On the use of autonomous unmanned vehicles in response to hazardous atmospheric release incidents

by
Michael Hutchinson

A Doctoral Thesis

Submitted in partial fulfilment of the requirements for the award of
Doctor of Philosophy of Loughborough University

March 2019

Loughborough University

Abstract

Recent events have induced a surge of interest in the methods of response to releases of hazardous materials or gases into the atmosphere. In the last decade there has been particular interest in mapping and quantifying emissions for regulatory purposes, emergency response, and environmental monitoring. Examples include: responding to events such as gas leaks, nuclear accidents or chemical, biological or radiological (CBR) accidents or attacks, and even exploring sources of methane emissions on the planet Mars.

This thesis presents a review of the potential responses to hazardous releases, which includes source localisation, boundary tracking, mapping and source term estimation. Following the review, source term estimation was identified as a promising approach to develop upon during the remainder of the thesis, with mapping to follow. Current literature on source term estimation is focused on using an array of static sensors to infer the location of the source and its emission rate. Formulated as an inverse problem, optimisation or Bayesian inference algorithms are used to fuse point-wise concentration measurements of the hazard with meteorological information and a dispersion model. The inverse problem is highly non-linear, ill-posed and subject to input data that is typically sporadic, noisy and sparse.

With the technological developments in sensing and robotics, sensor equipped unmanned vehicles are the modern approach to perform sensing tasks. In this thesis, the use of ground and aerial robots equipped with appropriate hazardous sensors are explored to estimate the source term of an atmospheric release. Previous work on the subject had been limited to simulations or tests using experimental datasets.

One of the main aims of this thesis was to extend work on source estimation using mobile sensors from theory and simulations to real world experiments. This aim was achieved for the first time in the literature by the five main contributions of this thesis. A joint Bayesian estimation and planning algorithm was developed to plan the robots path, taking into account the gain in information provided by a new manoeuvre. An experimental set-up was devised to test source estimation algorithms in a controlled environment using a ground robot. Successful experiments were achieved by developing a novel likelihood function to account for the intermittent, noisy readings from short sensor measurement sampling times. An unmanned aerial system was developed for source estimation experiments in uncontrolled outdoor environments and the Bayesian estimation algorithm was extended to consider uncertainty in all the dispersion parameters. After successful experiments the methodology was extended to consider a non-continuously releasing source and mapping algorithms were assessed for particularly unstable atmospheric conditions where the performance of the source estimation algorithms were degraded.

Acknowledgements

Firstly, I would like to thank my supervisor, Dr Cunjia Liu, for support during my PhD studies. His help formulating equations improved the quality of my publications, turning my code into understandable math.

I am grateful to my previous supervisor Dr Hyondong Oh who introduced me to the area of environment monitoring using unmanned vehicles and gave me the freedom to direct the research.

I would also like to thank Prof. Wen-Hua Chen for his guidance during my studies, his hard work in facilitating my research within the lab, and help looking into the next steps of my academic career.

I would like to give thanks to Paul Thomas, Paul Westoby and Grant Richardson of Dstl for useful discussions and support during a brief secondment at Porton Down, Salisbury. I am lucky to of had a casual discussion with Grant, where he joked that I could use incense sticks to simulate a hazardous source.

I am very pleased to have known the researches within the autonomous systems lab at Loughborough. The collaborative environment made this a great place to work. My particular thanks to Matthew Coombes, Pawel Ladosz and Jean Smith for their help in setting up robots, performing experiments, and for making time in the lab more enjoyable.

I am thankful to my parents for their continual support, and the rest of my friends and family for distraction from my work when it was needed.

To my girlfriend Alexandra, I am grateful for our shared commute and her ability to help with my headaches. Thank you for my random facts of the day.

This research was supported by the Loughborough University Department of Aeronautical and Automotive Engineering as well as the UK Ministry of Defence via the Defence and Security Accelerator, project numbers: ACC101517 and ACC500113.

Contents

List of Figures

List of Tables

Nomenclature

$\mathbb{E}$	Expectation function
$\mathbf{p}_k$	Sensor position vector
$\mathbf{p}_s$	Source posision vector
$\mathcal{M}$	Uncertainty augmented dispersion model
$\mathscr{I}$	Information function
ϕ_s	Wind direction
ψ	Available manouvres
σ_k	Standard deviation in likelihood funciton
σ_y	Turbulent diffusion parameter in y axis
σ_z	Turbulent diffusion parameter in z axis
τ_s	Source particle lifetime
Θ	Source parameter vector
Υ	Utility function
ζ_{s1}	Dispersion parameter
ζ_{s2}	Dispersion parameter
a_k	Robot manouvre vector
A_s	Scaled emission rate
C	Atmospheric transport and dispersion model
d_s	Diffusivity
M	Number of samples to approximate expected information
N	Number of Monte Carlo samples used in the particle filter

q_s	Source emission rate
R	Expected rate of particle encounters with a sensor
u_s	Wind speed
V	Voltage reading
w_k	Particle weight
x_s	Source cartesian coordinate
y_s	Source cartesian coordinate
z	Sensor measurement
z_s	Source cartesian coordinate

Acronyms

ABC approximate Bayesian computation

ABMP adaptive Bayesian motion planning

ATD Atmospheric Transport and Dispersion

BAE Bayesian adaptive exploration

CBR Chemical, Biological or Radiological

CFD computational fluid dynamics

DEMC differential evolution Monte carlo

GA genetic algorithm

GP gaussian plume

HAZMAT hazardous material

IP isotropic plume

IS importance sampling

MCMC Markov chain Monte Carlo

MH Metropolis Hastings

MOX metal oxide

MST mean search time

NN Neural Network

PC progressive correction

PCE polynomial chaos expansion

pdf probability density function

PID photoionisation detector

RMSE root mean squared error

ROS robot operating system

SCIPUFF second order closure untegrated puff

SD standard deviation

SLAM simultaneous localisation and mapping

SMC sequential Monte Carlo

SR success rate

STE source term estimation/reconstruction

UAV Unmanned Aerial Vehicle

Chapter 1

Introduction

In an event involving the release of hazardous airborne material, timely acquisition of information can save lives. This thesis describes research undertaken to enable an autonomous unmanned vehicle to gather such information, in an efficient, fully automated fashion, by searching for and estimating the source term of the release or by mapping the spread of hazardous material. The source term is a set of parameters that characterise the source of an atmospheric release of dispersive material. This includes several parameters that can be used for post hazard forensics and to forecast the spread of the material using an Atmospheric Transport and Dispersion (ATD) model. Key parameters of the source term are the location of the source of the release and its emission rate. An example use of the source term of a release, well-known by the general public, is forecasting the dispersion of ash after a volcanic eruption. The forecast is used by aviation authorities to avoid damage to aircraft and by governments to issue health warnings to children, the elderly and asthmatics.

Contrary to volcanic eruptions, most hazardous atmospheric releases, such as gas leaks or chemical spills, are not visible by satellite and the locations of the releases are unknown. In this thesis, an unmanned ground or aerial vehicle, equipped with in-situ hazardous sensors, is used to achieve a similar level of situational awareness provided by satellite observations of the ash clouds, for releases of greenhouse gases, hazardous gases or Chemical, Biological or Radiological (CBR) material.

Autonomous unmanned vehicles, such as unmanned aerial vehicles (UAV) have the ability to sample from the most desirable locations to gather high quality spatial temporal data. This can enable mapping of the distribution of hazardous material or estimation of the location of the hazardous release and the other parameters of the source term. UAVs are already in use by researchers, police forces, fire brigades and militaries around the world. The benefit of such platforms and their ability to enhance a human machine unit is undeniable. The application of UAVs to events as critical as hazardous gas leaks or CBR incidents is the most prudent course of action. Moreover, for research and government, they can be used to effectively monitor, explore, map and quantify sources of emissions.

Related work in the area of source term estimation has focused on using networks of static detectors or has been limited to simulated measurement data. One of the key features of this thesis is experimental validation of the algorithms, leading to novel results of source term estimation performed using a ground robot or a UAV.

1.1 Motivation

Finding the source of a gas, knowing an estimate of its emission rate, mapping or forecasting the spatial extent of a gas, or even simply confirming the presence or absence of hazardous airborne material in an area has immense benefit in emergency response and several other applications. The gaseous release could be man-made or naturally occurring, hazardous to the environment or to human health, or provide clues as to the location of resources. Examples of well-known naturally occurring releases include some sources of methane emissions or volcanic eruptions [1]. In these circumstances it is of great interest to identify and quantify these sources, and map or forecast the spread of the hazard, in order to assess the environmental, social and commercial impact.

Man-made releases are predominantly a result of industrial emissions, accidents such as chemical spills, or acts of terrorism and war. Characteristic examples include the Sarin gas terrorist attacks in Japan (1995), the famous chemical accidents of Bhopal, India (1984) and Seveso, Italy (1976), Nuclear disasters such as Fukushima (2012), and the recent use of chemical weapons and nerve agents in Syria (2013-2018). A prompt and accurate assessment of the whereabouts of the hazardous material and a prediction of its future dispersion and deposition is important to enable responders to undertake appropriate mitigation strategies and/or to extract troops/civilians from affected regions. Hazard predictions, however, require accurate knowledge of the release parameters (the so-called source term), as well as the local meteorological information. In many situations this information may be unknown, or highly variable.

Existing emergency response practices for hazardous material (HAZMAT) events require either a static network of pre-deployed sensors, which can be costly and necessitate substantial planning, or the manual collection of sensor measurements, e.g. using hand-held devices and dedicated manned vehicles, which places people at risk. The optimal response to releases of material hazardous to the environment or to human health would be stand-off, rapid, and reliable; keeping people out of danger, whilst maximising the efficiency of the response and minimising training costs. An autonomous UAV with integrated hazardous sensors has the potential to provide such a response. The goal of this thesis is to research methods that will enable it to do so.

1.2 Background

Potential responses to a harmful atmospheric release include mapping, boundary tracking, source localisation or source term estimation/reconstruction (STE) [2]. Mapping and boundary tracking both aim to provide a spatial approximation of the contaminated area. A benefit of mapping is the ability to approximate the distribution of the hazardous material without relying on a model. However, it could be challenging to handle large amounts of noise, large areas, intermittent sensing, and temporal variations in the hazard distribution. Boundary tracking shares similar challenges, in addition to the splitting up of contaminated regions. Source localisation will attempt to find the origin of the hazardous material. Although valuable, this does not provide information about the spread of hazardous material nor the quantity of the emission. STE methods will estimate the location of the release and the strength of the source. With this information, an ATD model can be used to approximate the spread of contamination and it will be possible to forecast the future and long term hazard; including estimates of deposition [3]. The main limitation of STE is the reliance on an ATD model to forecast the dispersion.

Estimation of the source term of an atmospheric release is most popularly achieved using a large network of static concentration sensors and meteorological stations as reviewed in [4] and [2]. Formulated as an inverse problem, the source parameters are estimated using optimisation or Bayesian inference algorithms based on those sensor readings. On the other hand, the development of smaller sensors and intelligent, autonomous robots, means that mobile platforms such as unmanned ground or aerial robots equipped with various sensors are the modern approach to perform sensing tasks. Applied to environmental monitoring tasks [5, 6, 7, 8], mobile platforms overcome issues such as maintenance, powering, networking, positioning and costs of large static networks of sensors. For source estimation and mapping, mobile sensors are preferred, as a single sensor has the potential to solve the entire problem by searching more desirable measurement locations and collecting more useful/informative, spatial-temporal data.

A reader unfamiliar with gas source localisation, atmospheric dispersion, or STE research could at first glance perceive the problem as rather trivial. For example, to localise a gas source, one would intuitively propose to trace the concentration gradient of the gas towards its origin. When in fact, it is an immensely challenging problem due to the random nature of turbulence and gas dispersion which can cause erratic fluctuations in concentration resulting in sporadic, highly volatile readings from the gas detectors [9, 10]. Indeed, from a biological point of view, living organisms that adopt a gradient based, or "chemotaxis", approach are of a microscopic scale such as Escherichia Coli bacteria [11]. On a larger scale the procedure is abandoned. For the readers comprehension, an example plume on the scale of the experiments conducted in this thesis is shown in Fig 1.1. The coloured smoke was used to visualise the effect of the UAV (seen in the centre of the figure) on the gas dispersion. In this example, despite a strongly emitting source, gaps in the

Figure 1.1: Visualisation of a UAV flying in the plume of a point source of emissions.

plume can be observed nonetheless.

STE methods incorporating static detectors can overcome this challenge by averaging the sensor measurements for a time period of a minute or more. Given the short flight time of a Unmanned Aerial Vehicle (UAV), and the requirement of a rapid response, this sampling time must be greatly decreased, resulting in significantly different outputs from the sensor; characterised by greater intermittency, or non-detections, and increased noise. Overcoming such a challenge is one of the key contributions of this thesis, and it is expected to be a contributing factor to why this thesis reports the first experimental results of source term estimation performed using a mobile platform.

1.3 Overview

1.4 Aims and objectives

The aims of this thesis are to:

- Determine the most appropriate autonomous response to releases of hazardous airborne material, which can eventually be exploited by end-users, to be further developed during this thesis.
- Develop an information based search and source estimation algorithm to efficiently and reliably localise the source of a hazardous release and determine its emission rate.
- Test an information based search and source term estimation algorithm, using a real autonomous ground robot equipped with a gas detector, in reproduce-able conditions outside of simulations and experimental datasets.

- Estimate the source term of an atmospheric release using point measurements of concentration from a UAV in outdoor conditions.
- Explore the performance of the system in different scenarios such as a non-continuous release of hazardous material.
- Explore other promising response methods such as plume mapping.

The objectives which must be met to achieve the aims are as follows:

- Perform a thorough literature review of potential methods of response to releases of hazardous airborne material.
- Develop an information based sensor planning algorithm to search for and estimate the source term of an atmospheric release.
- Develop experimental methodologies to test the system outside of simulation but in a reproducible manner.
- Extend the algorithm to handle the challenging conditions experienced outside of simulation environments.
- Develop experimental methodologies to test the system in realistic outdoor conditions.
- Develop and test an autonomous UAV for source term estimation in outdoor conditions.
- Extend the information based planning algorithm to three dimensions and perform experiments using the UAV.
- Extend the methodology to handle a non-continuous source and compare the UAV based approach against using static detectors in simulations.
- Develop a method to map the concentration distribution of a plume using unmanned vehicles and test it in multiple experimental environments.

To achieve the aims and objectives a mixture of research methodologies were adopted; ranging from initial analytic derivations, numerical simulations, to hardware development, integration and experiments.

1.5 Contributions

The contributions of this thesis are well summarised by a time line of the research and development conducted to take the work from an initial review of the literature and preliminary simulation results to controlled indoor experiments and subsequently uncontrolled outdoor experiments.

To initialise the research conducted as a part of this thesis, a thorough review of related work in the area was conducted to outline the field and determine the most promising approach that, through this thesis work, could potentially be employed in the field. Source term estimation, using Bayesian probabilistic algorithms and an unmanned ground or aerial vehicle, was identified as such an approach. This discovery led to the research and development conducted in the majority of the thesis. Moreover, mapping the contaminated area was also identified as an appropriate response and is also considered in this thesis, albeit, to a lesser extent.

Initially, the most common and tested Bayesian method used to estimate the source term of a release, previously using static detectors, was combined with an information based path planning algorithm which was adapted from the field of optimal experiment design. In an experiment design context, the method was developed to determine the most informative experiment to perform next based on the current information available. Applied to source term estimation using a mobile platform, the algorithm was shown to outperform conventional path planning methods such as a parallel sweep search pattern.

Given this promising result, the Bayesian estimation algorithm was reformulated and implemented in a recursive manner, more appropriate for the problem where sensor data are collected sequentially. The information based path planning algorithm was made more efficient by using the predictive measurement entropy as the planning reward, which lead to the new algorithm termed "Entrotaxis", for autonomous search and source term estimation in turbulent conditions. The method was compared with the state of the art approaches in the literature using a simulated scenario and an experimental dataset, where it was shown to achieve a more efficient autonomous search.

The next stage was to test the algorithm outside of simulations. This involved modifying the algorithm, designing an appropriate experiment, and setting up a robotic platform. Successful experiments were conducted in an indoor area with fans to simulate wind and a ground robot equipped with a low cost gas sensor. Several contributions were required to facilitate the successful experimental result, which was the first of its kind in the literature, where the source term of a diffusive release was estimated using a ground robot.

With the successful indoor result, the next stage was to assess the system in outdoor conditions using an aerial vehicle rather than a ground based system. In these challenging conditions the system was first verified using a parallel sweep flight pattern rather than the information based online planner. Gas sensing experiments using a UAV are rare. Using the unique data, two ATD models were compared for source term estimation and the effect on the results of the UAVs altitude, the step size in the sweep pattern, and the wind speed were assessed. The information based on-line planner was then tested in similar experimental conditions and the results were compared.

Following successful outdoor experiments showing the potential of the UAV based approach, the method was extended to handle a non-continuous release of hazardous material. The UAV based approach was compared to using static sensors in simulations.

During the outdoor experiments using the UAV it had been discovered that the system performed less well in low wind, highly unstable atmospheric conditions. In response to this a mapping algorithm was developed. Several regression based algorithms for mapping were compared in controlled indoor experiments using a ground robot and demonstrated in uncontrolled outdoor tests using a UAV.

Overall, the contributions presented in this thesis can be summarised as follows:

- This thesis has developed an information based search and STE algorithm and compared it with state of the art methods in simulations and on experimental datasets.
- The information based search algorithm has been implemented using a ground robot, in novel repeatable experiments, to validate the STE method incorporating an autonomous mobile platform for the first time.

  - To produce the successful experiments a new sensor model and likelihood function were developed, and the estimation algorithm was extended to consider uncertainty in all model parameters.
- This thesis presents novel STE experiments performed in uncontrolled outdoor conditions using an autonomous UAV.

  - The setup of a HAZMAT sensing UAV is described.

  - The performance of the STE algorithm subject to several parameters is analysed including the wind speed, flight altitude and the scale of the experiments.

  - Two dispersion model are subsequently compared using the unique experimental data to inform the appropriate use of the models in different scenarios.
- The information based planning algorithm is extended to three dimensions and assessed in outdoor experiments using the UAV.
- The method is extended to the scenario where the HAZMAT is released instantaneously rather than from a continuously emitting source.
- Several plume mapping algorithms are compared in simulations and in repeatable experiments using a ground robot. The most effective method is subsequently demonstrated in uncontrolled outdoor experiments using a UAV.

1.6 Outline

The outline of the thesis is as follows:

Chapter 2 - Literature review
This chapter presents a broad of review of potential responses to incidents involving the release of hazardous airborne material into the atmosphere, with particular emphasis on

source term estimation. The other approaches reviewed include mapping and source localisation.

Chapter 3 - Informative path planning for hazardous source reconstruction
This chapter describes an information based algorithm to search for and estimate the parameters of a diffusive release. The method is verified with simulations and compared against conventional approaches such as a uniform sweep flight pattern.

Chapter 4 - Entrotaxis as a strategy for autonomous search and source reconstruction in turbulent conditions
In this chapter, the Entrotaxis algorithm is described as a strategy for autonomous search and source reconstruction in turbulent conditions. The algorithm performs faster than that described in the previous chapter as estimation is performed sequentially and it is extended to handle more sporadic conditions and a particle counter based sensor. The algorithm is compared with other search algorithms using an experimental dataset collected in a water channel.

Chapter 5 - Information based search for an atmospheric release using a mobile robot
This chapter presents the first results of an intelligent search and source estimation algorithm using a real robot and sensor in experimental conditions. Several moderate extensions were made to the previous chapters to facilitate the results. Simple, safe, easily reproduce-able experiments were developed and described as part of the chapter.

Chapter 6 - Source term estimation of a hazardous airborne release using an unmanned aerial vehicle
The set-up of a UAV for gas sensing experiments is described in this chapter. Followed by experimental trials of the source term estimation algorithm using a uniform sweep flight pattern. The performance of the system is assessed with regards to the wind speed, the flight altitude of the UAV and the incremental step size between measurements during flight.

Chapter 7 - Information based search for a hazardous airborne release using an unmanned aerial vehicle
In this chapter the information based search and STE algorithm is extended to three dimensions and assessed in experimental trails.

Chapter 8 - Information based search for a non-continuous atmospheric release using a UAV
In this chapter the information based search and STE algorithm is extended to handle a

non-continuous release, rather then a plume of constant emission.

Chapter 9 - Plume mapping using point measurements from autonomous unmanned vehicles
In this Chapter, a Gaussian Process regression machine learning algorithm is applied to map the concentration of hazardous airborne material. The method described is compared with other approaches in repeatable indoor experiments using a ground robot and demonstrated in uncontrolled outdoor experiments using a UAV.

1.7 Publications

Journal articles

Hutchinson, M., Liu, C., & Chen, W. H.. (2019). UAV Based HAZMAT Response: Information-theoretic Hazardous Source Search and Reconstruction. In Robotics & Automation Magazine. IEEE. (in preparation)

Hutchinson, M., Liu, C., & Chen, W. H.. (2018). Source term estimation of a hazardous airborne release using an unmanned aerial vehicle. In Journal of Field Robotics. Wiley. DOI: 10.1002/rob.21844.

Hutchinson, M., Liu, C., & Chen, W. H.. (2018). Information Based Search for an Atmospheric Release Using a Mobile Robot: Algorithm and Experiments. IEEE Transactions on Control Systems Technology, (99), 1-15.

Hutchinson, M., Oh, H., & Chen, W. H. (2018). Entrotaxis as a strategy for autonomous search and source reconstruction in turbulent conditions. Information Fusion, 42, 179-189.

Hutchinson, M., Oh, H., & Chen, W. H. (2017). A review of source term estimation methods for atmospheric dispersion events using static or mobile sensors. Information Fusion, 36, 130-148.

Conference papers

Hutchinson, M., Ladosz, P., Liu, C., & Chen, W. H.. (2019, May). Experimental Assessment of Plume Mapping using Point Measurements from Unmanned Vehicles. In Robotics and Automation (ICRA), 2019 IEEE International Conference on. IEEE.

Hutchinson, M., Liu, C., & Chen, W. H.. (2018, May). Information based mobile sensor planning for source term estimation of a non-continuous atmospheric release. In Robotics and Automation (ICRA), 2018 IEEE International Conference on. IEEE.

Hu, L., Su, J., Hutchinson, M., Liu, C., & Chen, W. H. (2018). Bayesian Estimation of A Periodically-Releasing Biochemical Source Using Sensor Networks. UKACC 11th International Conference on Control (CONTROL). IEEE.

Hutchinson, M., Oh, H., & Chen, W. H. (2017). Adaptive Bayesian sensor motion planning for hazardous source term reconstruction. IFAC-PapersOnLine, 50(1), 2812-2817.

Book chapters

Ladosz, P., Coombes, M., Smith J. and M. Hutchinson, (2018). A Generic ROS based System for Rapid Development and Testing of Algorithms for Autonomous Ground and Aerial Vehicles. Robot Operating System (ROS) The Complete Reference. Springer International Publishing.

Chapter 2

Literature review

The first objective of this thesis is to review the potential methods of autonomous response to releases of HAZMAT into the atmosphere. As discussed in the Introduction, this topic has several important applications and many probable solutions. The potential methods that are reviewed in this chapter include:

- Localising the source of the release - to find where release is coming from.
- Tracking the boundary of the release - so that the area within which the concentration crosses a threshold is known.
- Mapping the concentration distribution of the release - to determine the spread and distribution of the hazardous material.
- Estimating the source term of the release using static sensors - to estimate the position of the source and its emission rate, the spread of the material can then be approximated using a model.
- Estimating the source term of the release using sensors placed on unmanned platforms - as above, but using mobile sensors rather then a static sensor network.

This literature review considers each method of response in order to identify the most appropriate area for further research, with regards to the value provided by the response and how realistically it can be achieved - with the goal of eventually providing some functions for a system used by emergency responders to facilitate a more effective response. Part of the review has been previously published by the author [2].

The review begins with a look at the available sensors and prototype robots proposed in the literature to sense gases, aquatic plumes, atmospheric emissions or airborne HAZMAT. The sensors considered are Commercial Off The Shelf (COTS) and the robots include ground, aerial, surface and underwater based sensing platforms.

Next the review considers each of the identified response methods, looking at the variety of techniques therein to identify the state of the art and potential for improvements or

extensions. The current limitations of the state of the art are identified and areas for future research are suggested. At the end of the chapter the approaches are compared and used to guide the work conducted during the remainder of the thesis.

2.1 Atmospheric concentration measurement systems

In early work of atmospheric sensing static sensors were most commonly used. This soon led to sensors placed upon vehicles such as cars or aircraft. The modern approach to many sensing tasks is to mount sensors on unmanned platforms. The unmanned platforms could be ground or aerial based, and be controlled remotely or autonomously. In this section the sensors that may be used on unmanned platforms are reviewed, looking at their advantages and disadvantages for incorporating into the system to be developed during this thesis. The set-up of several unmanned sensing platforms seen in the literature are also reviewed, where they have been proposed for various applications and conditions. The sensing platforms range from ground, aerial, or aquatic robots, however, emphasis is given to UAVs as this is the focus of the thesis.

2.1.1 Atmospheric concentration sensors

Atmospheric concentration sensors are devices that respond to changes in the atmospheric composition. The sensors can vary greatly in sensitivity, selectivity, cost, size, weight, response time, and power consumption. The sensors are classified by their principles of operation such as thermal, electrochemical, conductometric, mass or optical. They can also be classified among in-situ and remote sensors. In-situ sensors require direct interaction between the sensitive layer of the sensor and the target compound, meaning the measurement from the sensor corresponds only to a small area around the sensitive part of the sensor. Remote sensors take a distance measurement of a phenomenon so that direct interaction with the target compound is not necessary. The general principle of all the sensors is that a change in the atmospheric concentration generates a measurable, somewhat repeatable response. The different sensors and their applicability to robotic sensing missions are briefly assessed in the next few sections, a more thorough review is given in [12].

2.1.1.1 Spectrometers

Spectrometers have the ability to measure spectral components of a physical phenomenon. One such device used for analysing gases is known as an ion mobility spectrometer (IMS). IMSs are based on the time of flight of ionised samples. The measured time of flight of the samples through a short distance within the device is compared with a library of known compounds to identify the material. There are several sensors based on IMS technology, a popular and lightweight sensor is the LCD 3.3 IMS from Smiths detection, shown in Fig

Figure 2.1: The LCD 3.3 IMS sensor from Smiths Detection[1].

2.1. It is a small hand-held device used for the detection of chemical warfare agents (CWA) and toxic industrial compounds (TICs). The sensor is one of few spectrometers small and lightweight enough for UAV deployment, weighting in at 650g (including batteries, screen and casing), with a fast response time ($\leq$10 seconds), which refers to the delay between contact with a contaminant and its detection. However, the device is expensive and has a narrow detection range.

There are several other spectrometers based on different technologies, they typically weigh or cost more than an IMS.

2.1.1.2 Conductometric sensors

Conductometric sensors measure the presence of gaseous compounds by changes in conductance in the sensitive layer of the device, some example sensors are shown in Fig 2.2. Changes in conductance are caused by different mechanisms depending on the sensor type, such as though redox reactions or chemosorption. Within the literature involving mobile platforms, Metal Oxide (MOX) gas sensors have been the most widely used due to their commercial availability, high sensitivity, long life span and their reasonable response and recovery times. MOX based sensors consists of a heating element inside a ceramic tube coated with a semiconductor. The selectivity of these sensors is adjusted either by doping the surface of the semiconductor with different additives or by changing the operating temperature. The presence of reductive gases causes a drop in the resistance of the semiconductor. The resistance increases as the concentration of the target gas is reduced. Particular advantages of MOX sensors to deployment on mobile platforms are their very light weight and low cost. The disadvantages of MOX gas sensors are their cross sensitivity to humidity and temperature, lack of selectivity to target gases (i.e. they respond to several interfering materials), difficult calibration and the requirement of some warm up time for the sensor reading to settle.

Other conductometric sensors include electrochemical cells and pellistor sensors. Pellistors are used to detect flammable gases due to combustion within the sensor which changes

[1]https://www.smithsdetection.com/products/lcd-3-3/

Figure 2.2: (a) MICS 5524 MOX sensor from SGX sensortech[2], (b) An Alphasense pellistor[3]and (c) An electrochemical sensor from Alphasense[4].

the resistance proportionally to the concentration of explosive gases. Electrochemical sensors use oxidation or reduction to detect chemicals. They are low cost, lightweight and selective to the target gas making them useful for several applications. However, the sensors have a long response time, ranging from 30 to 60s, and quite low sensitivity (depending on the target gas), making them less suitable for mobile robot applications.

2.1.1.3 Photo ionisation detectors

Photo ionisation detectors (PID) use high energy photons, typically ultraviolet, to break gas molecules into positively charged ions. Most PID sensors available commercially use a 10.6eV ultraviolet lamp. Compounds that enter the sensor are ionised by the lamp which causes them to become positively charged. The positively charged ions produce a current which is the output of the detector. The current output is proportional to the concentration of measured gas. PID sensors are not selective, as the UV light from the detector ionises all molecules that have an ionisation energy below the value of the lamp (commonly 10.6eV). However, if the target gas is known, and there are not any other interferences, they can provide an accurate concentration measurement. PIDs are more expensive than MOX sensors but significantly cheaper than IMS sensors. They can be very lightweight, small sensors (similar to MOX), or come as part of a commercially available device as shown in Fig 2.3. An advantage of PID sensors is their very fast response and recovery times.

2.1.1.4 Remote sensors

Remote sensors are able to take a distant measurement of a phenomenon of interest. Applied to sensing of airborne material or gases, concentration measurements are made quantifying the interaction between the target compound and electromagnetic energy. Depending on the method of remote sensing, the electromagnetic energy can come from an

[2]https://sgx.cdistore.com/Products/Detail/MICS5524-SGX-Sensortech/333420/
[3]http://www.alphasense.com/index.php/products/pellistors/
[4]http://www.alphasense.com/index.php/safety/products/

Figure 2.3: (a) PID sensors from Alphasense [5]and (b) The MiniRAE 3000 PID sensor from RAE Systems[6].

artificial or natural source. Active sensing methods emit an artificial source of electromagnetic radiation whereas passive sensors rely on natural sources such as sunlight.

Active sensors typically use absorption spectroscopy to measure the concentration of a gas. Different gas molecules absorb various amounts of energy depending on the wavelength of the electromagnet radiation. The active sensor emits radiation at a particular band depending on the target gas, achieving a high degree of selectivity. Concentration measurements of the gas are made using the Beer Lambert law [13].

The remote sensors vary depending on the target gas. For example differential optical absorption spectroscopy (DOAS) use absorption of UV light to detect nitrogen and oxygen. Tunable diode laser absorption spectroscopy (TDLAS) sensors emit a laser beam with a wavelength set depending on the target gas. The diode is driven on and off the absorption band, and the difference in the two beams is used to determine whether the target gas is present or not. TDLAS sensor can achieve a high degree of selectivity but are quite expensive. It will also be effected by blocking of the beams, for example, by dust in the air. Fourier transform infra red (FTIR) devices are able to detect multiple target gases. They require an emitter and a receiver with line of sight. The frequency of the infra-red waves between the emitter and receiver is compared with a database to determine the compound. While FTIR devices are highly selective and can detect multiple compounds, they are very expensive.

Passive remote sensors include multi spectral and Thermal infra red (IR) cameras. These benefit from the ability to capture an image of the target gas plume. Multi spectral cameras are able to identify multiple gases and their spatial distribution. However they have low accuracy, are affected by weather conditions, and are expensive. IR cameras can similarly visualise a plume, however, they are unable to detect gas concentrations.

[5]http://www.alphasense.com/index.php/products/pid-air/
[6]https://www.raesystems.com/products/minirae-3000-wireless-handheld-voc-monitor

Figure 2.4: (a) TDLAS methane detector[7]and (b) FTIR chemical warfare agent and toxic chemical detector[8].

2.1.2 Unmanned sensing platforms

Unmanned sensing platforms proposed in the literature are essentially an integration of existing autonomous robots with atmospheric sensors with some on-board processing or wireless communication system in place. In this Section, existing prototype robots proposed in the literature are summarised and used to guide the design of the experimental platform used in this thesis.

2.1.2.1 Ground robots

Ground based robots are popular platforms for atmospheric concentration sensing with several proposed applications including: environmental monitoring, localising odour sources in indoor or outdoor environments, monitoring methane emissions or in response to chemical spills. Some of the prototype ground based platforms are shown in Fig 2.5. Besides the integration of an atmospheric concentration sensor with the platform, the systems are also commonly equipped with a camera for tele-operation, a LIDAR for simultaneous localisation and mapping (SLAM) and obstacle avoidance, and an anemometer. Some of the systems are equipped with a range of low cost sensors to improve the detection probabilities of the system or to attempt to determine the gas that is present by comparing the response of multiple sensors [14], otherwise known as gas discrimination.

The main advantages of ground robots as oppose to aerial robots are common among most applications, such as battery life and the ability to carry larger, heavier sensors. Other advantages are specific to the problem, for example, ground robots will effect the meteorology and sensing ability of detectors significantly less than a aerial vehicle with spinning rotors which will have a large affect on wind and pressure. The disadvantages

[7]http://www.pergam-suisse.ch/en/products/lmm/
[8]https://www.bruker.com/products/cbrne-detection/ft-ir/rapidplus-rapidplus-control-20-vom/overview.html

come from the limit in 3D sensing abilities, speed, manoeuvrability, and the ability to traverse obstacles or harsh terrain.

2.1.2.2 Aerial robots

The ability to sense a gas from a UAV has numerous proposed applications including: detecting gas leaks [22, 23, 24]; monitoring various sources of air pollution [25, 26, 27, 28]; measuring important variables in greenhouses [6]; and exploring sources of methane emissions [29, 30]. The UAVs used in aerial gas sensing research include both fixed wing and rotary wing platforms [31]. Some examples in the literature are shown in Fig 2.6. The main advantage of using UAVs comes from their ability to cover large areas quickly, to easily handle cluttered ground environments, and 3D movement for data collection at various altitudes; which will be useful for a system designed to sample from both buoyant or dense gas plumes. The disadvantages come from the limit in payload which will affect the sensor that can be carried and the limited flight time of the vehicles.

One of the dominant factors to consider when measuring a gas using a UAV is the influence of the rotors on the dispersion of the gas and the output from the sensor. This effect has been taken into consideration in the past and research has been conducted to determine the optimal position of the gas detector and the effect on the sensor measurement [6, 25, 22]. Some of the potential sensor positions proposed include: under the rotors of the UAV, in the centre of the platform raised above or below it, in the space between the UAV rotors, and extended on an arm away from the platform and its effect on the gas. Through computational fluid dynamics (CFD) studies, smoke visualisation experiments, and pressure and airflow measurements around the UAV, some conclusions can be drawn, despite conflicting results. The general consensus is that the effect of the rotors is to decrease the measurement from the gas detector and increase its uncertainty [26]. The most accurate measurements would come from a sensor outside of the disturbed region of airflow, however, this would be more likely to cause stability issues whilst in flight. A pumped system could be implemented on the vehicle, where the inlet would be away from the platform, still, this would add undesirable weight to the system. For these reasons, the most common placement seen in the literature is in a raised position, in the centre of the platform [6, 28]. The focus of this thesis is on developing algorithms for monitoring hazardous releases using a UAV, consequently, the effect of the rotors has not been prioritised. Nevertheless, the effect on the results is discussed in the experimental Chapters of the thesis. Given the huge increase in applications and experiments involving gas sensing on UAVs, it is envisaged that bespoke new sensors, designed for UAVs will have a great benefit and will be an important area for future research.

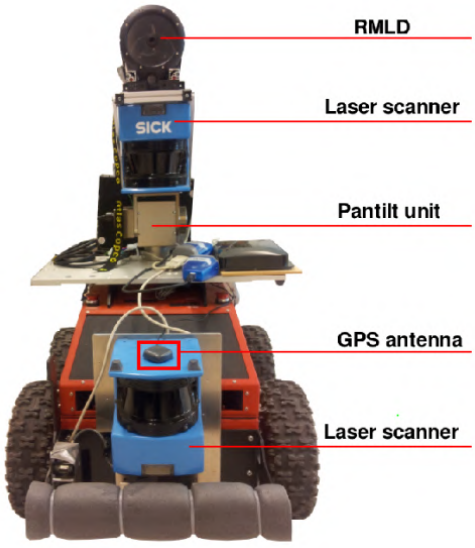

(a) Gasbot1 [15, 16]

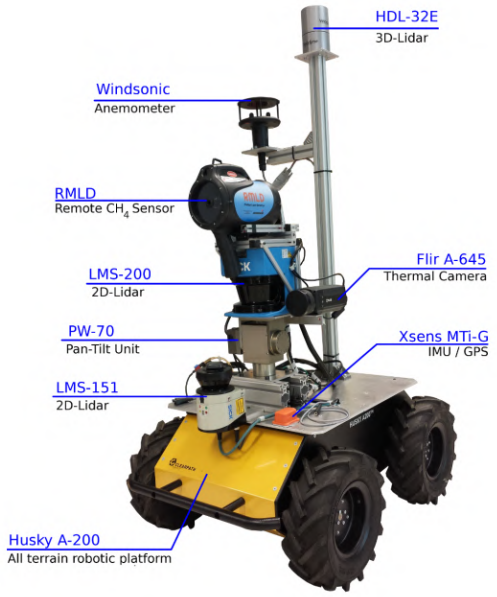

(b) Gasbot2 [17]

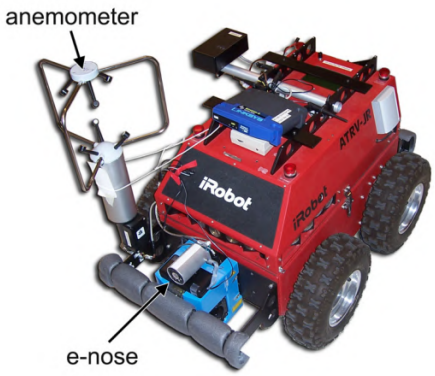

(c) Rasmus pollution survey robot [18]

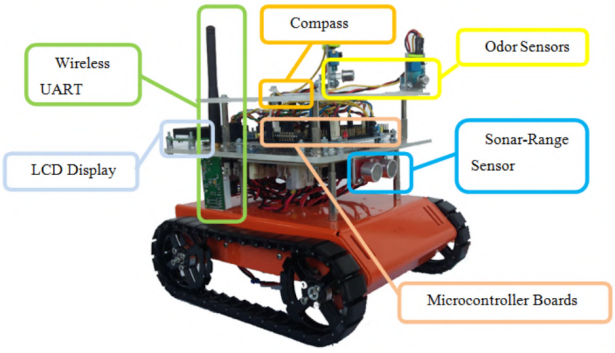

(d) Al-Fath odour sensing robot [19]

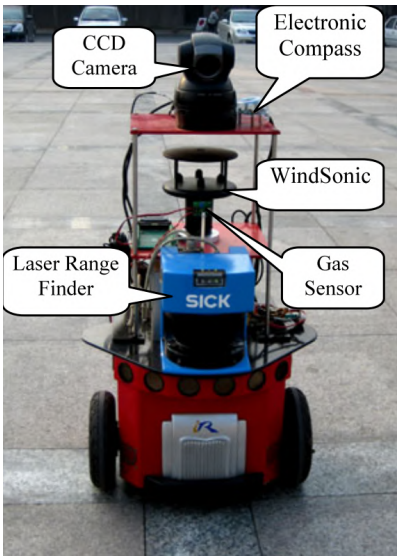

(e) Odour localisation robot [20]

(f) MrCollie odour sensing robot [21]

Figure 2.5: Existing ground robot prototypes for atmospheric concentration sensing

(a) [32]

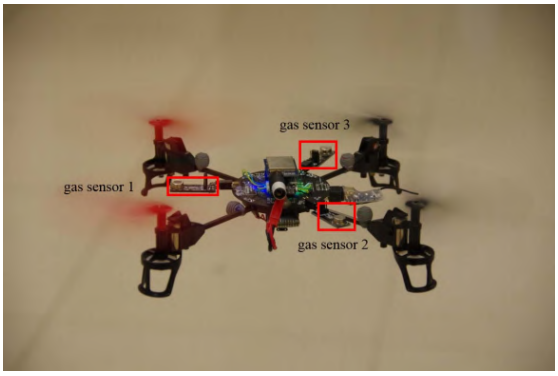

(b) [24]

(c) [29]

(d) [23]

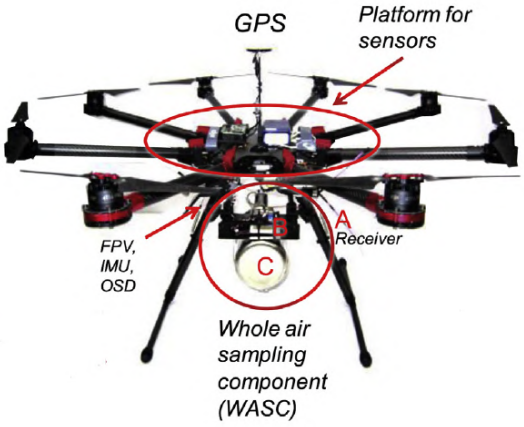

(e) [25]

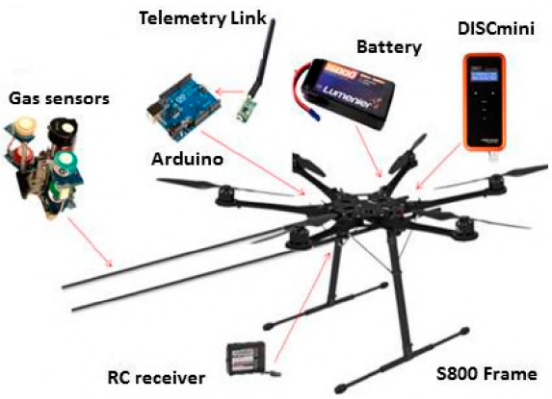

(f) [26]

Figure 2.6: Existing aerial robot prototypes for atmospheric concentration sensing.

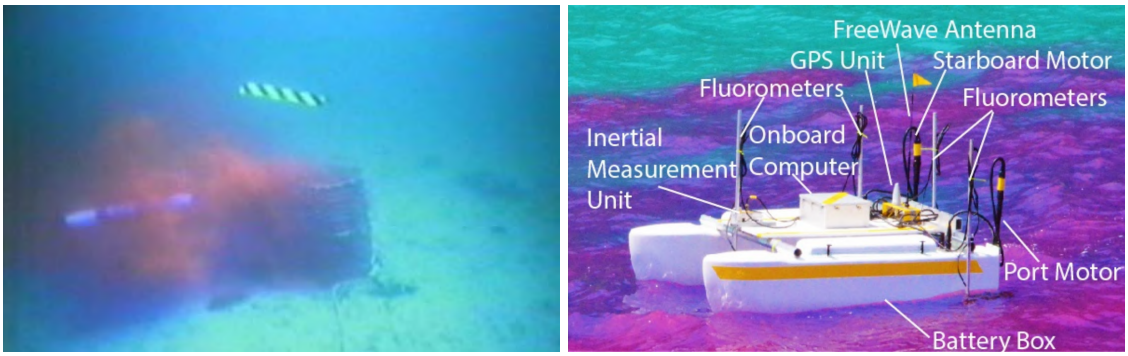

Figure 2.7: An underwater [33] and a surface robot [34] for aquatic concentration sensing.

2.1.2.3 Aquatic robots

Although not directly related to the problem of atmospheric concentration sensing, aquatic robots have also been used to detect concentrations of contaminants and plumes in oceans or lakes. Unmanned surface and underwater robots have both been developed as shown in Fig 2.7. Applications of these robots include monitoring underwater plumes and oil spills. Several algorithms have been developed for use by aquatic robots to locate plume sources or to track plume boundaries. Due to the higher density of the fluid medium and less turbulence, the oceanic plume propagate more slowly and with less areas of intermittent patches of contaminant; making difficult tasks such as boundary tracking, mapping or source localisation slightly easier.

2.1.3 Summary

In this subsection atmospheric concentration measurement sensors and some robotic platforms proposed in the literature for atmospheric sensing were reviewed, considering their unique advantages and disadvantages. The insights gained will be used to guide the development of the experimental platform used for the validation of the algorithms created in this thesis. The concentration measurement sensor vary greatly based on the sensing technology used, the target compound, cost and weight. Most of the proposed robots were equipped with the low cast MOX sensors which were highly sensitive for their low cost. Their main limitations are cross sensitivity to humidity and temperature, difficult calibration, and a lack of selectivity to a target gas, however attempts were made to address this by fusion of a range of different low cost conductometric sensors. Spectrometers are a high cost, slightly heavier sensor with a lot of selectivity to the target gas. A TDLAS sensor has been mounted on ground robots and recently on an aerial platform [30]. A good trade off between the low cost MOX and the expensive spectrometers is PID sensors. While these devices are more expensive than MOX sensors and do not have the selectivity of spectrometers such as the TDLAS or IMS sensors; they are lightweight, small, highly sensitive to a range of compounds, have very fast response and recovery times and are easily calibrated. These reasons among many were deciding factors on the experimental

set-up used in this thesis - a UAV mounted with PID detectors. However, a commercial system is expected to hold a range of sensors depending on its application, the budget, and the target compounds. It should be noted that the algorithms developed in this thesis are generic, and can be used with different sensing systems.

2.2 Source localisation

The goal of source localisation, with regards to atmospheric releases, is to identify the location of the source of the emitting material. Knowing the location of a releasing source can support operations in several ways, for example: inspecting pipelines for cracks, identifying the source of an accidental or intentional HAZMAT release, locating sources of greenhouse emissions, or inspecting industrial facilities for chemical leaks or pollution. Source localisation has received substantial interest lately, with methods incorporating mobile robots proposed ranging from simple gradient climbing algorithms to more complex techniques to account for sporadic measurements of concentration. As this is not the primary topic of this thesis, only a brief overview of source localisation is presented in this section. For further reading, detailed reviews on the topic are presented in [35] and [36]. The majority of experiments used to assess source localisation algorithm are performed in indoor environments with artificial wind produced by fans. However, some notable examples of outdoor experiments include [20] and [32], where particle filter based algorithms are used to estimate the source location using an unmanned ground or aerial vehicle. They are among other proposed methods reviewed in this section.

2.2.1 Bio-inspired algorithms

Chemotaxis are used throughout the literature for source seeking [37, 38]. The method was biologically inspired from the behaviour of a number of organisms (Moths, Lobsters, E-coli bacteria, Dung beetles, and Blue crabs). Most chemotaxic methods focused on climbing a gradient of the concentration value. The gradient was determined by taking measurements of the concentration at spatially separated positions. These methods relied on the assumption that the concentration gradient would consistently be positive in the direction of the source; this is often not a valid assumption for atmospheric dispersion due to turbulence.

Anemotaxis are another method that has been used in the literature [39, 40]. This technique used knowledge of the motion of fluid to help find the source. Several researchers have combined chemical concentration and fluid flow measurements to find an odour source. Some techniques include:

- The Zigzag/Dung Beetle method, which involved moving upwind within the odour plume in a zigzagging motion [39]
- Plume-centred upwind search [40]

- Silkworm moth inspired algorithm [37, 41]

The male silkworm moth, for example, displays a mixture of crosswind casting followed by an upwind surge upon detection of female pheromone [42]. The moth has been a popular subject of biological and robotics research on account of the extraordinary efficiency observed, despite the challenging conditions, whilst searching for a female mate releasing sexual pheromone [43, 10].

Fluxotaxis is a source seeking technique that incorporates fluid and chemical concentration measurements and estimation of the mass flux. Zarzhitsky et al. [44] developed a Fluxotaxic algorithm for a swarm, which found the source by climbing up the mass flux gradient [44, 45, 46, 47]. Computational fluid dynamics had been used to estimate the average bearing of the flow. The technique outperformed several chemotaxis and anemotaxis methods during simulations though there was no experimental comparison.

Bio inspired source localisation algorithms benefit from their low computational cost and the fact that they do not rely upon a model. A limitation of the methods is a lack of extendibility such as the ability to extend them to consider obstacles in the environment.

2.2.2 Gas patch path reconstruction

Gas patch path reconstruction methods of source localisation estimate the position of a source iteratively by linking positive sensor detections of hazardous material, or odour, and wind measurements. The wind and gas/odour data are used to define an observation window, where the detected material could have came from. This is first proposed and implemented on a ground robot, and tested in outdoor open conditions in [20]. In the experiments, the method was compared with a Bayesian based method from [48] which is described in the next subsection. Both source localisation algorithms are compared using a robot path generated from a surge and cast algorithm [49]. The method used binary measurements from a MOX gas sensor to take into account its slow response, where the measurements represent detections or non detections of concentration. The gas patch path reconstruction is implemented probabilistically using a particle filter. The method takes into account time varying wind, however, it assumes that the mean airflow is approximately uniform.

The gas patch path reconstruction method was extended in [32] to account for non uniform airflow and using a UAV rather than a ground vehicle. Multiple path planning methods during the localisation simulations and experiments including a surge-cast, zigzag and pseudo gradient based algorithms. The pseudo gradient based algorithm used measurements taken at different positions and knowledge of the wind direction. It outperformed the other path planning methods with regards to success rate of localisations and localisation accuracy in both simulations and experiments. The method extended that of [20] by using the uncertainty in the wind direction to create a patch path envelope (PPE), which describes the envelope of an area the gas patch has passed with high probability.

The paper [32] presents the first results of gas source localisation performed using a UAV and remains to be the state of the art, with regards to experimentally verified methods, in the literature on source localisation. The experimental results were impressive, however, there were still some limitations at this stage: the search area was quite narrow and two dimensional, a fan at the source was used to create a nice flow to help spread the gas, the UAVs altitude was held manually, it was initiated from within the gas plume, and finally, the emission rate of the source was not estimated. The work has provided valuable insights onto which this thesis will aim to build upon.

2.2.3 Bayesian inference based methods

Bayesian methods introduced probabilistic robotics to the source localisation problem [33, 48]. In [48], Pang and Farrell modelled the plume using stochastic methods based on Bayesian reasoning. A hidden Markov model (HMM) was used to implement the stochastic approach for plume modelling and predicting the most likely location of a source. The approach was tested in simulations and with experimental data. The global wind field was used to integrate upwind and predict the path of the contaminant. In [10], Vergasolla et al. proposed a search strategy based on information theoretic principles, referred to as Infotaxis. A measurement strategy was adopted, which measured the rate of particle encounters rather than a concentration reading. In a lattice environment, the searcher would determine the move that maximised the expected information gain in the form of entropy reduction or increase in particle encounters. The expectations were based on the information currently available, which was the posterior field. The method capitalised on the fact that the closer to the source, the higher the rate of information acquisition (particle encounters), hence tracking the rate of information acquisition would guide the searcher to the source similarly to the concentration gradients in chemotaxis. The method could handle situations of sporadic and intermittent concentration information where the chemotaxis algorithms would struggle. The infotaxis search attempts to find a balance between exploring to gain more information and exploiting the information currently available. This method was shown to successfully find the source where the data was intermittent and sporadic. Following [10], several researchers have studied the efficacy of infotaxis and proposed modifications and extensions [50, 51, 52, 53, 54]. Experimental studies of such an approach have so far been limited to indoor areas with artificially generated wind [53].

A critical extension of the Bayesian inference based approach was its implementation in the sequential Monte Carlo framework, using a particle filter, alleviating its grid based implementation and allowing the source strength to be included as a parameter to be estimated [55]. This was essentially now estimating the source term of the release, therefore, further description of this work is left for Section 2.6: source term estimation using mobile sensors.

The Bayesian based inference methods benefit from their ability to handle uncertainties using probabilistic methods. They also allow themselves for natural extensions to consider obstacles in the environment, to search cooperatively with a team of robots, and to incorporate other source parameters into the Bayesian estimation algorithms. The limitations of the methods so far are a lack of experimental validation outdoors, and the assumption of constant uniform wind.

2.2.4 Statistical methods

An alternative approach to source localisation does not attempt to direct a robot, or searcher, to the source of the emission. Rather, this technique capitalises on an interesting observation on sensing characteristics in plumes; where variance and fluctuations in gas concentration tend to be greater nearer the source [56]. This feature has been used to simultaneously estimate the source position whilst mapping the gas distribution. Methods proposed include the kernel DM+V algorithm, which uses in-situ point measurements to map the concentration mean and variance [18, 56], and a gas tomography algorithm which uses integral measurements from a tunable diode laser absorption spectroscopy (TDLAS) sensor to map the mean and fluctuations in concentration [17]. The results of experimental trials conducted in different indoor and outdoor environments verified the approach using data collected during sweep patterns performed using aerial and ground based robots and various sources [56]. The main limitation of these methods is the requirement to collect measurements at a large number of locations in order to produce a map of the hazardous area. The approach shall be described in more detail in the mapping section of the literature review (Section 2.4).

2.2.5 Summary

Source localisation algorithms have featured many techniques that have been dependant on the quality of information available to the robot. Gradient climbing methods such as chemotaxis perform well in concentration fields with well defined gradients; however, in turbulent flows or with a noisy sensor, the gradient does not always lead directly to the source. Several biologically inspired algorithms have been proposed using a combination of chemotaxis and anemotaxis to capitalise on available wind information. The methods based upon probability and statistics (i.e. the Bayesian based methods using the gas patch path prediction or model based inference, and the statistical mapping methods) yield a benefit due to their probabilistic aspect, where models can be used and uncertainties in measurements and environments can be accounted for. Thus, the methods have been demonstrated in realistic indoor and outdoor stochastic environments. Another benefit is the ability to extend the methods to handle obstacles in the environment, indoor and outdoor scenarios, and to cooperate a team or swarm of robots.

The main concern of source localisation methods in the literature is in the experimental

evaluation of the proposed approaches. Atmospheric dispersion, and measurement/sampling of dispersing material, is a complex phenomena which is challenging to reproduce with models and in simulations. Therefore, experimental evaluation of the methods is important. However, this brings in other challenges with regards to the reproduce-ability of the experiments, fair comparisons of methods that require different inputs, the amount of different scenarios to consider, the time consuming set-up of the experiments and gas sensitive robots, and finally, the criteria that is used for comparing methods. Besides experimental evaluation, the methods so far still face challenges with regards to changing wind conditions, searching in 3 dimensions, and searching in environments with obstacles.

2.3 Boundary tracking

Boundary tracking algorithms aim to determine the edge of a region, or where the value of a scalar crosses a threshold. Researchers have explored boundary tracking algorithms to monitor oil spills, algae growth, volcanic ash clouds, contaminant gases, nuclear radiation levels, and generalised scaler fields. In the literature, boundary tracking methods have been proposed using purely control algorithms, and algorithms incorporating estimation and control. Most methods use point measurements of the concentration value or scalar field intensity provided by sensors on-board mobile robots. The point measurements can be used directly or as a binary signal to determine whether or not the sensor is inside or out of the affected/contaminated region. Alternatively, researchers have proposed to estimate of the gradient or Hessian of the contaminant obtained either through spatially separated simultaneous measurements by multiple sensors or via consecutive measurements from a single sensor. The majority of researchers have assumed slow moving, clearly defined, 2-D boundaries and accurate sensors. Some have attempted to extend the state of the art, researching the effect of sensor noise and studying 3-D boundaries [57]. The remainder of this section provides a brief description of the boundary tracking algorithms found in the literature.

2.3.1 Control law based methods

2.3.1.1 Bang-bang control

Bang-bang control is a simple algorithm which involves switching abruptly between two states. In the case of tracking a boundary, the turning direction of the vehicle is changed upon crossing the contour boundary. Several papers in the literature have researched the use of bang-bang control for tracking an environmental boundary. Kemp et al. [58] implemented a bang-bang control algorithm that required only a concentration sensor to monitor an underwater perimeter using unmanned underwater vehicles (UUVs). Some drawbacks of the method include: i) with a large crossing angle, the tracking can become very inefficient; ii) noise can cause the UUV to turn the wrong way and fail to track the

boundary; and iii) narrow bottle necks in the boundary may cause sections to be missed. A turning angle correction was proposed by Bertozzi et al. [59] to improve efficiency and a cumulative sum algorithm was implemented to provide robustness to noise. In [60], this method was extended to multiple vehicles. In [61], the authors used random coverage, collision avoidance and a bang-bang angular velocity controllers to detect and surround an oil spill. In [62], a bang-bang controller was used to follow contours of a radiation field with an autonomous helicopter. The applicability of these sensor movement strategies has only been evaluated for static phenomena, or the authors assumed that the movement of the sensing vehicles was much faster than that of the observed phenomenon. In [63] however, Brink adapts the method in [59] to track the boundary of a dynamic plume in an environment where a low-density static sensor network was installed.

2.3.1.2 Sliding mode control

When applied to boundary tracking, sliding mode control [64] is similar to bang-bang control as both methods change the turning direction of the vehicle based on its position relative to the contour. Sliding mode control can produce more efficient tracking as the vehicle turns before exiting/entering the contour. The sliding variable was defined as the difference between the desired/threshold density and the measured density of the contaminant. In [64], a sliding mode control law was used to steer a vehicle to a location where the distribution assumed a pre-specified value and afterwards ensured circulation of the vehicle along this set at the prescribed speed. In simulation, the algorithm tracked a boundary with noise added to the concentration data. In [65], this method was extended to multiple vehicles where a guidance law that altered the longitudinal speed was used to ensure effective distribution of the team. In [66], a real world experiment was performed to justify the navigation and guidance algorithms. The experiments showed some robustness to common sources of uncertainties in robotic applications. The effect of chattering which is common in sliding mode based approaches was not observed in the experiments. In [67] a sliding mode control algorithm was proposed and demonstrated on a realistic example pertaining to synthetic volcanic eruption dispersion data generated by the NAME ATD model [68].

2.3.1.3 Formation control

Based on estimated concentration gradient, Hessian matrix, and curvature of the environmental contour line, Zhang and Leonard [69] used a formation of Newtonian particles to track level sets of a field at unitary speed. The desired formation was maintained by a formation shape control law based on Jacobi transform. The Jacobi transform decoupled the dynamics of the formation centre from the dynamics of the formation shape, which allowed separate control laws to be developed. Following a differential geometric approach, steering control laws were developed separately that controlled the formation centre to

detect and move to a desired level surface and track a curve on the surface with known curvatures. In [70, 71], the estimates from the cooperative filter were used in a provably convergent motion control law that drove the centre of the formation along level curves of an environmental field. The method was later extended [71] to track a 3-D surface.

2.3.2 Estimation and control

2.3.2.1 Approximation of boundaries

In [72], White et al. presented a method of approximating a cloud boundary using a 2-D splinegon defined by a set of vertices linked by segments of constant curvature. The method was inspired by the fact that it is beneficial to be able to express the predicted dispersion of a contaminant cloud in a compact form so that it can be shared among a UAV group with minimal communication overhead and maximum utility in guidance algorithms. The research in [72] is one of very few methods that estimate the dispersion of the cloud in a low computational manner. The splinegon algorithm was tested against contours produced using the second order closure untegrated puff (SCIPUFF) dispersion model and showed a good representation; however, there was some error in predicting the future dispersion of the cloud. The dispersion estimation used a simple linear equation and could be a potential area for improvement using improved estimation techniques. Subchan et al. [73] presented a path planning algorithm comprised of Dubins paths and straight lines to guide UAVs to approximate a boundary. Equipped with a relevant sensor, the UAVs recorded the entry and exit points of the cloud. These points were used as vertex data in construction of a splinegon [72] that represented the contaminant cloud. In [74, 75], Sinha et al. proposed two methods for coordinating a group of UAVs to gather the vertex data. In [75], the paths of the UAVs were designed progressively, after every transition through the cloud.

2.3.2.2 Model predictive control

In [76], Zhang and Pei used model predictive control (MPC) to track the boundary of an oil spill using a single UAV. Universal Kriging was used to predict the future state of the system for use in the MPC. The advantage of the Kriging method was that it is an optimal interpolator in the sense that the estimates were unbiased and the minimum variance was known, so that it could relatively accurately construct the environment map. In addition, the advantage of the MPC was its constraint handling capacity. Nonlinear MPC was used to estimate the future states at sampling instants and determine the optimal manoeuvre based on minimising a cost function with control constraints. The cost function was derived from the difference between measured concentration and the desired threshold with a penalty weight added to constrain the angular rate of the vehicle. The method was tested on simulated data based on the advection-diffusion equation which demonstrated

the proposed method was feasible and effective; however, this was in the absence of sensor noise and the contaminant boundary was relatively well defined and bounded.

Euler et al. [77] proposed an adaptive sampling strategy to track multiple concentration levels of an atmospheric plume by a team of UAVs. The approach combined uncertainty and correlation-based concentration estimates to generate sampling points based on already gathered data. The adaptive generation of sampling locations was coupled to a distributed MPC for planning optimal vehicle trajectories under collision and communication constraints. The domain area was represented as a grid of discrete cells. Each cell stored a Gaussian distribution defined by the expected concentration value and variance. A correlation among adjacent measurements was assumed and used to infer information about the concentration at locations surrounding the sampling point. New sampling points were selected based on the maximum variance of reachable positions. Numerical simulation results demonstrated the ability of the method to track a boundary with noise added to the data. The major limitation was in the amount of time taken to generate an estimate of the perimeter, caused by sampling times used to handle noise.

2.3.2.3 Support vector learning

Kim et al. [78] used mobile sensors to estimate the boundary of physical events such as oil spills. The boundary estimation problem was set in the form of a classification problem of the region in which the physical events occur. Support vector domain description (SVDD) was employed, which was able to represent boundaries in a mathematical form regardless of the shape. Furthermore, by using the hyper-dimensional radius function obtained from SVDD, a velocity vector field was generated which gave asymptotic convergence to the boundary with circulation at the desired speed. The desired speed was adjusted to coordinate the mobile sensor so that their intra-vehicular spaces were maximised for efficient estimation of the boundary and fast reaction when the boundary changes. The method was tested in both simulations and experiments though the boundary was clearly defined and bounded with no account for sensor noise. It was noted by the authors [78] that future work would focus on time-varying boundaries and other methods such as the MPC.

2.3.2.4 Optimisation

In [79], Srinivasan and Ramamritham estimated the contour of a specified concentration in a bounded region with mobile sensors. The spatial domain was modelled as a grid and the sensor was assumed to be able to measure the concentration at its current and neighbouring grid points. The contour was tracked by minimising a cost function based on the difference between the desired and measured concentration of pollutant. The ability to minimise the cost function and track the boundary was assessed for three optimisation algorithms: i) the greedy algorithm; ii) simulated annealing; and iii) a newly proposed collaborative algorithm based on minimising centroid distance. It was found that the collaborative

method estimated the contour with less error and latency. The method was capable of estimating complex shaped contours though it required a number of assumptions such as: a well-defined closed curve, an interior point known by the sensors, no sensor error, and that the sensor could determine concentrations at its neighbouring grid locations. In [80], Srinivasan et al. improved the method and named it ACE (adaptive contour estimation). The method estimated and exploited information regarding the gradients in the field to move towards the contour. In numerical simulations, ACE was shown to significantly reduce latency in contour estimation when compared to directly approaching the contour.

Glow-worm swarm optimisation (GSO) is an algorithm originally proposed in [81] primarily to detect multiple optima of a function and considered to be ideal for implementation in multi-robotics platforms. In [82], this method was applied to simultaneously detect multiple emission sources and map the boundary. Subsequently, the methodology was also extended to map 3-D boundaries [57]. The algorithm finds the source by following the gradient until it reaches a maximum; conversely, it finds the boundary by following the gradient in the negative direction until it reaches a threshold concentration. The method was successful in simulations [82] using 150 agents to map a boundary and detect three sources. Although the algorithm performed well, the use of such a large number of agents is not ideal. Other problems arise in becoming stuck in local minima or maxima if the assumption of the distribution of the field does not hold.

2.3.2.5 Neural networks

In [83], Sun et al. used a radial basis function Neural Network (NN) control method to address the problem of environmental contour line tracking using a non-holonomic mobile robot. A radial basis function NN was used to approximate a non-linear function containing the uncertain model terms and the elements of the Hessian matrix of the environmental concentration function. Then, the NN approximation was combined with robust control to construct a robust adaptive NN controller for the mobile robot to track the desired environment boundary. The method was tested using Lyapunov functions to show accurate tracking of a well-defined, bounded contour line in the absence of sensor noise.

2.3.2.6 Model based prediction and control

Li et al. developed a control strategy to track the front of an evolving dynamic plume in a marine environment modelled by the advection-diffusion equation [84]. Instead of using only concentration gradient measurements, the transport and dispersion model was incorporated into the control design. An observer was designed to estimate the dynamic movement of the plume front, and a feedback control law was constructed for a robot to track it. The method was extended to a multi-robot scenario where the control laws were designed to account for a robot team in a nearest neighbour communication topology. The

methods were tested in simulations without consideration of noise.

In [85], Fahad et al. tested the method presented above in a more realistic environmental model set-up. A probabilistic Lagrangian environmental model was used, which can capture both the time-averaged, idealised structure and the instantaneous, realistic structure of a dynamic plume. The simulation demonstrated how a single robot was capable of patrolling a plume front using the control law designed in [84] where the plume front was noisy and fairly realistic. It was found that the sensor measurement of the concentration and estimation of the gradient and divergence of the concentration were of vital importance to the success of the plume tracking. It was assumed that the sensors were area-level measurement sensors (such as ultraviolet, infra-red, visible band, radar or passive microwave sensors) rather than point detectors (such as chemical sensors). If the sampling radius was reduced to a very small value, the plume concentration had very high variance so that the controller struggled to produce accurate tracking results.

To extend the aforementioned approach and subsequently validate it in real experiments, a gradient and divergence estimation method is presented in [86]. The method enables concentration levels to be tracked using point measurements of concentration only. Field experiments using an unmanned surface vessel (USV) demonstrated the boundary tracking system, tracking a plume of dye in the ocean as it disperses. This is a significant achievement and a rare result in the literature, where a boundary tracking algorithm is tested in real conditions. However, it is worth noting that oceanic plumes are significantly more stable than in the atmosphere, making the boundary and measurements from the concentration sensor much more stable.

2.3.3 Summary

A range of methods have been proposed to track the boundary of environmental fields. The methods vary in their measurements of the field such as binary, concentration values (point measurements), gradients or curvature and also in the types of tracking algorithms used to trace the boundary. The effect of 3-D boundaries, sensor noise, and dynamics has been briefly explored with a large area available for potential improvements.

The main limitations of the boundary tracking methods, applied to atmospheric plumes, are the ability to handle noisy and intermittent measurements. This is expected to be the reason why there are currently no reports in the literature of atmospheric boundary tracking performed using a real dispersive source and sensor. Current work is limited to simulations with minimal noise. Additional problems that are yet to be tackled are how to handle the splitting up of contaminated regions or boundary tracking in environments with obstacles. The only reports of experimental results of boundary tracking are for underwater plumes, where there is significantly less noise and turbulence, creating a more clearly defined boundary.

2.4 Mapping

Mapping the spatial distribution of the concentration of a gas has important applications in environmental monitoring, air quality assessments, and in response to accidents or deliberate spills of hazardous chemicals [87]. A spatial approximation of the spread of the gas can provide valuable information for urban planning, about emissions, and to support emergency responders with important knowledge to help them act more effectively. Mapping of a gas cloud typically involves linking several spatial temporal observations from point-wise concentration detectors which can be spread on the ground or placed upon unmanned vehicles. One of the advantages of mapping the ability to provide a detailed map of the hazard distribution, not only the boundary, and without relying on a model. The approach can still be affected by noisy observations, turbulence, and intermittent readings from the sensors, however, these phenomena should be handled by a robust algorithm. A limitation of mapping is the need for many spatial temporal measurements, and how by time a map is produced, the spread of the material is likely to have changed. Intelligent path planning and cooperation among a swarm of sensing platforms could solve this issue.

Besides approximating the distribution of an atmospheric plume, mapping has several other unrelated applications, particularly in environmental monitoring, such as: determining the spread of bacteria/algae in a lake, mapping atmospheric or oceanic properties such as oxygen content or temperature distributions, mapping soil/plant properties for agriculture, mapping magnetic fields, approximating a map of wireless signal strength, or, a critical area of robotic navigation, Simultaneous Localisation and Mapping (SLAM). Due to the large amount of applications, mapping is a popular subject in the literature. Several of the proposed methods are problem agnostic, and work by simply introducing a new sensor for the specific task. In addition to the methods used to fuse measurements to form a map, another popular area is how to plan the path of an unmanned vehicle, or swarm, in order to produce an accurate map considering efficiency, accuracy, and the operational time/range of the systems. This section will consider both areas in turn.

Plume mapping methods in the literature range from simple interpolations methods to statistical, probabilistic and machine learning based techniques. The methods have been used in conjunction with multiple or single sensing robots, in indoor or outdoor environments, and considered the effect of varying plume properties over time on the mapping result. In this thesis the mapping methods are split among machine learning based methods, a statistical method called the kernel DM+V algorithm, and a Gaussian Markov random field based approach.

2.4.0.1 Machine learning

Machine learning based approaches to mapping are mostly comprised of Gaussian Process machine learning algorithm and extensions. The method has been used to map several spatial phenomena such as wireless signal strength, bacteria distributions, temperature distribution, and magnetic field strengths. In this section, only plume mapping applications are considered.

In [88], a Gaussian Process regression algorithm (referred to as Kriging in the paper) was used to map a chemical plume based on point measurements from multiple ground robots. Several path planning algorithms were compared for the robots to produce an approximation of the chemical distribution including a uniform sweeping search and optimisation based path planning algorithms: decentralized and asynchronous particle swarm optimisation (DAPSO), bacterial foraging optimisation (BFO), and ant colony optimisation (ACO). Experiments were performed in a small enclosed arena with an ethanol source and ground robots equipped with MOX senses. The DAPSO algorithm was found to achieve slightly better performance during the experiments, where performance was measured by the distance between the greatest concentration peak and the time taken. Not taking into account task completion time, the uniform sweep search achieved the smallest difference between peak concentration and the source. The paper did not consider the overall accuracy of the modelled chemical distribution.

Sparse Gaussian Process mixtures (GPM) was used to map a gas distribution in [89]. The use of GPMs enabled the prediction to better capture the concentration peak near the source and the "flatness" in areas without any contamination. The sparse aspect made the mapping more efficient by limiting the number of samples required to learn the gas distribution. The performance of the proposed sparse GPM method was compared to the original kernel DM+V algorithm (described in the next section) and the standard Gaussian process algorithm using experimental datasets in an indoor environment, an indoor corridor and an outdoor open area. The datasets consisted of two uniform sweeps of the test environments, where the first sweep would be used for learning and the second for a ground truth. This limits the validity of the results, as sensor data taken at different times in uncontrolled environments does not represent a proper ground truth (In an uncontrolled environment, such as natural conditions outdoors or indoors, the gas distribution changes over time predominantly due to small variations in the wind. Therefore, point measurements of the plume taken at different times should not be used to form learning data and ground truth data.). Regardless, the proposed method was shown to outperform the other approaches using this validation approach. More realistic and accurate methods of validating mapping algorithms using real experimental data are challenging and have not been found in the literature.

2.4.0.2 The kernel DM+V algorithm

The Kernel extrapolation distribution mapping (Kernel DM+V) algorithm has been under development for some time by several researches at Örebro University, Sweden. The approach maps a gas distributions mean and variance given a set of point measurements of concentration mean and variance [18]. The distribution modelling task is treated as a density estimation problem, where gas sensor measurements are interpreted as noisy samples from the desired distribution. The method was tested on a dataset in an environment with multiple rooms, a corridor and an open outdoor area.

Subsequently, the kernal DM+V algorithm was tested using measurements from a UAV in an outdoor environment [90], to the best of the authors knowlege, this is the first time a UAV has been used to produce a map of an airborne plume. However, there was not any analysis of the predicted map with regards to comparisons with a ground truth. The paper also presented a path planning strategy based on artificial potential fields, in addition to the uniform sweep paths to collect the measurement data.

The method was integrated with SLAM though a map merging technique in [91]. Real experiments were used to generate a map indoor overlaid on an occupancy map generated using a Lidar and hector SLAM. The accuracy of the mapping was assessed only by the distance between the concentration and variance peaks, and the source location. The method has also been extended to consider the wind information during the mapping [92], to generate 3D concentration maps [93], and to consider the effect of time on the mapping [94].

2.4.0.3 Gaussian Markov random field

In [95] the spatial distribution of a gas in an indoor environment was modelled as a Gaussian Markov random field (GMRF). This enabled the system to take into account the vanishing information of gas readings over time and the influence of objects in the environment by considering correlations among different areas, such as separate rooms with closed or open doors. In time variant simulations where a gas source was turned on and off the method was shown to outperform the Kernel DM+V algorithm from [18]. The method was also assessed in an indoor experiment with an ethanol source and a ground robot equipped with a PID sensor. However, the GMRF and Kernel DM+V methods were only compared empirically. The paper did not include a comparison with the time dependent extension of the Kernel DM+V algorithm [94].

2.4.1 Summary

The problem of plume mapping is a particularly challenging spatial mapping task, due to the intermittent and noisy measurements from the sensors, three dimensions of the problem, and the temporal changes caused by changing meteorology and turbulence. Additionally, due to the nature of the problem, mapping tasks will often be in cluttered, urban, or

indoor scenarios, adding an additional challenge - how to navigate autonomously in these environments and the effect on the mapping performance. Overall, the methods perform well in simulations and appear to perform well in uncontrolled experiments indoors or outdoors. In particular, Gaussian Process machine learning techniques, the kernel DM+V, and the GMRF methods produce a map of the hazard concentration and the uncertainty, which can provide additional information for an active mapping algorithm, which will plan the path of the unmanned vehicle on-line. Path planning algorithms have the ability to improve the efficiency of the mapping result, and to facilitate autonomous mapping in indoor or cluttered environments. They also could enable a mission to be tailored, for example, to bias information collection in areas of higher concentration.

Path planning for mapping tasks, not specific to atmospheric plumes, in the literature, range from simple sweeping paths, to methods based on coverage, artificial potential fields, multi-vehicle cooperation and informative path planning (IPP) approaches. There are several path planning methods that have been proposed for many mapping tasks but not yet applied to the problem of plume mapping - such as the informative path planing method, otherwise known as robotic information gathering (RIG), which has been applied to many other problems such as mapping the distribution of toxic bacteria in a lake, wireless signal strength over an area, or temperature in the ocean. Methods specifically applied to mapping dispersive plumes include the optimisation based approaches proposed in [88] where they were shown to have significant performance benefits over conventional planning approaches, providing motivation for further research in the area.

Finally, to the best of the authors knowledge, proper experimental evaluation of gas distribution or plume mapping algorithms is not available in the literature. The previous work was assessed in simulations, empirically, or by using sensor data taken at different times in uncontrolled environments, which does not represent a proper ground truth (In an uncontrolled environment, such as natural conditions outdoors or indoors, the gas distribution changes over time predominantly due to small variations in the wind and sampling times that are inadequate to capture the mean concentration. Therefore, the point measurements of the plume taken at different times cannot be used to form learning data and ground truth data.). Furthermore, the effect of measurement sampling times, which has a great effect on the noise and sporadicity, has not yet been considered. Sampling times in the literature were relatively high meaning a long time was taken to produce a map of the plume, typically at least one hour.

2.5 Source term estimation using static sensors

The goal of STE is to estimate the parameters that describe the source of a release: namely its location and strength. Such information is useful on its own, however, it can additionally be used to forecast the spread of the airborne HAZMAT using an ATD model. The forecast will provide an estimate of the HAZMAT distribution, similarly to boundary

tracking or plume mapping. However, the accuracy of the prediction is dependant on the accuracy of the source estimate and the dispersion model used. STE is the focus of this thesis, and therefore the literature review is more thorough in this area.

Traditionally, with regards to CBRN source term estimation (STE), a network of atmospheric concentration and meteorological sensors are used to estimate the source term as illustrated in Fig. 2.9. A benefit of this approach lies in early detection near places of strategic importance (e.g nuclear power-plant sites) where sensors can be pre deployed. However, for accidents or deliberate attacks in random places, it is infeasible to cover all regions of importance with sensors dense enough to determine the source before it has spread significantly. The determination of the source parameters from static sensor measurements is a problem in inverse modelling; the inverse problem is highly non-linear, ill-posed [96] and subject to input data that is typically sporadic, noisy and sparse [97]. The inverse problem has been tackled using two dominant approaches: i) optimisation methods and ii) probabilistic approaches based on Bayesian inference. Regardless of the approach, inferred source parameters are run in a forward ATD model to generate predicted concentrations that are compared with the observations in a cost or likelihood function. The overall goal of these methods is to find the best or most likely match between the predicted and observed data, as illustrated in Fig. 2.8.

The major difference between the optimisation and Bayesian approaches is in the probabilistic aspect of the Bayesian approach. The Bayesian approach allows inputs and models used in the algorithm to be specified via a probability density function (pdf), taking into account uncertainties in the input data and the chosen ATD model. With probabilistic inputs, the final output of the algorithm will be in the form of a pdf, thereby, producing an estimate of the source term with associated confidence levels. In contrast, the optimisation approach takes inputs without uncertainty and attempts to find a single optimal solution to the problem. Both methods have been shown to perform well in simulations; however, it was discovered that there is a significant room for improvement for both when tested on experimental data [98]. Aside from the main estimation algorithm used, the STE algorithms developed have several other differences making a direct comparison difficult. Some of the differences include:

- The source term parameters that are estimated
- Likelihood/Cost function used to measure the goodness of fit
- Type of release (continuous, non-continuous, instantaneous, point source or area source)
- The forward atmospheric dispersion model used (simple, complex, puff based, CFD etc.)
- Domain size

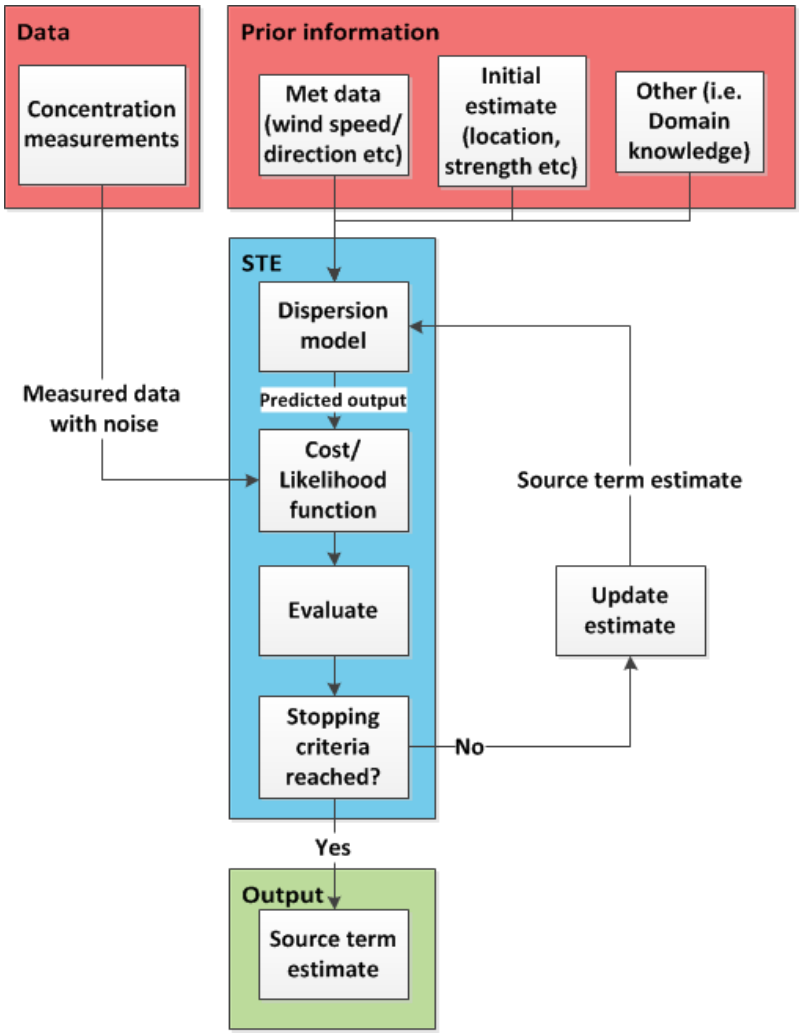

Figure 2.8: Flow diagram of a generic STE algorithm.

- Prior information assumed about the source

The source term parameters that are estimated can be extended to take into account uncertainties in any of the meteorological or dispersion variables, which may be dependent on the chosen ATD model. Note that this review has been limited to models that estimate at least the source strength and location. Under such scenarios it is common to assume a constant release rate. The literature is rich with estimation methods for releases of known origin and varying release rate such as the Fukushima accident. For this scenario, Kalman filters and variational data assimilation approaches have been more popular [4].

Source estimation of multiple releases is a particularly complex problem which has been tackled in more recent research. Several forms of likelihood and cost functions have been used throughout the literature which will be discussed in the following sections. The type of release has varied from: i) a steady state plume, ii) a dynamic plume and iii) an instantaneous release or puff. Most research has focused on continuous steady state plumes using the Gaussian plume equation. Dynamic plumes and instantaneous releases yield a more demanding problem which is more applicable to emergency response situations.

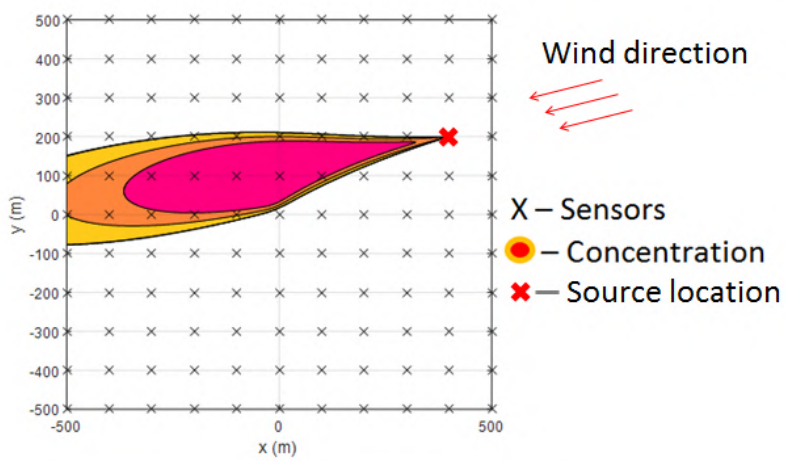

Figure 2.9: Example diagram of a static sensor network.

The domain size can range from small scale (<km) to continental scale; however, with a relevant dispersion model, the majority of techniques can be applied to any domain size [99]. Several forms of prior information have been used throughout the literature including meteorological variables, the geometry of the network and parameter bounds such as the time of release, release rate and domain size.

This section of the thesis is split among the optimisation and Bayesian based source estimation methods incorporating static sensors.

2.5.1 Optimisation

The optimisation approach to STE aims to find the combination of parameters that minimises a cost/objective function J. The objective function has taken many forms, although most often it is derived from the sum of the squared differences between predicted C_k and observed concentrations z_k. Where C_k are obtained from an ATD model run using the inferred source term and z_k are concentration data from deployed sensors. It is assumed that the parameter combination that produces the minimal difference is the optimal estimate of the source term. Most optimisation techniques employ an iterative process, where the objective function is minimised by using different update rules to provide new improved estimates of the parameters.

The main focus of research on the optimisation approach has been on assessing the performance of existing algorithms in optimising a cost function, however the different methods have also explored various cost functions and the use of better initial estimates. A variety of methods have been used to optimise the objective function such as gradient-based methods [100, 101], direct search methods (e.g. the pattern search method [102]), and intelligent optimisation methods (e.g. simulated annealing [103] and the genetic algorithm [104, 105, 106]). Details about the specific optimisation approaches are described in this section.

2.5.1.1 Gradient based

This sub-section describes gradient-based STE algorithms found in the literature. The methods used are the extension of the least squares technique known as Re-normalisation or regularised least squares.

2.5.1.1.1 Least squares The aim of least squares estimation is to minimise the sum of the squares of the residuals between measured z_k and predicted C_k concentrations for the total number of measurements N. The cost function can be written as:

$$J = \sum_{k=1}^{N} (C_k - z_k)^2 . \tag{2.1}$$

The least-squares method is applicable only for an over-determined inverse problem. The iterative minimisation of the cost function Eq. (2.1) requires an initial guess of source term [107]. Since the least squares optimisation method is not a global optimisation technique, it is largely dependent on a good initial guess, otherwise it may get stuck in a local minimum leading to a poor solution due to the non-linearity of the solution space.

2.5.1.1.2 Re-normalisation Re-normalisation or regularised least squares is a strategy for linear assimilation of concentration measurements to identify the unknown releases [108, 109]. The method exploits the natural statistics provided by the geometry of the monitoring network. These statistics are expressed in the form of a weight function derived by a minimum entropy criterion, which prevents the over-estimation of the available information that would lead to the artefacts especially close to the detectors. These weight functions serve as a priori information about the release apparent to the monitoring network and provide regularisation, thus limiting the search space of the algorithm and providing an initial guess. The weight functions could be computed iteratively using an algorithm proposed by Issartel [109]; besides, a minimum norm weighted solution provides an estimate for the distributed emissions and is seen as a generalised inverse solution to the under-determined class of linear inverse problems [110]. Overall, the re-normalisation approach utilises the adjoint source-receptor relationship and constructs a source estimate among a vector space of acceptable sources, which describes the possible distribution of the emission sources [111]. The method is applicable for both over-determined and under-determined problems.

Sharan et al. [101] used regularised least squares to determine the source term of a point release using the fact that the maximum of the source estimate will coincide with the location of the release. An advection-diffusion based dispersion model [112] was used to generate an adjoint model of the source-receptor relationship. Unlike many other STE methods, the domain was discretised into a grid, where the size was dependant on the density of the sensor network. The method was extended in [113] for identification of an elevated release with an inversion error estimate. The algorithm was further extended

to identify multiple-point releases [114] where the number of releases was known. Two steps were applied to reduce the computational time of the algorithm. First, regions associated with weak weight functions were removed. Then, only one in five grid points in each direction were considered, and this was iteratively refined to obtain an estimate of the source. In [100], Singh and Rani applied the algorithm to data from the FFT07 experiment [115]. A sensitivity analysis was performed to determine the effect of the number of measurements on the inversion results. It was found that on average nine measurements were required to sufficiently identify the source parameters and the accuracy of estimation was subject to the locations of sensors downwind and crosswind of the release. In [116], Singh and Rani applied the framework to multiple source scenarios of the FFT07 dataset. Recently, Kumar et al. [117, 118] have extended the regularised least squares inversion approach to urban environments, where CFD has replaced the underlying ATD model [119]. The method is tested on experimental data from the Mock Urban Setting Test (MUST) field experiment under various stability conditions. Reasonable accuracy was demonstrated in an experimental setting, with an idealized urban geometry.

2.5.1.1.3 Broyden-Fletcher-Goldfarb-Shanno algorithm (BFGS) The BFGS algorithm [120] is one of the most popular quasi-Newton optimisation techniques. The method is used to rapidly search for extrema of a function. It is similar to Newtons method however the inverse of the Hessian is approximated directly, greatly reducing computational requirements. On its own, the algorithm would struggle to determine the source term since it can become stuck in local minima. To overcome this issue, the Inverse ATD models have been used to generate a suitable initial guess.

In [121], Bieringer et al. used the BFGS algorithm to refine an initial guess of source parameters obtained from an inverse SCIPUFF run. To reduce computation, the simple Gaussian plume equation was used in the iterative optimisation. This equation was enhanced by using dispersion coefficients generated from the SCIPUFF run. The paper attempted to produce a final estimate where the final SCIPUFF and Gaussian plume runs matched as closely as possible with each other and the sensor readings. The algorithm was tested on experimental data from the FFT07 experiment to show similar performance to previous SCIPUFF based methods however with reduced computational complexity. The method was created to be computationally efficient for emergency scenarios where a timely solution would be critical. It was tested more rigorously than previous algorithms under scenarios including: different numbers of sensors, inconsistencies in observations and large distances between sensors and source. The performance was degraded in cases where the measured gradients in the concentration field were reduced (such as longer source to sensor distances, fewer sensors, larger sensor spacing etc.). The need for proper concentration gradients highlights the importance of having null sensor measurements that effectively characterise the spatial extent of the plume.

2.5.1.2 Meta-heuristics

Meta-heuristic optimisation algorithms have been among the most popular of the STE algorithms in the literature. They benefit from their global search performance in order to prevent the estimate from becoming stuck in a local minimum. The algorithms reviewed in this section include the pattern search method (PSM), simulated annealing (SA) and the genetic algorithm (GA). The algorithms use different methods to iterate until convergence to a solution based on evaluation of a cost function. The methods differ by the means in which they alter the parameters to find improved solutions.

2.5.1.2.1 Pattern search method The pattern search method (PSM) is one of the basic optimisation methods, consisting of two simple steps. The first step defines the theoretical parameters (source strength Q and location x, y) and their initial values. In the second step, the algorithm varies each parameter by increasing or decreasing their values from the current point applying a constant factor, known as the axis direction move. The cost function is then calculated for the new set of parameter values (the difference between calculated and measured concentration). If there is no increase or decrease of the cost function value compared with the values of the previous points, the step size is halved (the pattern move) and the process is repeated until the termination criteria are reached [122].

In [102], Zheng and Chen developed a PSM to determine the strength and locations of a contaminant source. The method was shown to be more efficient than other intelligent optimisation methods such as the GA, however it was limited as the PSM is a local optimisation method, meaning that it was highly dependent on its initial value. To overcome this limitation, Zheng and Chen [123] developed a hybrid algorithm that incorporated the global search performance of the GA with local search performance of the PSM. The GA algorithm was used to produce a reasonable initial value for use in the PSM. The algorithm was able to define the location and strength of a contaminant source with great accuracy. The algorithms performance was compared with that of an original GA to find an increase in accuracy and efficiency.

2.5.1.2.2 Simulated annealing The simulated annealing (SA) algorithm is a global optimisation algorithm that was introduced by Kirkpatrick et al. [124]. It is based on an analogy of thermodynamics, specifically the process of heating and controlled cooling of a material to reduce defects. This process directly depends on thermodynamic energy E. Once applying this thermodynamic analogy to the optimisation problem, the goal is to bring the system from its initial state to a convergent state in which the system uses minimum possible energy. The rule for accepting change in state is based on the Boltzmann

probability distribution [103], given as:

$$R \sim u\,(0,1) < \exp\left(-\frac{E_n - E_{n-1}}{T_n}\right) \tag{2.2}$$

where R is a random number from the uniform distribution u between zero and one, E_n is the energy of the system (similar to a cost function) and T_n is the temperature or cooling parameter. This enables the algorithm to occasionally accept parameter sets that increase E_n, thus achieving global search performance as it is able to escape from local minima. The algorithm repeats, generating new parameter estimates randomly, until it converges to a solution. Throughout the simulation, T_n is decreased to improve the convergence behaviour of the system.

Thomson et al. [103] applied SA to locate a gas source from measurements of concentration and wind data. The search algorithm was employed to find the source location and emission rate. SA was found to be advantageous as it helps prevent the search algorithm from converging to local minima that might surround the targeted global minimum. Three cost functions with different regularisation terms were evaluated, and the cost function that minimises the total source emissions was found to be the most robust, producing successful event reconstructions.

2.5.1.2.3 Genetic algorithm The genetic algorithm (GA) is a popular global optimisation technique used in numerous STE algorithms. It is classified as one of the artificial intelligent optimisation methods. Similarly to most optimisation techniques, the GA is based on iterations, but the major difference of the algorithm is in the alteration of parameter estimates to generate new solution candidates. This is inspired by the process of natural evolution [125]. The process of the GA can be summarised by the following steps:

1. Initialisation: A random population of candidate solutions called chromosomes are generated.

2. Selection: A cost function is evaluated to measure the quality (fitness) of the solutions.

3. Mating: High quality solutions are mated with each other to generate new parameter estimates while creating a second generation population of solutions. The second generation contains a higher quality of chromosomes than the earlier generation.

4. Mutation: As is the process in evolution, a selection of chromosomes are mutated in order to generate more new solutions.

5. Convergence or termination check is performed.

6. Repeat 2)∼5)

Several variations of the GA exist: incorporating different mutation, mating and population generation strategies. It is important to tune parameters such as population size and mutation rate to optimise the performance of the algorithm with regards to efficiency, accuracy and avoidance of local minima. In [126], Haupt et al. first demonstrated the ability of the GA to link readings from receptor data with the Gaussian plume ATD model. Later in [104], Allen et al. used this method to characterise a pollutant source by estimating its two dimensional location, strength and the surface wind direction. Including the surface wind direction as a parameter to be optimised in the GA could account for the sparse resolution of meteorological wind field data and any error therein [104]. The algorithm performed very well during twin experiments (where the Gaussian plume was used to create synthetic data), and performance was decreased with sensor grids with less than 8x8 receptors. It is worthwhile noting that the algorithm showed reasonable performance under sensor noise provided that the noise was less than the signal [104]. To further refine the final estimate of the source term, a hybrid GA was formulated in [105]. A traditional gradient descent algorithm (the Nelder-Meade Downhill Simplex (NMDS)) was run after the GA. The GA produced a suitable initial estimate to prevent the NMDS from becoming stuck in a non global minima. The hybrid algorithm was benefited from the speed and performance of NMDS in a local search with the global search performance of the GA.

To improve the performance of the algorithm in more realistic scenarios, Allen et al. [106] replaced the simple Gaussian plume model with SCIPUFF. The sensitivity of the GA in STE was assessed in [127]. The paper investigated the number of sensors necessary to identify source location, height, strength, surface wind direction, surface wind speed, and time of release. It was found that the number of sensors required varied depending on the signal to noise ratio.

In [128] Annunzio et al. combined the GA with the adjoint method in an Entity and Field framework (where entities are Gaussian plumes) for an improved estimate of the source term. The approach estimates the axis of the plume/puff while providing an estimate of the wind direction and the spread of the contaminant. The source was located using a GA with a cost function based on contaminant spread.

To estimate the source terms in a scenario of multiple releases, Annunzio et al. [129] extend the Entity and Field framework approach to use multiple entities. The number of entities was increased to improve the concentration field approximation. When increasing the number of entities did not yield an improved field approximation, the number of sources was found. As there were too many correlated unknowns (i.e. entity mass m, release time t and wind speed u), the source strength was not estimated. Instead, a scaling variable was determined during the optimisation process $m/u\Delta t$. Based on a comparison by Platt and Deriggi [98] using the FFT07 experimental data, the algorithm obtained a better source location estimate than several other optimisation and Bayesian-based approaches.

2.5.1.3 Summary on optimisation

Optimisation methods provide a single point estimate of source parameters by minimising discrepancies between predicted and measured concentrations. The gradient climbing methods are limited as without a suitable initial guess they can become stuck in an incorrect local minima. However, with a reasonable initial estimate, for instance by using the adjoint, or a backwards run, the algorithm can converge to a solution quite rapidly. Intelligent global search algorithms such as the GA, SA and the PSM have been classified as Meta-heuristics in this thesis. The methods benefit over gradient descent methods as they can handle poor initial estimates as they employ methods to prevent becoming stuck in local minima.

Many modifications of the original algorithms have been presented, in which some interesting features include:

- The wind direction in the parameter space to account for sparse meteorological data [104].
- Hybrid algorithms to gain the benefits of global and local search [105].
- Prior information to limit the search space of the algorithms [109].
- The combination of global search algorithms or a backwards dispersion model run to generate a good initial guess to be refined by a local search algorithm [128].
- Complex ATD models to improve the simple Gaussian plume equation resulting in improved accuracy without increasing too much computational load [121].
- Null sensor readings to narrow down where the source *is not* present [121].

In twin experiments, the majority of optimisation methods perform well [130]. When tested upon experimental data, the accuracy of the solution is heavily reliant upon the ATD model and knowledge of the atmospheric conditions/stability. Several more complex ATD models exist that may overcome this issue. Unfortunately, for an accurate simulation, a vast amount of meteorological parameters were also required. Furthermore, the benefit of a more accurate dispersion model may be outweighed by the increase in the computational time.

2.5.2 Bayesian inference

Bayesian-based methods of STE allow probabilistic considerations to be introduced to the problem in order to account for uncertainties in input data. Another way of exploiting the Bayesian approach consists in seeking not just for one optimal solution, but obtaining the probability density function (pdf) of the estimated source parameters. In this case, the source is defined by a set of parameters, which are the quantities of interest. By means of stochastic sampling, the posterior probability distribution of these parameters is evaluated

to fully describe the parameters of the source and the uncertainty on them. The goal of STE is then to look for the most probable parameters for the source in terms of posterior probability.

Bayes theorem estimates the probability of a hypothesis or inference being true, given a new piece of evidence as given [131]:

$$Posterior \propto \frac{Prior \times Likelihood}{Evidence} \rightarrow p(\Theta|z, M, I) \propto \frac{p(\Theta|I) \times p(z|\Theta, M, I)}{p(z|M, I)} \tag{2.3}$$

where the theorem estimates the probability of a hypothesis Θ being true, given the data (measurements) D, model M and prior information I. The prior distribution $p(\Theta|I)$ expresses the state of knowledge about Θ prior to the arrival of data z. The likelihood function $p(z|\Theta, M, I)$ describes the probability of the data z, assuming the hypothesis Θ is true. This is also known as the sampling distribution when considered as a function of the data. The posterior distribution $p(\Theta|z, M, I)$ is the full solution to the inference problem and, converse to the likelihood, expresses the probability of Θ given z. The final goal is to conduct inference over the parameters which define Θ, and the posterior expresses the complete state of knowledge of these parameters given all of the available data. Once completed, post processing is often required in order to extract useful summary information from the posterior.

The evidence (sometimes known as the marginal likelihood) $p(z|M, I)$ is so-named because it measures the support for the hypothesis of interest. For inference problems where only a single hypothesis has been or will ever be considered, the evidence is an unimportant constant of proportionality. When applied to STE, the hypothesis Θ is an inferred set of parameters that describe the source term, the data z are the measured concentrations from the sensors, the model M is an ATD model, and the prior information I can be any information related to the problem. In early work where only a single source is considered, the evidence term is neglected so Eq. (2.3) may be simplified to:

$$Posterior \propto Prior \times Likelihood \rightarrow p(\Theta|z, M, I) \propto p(\Theta|I) \times p(z|\Theta, M, I). \tag{2.4}$$

The likelihood function is used to quantify the probability of discrepancy between the measured and predicted concentrations at each sensor. Predictions are made by inputting the inferred parameters into an ATD model. The prior probability is used to encompass any information about the source parameters known prior to any detection. It is often assumed little prior information is known beforehand and therefore this is often initially given a uniform distribution. The posterior probability of the parameters is then proportional to the likelihood. When the inference is performed in a sequential process, the prior is set as the posterior of the previous iteration.

Monte Carlo (MC) sampling methods are employed to determine an accurate estimate

of the posterior pdf for the source parameters Θ. Parameter estimates and uncertainty can be determined from the statistics of the posterior, commonly the mean and the standard deviations. In a high dimensional space, where there are many parameters inferred, the computational effort increases exponentially. For this reason, efficient sampling techniques are used such as the popular Markov Chain Monte Carlo (MCMC) and Sequential Monte Carlo (SMC). The sequential aspect of SMC enables it to update the data as it arrives making it more applicable to dynamic plumes. In the following sections, different improvements and modifications of the Bayesian approach to STE conducted in the literature are discussed. Improvements have been made in terms of computational efficiency of the algorithms, accuracy, improvements to the likelihood function, extension of the methods to handle multiple-source release scenarios and urban environments and how the algorithm could be enhanced to gain robustness under sensor noise. The Bayesian-based methods explored in this section include: MCMC [132, 133, 134], SMC [132, 135, 136, 137], differential evolution Monte Carlo (DEMC) [138] and polynomial chaos quadrature (PCQ) [139] among others..

2.5.2.1 Markov Chain Monte Carlo (MCMC)

MCMC methods are used to efficiently sample from probability distributions by constructing a Markov Chain with the desired distribution equivalent to its equilibrium distribution [140]. With an initial random or informed starting point, a Markov chain is created where new inferences are drawn from the current link in the chain. The likelihood of the current inference is evaluated and based on acceptance criteria, it is either rejected or accepted as the next link in the Markov chain. Several techniques have been proposed to generate and accept new inferences. The most popular one is the Metropolis Hastings (MH) algorithm [141], described by the following steps.

Step 1 – Initialisation: Propose a starting estimate of the source parameters: Θ_1

For $i = 1 : N$

Step 2 – Proposal: Generate a new estimate $\bar{\Theta}$. Sample from the proposal distribution $q(\cdot)$:

$$\bar{\Theta} \sim q(\bar{\Theta}|\Theta_i)$$

Step 3 – Evaluate the MH acceptance probability:

$$\alpha = \frac{p(\bar{\Theta}|z, M, I)q(\Theta_i|\bar{\Theta})}{p(\Theta_i)|z, M, I)q(\bar{\Theta}|\Theta_i)}$$

Step 4 – Accept or reject new parameters into the markov chain:

$$\Theta_{i+1} = \begin{cases} \bar{\Theta} & \text{if } \alpha \geq u[0,1], \\ \Theta_i & otherwise, \end{cases}$$

where u represents the uniform distribution. The initialisation process involves selecting an initial guess of the source parameters. This should be based on prior information as the initial guess can have a significant impact on the convergence of the algorithm. The next proposal is generated by sampling from the end of the previous link in the Markov Chain. A random walk is the most popular technique, however in the literature more informed techniques have been proposed. During Step 3, the probability of the proposal being accepted is calculated based on the posterior distribution and proposal density of the prior estimate and of that proposed. In Step 4, this is compared with a random number to determine whether or not it is accepted as the next link in the Markov Chain [132].

The MCMC algorithms have been popular in STE due to the computational benefit over the more traditional Monte Carlo method. In [132], Johannesson et al. proposed a number of benefits and implementations of the MCMC algorithms for inverse problems including STE of ATD events. Several approaches to generating proposals were discussed including the Gibbs sampler, random walk and Langevin diffusion which was suggested to yield the most effective random walk. In [133] Borysiewicz et al. compared several MCMC algorithms for STE. Those compared include:

- Standard MCMC
- MCMC via maximal likelihood
- MCMC via rejuvenation and extension
- MCMC via rejuvenation, modification and extension

MCMC via rejuvenation, modification and extension was proposed to be the most effective during a number of synthetic tests which included an assessment of their efficiency when smaller amounts of measurements were available. In [142], Senocak et al. extended the MCMC algorithm for STE to incorporate null/zero sensor measurements. Another extension was an enhancement of the simple Gaussian plume model by incorporating the turbulent diffusion parameters into the parameter space, thus better matching of predicted and observed concentrations.

In [134], Keats et al. estimated the source strength and location of a contaminant plume in an urban environment with the MCMC MH algorithm. A key feature of the method was the adjoint based source-receptor relationship which greatly reduced the computational burden as the advection-diffusion equation was solved only once for each detector as opposed to solving for every combination of source parameters. The method was tested on experimental data from the Joint Urban 2003 atmospheric dispersion study, and the true parameters were shown to be located within one standard deviation of the estimate. In [143], Yee et al. successfully extended the aforementioned method [134] to estimate the parameters of multiple sources during synthetic simulations where the number of sources was known a priori. Here the MH procedure was applied with simulated tempering (ST) [144]. ST was used to alter the likelihood function in a way that the effects of the

measured concentration data were introduced gradually. This allowed the algorithm to explore the prior distribution for a number of different source parameter hypotheses, helping with the burn in phase of the MCMC algorithm by delaying sampling from the posterior. In [145], Yee used a reversible jump MCMC algorithm to detect multiple sources where the number of sources was unknown a priori. The reversible jump sampling algorithm which was first introduced by Green. [146] enables the Markov Chain to jump between model spaces of different dimensions. In this STE case, a different dimension referred to a different number of sources. The jump could either add a single new source or remove an existing source from the inferred parameters. The methods successfully estimated the number of sources when tested on synthetic data.

In [147], Yee improved the method by employing a simulated annealing scheme to move between the hypothesis space, increasing the mixing rate of the Markov Chains, which leads to faster convergence. Similarly to ST in [143], the algorithm alters the likelihood function over time to facilitate the burn-in phase of MCMC. The algorithm was tested on data from the FFT07 experiment, resulting in good performance of identifying the parameters of up to four sources along with their associated uncertainties. However, large parameter space by adding the number of sources into the estimation problem caused a slow computational speed. This issue was addressed in [148], where a model selection approach was proposed to determine the number of sources. The number of sources was determined by finding the minimum number of sources necessary to represent the concentration signal in the data. The accuracy of the method was similar to [147, 143] with the computational load significantly reduced.

In [149], Wade and Senocak. presented another method to determine the parameters of an unknown number of sources using the Bayesian MCMC algorithm. The method used a ranking system inspired by the environmental protection agencies (EPA) metric to determine the quality of ATD models. The method successfully determined the correct number of sources on experimental data from the FFT07 experiment. The major drawback of the method, however, was its need to run simulations for each number of sources.

It is worthwhile noting that most algorithms above performed well on synthetic data and on data from the FFT07 experiment. This experiment was conducted in an idealistic scenario, featuring a high number of sensors, releases in the vicinity of the sensor array and a rich amount of meteorological data available. A real world application was presented in [150] by Yee et al. Here, the location and emission rate of a source (from the Chalk River Laboratories medical isotope production facility) was estimated using a small number of activity concentration measurements of a noble gas (Xenon-133) obtained from three stations that form part of the International Monitoring System radionuclide network [150]. It was discovered that the key difficulty in the STE lay in the correct specification of the model errors. The initial algorithm obtained a reasonable estimate of the source parameters though the precision of the estimate was poor as the uncertainty bounds of the estimated source parameters did not include the actual values. An alterna-

tive measurement model was proposed, which incorporated scale factors of the predicted concentrations in order to compensate for the model errors [150].

2.5.2.2 Sequential Monte Carlo (SMC)

SMC is another technique used for efficient sampling. Unlike MCMC, the method is inherently parallel which allows all Monte Carlo proposals to be generated and evaluated simultaneously [151]. For this reason, it is considered to be computationally more efficient than MCMC provided the algorithm converges well. Another benefit is the sequential nature of SMC, allowing new data to run in the algorithm as it becomes available [151]. The approach approximates a posterior distribution $p(\Theta|z, M, I)$ by a set of weighted random samples $\{\Theta_k^{(i)}, w_k^{(i)}\}_{i=1}^N$. A popular SMC method uses importance sampling (IS). This involves taking a certain number of samples from the current estimate of the source parameters, weighting them and using these weights to form a new posterior distribution, which new samples are drawn from. The steps are outlined as follows:

Step 1 – Initialisation: Propose an initial importance sample:

$$\Theta_{k_0} = \{\Theta_{k_0}^{(i)}, w_{k_0}\}_{i=1}^N$$

For $k = k_0 : K$

Step 2 – Proposal: Generate a new estimate. Sample from the proposal distribution $q(\cdot)$:

For $i = 1 : N$, sample

$$\tilde{\Theta}_{1:k}^{(i)} \sim q_k(\tilde{\Theta}_{1:k}) = q_k(\tilde{\Theta}_k|\tilde{\Theta}_{1:k-1})q_k(\tilde{\Theta}_{1:k-1})$$

Step 3 – Update importance weights:

For $i = 1 : N$, evaluate importance weights

$$\tilde{w}_{1:k}^{(i)} \propto \frac{\pi_k(\tilde{\Theta}_{1:k}^{(i)})}{q_k(\tilde{\Theta}_{1:k}^{(i)})} \propto \frac{p(z_k|\tilde{\Theta}_k^i, M, I)p(\tilde{\Theta}_k|\tilde{\Theta}_{1:k-1})}{q_k(\tilde{\Theta}_k|\tilde{\Theta}_{1:k-1})} \frac{\pi_{k-1}(\tilde{\Theta}_{1:k-1}^{(i)})}{q_k(\tilde{\Theta}_{1:k-1}^{(i)})}$$

Step 4 – Normalise weightings:

$$\text{Let} \quad \Theta_{1:k}^{(i)} = \tilde{\Theta}_{1:k}^{(i)} \quad \text{and} \quad w_{1:k}^{(i)} = \frac{\tilde{w}_{1:k}^{(i)}}{\sum_{j=1}^N \tilde{w}_{1:k}^{(j)}}$$

Step 5 – Approximate the posterior distribution:

$$\pi(\Theta_k) \simeq \sum_{i=1}^N w_k^i \delta(\Theta_k - \Theta_k^i)$$

In [132], Johannesson et al. first proposed SMC for STE of an atmospheric release. The article provides an introduction to the SMC algorithm for Bayesian inference and some

sampling techniques including a hybrid MCMC-SMC algorithm. In [135], Gunatilaka et al. used SMC with a progressive correction (PC) technique to converge to a solution for STE. Some limitations of the Gaussian plume model were addressed. In particular, as the assumption of uniform wind speed and diffusivity caused the plume height and ground level concentration to be underestimated. The concentration read by the sensors was represented by the sum of the mean and fluctuating components where the mean was derived from an analytic solution of the turbulent diffusion equation and the fluctuating part modelled by a pdf. The performance of the algorithm was tested on synthetic data for a range of sensor grid densities. Reasonable performance was attained using grid densities as small as three by three.

In [136], Wawrzynczak et al. estimated the source strength, location, and ATD coefficients using SMC. Sequential importance re-sampling (SIR) was used which combines IS with a re-sampling procedure. Re-sampling was used to replace samples with low importance weights with those from a higher weighting. The algorithm was implemented first by running several iterations of multiple MCMC chains using MH and a random walk. After a number of iterations, the importance weights were found and the initial SMC sample was drawn. The paper compared the performance of the MCMC and SMC algorithms using synthetic data generated using SCIPUFF. It was found that SMC performed significantly better in obtaining the location estimate of the source. However, neither found the correct release rate. This was expected to be caused by differences among the Gaussian dispersion model and SCIPUFF. Additionally, no results were presented for the estimate of the ATD coefficients, which were said to differ among the SCIPUFF and Gaussian puff models in its estimation.

One reason many STE algorithms lose substantial performance when tested on experimental data arise from poor probabilistic models of the likelihood function. Errors in the measurements come from both sensor noise and modelling inaccuracies, both of which are difficult to specify precisely. Issues due to a lack of knowledge of the correct form of the likelihood function were addressed by Lane et al. [137]. The method used approximate Bayesian computation (ABC) to replace the likelihood function in the SMC algorithm with a measure of the difference between predicted and measured concentrations. The method was able to estimate the strength and location of a release, in addition to the release time. Multiple hazardous releases were handled via a trans-dimensional version of the ABC-SMC algorithm. Ristic et al. [152] used ABC-SMC with multiple dispersion models to find the most relevant ATD model for the release scenario. A rejection sampler was used, which removes inferences that do not match the observed data within a specified tolerance. An adaptive iterative multiple model ABC sampler was proposed to increase the acceptance rate of the rejection sampler by adaptively generating the proposal distribution for each sample. The algorithm was tested on experimental data sets collected by COANDA Research and Development Corporation which used a recirculating water channel specifically designed for dispersion modelling. Results were shown for scenarios

with and without obstacles. Without obstacles, very good results were obtained although, in the presence of obstacles, the estimate of the upwind source location was affected by producing a bimodal posterior distribution.

In [153], Gunatilaka et al. used binary sensor measurements where the threshold was unknown to determine the parameters of a biochemical source. The achievable accuracy of binary measurements for dispersion events was previously explored using the Cramer Rao bounds by Ristic et al. [154] resulting in promising results. The algorithm found a solution iteratively using SMC IS with PC. The wind speed was included in the parameter space to account for uncertainty in the prior meteorological data. The method was tested on experimental data showing that the algorithm could reasonably estimate the source location, wind speed and a normalised release rate. Due to the unknown sensor threshold, it was unable to determine the exact source strength; only the source strength normalised by the assumed sensor threshold could be estimated.

2.5.2.3 Differential Evolution Monte Carlo (DEMC)

DEMC is a combination of differential evolution (DE) and the Bayesian MCMC methods. Essentially, it is an MCMC version of the GA [155]. The method is a population MCMC algorithm in which multiple Markov Chains are run in parallel. The selection process is based on the Metropolis acceptance ratio and the main difference to the MCMC lies in the generation of new proposals via a jump. Instead of a tuned random walk or multivariate normal distribution, DEMC uses multiple chains to adaptively determine the jump proposal based on the difference among them.

In [138], Robins et al. used DEMC to determine the source term of a biological [156] or chemical [157] release. DEMC was used to enable the jump size to adapt itself to the current state of the posterior estimate, thus alleviating responsibility from the user to specify a reasonable jump size. To reduce the number of expensive dispersion calculation runs, a two step decision process was used. The first accepted or rejected the proposal based on prior information. If it was accepted, it was passed to the dispersion model. Unlike much of the related work, the method had a large focus on operational aspects in emergency response such as incorporating time variant data, additional data collected by newly alerted sensors, and the removal of older data and inferences. The approach used a probabilistic sensor model proposed in [158] based on an analysis of experimental data.

2.5.2.4 Polynomial Chaos Expansion (PCE)

The polynomial chaos-based estimation algorithms have received increasing attention in research recently. They arise from an extension of the homogeneous chaos idea developed by Wiener [159] as a non-sampling based method to determine the evolution of uncertainty in a dynamical system. The main principle of the polynomial chaos expansion (PCE) approach when applied to inverse problems such as STE is to expand random variables using

polynomial basis functions. Suitably chosen polynomials converge rapidly to a solution of the posterior probability distribution. To manage the non-polynomial nonlinearity difficulties in polynomial chaos integration, Dalbey et al. proposed a formulation known as polynomial chaos quadrature (PCQ) [160]. PCQ replaces the projection step of PCE with numerical quadrature. The resulting method can be viewed as a Monte Carlo evaluation of system equations with sample points being selected by quadrature rules.

In [139], Madankan et al. used a PCE based minimum variance approach for STE. PCQ was implemented using the conjugate unscented transform method [161] to generate new sampling points from the posterior distribution using the Bayesian framework. The paper compared the performance of PCQ with SMC and an extended Kalman filter (EKF) to determine the source parameters of an atmospheric release using SCIPUFF as the underlying ATD model. It was found that the PCQ technique outperformed the EKF in terms of accuracy and the SMC method in computational speed.

2.5.2.5 Summary on Bayesian inference

Bayesian-based approaches to STE were described in this section. The major benefit of methods was in the output of posterior pdfs to determine parameter estimates with associated uncertainties or confidence level. The methods presented implementations of efficient sampling methods to determine the source term. The algorithms varied in the source parameters estimated, specification of the likelihood function, ATD models used and several schemes to improve performance with regards to computational efficiency, solution accuracy and robustness. A range of scenarios have been considered including utilising varying meteorological information, steady or dynamic plumes, long/short range dispersion events, urban/plain environments and single/multiple releases.

One of the advantages of the Bayesian-based approaches was in specifying probability distributions of the measured and modelled data. In most cases, this had been assumed to take a Gaussian distribution. In [138], more complex models were derived based on the characteristics of particular sensors and the agent.

Several approaches have been proposed to reduce the computational time of the algorithms. This was predominantly done by reducing the number of ATD model runs. This was achieved via: i) a two step inference acceptance criteria so poor samples are not run in a dispersion model [138]; ii) the adjoint source-receptor relationship [134] and iii) by storing a library of pre-computed ATD simulations. The focus of DEMC and PCQ was on reducing the number of iterations required in an MCMC-like algorithm by generating better inferences.

The event of multiple releases posed a significant problem. Methods to determine the number of sources and to correctly characterise them required significantly more computational time. Earlier methods simply ran the original Bayesian algorithms with a specified number of sources and parameters in the parameter space and determined the appropriate

number which is most closely matched with the data. Yee [147] determined the number of sources using simulated annealing to move a Markov Chain among parameter spaces and later work used a more efficient model selection method [148].

Upon testing in realistic scenarios or on experimental data, several problems were also identified including the limitation of theoretical/ideal dispersion models (e.g. Gaussian plume model) and the difficulty in attaining accurate representations of model errors and noise. Yee discovered the significance of the representation of model errors and the loss in accuracy caused by differences between the dispersion model and the real dispersion event [150]. Other limitations included computational time despite several improvements to reduce it, the amount of prior information required and the increase in computational burden when the parameter space expands beyond the location and source strength. Ristic et al. proposed several strategies to overcome the problems such as: making use of ABC to account for the fact it is nearly impossible to accurately know the exact model and sensor errors [137]; the use of multiple dispersion models to find the most appropriate one for the current scenario [152]; the use of binary measurements to reduce noise effects and enable the use of cheaper sensors [154]; and the use of binary sensors where the threshold was unknown was explored in [153] to account for sensor bias/drift and for easy inclusion of alternative data sources.

An example of the limitation of the Gaussian dispersion model was found in [136], where the Gaussian plume dispersion model was unable to accurately estimate the strength of release from simulated data generated using SCIPUFF. A trade-off is required between the accuracy of the dispersion model and its calculation speed. The difficulty of estimating the strength of the release was highlighted further in [98] where algorithms attempted to estimate the strength of release from experimental data. Among eight different algorithm developers, incorporating a number of techniques, only a few of them were able to consistently estimate the strength to within a factor of ten.

2.5.3 Summary

The STE methods examined have been split into optimisation and Bayesian-based approaches. At the end of each subsection, a summary of each of the techniques was given discussing innovative ideas and problems found within the literature. Within each section, there was a range of ideas and implementations of the algorithms; in the following, we will discuss the application of the general frameworks and describe the key problems found within the literature of STE.

The Bayesian methods benefit from producing a final estimate with confidence levels and the fact that prior information can be incorporated into the algorithm with a probability distribution. Any inaccuracies due to modelling errors or sensor noise could be accounted for with appropriate distributions, though these might be difficult to characterise perfectly, in particular, when applied to a real scenario.

The optimisation methods produce a single point estimate of the source parameters. The methods suffer from their inability to include confidence intervals on any prior information it may use or in the final estimate. In spite of this, the optimisation methods are often less computationally expensive and may converge faster than Bayesian methods. They also benefit from the requirement of little or no prior information, though the more available can result in better performance.

Incorporating the adjoint source-receptor relationship or back trajectories methods produces a point estimate of the source by inverting meteorological variables and back tracking from triggered sensors. The method is very fast but highly dependent on accurate rich meteorological information and accurate dispersion models. As a technique to gain an initial estimate to be optimised, it has shown significant performance benefits. The back trajectory algorithms show how the system can benefit from null sensor readings, as these can be used to narrow down the search space for possible source locations. In other words, it helps by providing more information about where the source is not present. By narrowing down the search space, the accuracy of the source term estimate can be increased significantly and computational time reduced. A summary of the STE algorithms that have been reviewed is given in Table 2.2 which is accompanied by Table 2.1 to describe the variables and acronyms that have not been previously defined in the thesis. The algorithms described were created for a static network; however, with some modification, most would be applicable to data gathered by mobiles sensors.

Table 2.1: Variables and Acronyms used in Table 2.2

Variable	**Description**
q	Source strength or release rate
n	Number of sources
x,y,z	Location coordinates, typically downwind, crosswind, height
t_0	Release time
t	Release duration
u	Wind speed
ϕ	Wind direction
ζ	Dispersion model parameters, dependant on the model used
SS	Steady state
LS	Lagrangian stochastic

To summarise the literature in STE, it can be seen that a number of methods produce very good performance in an idealistic scenario of little or no noise, a plain flat environment, plenty of sensors and a single source. Difficulties arise when these conditions are not met, which is generally the case in real scenarios. The difficulties found in STE when moving from a theoretical to a realistic setting are common to most research fields. Some of the key issues are listed in Table 2.3. In the following section, the use of mobile sensors to solve the source term estimation problem are reviewed. Mobile sensors provide several benefits to solve many of the limitations encountered by static networks.

Table 2.2: Summary of STE methods

Ref.	Date	Paramters	Type	Source	Algorithm	Domain knowledge	Met var	Dispersion model
[132]	2004	x,y,q	Plume	Single	SMC-MCMC MH	NA	u,ϕ,ζ	INPUFF
[133]	2012	x,y,q,ζ	SS plume	Single	MCMC MH	NA	u,ϕ	Gaussian plume
[142]	2008	x,y,q,ϕ,u,H,ζ	SS plume	Single	MCMC MH	Uniform priors	NA	Gaussian plume
[134]	2007	x,y,z,q	SS plume	Single	MCMC MH	Urban map	u,ϕ,ζ	Adv-diff
[143]	2007	x,y,q,n	SS plume	Multiple	MCMC SA	n	u,ϕ,ζ	Adv-diff
[145]	2007	x,y,q,n,t	Plume	Multiple	RJ MCMC	Time prior	u,ϕ,ζ	Backward-time LS
[147]	2010	x,y,q,n,t	Plume	Multiple	MCMC SA	Time prior	u,ϕ,ζ	Adv-diff
[148]	2012	x,y,q,n,t	Plume	Multiple	MCMC MS	Time prior	u,ϕ,ζ	Backward-time LS
[162]	2010	x,y,t,ϕ,ζ	Plume	Multiple	MCMC MH	Informative priors, n	u	absorption-drift-diff
[135]	2008	x,y,q	SS plume	Single	MC IS PC	NA	u,ϕ,ζ	Turbulent diff equ
[163]	2014	x,y,z,q,u,ζ	SS plume	Single	MC IS MH PC	NA	u,ϕ	Gaussian plume
[154]	2014	x,y,z,q,u,ζ	SS plume	Single	MCMC MH	NA	u,ϕ	Gaussian plume
[152]	2014	x,y,z,ζ,q/u,	SS plume	Single	ABC-SMC	Informative priors	u,ϕ	Various
[137]	2009	x,y,z,t_0,n,q	Plume	Multiple	ABC-SMC	Gaussian priors	u,ϕ,ζ	Gaussian plume
[153]	2016	x,y,q,u	SS plume	Single	MC IS PC	Urban map	u,ϕ,ζ	Turbulent Adv-diff
[149]	2013	x,y,q/u,ϕ,ζ,n	SS plume	Multiple	MCMC MH	Uniform priors	NA	Gaussian plume
[138]	2009	x,y,q,t_0,t	Plume	Single	DEMC	Parameter bounds	U,ϕ,ζ	Gaussian plume
[164]	2015	x,y,q	SS plume	Single	EnKF	NA	U,ϕ,ζ	Gaussian plume
[139]	2012	x,y,q	SS plume	Single	gPCq minVar	NA	U,ϕ,ζ	SCIPUFF
[100]	2014	x,y,q	SS plume	Single	Least squares	Geometry exploitation	u,ϕ,ζ	Advection-diffusion
[116]	2015	x,y,q	SS plume	Multiple	Least squares	Geometry exploitation, n	u,ϕ,ζ	Advection-diffusion
[117]	2015	x,y,q	SS plume	Single	Least squares	Urban geometry	u,ϕ,ζ	CFD
[165]	2014	x,y,q	SS plume	Single	MRE-PSO	Parameter bounds	u,ϕ,ζ	Gaussian plume
[102]	2010	x,y,q,t	Plume	Single	PSM	NA	u,ϕ,ζ	Gaussian plume
[103]	2006	x,y,q	SS plume	Single	SA	NA	u,ϕ,ζ	Gaussian plume
[104][105]	2007	x,y,q,ϕ	SS plume	Single	GA-NMDS	u	ζ	Gaussian plume
[106]	2008	x,y,q,t,n	Plume	Multiple	GA	x,y,q,t Inv SCIPUFF	u,ϕ,ζ	SCIPUFF
[128] [129]	2012	x,y,q/tu,ζ,ϕ,n	Plume/Puff	Multiple	GA	Plume axis/spread	NA	Gaussian plume/puff
[121]	2015	x,y,z,q,t,u,ϕ,n	Plume/Puff	Multiple	BFGS	x,y,q,t Inv SCIPUFF	u,ϕ,ζ	SCIPUFF & HLEPM

Table 2.3: Key difficulties in STE

Prior knowledge	**Sensing**	**Sensor locations**
Meteorological data	Noise	Not enough triggered sensors
Parameter space	Bias/drift	Poor sensor locations
Domain knowledge	Sampling frequency	
Modelling issues	**Release scenario**	**Computational time**
Dispersion modelling	Multiple sources	Accuracy vs cost
Sensor modelling	Environment	Estimation algorithms
Modelling errors	Release type	

2.6 Source term estimation using mobile sensors

STE using mobile sensors is a relatively immature area of research. The increase in performance and decrease in cost of small computers and electronics has made it a more appealing and feasible option than in the past. Mobile sensors could be used independently, or in conjunction with static sensors. They can overcome many of the limitations imposed by a static network. Firstly, it is infeasible to cover all regions of importance with static sensors, particularly a dense enough grid of static sensors for STE to be performed before the contaminant has spread significantly. Sensors are expensive, as will be their communication network, powering, maintenance and protective holdings. Mobile sensors enable measurements to be taken from more informative locations. This introduces a new area of research to STE, with relation to sensor path planning strategies to provide an accurate estimate of the source term in the least amount of time. In the literature, sensor movement strategies for STE include expert systems, where the sensors follow a set of pre-set guidance rules and information driven motion control, where the movement of the sensor is based on estimates of the expected information gained. The aforementioned techniques are described in more detail in the remainder of this section.

2.6.1 Pre-planned rules

In [166], Kuroki et al. used an expert system of navigation rules to guide a UAV to determine the strength and location of a contaminant source. Concentration data was collected throughout the flight and used in the GA described in [127] to estimate the source term. The method required a single concentration sensor on the ground in order to help guide the UAV. The rules then guide the UAV to fly towards the sensor, downwind and then crosswind to gather concentration data. In simulations, an improved estimate was found than using the GA with an 8x8 grid of sensors, with less computation required. Tests were done for both Gaussian plume and puff models. Particular difficulty was found with the puff model where a high amount of UAVs and plume traverses were required to estimate the source location.

Hirst et al. [167] used the Bayesian framework to estimate the location and strength of multiple methane sources with remotely obtained concentration data gathered using an

aircraft. The aircraft was flown by a human pilot in a somewhat pre planned manner where it would fly in consecutive crosswind directions, downwind of the source. Concentration measurements were modelled as the sum of spatially and temporally smooth atmospheric background concentration, augmented by concentrations due to local sources. The underlying dispersion model was a Gaussian plume atmospheric eddy dispersion model. Initial estimates of background concentrations and source emission rates were found using optimisation over a discrete grid of potential source locations. Refined estimates (including uncertainty) of the number, emission rates and locations of sources were then found using a reversible jump MCMC algorithm. Other parameters estimated include the source area, atmospheric background concentrations, and model parameters including plume spread and Lagrangian turbulence time scale. The method was tested on synthetic and real data. Two real scenarios were considered, first featuring two landfills in a $1600km^2$ area and then a gas flare stack in a $225km^2$ area. Experiments showed good performance of the algorithms. An interesting feature was an extra source estimated downwind of the actual source. This was attributed to bias in wind directions.

2.6.2 Informative path planning

An information guided search strategy can be formulated as a partially observed Markov decision process (POMDP) [168]. This consists of an information state, a set of possible actions and a reward function. With regards to STE, the information state is the current estimate of the source parameters. The set of possible actions are the locations where the robot can move next, and the reward function determines a measure of the amount of information gained for each manoeuvre. The reward function can take several forms, such as Kullback-Lieber divergence [169] (variation of entropy), Rényi divergence [170] or a measure of the mutual information.

2.6.2.1 Information gain

In [171], Ristic and Gunatilaka presented an algorithm to detect and estimate the location and intensity of a radiological point source. The estimation was carried out in the Bayesian framework using a particle filter. The sensor motion and radiation exposure time were controlled by the algorithm. The search began with a predefined motion until a detection was made, and then control vectors were selected based on reducing the observation time. The selection of control vectors was done using a multiple step ahead maximisation of the Fisher information gain (Hessian of the Kullback-Leibler divergence). In [172], this was extended to the estimation of multiple point sources using the Rényi divergence between the current and future posterior densities. This enabled decision making using maximum information gain for the entire search duration regardless of the estimate of the number of sources. The method was tested on experimental data with one and two source scenarios and compared with a uniform random and deterministic search. The information driven

search obtained much more accurate estimates of the location and strength of the source with similar but slightly faster search time.

In [173], Ristic et al. presented a method to determine the location of a diffusive source in an unknown environment featuring randomly placed obstacles. The method used a particle filter to simultaneously estimate the source parameters, the map of the search domain and the location of the searcher in the map. The map was represented as a lattice where missing links represented obstacles and the source was assumed to be located at a node. The gas and searcher travelled down links in the lattice and concentration measurements were taken from the nodes. Concentration measurements were taken from a Poisson distribution to mimic the sporadic nature of measurements. The searcher travelled along the grid and stopped at the nodes to take measurements of gas concentration and to determine the existence of neighbouring links (available paths). At each step, the searcher remained at its current node or move along one link. Movement was based on information gain similar to that mentioned previously [172]. Numerical simulations demonstrated the concept with a high rate of success.

In [174], a number of different search strategies based on information theoretic rewards were compared for determining the location of a diffusive source in turbulent flows. The reward functions compared include: Infotaxic reward, Infotaxic II reward and Bhattacharyya distance. The Infotaxic reward is based on the expected information gain for a single step ahead. It is based on the assumption that the source location coincides with one of the nodes of the square lattice introduced to restrict motion of the searcher. The reward is defined as the decrement of the entropy. The Infotaxic II reward is a slight modification to account for the case where the source may not coincide with a node of the lattice. The Bhattacharyya distance is a particular type of Renyi divergence, which measures the similarity between two densities. In this context, the densities are the posterior distributions at the current time and that expected in the next step. The control is selected based on the maximum reward. The techniques were compared on synthetic and experimental data implemented using the SMC method. It was found that the ratio between the search and sensing areas was a key factor to the performance. With a larger search area, systematic search such as parallel sweep outperformed information theoretic searches. However, with a smaller search area, the cognitive strategies were far more efficient. It was also found that for a smaller search area, the Infotaxic reward performed slightly worse than the others and this was attributed to its more exploratory behaviour.

2.6.2.2 Mutual information

In [175], Madankan et al. presented an information driven sensor movement strategy that attempted to maximise the mutual information between the model output and data measurements. A combination of generalised polynomial chaos and Bayesian inference were used for data assimilation similar to the previous work that used static sensors [139].

A sensor movement strategy was created to move a group of UAVs to maximise the mutual information between the sequence of observational data and the source parameters over the time. To reduce computational complexity a limited look-ahead policy was used and the optimal positions of the UAVs were chosen individually. This means the only cooperation among them was to maintain a distance from one another. This approach was compared with a static network approach using synthetic data on a source estimation task where it was assumed the location was known (so only the source strength was estimated). The results show significant improvements in accuracy and confidence in the estimation.

2.6.2.3 Uncertainty driven

The use of multiple robots has also been proposed, employing an uncertainty driven exploration strategy to plan their path whilst estimating the locations and intensities of multiple sources [176]. This method was tested with real robots in hardware in the loop simulations using simulated gas sensor data.

2.6.3 Summary

The main area of research in mobile sensors for STE has been in developing intelligent path planning strategies for maximum information gained by the sensors. The STE algorithms themselves are similar to those reviewed earlier using static networks. Pre-planned rules have shown to be capable of moving the sensor to determine the source term provided there is enough information on the wind and there exists at least one static sensor within the contaminant plume. Informative path planning strategies have featured maximising information in terms of entropy gain and mutual information. In [173], the need to sample from a position for a significant amount of time was highlighted whilst using a Lagrangian stochastic dispersion model in order to gain a more accurate concentration estimation from noisy sensor readings. The effect of search area was studied and its impact on the performance of reactive or informative search strategies.

The information based or uncertainty driven probabilistic approaches can be beneficial as they take into account the utility of the next measurement when making manoeuvre decisions. In simulations and on experimental datasets based studies, information based search planning strategies have been shown to outperform conventional approaches such as a uniform sweep [172]. However, experimental results of STE performed on-line using a mobile sensor are yet to be found. Besides simulated data, previous work has used experimental datasets, whereby the artificial searcher could move to neighbouring locations to take a new measurement. This was done on a dataset collected in a turbulent water channel and for a radiological dataset [172, 55]. The most closely related experimental result used a manned aircraft equipped with a highly sensitive methane detector. Observations during sweep search patterns were used to estimate the source terms of methane releases from landfill sites using a reversible jump Markov chain Monte Carlo algorithm [167].

Mobiles sensors overcome several of the limitations of using a static network to perform source term estimation, however, they still have some common challenges. Mainly, the effect of varying wind conditions and different types of releases (i.e. continuous, non continuous, instantaneous etc).

2.7 Literature summary

This review has considered the potential methods of response to releases of hazardous material into the atmosphere. The review has in turn looked at atmospheric concentration sensors, mobile robotic platforms, and algorithms for source localisation, boundary tracking, mapping, and source term estimation using static or mobile sensors.

Overall, the primary difficulty experienced by all the proposed methods appears to be in the sporadic nature of sensor measurements caused by turbulence, missed detections, and random changes in wind speed and direction. The majority of the proposed approaches in the literature had been validated in simulations where the difficulty could be better controlled. In fact, to the best of the authors knowledge, there are not any experimentally validated boundary tracking algorithms considering a source releasing dispersive material into the atmosphere (boundary tracking results involving aquatic plumes exist however aquatic plumes are significantly less dynamic). This is expected to be due to the tremendous challenge of the boundary tracking problem subject to large amount of noise, splitting up of regions, and dynamics of the phenomena.

There are several examples of source localisation, mapping, and source term estimation using static sensors that have been demonstrated under the challenging natural outdoor conditions. However, the source localisation methods have so far been demonstrated in small test areas, are still effected by changing wind conditions despite some robustness, assume an open environment, and do not estimate other parameters of the source; therefore they do not provide information about the spread of the HAZMAT. The mapping algorithms proposed have been demonstrated in multiple environments, and recently have considered time variant plumes. In spite of this, a proper method of validating mapping algorithms using a real dispersive source and sensor has not yet been proposed. Source term estimation algorithms incorporating static sensors have been developed to handle several challenging conditions such as variable wind, however, they can become computationally expensive, have limited accuracy depending on the number of sensors and their placement, and are only applicable in areas of high importance where a sensor network has been installed. Source term estimation using mobile sensors is a promising method of response, however, results outside of simulations or using experimental datasets have not previously been produced; this is expected to be due to challenges with regards to the reliability of the algorithms in more realistic conditions and the difficulty of performing the experiments themselves considering the set-up of the experiment environment and the robotic platform, including its integration with sensors. Filling this gap, by the design and

development of new, probabilistic, robust algorithms, is a key contribution of this thesis. This was achieved by the systematic development of the algorithms from increasingly challenging simulations and experiments leading to STE being performed in a natural outdoor environment using an autonomous UAV. In addition, a method of validating mapping algorithms is proposed, using a real dispersive source and sensor, albeit, in a controlled environment.

Chapter 3

Informative path planning for hazardous source reconstruction

A probabilistic approach to estimate the source term of a HAZMAT release appears to be the most promising method. In this chapter, the most common STE algorithm that was used for static sensors is fused with an information based planning strategy, to guide a moveable sensor to estimate the source term of a release. The performance of the path planning strategy is compared to several other methods such as a conventional sweep pattern. The information based planning strategy described in this chapter is inspired by work from the field of optimal experiment design known as Bayesian adaptive exploration (BAE) [177]. BAE provides an iterative observation-inference-design framework for probabilistic and on-line experimental design. The method was first applied to the problem of STE in [178] to explore how to optimally place a single additional static sensor to an existing network. BAE has been adapted for path planning of a mobile sensor to manoeuvre to the most informative measurement locations, which combines search for the contaminant source and STE under a single framework. The proposed algorithm is compared with traditional techniques under various levels of noise while showing robustness to large amounts of noise as a result of Bayesian sampling techniques.

This chapter is based upon work that has been published by the author in [179]. The remainder of the chapter is organised as follows. In Section 3.1, the problem is presented including information about the domain and the forward dispersion model used. In Section 3.2, the adaptive Bayesian sensor motion planning is described. In Section 4 3.3, the computational algorithms that were used to implement the conceptual solution are described. An illustrative run and Monte Carlo simulations with other strategies are given in Section 3.4. Finally, the chapter is summarised in Section 3.5.

3.1 Problem description

When signs of a possible harmful contaminant release are brought to the attention of emergency services, the responders must determine the location of the emitting source, and predict the spread of contamination in order to react efficiently. To avoid putting the emergency responders in danger, an unmanned vehicle equipped with an appropriate sensor can be sent into the search area to assess the severity of contamination. The vehicle is to navigate within the search area collecting concentration measurements which will be used in an estimation algorithm to determine the source term. Sensor measurements can require a long sampling time to gain an accurate concentration reading, so it is important to need as few as possible, whilst producing a high level of STE accuracy. The aim is to rapidly gain a reliable estimate of the source term for its use in an ATD model.

In this chapter, the dispersion of contaminant is assumed to occur in an outdoor open area, and to have reached a steady state. Due to its low computational burden and reasonable accuracy under short ranges, the Gaussian plume dispersion equation [180] is used as the forward ATD model to infer the expected concentrations $\mathcal{M}(\mathbf{p}_k, \Theta_k)$ at a given position ($\mathbf{p}_k = x_k, y_k, z_k$), given hypothesised source parameters Θ_k:

$$\mathcal{M}(\mathbf{p}_k, \Theta_k) = \frac{q_s}{u_s \sigma_y \sigma_z 2\pi} \exp\left(\frac{-c_k^2}{2\sigma_y^2}\right) \times \left[\exp\left(\frac{-(z_k - z_s)^2}{2\sigma_z^2}\right) + \exp\left(\frac{-(z_k + z_s)^2}{2\sigma_z^2}\right)\right], \tag{3.1}$$

where c_k is the crosswind distance from the source positioned at ($\mathbf{p}_s = x_s, y_s, z_s$) with emission rate q_s. u_s is the mean wind speed and σ_y, σ_z are turbulent diffusion parameters that are estimated based on Pasquill's atmospheric stability class [180].

Most meteorological variables can be known within a certain degree of accuracy from existing sensors across the globe. We assume that these variables have been provided and that the source is located on the ground ($z_s = 0$). The source term parameters remaining to be estimated are the location (x_s, y_s) and the release rate (q_s) of the source. We assume the source parameters are within a search space Ω. The source term vector Θ_{k+1} is then defined as:

$$\Theta_{k+1} = [x_s, y_s, q_s]^\mathsf{T} \quad \text{where} \quad (x_s, y_s, q_s) \in \Omega. \tag{3.2}$$

We assume that the vehicle knows its location (x_k, y_k) at the current time step k and it is equipped with the appropriate concentration sensor. The available manoeuvres for the vehicle are $\Psi = \{\uparrow, \downarrow, \leftarrow, \rightarrow\}$, referring to a move up, down, left or right, by a fixed distance. The goal of the algorithm is to choose the manoeuvre $\mathbf{a}_k^* \in \Psi$ that provides the most information about the unknown source term in the next iteration Θ_{k+1}.

3.2 Adaptive Bayesian sensor motion planning

Bayesian adaptive exploration, proposed by [177], is adapted for mobile sensor motion planning. For the remainder of the thesis, the approach shall be referred to as adaptive Bayesian motion planning (ABMP). The process iterates an observation, inference and design cycle as illustrated in Fig. 3.1.

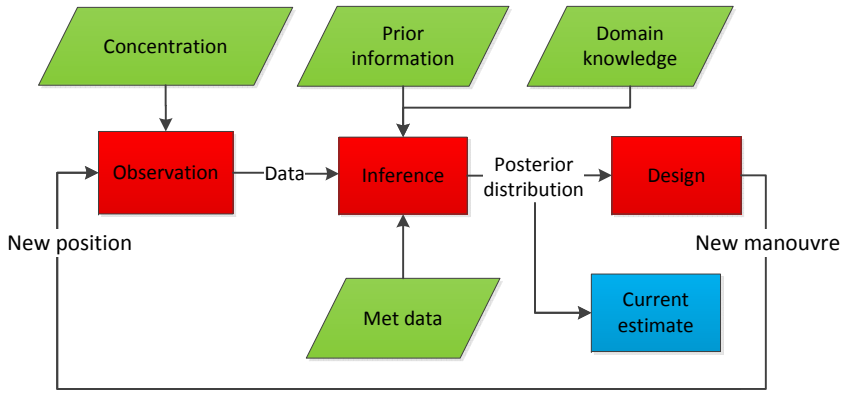

Figure 3.1: Adaptive Bayesian motion planning algorithm flowchart

The observation phase is rather simple and essentially involves taking a measurement of the phenomena; which is the contaminant concentration in this implementation. In the inference phase, Bayesian inference is used to gain an estimate of the source term to reveal the current state of knowledge about the release, in the form of a posterior pdf. During the design phase, the optimal manoeuvre is selected, which is expected to yield the most information for the next inference cycle. The optimal manoeuvre is determined using the idea of maximum entropy sampling, where it is believed that the most is learnt by sampling from where the least is known [181]. In the following section, the steps are described in more detail.

3.2.1 Observation

Concentration observations z_k are assumed to be composed of the true signal $\bar{z}_{k,true}$ and associated errors $\bar{v}_k$, resulting in the following observational model (neglecting modelling errors).

$$z_k = \bar{z}_{k,true} + \bar{v}_k = \mathcal{M}\left(\mathbf{p}_k, \Theta_{k,true}\right) + \bar{v}_k. \tag{3.3}$$

Errors can arise from errors in meteorological data, sensing, atmospheric turbulence or modelling discrepancies [182]. For simplicity, meteorological errors are ignored at this stage. Errors due to sensing, turbulence and modelling are assumed to be jointly represented by a normal distribution.

3.2.2 Inference

In such a scenario where input variables and underlying models are uncertain, a probabilistic approach is preferred over optimisation so that uncertainty in the source term can be captured within a posterior pdf. Bayes' theorem is used to define the posterior pdf of the source term Θ_{k+1} given the observations $\mathbf{z}_{1:k+1}$, prior information, and an appropriate ATD model. In this work, Bayes' theorem is expressed as (3.4), where I represents prior information about the release and the ATD model used. Essentially, this means that the posterior distribution is proportional to the product of the prior and the likelihood.

$$p(\Theta_{k+1}|\mathbf{z}_{1:k+1}, I) \propto p(\Theta_{k+1}|\mathbf{z}_{1:k}, I)p(\mathbf{z}_{k+1}|\Theta_{k+1}, I). \tag{3.4}$$

The prior on all parameters is assumed to be uniformly distributed within the search domain Ω. A Gaussian form of the likelihood is used similarly to [134]:

$$p(\mathbf{z}_{k+1}|\Theta_{k+1}, I) = \prod_{i=1}^{k+1} \frac{1}{\sigma_i\sqrt{2\pi}} \exp\left[-\frac{(z_i - \mathcal{M}(\mathbf{p}_i, \Theta_{k+1}))^2}{2\sigma_i^2}\right], \tag{3.5}$$

where z_i are the observed concentration data at positions $\mathbf{p}_i$, and $\mathcal{M}(\mathbf{p}_i, \Theta_{k+1})$ are predicted concentrations at the corresponding locations obtained by running inferred parameters Θ_{k+1} in an ATD model (3.1). σ_i refers to the error variance, this should be set to encapsulate errors between the predicted and measured concentrations; it also has a strong effect on the acceptance rate of the inference algorithm.

3.2.3 Design

The goal of the design phase is to choose the manoeuvre a_k that is expected to be the most informative, by following a similar approach described in [177]:

$$\mathbf{a}_k^* = \arg\max_{\mathbf{a}_k \in \Psi} \mathbb{E}[\mathscr{I}(a_k)] \tag{3.6}$$

where $\mathbb{E}[\mathscr{I}(\Theta_{k+1}|\mathbf{z}_{1:k}, \hat{z}_{k+1}(\mathbf{a}_k))]$ is the expected information provided by taking manoeuvre a_k. This is defined as the information gained about the posterior distribution given the new data $\hat{z}_{k+1}(\mathbf{a}_k)$, multiplied by the probability of the new data (3.7):

$$\mathbb{E}[\mathscr{I}(a_k)] = \int_{\hat{z}_{k+1} \in \mathcal{Z}} p(\hat{z}_{k+1}(\mathbf{a}_k)|\mathbf{z}_{1:k}) \mathscr{I}(\Theta_{k+1}|\mathbf{z}_{1:k}, \hat{z}_{k+1}(\mathbf{a}_k)) \, \mathrm{d}\hat{z}_{k+1}, \tag{3.7}$$

where $\mathcal{Z}$ is the range of the possible future measurements at the future sampling position. To quantify the measure of information $\mathscr{I}(\Theta_{k+1}|\mathbf{z}_{1:k}, \hat{z}_{k+1}(\mathbf{a}_k))$, several derivations have been proposed from the literature on information theory. In this work, the negative Shannon entropy has been used given by the following Eq. (3.8). This quantity of information

provides a measure of the spread of a distribution:

$$\mathscr{I}(\Theta_{k+1}|\mathbf{z}_{1:k}, \hat{z}_{k+1}(\mathbf{a}_k)) = \int_{\Theta_{k+1}} p(\Theta_{k+1}|\mathbf{z}_{1:k}, \hat{z}_{k+1}(\mathbf{a}_k)) \times \log p(\Theta_{k+1}|\mathbf{z}_{1:k}, \hat{z}_{k+1}(\mathbf{a}_k))\, \mathrm{d}\Theta_{k+1}. \tag{3.8}$$

where $p(\Theta_{k+1}|\mathbf{z}_{1:k}, \hat{z}_{k+1}(\mathbf{a}_k))$ is the posterior for source term parameters considering future data $\hat{z}_{k+1}(\mathbf{a}_k)$. Note, the prior information I has been ignored from the equation to improve readability. In order to simplify Eq. (3.7), let us look at the joint distribution for Θ_{k+1} and $\hat{z}_{k+1}(\mathbf{a}_k)$ and using the product rule to factor it as given:

$$\begin{aligned}
\mathscr{I}(\hat{z}_{k+1}(\mathbf{a}_k), \Theta_{k+1}) =& \int\int p(\hat{z}_{k+1}(\mathbf{a}_k), \Theta_{k+1}|\mathbf{z}_{1:k}) \\
&\times \log p(\hat{z}_{k+1}(\mathbf{a}_k), \Theta_{k+1}|\mathbf{z}_{1:k})\, \mathrm{d}\Theta_{k+1}\mathrm{d}\hat{z}_{k+1}(\mathbf{a}_k) \\
=& \int\int p(\hat{z}_{k+1}(\mathbf{a}_k), \Theta_{k+1}|\mathbf{z}_{1:k}) \log p(\Theta_{k+1}|\mathbf{z}_{1:k})\, \mathrm{d}\Theta_{k+1}\mathrm{d}\hat{z}_{k+1}(\mathbf{a}_k) \\
&+ \int\int p(\hat{z}_{k+1}(\mathbf{a}_k), \Theta_{k+1}|\mathbf{z}_{1:k}) \log p(\hat{z}_{k+1}(\mathbf{a}_k)|\Theta_{k+1}, \mathbf{z}_{1:k})\, \mathrm{d}\Theta_{k+1}\mathrm{d}\hat{z}_{k+1}(\mathbf{a}_k) \\
=& \mathscr{I}(\Theta_{k+1}|\mathbf{z}_{1:k}) + \int p(\Theta_{k+1}|\mathbf{z}_{1:k}) \mathscr{I}(\hat{z}_{k+1}(\mathbf{a}_k)|\Theta_{k+1}, \mathbf{z}_{1:k})\, \mathrm{d}\Theta_{k+1}.
\end{aligned} \tag{3.9}$$

Repeating the above calculation but switching the order of factorising $\hat{z}_{k+1}(\mathbf{a}_k)$ and Θ_{k+1} gives:

$$\begin{aligned}
&\mathscr{I}(\hat{z}_{k+1}(\mathbf{a}_k), \Theta_{k+1}) = \\
&\qquad \mathscr{I}(\hat{z}_{k+1}(\mathbf{a}_k)|\mathbf{z}_{1:k}) + \int p(\hat{z}_{k+1}(\mathbf{a}_k)|\mathbf{z}_{1:k}) v(\Theta_{k+1}|\hat{z}_{k+1}(\mathbf{a}_k), \mathbf{z}_{1:k})\, \mathrm{d}\hat{z}_{k+1}(\mathbf{a}_k).
\end{aligned} \tag{3.10}$$

Equating Eqs. (3.9) and (3.10) and noting that the integral in (3.10) is equivalent to the expected information from (3.7) yields:

$$\begin{aligned}
&\mathbb{E}[\mathscr{I}(a_k)] = \\
&\qquad \mathscr{I}(\Theta_{k+1}|\mathbf{z}_{1:k}) + \int p(\Theta_{k+1}|\mathbf{z}_{1:k}) \mathscr{I}(\hat{z}_{k+1}(\mathbf{a}_k)|\Theta_{k+1}, \mathbf{z}_{1:k})\, \mathrm{d}\Theta_{k+1} - \mathscr{I}(\hat{z}_{k+1}(\mathbf{a}_k)|\mathbf{z}_{1:k}).
\end{aligned} \tag{3.11}$$

The first term in (3.11) refers to the information in the posterior distribution from the previous time step which is independent from the future measurement, so it shall remain constant. The second term refers to the average information contained in the sampling distribution. In cases where the noise variance varies with the signal, this is an important quantity; however, if the noise is constant regardless of the signal, then this term is also constant. The final term is the entropy (considering a minus sign) in the predictive distribution which needs to be calculated. Using (3.8), the expected information can be

represented as:

$$\begin{aligned}\mathbb{E}[\mathscr{I}(a_k)] &= C_{a_k} - \mathscr{I}(\hat{z}_{k+1}(\mathbf{a}_k)|\mathbf{z}_{1:k}) \\ &= C_{a_k} - \int p(\hat{z}_{k+1}(\mathbf{a}_k)|\mathbf{z}_{1:k}) \log p(\hat{z}_{k+1}(\mathbf{a}_k)|\mathbf{z}_{1:k}) \, \mathrm{d}\hat{z}_{k+1}(\mathbf{a}_k),\end{aligned} \tag{3.12}$$

where C_{a_k} represents a constant formed from the first two terms of (3.11). In order to choose the most informative manoeuvre using (3.6), we need to maximise (3.12). This means that the best move is to go toward the location whose predictive distribution has maximum entropy (equivalently, the least information); such a principle is known as maximum entropy sampling [181]. In other words, the most informative manoeuvre is where the predictive distribution has the most spread.

3.3 Computational approach

The inference and the design stages of the algorithm involve solving multidimensional integrals that cannot be done analytically. In this section, the computational approach used to implement the conceptual solution for ABMP is described.

3.3.1 Inference

Since the posterior distribution of source parameters (3.4) cannot be obtained analytically, it shall be approximated using a numerical techniques such as Monte Carlo methods. However, as it is computationally expensive, an efficient sampling technique is required to approximate the posterior distribution. Within the literature on STE, as discussed in the previous chapter, several techniques have been proposed: i) Markov chain Monte Carlo (MCMC) [134, 142]; ii) sequential Monte Carlo (SMC) [183]; and iii) differential evolution Monte carlo (DEMC) [138]. In this chapter, we use the MH MCMC algorithm [184]. As this is a popular approach used in the majority of MCMC based STE algorithms, and it is discussed in some detail in the literature review, it will not be described any further in this chapter. For more information on MCMC for STE, the reader is directed to [134].

The output of the MCMC algorithm is a posterior distribution for the source parameters (3.4), represented by a Markov chain. In subsequent iterations of the ABMP algorithm, a new Markov chain is initiated each time new data has been collected. The starting point of the new Markov chain is at the mean value of each source parameter from the previous iteration.

3.3.2 Design

Once a posterior distribution of source parameters has been obtained using MCMC; The pdf in Eq (3.12) can be approximated using a set of N samples $\{\Theta_{k+1}^n\}_{n=1}^N$ for which the

information can be estimated:

$$\begin{aligned} p(\hat{z}_{k+1}(\mathbf{a}_k)|\mathbf{z}_{1:k}) &= \int p(\hat{z}_{k+1}(\mathbf{a}_k)|\Theta_{k+1}) p(\Theta_{k+1}|\mathbf{z}_{1:k}) \, \mathrm{d}\Theta_{k+1} \\ &\approx \frac{1}{N} \sum_{n=1}^{N} p(\hat{z}_{k+1}(\mathbf{a}_k)|\Theta_{k+1}^n) = \bar{p}(\hat{z}_{k+1}(\mathbf{a}_k)^m). \end{aligned} \tag{3.13}$$

The average information from a set of samples for a specific manoeuvre is used as a measure of the expected information [177]:

$$\mathbb{E}[\mathscr{I}(a_k)] \approx -\frac{1}{M} \sum_{m=1}^{M} \log \bar{p}(\hat{z}_{k+1}(\mathbf{a}_k)). \tag{3.14}$$

The overall ABMP algorithm is described in Algorithm 1.

Algorithm 1 Adaptive Bayesian motion planning

for k = 0,1,2,..., max time steps **do**
  $z_{k+1} \leftarrow$ take new measurment
  $p(\Theta_{k+1}|\mathbf{z}_{1:k+1}) \leftarrow$ run MCMC algorithm
  $\{\Theta_{k+1}^n\} \leftarrow$ draw N samples from above distribution
  choose integer $M \leq N$
  for all $a_k \in \Psi$ **do**
    consider potential position $(x_{k+1}^{a_k}, y_{k+1}^{a_k})$
    for m = 1:M **do**
      $\Theta_{k+1}^{a_k,m} \leftarrow$ draw uniformly from $\{\Theta_{k+1}^n\}$
      $\hat{z}_{k+1}(\mathbf{a}_k)^m \leftarrow$ sample from $p(\hat{z}_{k+1}(\mathbf{a}_k)|\Theta_{k+1}^{a_k,m})$
      determine $\bar{p}(\hat{z}_{k+1}(\mathbf{a}_k)^m) \leftarrow$ Eq. (3.13)
    end for
    determine $\mathbb{E}[\mathscr{I}(a_k)] \leftarrow$ Eq. (3.14)
  end for
  $a_k^* = arg\ \max\{\mathbb{E}[\mathscr{I}(a_k)]\} \leftarrow$ new manoeuvre
  $(x_{k+1}, y_{k+1}) = (x_k, y_k) + a_k^* \leftarrow$ new position
end for

3.4 Numerical simulations

3.4.1 Illustrative run

An example run of the algorithm at various time steps is presented in Fig. 3.2. Synthetic concentration measurement data were created using the Gaussian plume dispersion model (3.1) infected with normally distributed noise with mean zero and standard deviation equal to 50% of the signal. In the early stages of the simulation, the sensor moved crosswind before moving towards the location of the source. In simulations under higher noise, as illustrated in Fig. 3.3, the algorithm was naturally more explorative without any tuning of parameters. This showed a strong balance between explorative and exploitative behaviour

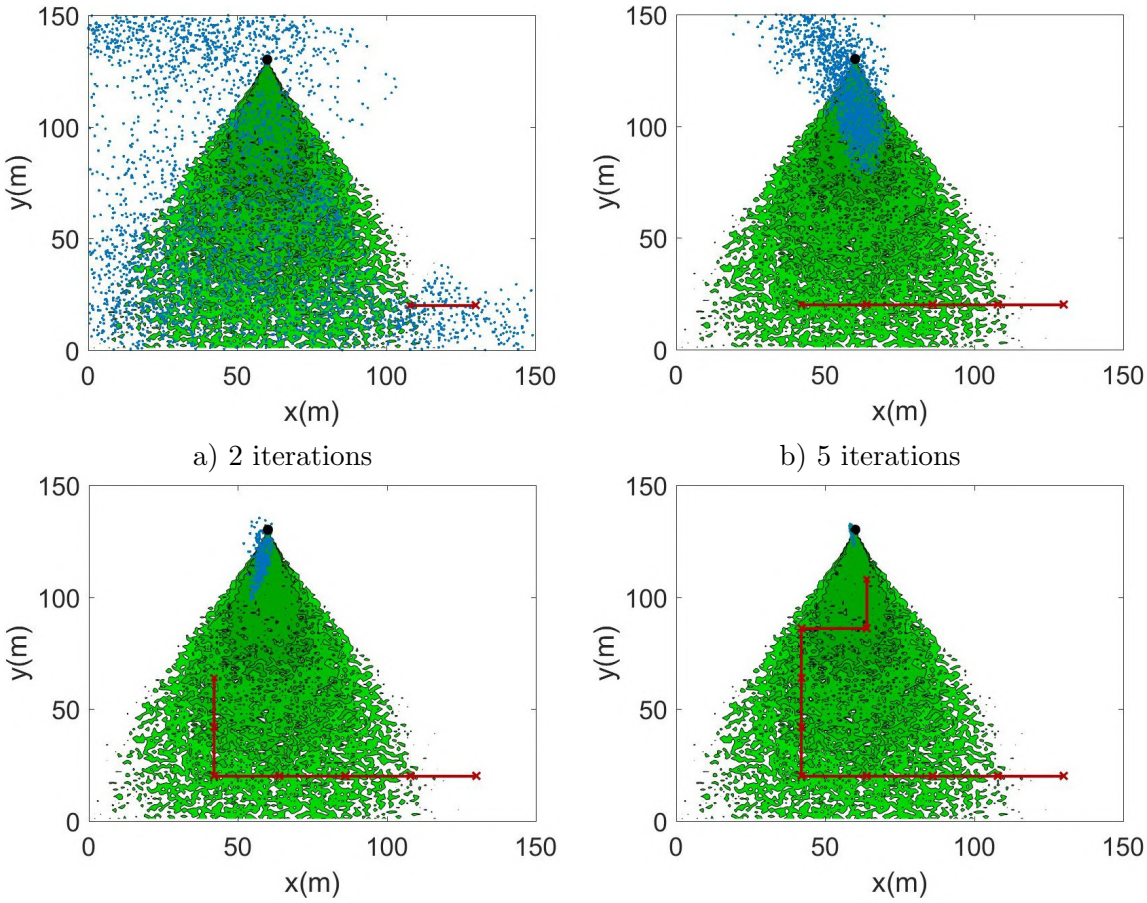

a) 2 iterations b) 5 iterations

c) 7 iterations d) 10 iterations

Figure 3.2: Example run of the ABMP algorithm. The shaded green region represents the contaminant with source position indicated by the black circle. Blue dots represent the Markov chain posterior for source location. Red crosses represent the measuring locations of the sensor following the red lined vehicle path.

which is crucial for efficient yet robust autonomous search behaviour. Interestingly, in early stages of the simulations, the posterior distribution for the source location, as illustrated in Fig. 3.2, formed a shape that resembled an inverse run of the Gaussian plume. In some STE algorithms, an inverse run was initially used to narrow down possible source locations [121]. This could be implemented in future work to possibly reduce the number of steps used in the inference phase of the algorithm.

By using ABMP, the unmanned vehicle is capable of estimating the source term regardless of its starting location or the location of the plume, provided it existed within the search domain. Towards the end of the search, the acceptance rate of the MCMC inference decreases, this is not a problem as the results produced are still accurate. However, addressing this in the future could yield a better approximation of the posterior distribution.

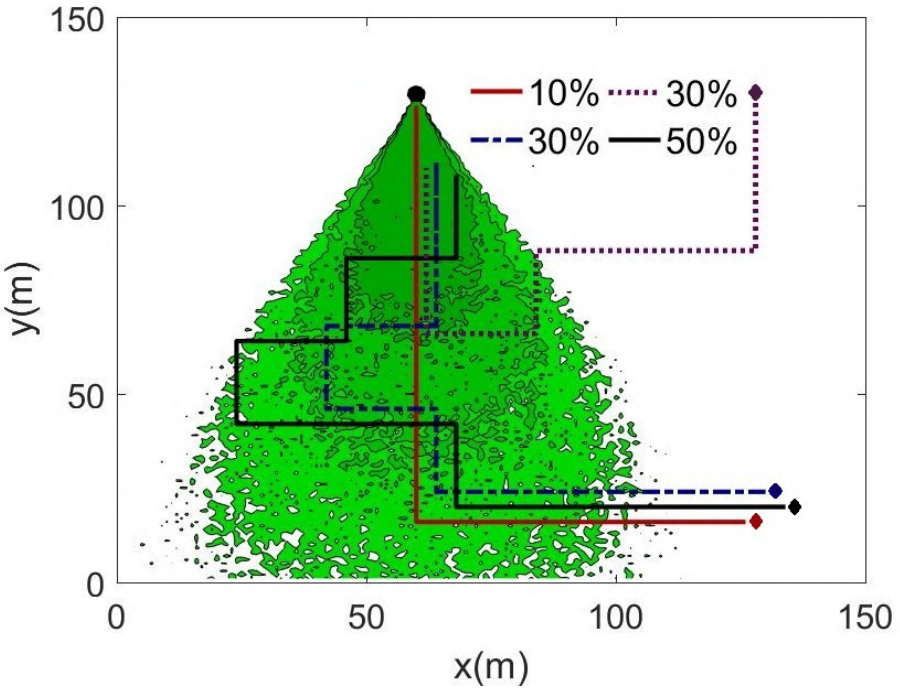

Figure 3.3: Example paths of ABMP under various levels of noise (two 30% paths are generated from different initial positions, indicated by coloured diamonds).

3.4.2 Monte Carlo comparison

Monte Carlo simulations were used to assess the performance of the algorithm in comparison to a uniform sweep, random movement and a source seeking algorithm. The source seeking algorithm followed the ABMP procedure partially; however, it moves towards the current estimate of the source position based on the mean values from the inference algorithm. Examples of the paths of each are shown in Fig. 3.4 under identical conditions as Fig. 3.2. For the Monte Carlo comparisons, the Gaussian plume equation (3.1) was used to generate synthetic data infected with normally distributed noise with mean zero and standard deviations equal to 10% and 50% of the signal. The contaminant plume was generated at random locations, with randomly varying wind direction. The results of the average root mean squared error (RMSE) for the mean parameter estimates after 100 Monte Carlo simulations are presented in Table 3.1.

Table 3.1: Performance comparison over a hundred Monte Carlo simulations

Strategy	Random search		Uniform search		Source seeking		ABMP	
Noise	10%	50%	10%	50%	10%	50%	10%	50%
RMSE in x (m)	11.96	15.54	7.50	11.16	9.35	13.42	**1.74**	5.95
RMSE in y (m)	12.10	14.63	7.34	8.79	9.42	13.09	**1.95**	6.67
RMSE in q (g/s)	0.29	0.33	0.21	0.30	0.26	0.32	**0.15**	0.28
Number of moves	21.55	22.89	19.08	20.65	12.71	12.87	**10.68**	11.71

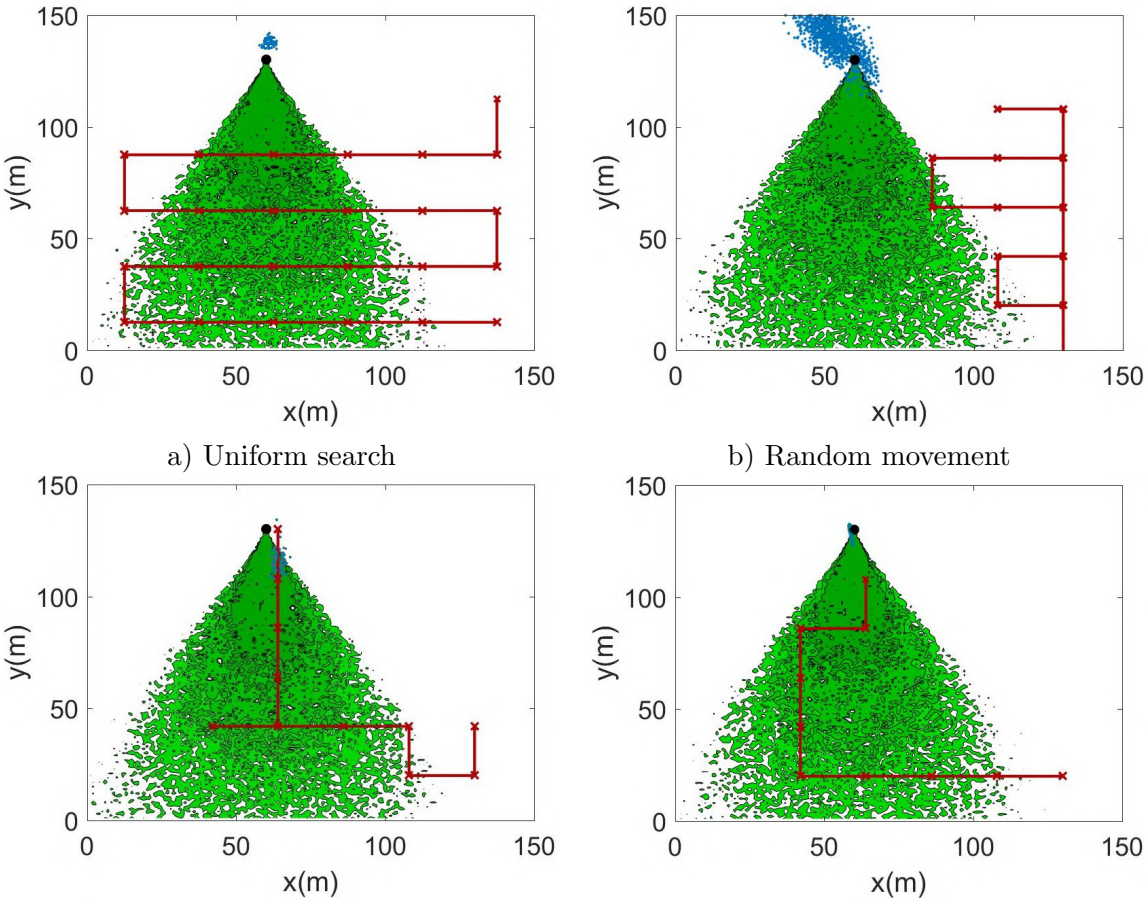

a) Uniform search b) Random movement

c) Source seeking d) ABMP

Figure 3.4: Example path and search results for a) uniform sweep; b) random movement; c) source seeking; and d) ABMP.

Plots of the number of measurements versus the average RMSE for the Monte Carlo simulations subject to 10% normally distributed noise have been plotted in Fig. 3.5. The graphs clearly demonstrate the overall benefit with regards to the accuracy and convergence time of the algorithm in estimation of the source term parameters.

3.5 Chapter summary

A Bayesian based source term estimation algorithm, originally proposed to fuse measurements from static detectors, has been augmented with an information based planning strategy to guide a single mobile sensor to solve the problem. The adaptive Bayesian exploration algorithm has been proposed; to guide a mobile sensor to the most informative sensing locations for STE rather then relying on a conventional pre planned path, random movement, or a purely source seeking plan. The algorithm guides the robot searcher to where most information is expected to be gained, rather than towards where the estimation algorithm expects the source to be found. The popular Bayesian estimation algorithm, MCMC, was used for inference of the source parameters whilst motion planning was implemented by sampling from the output posterior distribution to find the

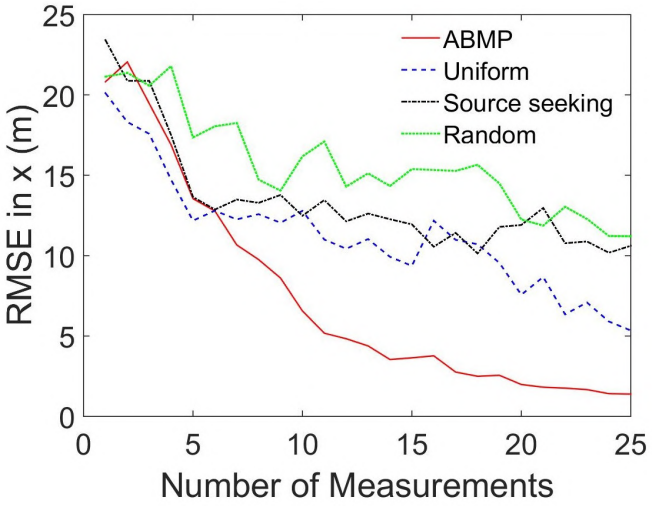

a) RMSE for x

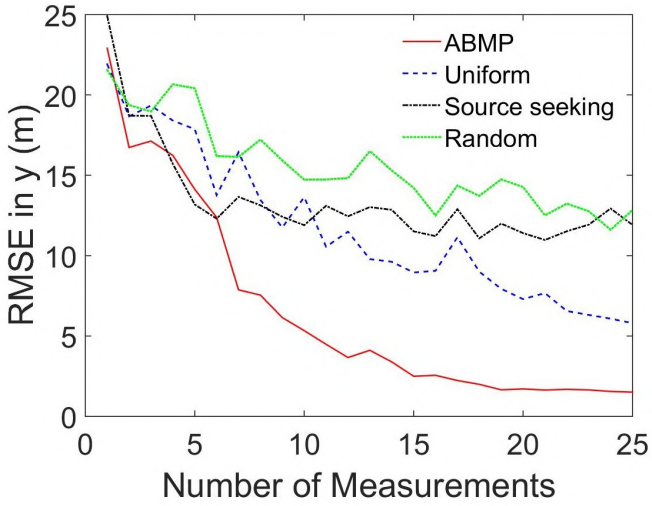

b) RMSE for y

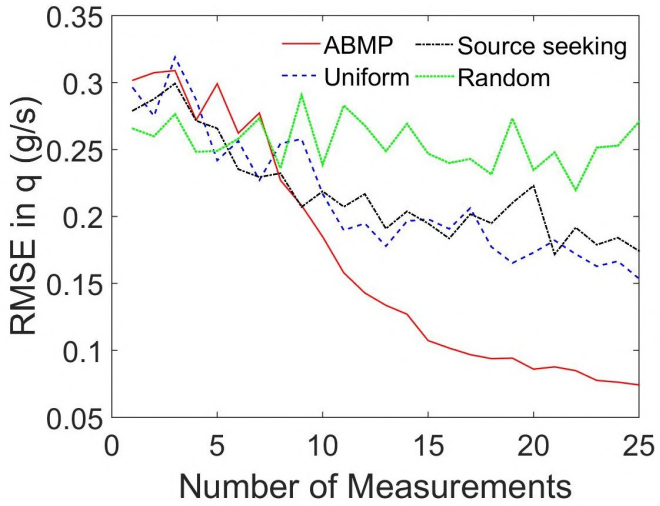

c) RMSE for q

Figure 3.5: Monte Carlo results of RMSE vs the number of measurements.

location of maximum entropy of the predictive measurement distribution. In simulations, the approach was capable of handling a large amount of sensor error. Even with a poor starting position outside of the contaminated area, or upwind, the algorithm was able to efficiently find the source and predict its emission rate. Monte Carlo simulations compared the ABMP STE method with other path planning approaches. The proposed information based technique significantly outperformed the alternative and more conventional methods with regards to the search time and the accuracy of the estimation.

This chapter has presented promising results by integrating a popular STE algorithm with an information based planning strategy. Given the promising result, there is motivation to tailor the STE algorithm for use with a mobile sensor. This means solving the STE problem in a recursive manner rather than using a batch process, as seen in the MCMC algorithm, to greatly improve computational efficiency. Additionally, the algorithm should be extended to handle different measurement input characteristics, such as a particle count sensor rather then a concentration sensor. Both of these extensions are considered in the following chapter.

Chapter 4

Entrotaxis as a strategy for autonomous search and source reconstruction in turbulent conditions

This chapter presents extensions of the work from the previous chapter by introducing a more efficient estimation algorithm that runs recursively, by considering a more challenging scenario, and comparing the algorithm with the state of the art. A strategy is developed to perform an efficient autonomous search to find an emitting source of sporadic cues of noisy information. The HAZMAT source considered is emitting a small but constant amount of particles into the atmosphere, where the weak source and turbulence cause irregular gradients and intermittent patches of sensory cues. Therefore, the observation model from the previous chapter is changed to consider discrete measurements from a particle count sensor. The search problem is now much more sparse, with limited sensory cues in the form of particle encounters with the sensor. Bayesian inference, implemented via the sequential Monte Carlo (SMC) method (rather than MCMC), is used to update posterior probability distributions of the source location and emission rate in response to the sensor measurements. Posterior sampling is then used to approximate a reward function, leading to the manoeuvre to where the entropy of the predictive distribution is the greatest. The algorithm formulated in the chapter is termed 'Entrotaxis', as it guides the path of the searching robot based on the maximum entropy sampling principles introduced in the previous chapter. The performance and search behaviour of the proposed method is compared with the state of the art algorithm, Infotaxis [10], for searching in sparse and turbulent conditions where typical gradient-based approaches become inefficient or fail. The algorithms are assessed via Monte Carlo simulations with simulated data and an experimental dataset. Whilst outperforming the Infotaxis algorithm in most of our simulated scenarios, by achieving a faster mean search time, the proposed strategy is also

more computationally efficient during the decision making process.

This chapter is based upon work that has been published by the author in [185]. The remainder of this chapter is organised as follows. In Section 4.1 inspiration is drawn from the searches seen in nature and from the literature in the area of autonomous search. In Section 4.2, the problem addressed in this chapter is mathematically formulated, including equations that model the spread of the emitted particles and the number of particle encounters with the sensor. In Section 4.3, the conceptual solution of the Entrotaxis algorithm is described, covering parameter estimation and mobile sensor control. In Section 4.4, we describe the sequential Monte Carlo implementation of the Entrotaxis algorithm. In Section 4.5, an illustrative run is presented, the Infotaxis II algorithm is briefly described, and numerical simulations compare the difference in performance and search characteristics between the two strategies. The results using an experimental dataset are given in Section 4.6, and finally, Section 4.7 summarises the chapter.

4.1 Related work

The search for an emitting source of weak, intermittent or noisy signals is an important task for mankind and the natural world. Within the animal kingdom, maximising searching efficiency is of great importance where food sources can be sparse and the mating race is competitive.

Searching strategies are adapted to capitalise upon the availability of sensing cues or prior information. In the absence of information or cues, it is common to execute a systematic or random search. Systematic search paths, such as parallel sweeps and Archimedean spirals [186], are effective methods provided that the target of interest is stationary, there is no available information, and if efficiency is not the priority. In early works of search theory, systematic searches were studied by the US navy, to optimise aircraft flight paths whilst hunting submarines [186]. In the animal kingdom systematic trajectories are rarely observed, nonetheless there is evidence to suggest that desert ants follow an Archimedean spiral path whilst foraging [187]. Random searches can be argued to be the most prevalent in nature. For instance, Albatrosses, among many other species, have been observed to display lévy flight patterns [188] whilst hunting. A large dataset of the movement of open-ocean predatory fish provides supporting evidence that hunters follow lévy patterns where prey is sparse, although it is suggested Brownian motion is observed when prey is abundant [189]. Regardless, the lévy hypothesis is a source of dispute within the literature and alternative hypotheses may be more probable [190].

When prior knowledge or sensing cues are available, the search strategy is adapted to exploit the extra information. Chemotaxic strategies use concentration gradients to direct motion towards an emitting source. Bacteria, such as Escherichia coli, use Chemotaxis to move towards the greatest supply of energy by slowly climbing positive concentration gradients [11]. However, in sparse sensing conditions, which can be caused by a weak source,

large distances or turbulent mixing, Chemotaxic strategies are abandoned as irregular gradients and intermittent sensing cause them to lose performance or fail. Anemotaxis concerns the use of wind information to help guide the searcher, a strategy which has been observed in honeybees [191] and the male silkworm moth [42], among others.

Most of the aforementioned biologically-inspired search strategies can be regarded as reactive, where observations trigger predefined movement sequences to localise a source [41, 53]. Alternatively, approaches have been developed based on information-theoretic principles, otherwise known as cognitive strategies. Information theory was first applied to the search problem to optimise effort during aerial reconnaissance [192]. The Shannon entropy, from the theory of information and communication, was used to compare the effectiveness of different pre-planned strategies. Recent cognitive search strategies make decisions on-line, formulated as a partially-observable Markov decision process (POMDP) [193]. The POMDP framework utilises state, action and reward. For our problem, the state refers to the current knowledge about the source, the actions are movements towards potential future measurement locations and the reward is a quantity to describe the gain in information supplied by the corresponding action. Infotaxis is a cognitive search strategy proven to be effective in the sparse sensing conditions where gradient based approaches would be unsuitable [10]. By assuming environmental parameters and the source strength were known, Bayes rule was applied to update a probabilistic map of the source location throughout the search, in response to sparse sensory cues in the form of particle encounters with a sensor [48]. Considering one-step ahead manoeuvres on a square lattice, the most informative actions were selected based on minimising the expected entropy of the posterior distribution, with an adaptive term to bias the searcher's movements towards the source as levels of uncertainty were reduced. The strategy showed robustness to significantly sparse conditions and has thus inspired several studies proposing modifications and extensions [194, 195]. A critical extension of the algorithm was its implementation in the sequential Monte Carlo framework, using a particle filter, alleviating its grid based implementation and allowing the source strength to be included as a parameter to be estimated [55]. Several reward functions were compared including an Infotaxic II reward, which removed the Infotaxis' bias towards the source, and a reward based on the Bhattacharyya distance. Although the differences among strategies were marginal, the Infotaxis II reward slightly outperformed the others in numerical simulations.

Perhaps the strongest argument that favours a reactive search strategy over the cognitive approach is the higher computational cost of the cognitive search. Aside from the possible complexity of the underlying dispersion and sensor models, the cognitive strategies require a new posterior distribution to be calculated, for each possible future measurement, at each considered location. This could pose a serious problem in conditions where the number of possible measurements or actions increases, or in the development of multiple-step ahead or collaborative multi-agent search strategies. Despite the computational burden, cognitive strategies are preferred due to their probabilistic nature. They

have been shown to be more robust in sparse conditions [53], and additional parameters (such as the source strength and potentially the time of release) can be estimated. The latter falls into the domain of source term estimation.

This chapter proposes an alternative cognitive search and source term estimation strategy, termed as Entrotaxis. Similar to previous work [55], the sequential Monte Carlo framework is used to update probability distributions of source parameters. Maximum entropy sampling principles are newly used to guide the searcher [181], hence the name 'Entrotaxis' by following the naming convention in the literature [10, 55]. The approach follows a similar procedure to Infotaxis II [55] in a way that a probabilistic representation of the source is used; however, the reward function considers the entropy of the predictive measurement distribution as opposed to the entropy of the expected posterior. Essentially, Entrotaxis will guide the searcher to where there is the most uncertainty in the next measurement, while Infotaxis will move the searcher to where the next measurement is expected to minimise the uncertainty in the posterior distribution. The maximum entropy sampling principles upon which the algorithm is built are rather intuitive, where it is considered the most is learnt by sampling from where the least is known. This approach has proven to be effective in the literature on optimal Bayesian experimental design [181]. Whilst outperforming the Infotaxis algorithm in several conditions by more rapidly localising the source, the proposed Entrotaxis strategy is also slightly more computationally efficient as hypothesised posterior distributions do not have to be computed in the decision making.

4.2 Problem description

The autonomous search algorithm is to guide a searcher to localise and reconstruct the source of a constant emission of particles characterised by the unknown source term vector $\Theta_s = [\mathbf{p}_s \; q_s]^\mathsf{T}$, where $q_s \in \mathbb{R}^+$ is the emission rate of the source located at $\mathbf{p}_s = [x_s \; y_s]^\mathsf{T} \in \Omega$, where $\Omega \subset \mathbb{R}^2$ denotes the search area. The autonomous searching agent located at $\mathbf{p}_k = [x_k \; y_k]^\mathsf{T} \in \Omega$ and equipped with a particle detector of area r, is to navigate the environment, choosing from the admissible set of actions $\Psi = \{\uparrow, \downarrow, \leftarrow, \rightarrow\}$, the move $\mathbf{a}_k^* \in \Psi$ that is expected to yield the most information.

The searcher shall collect measurements in the form of the number of particle encounters $z_k \in \mathbb{Z}^+$ with the sensor. The particles emitted from the source disperse through the domain under turbulent transport conditions. The three dimensional dispersion model $R(\mathbf{p}_k|\Theta_s)$ presented in [10] is adopted to denote the rate of particles encountered by a spherical sensor of radius r at position $\mathbf{p}_k$ from the source defined by the source term vector Θ_s. Particles emitted from the source have a finite lifetime τ, propagate with isotropic effective diffusivity σ (which approximates the combined effect of turbulent and molecular diffusion) and are advected by a mean current or wind u [10]. Adopting a sign convention

that sets the wind in the direction of the negative y axis yields the analytical solution:

$$R\left(\mathbf{p}_k|\Theta_s\right) = \frac{rq_s}{||\mathbf{p}_k - \mathbf{p}_s||} \exp\left[\frac{-||\mathbf{p}_k - \mathbf{p}_s||}{\lambda}\right] \exp\left[\frac{-(y_k - y_s)u}{2\sigma}\right], \tag{4.1}$$

where

$$\lambda = \sqrt{\frac{\sigma\tau}{1 + \frac{u^2\tau}{4\sigma}}}. \tag{4.2}$$

The mean number of particle encounters expected by the sensor is simply the product of the rate of encounters and the sampling time $\mu_k = R\left(\mathbf{p}_k|\Theta_s\right) t_0$. An example plot of the mean rate of encounters is given in Fig. 4.1.

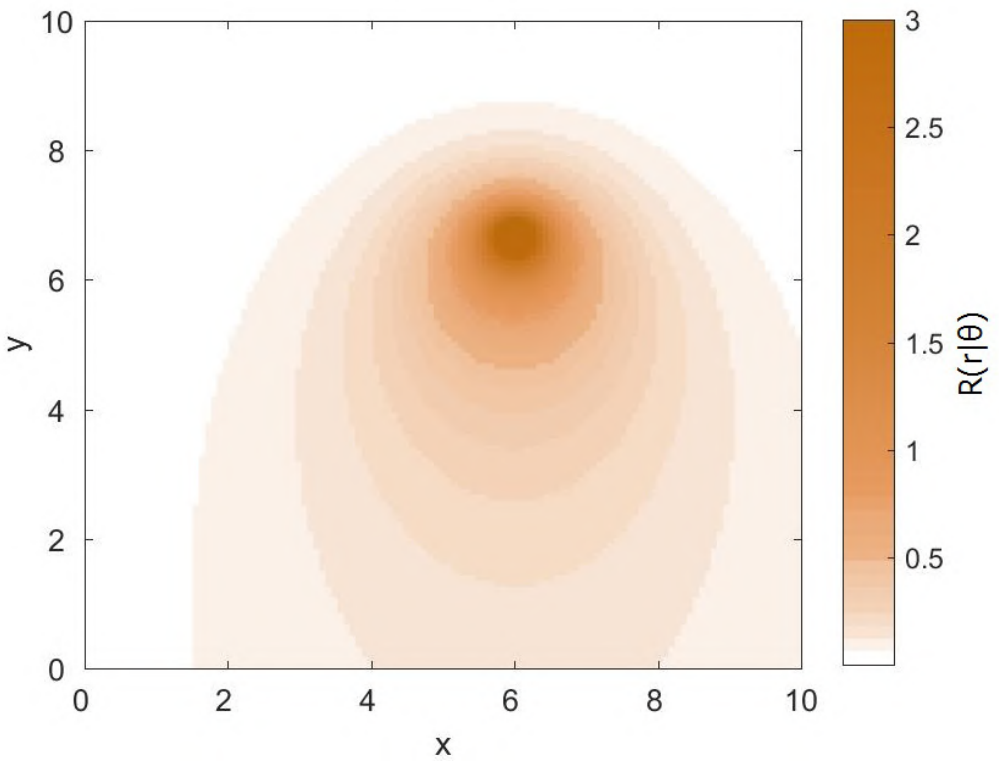

Figure 4.1: The mean rate of particle encounters with a sensor of size $r = 1$ after time interval $t_0 = 1$ and parameters $q_s = 1, x_s = 6, y_s = 6.67, u = 1, \tau = 250$ and $\sigma = 1$.

The stochastic process of particle encounters with the sensor, given the mean rate, is modelled by a Poisson distribution [10] which denotes the probability that the sensor located at $\mathbf{p}_k$ will encounter $z_k \in \mathbb{Z}^+$ particles during the sampling time interval t_0 as given:

$$p(z_k|\mu_k) = \frac{\mu_k^{z_k}}{z_k!} e^{-\mu_k}. \tag{4.3}$$

An example of what the searcher may observe at a fixed point in time is illustrated in Fig. 4.2, by running the Poisson sensor model over the mean rate of particle encounters from Fig. 4.1. The plot demonstrates the significant challenge imposed on source localisation by sparse and turbulent conditions.

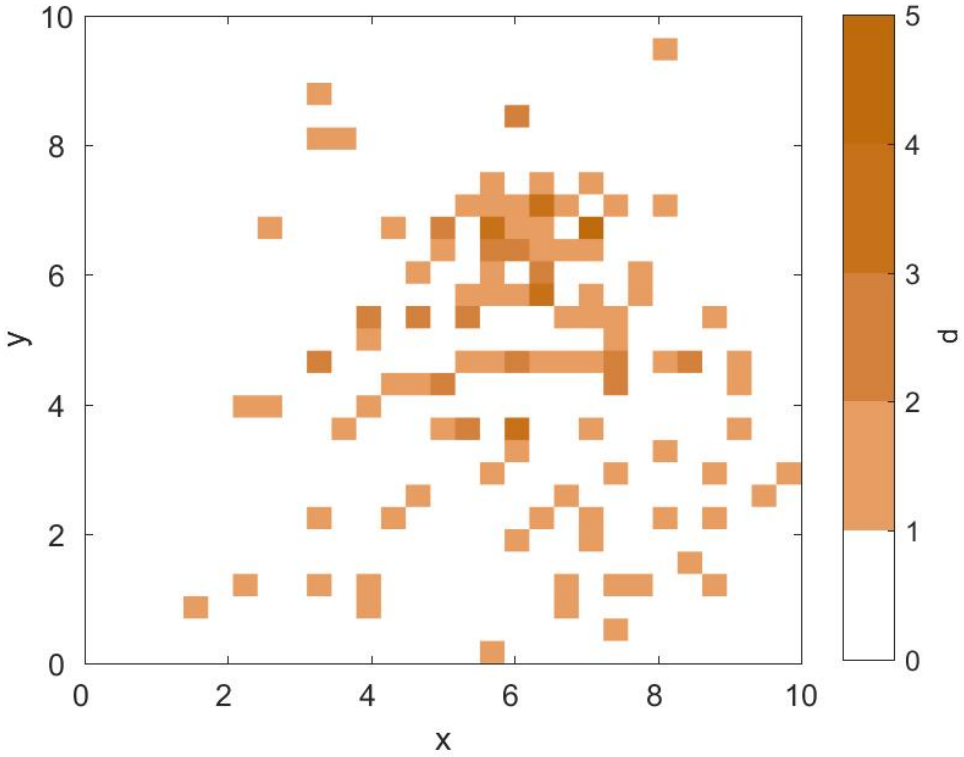

Figure 4.2: Example number of particles encountered $z_k(\mathbf{p}_k)$ by the sensor at searcher nodes, obtained by running the Poisson sensor model on Fig. 4.1.

We assume that the average particle lifetime τ and the environmental parameters σ and u are known, with the source term vector Θ_s remaining to be estimated.

4.3 Conceptual solution

The proposed Entrotaxis algorithm consists of estimation of the source parameter vector Θ_s, followed by an analysis to determine the most informative manoeuvre for a mobile sensor. Estimation is carried out using the Bayesian framework to estimate the source parameters in the presence of uncertainty. Information theory is used to identify the most informative manoeuvre, which is defined as the location where the entropy of the predictive distribution is at its maximum. In other words, the searcher moves to the position where the least is known about the next measurement. This is the maximum entropy sampling principle, which has been popular in research on optimal design of experiments [181]. The principle was demonstrated in the previous chapter, to show significant performance improvements against conventional path planning methods, such as a uniform sweeping path.

4.3.1 Estimation

In a similar manner to the previous chapter, a probabilistic framework is used to estimate the source parameters in response to uncertain information, this time, in the form of particle encounters with a sensor. The current state of knowledge regarding the parameters is represented by the posterior probability density function (pdf) $p(\Theta_k|\mathbf{z}_{1:k})$, where $\mathbf{z}_{1:k} := \{z_1(\mathbf{p}_1), ..., z_k(\mathbf{p}_k)\}$ refers to the measurement data at visited locations. The posterior pdf is subsequently updated according to Bayes rule as sensory data are acquired:

$$p(\Theta_k|\mathbf{z}_{1:k}) = \frac{p(z_k(\mathbf{p}_k)|\Theta_k)p(\Theta_k|\mathbf{z}_{1:k-1})}{p(z_k(\mathbf{p}_k)|\mathbf{z}_{1:k-1})} \tag{4.4}$$

where

$$p(z_k(\mathbf{p}_k)|\mathbf{z}_{1:k-1}) = \int p(z_k(\mathbf{p}_k)|\Theta_k)p(\Theta_k|\mathbf{z}_{1:k-1})\,\mathrm{d}\Theta_{k+1}. \tag{4.5}$$

If information concerning the source term is available prior to the search, it can be exploited through an appropriate distribution to represent the prior knowledge known about the release. However, in the absence of information, the initial prior distribution $\pi(\Theta_0) \equiv p(\Theta_0)$ can be set to an uninformative distribution. In this chapter, and in the majority of the thesis, a uniform distribution is used that is bounded by the domain Ω. Unless otherwise stated, it us assumed that no additional prior information is available about the source location. In subsequent iterations, the prior distributions are replaced to reflect the information gained from the previous sequence.

The likelihood function approximates the probability of the observed data $z_k(\mathbf{p}_k)$, given a hypothesised source parameter estimate Θ_k. A Poisson sensor model Eq. (4.3) is used as the likelihood function based on the discrete particle count sensor data:

$$p(z_k(\mathbf{p}_k)|\Theta_k) = \frac{(R\,(\mathbf{p}_k|\Theta_k)\,t_0)^{z_k(\mathbf{p}_k)}}{z_k(\mathbf{p}_k)!}e^{-R(\mathbf{p}_k|\Theta_k)t_0}, \tag{4.6}$$

where $R\,(\mathbf{p}_k|\Theta_k)$ is the inferred mean rate of particle encounters. The Bayesian estimation of source parameters is implemented recursively in the sequential Monte Carlo framework using a particle filter [196], which will be described in Section 4.4.

4.3.2 Decision making for mobile sensor control

The goal of sensor control is to choose the manoeuvre $\mathbf{a}_k^*$ from an admissible set of actions $\psi = \{\uparrow, \downarrow, \leftarrow, \rightarrow\}$, that is expected to yield the most information $E\mathscr{I}(a_k)$, as given:

$$\mathbf{a}_k^* = \arg\max_{\mathbf{a}_k \in \psi}\{\mathbb{E}[\mathscr{I}(a_k)]\}. \tag{4.7}$$

In Eq. (4.7), the expected information $\mathbb{E}[\mathscr{I}(a_k)]$ is defined from maximum entropy sampling principles as the manoeuvre to the position where the entropy of the predictive distribution is the greatest. This strategy is adapted from the literature on Bayesian

experimental design [181]. Note that, in the widely-used Infotaxis strategy, it was common to offer an option to remain at the current position [10, 55]. Adhering to the fundamentals of maximum entropy sampling, where we wish to sample from the position of the greatest level of uncertainty, this option has been removed.

In this work, the Shannon entropy $\mathscr{I}(\cdot)$ is used as the expected information measure, resulting in:

$$\mathbb{E}[\mathscr{I}(a_k)] = -\int p(\hat{z}_{k+1}(\mathbf{a}_k)|\mathbf{z}_{1:k}) \log p(\hat{z}_{k+1}(\mathbf{a}_k)|\mathbf{z}_{1:k}) \, \mathrm{d}\hat{z}_{k+1}, \tag{4.8}$$

where $\hat{z}_{k+1}(\mathbf{a}_k)$ refers to the unknown measurement at the potential sampling position $\mathbf{a}_k$. Until the manoeuvre is made, this data is unknown. The method applied to approximate Eq. (4.8) will be described in the decision making implementation in Section 4.4.

The sensor control strategy provides the full search algorithm under a single framework, which provides balanced exploration and exploitation by adapting to the state of the posterior pdf of the source parameters. The approach naturally moves towards the source location, as the posterior estimate becomes more certain.

4.4 Implementation

The Bayesian estimation of the source term parameters is estimated recursively in the sequential Monte Carlo framework using a particle filter. The output is an approximation of the posterior distribution $p(\Theta_k|\mathbf{z}_{1:k})$, which represents the current state of knowledge about the source parameters. Given the posterior distribution in the form of a weighted sample of particles (which shall be referred to as random samples to avoid confusion with emitted particles from the source), the integral in Eq. (4.8) can be approximated by posterior sampling so that the expected most informative manoeuvre can be selected.

4.4.1 Estimation

The conceptual estimation of source parameters is implemented using a particle filter. The posterior from Eq. (4.4) is approximated by a set of N weighted samples $\{(\Theta_k^{(i)}, w_k^{(i)})\}_{1\leq i\leq N}$, where $\Theta_k^{(i)}$ is a point estimate representing a potential source term and $w_k^{(i)}$ is its corresponding normalised weighting such that $\sum_{i=1}^{N} w_k^{(i)} = 1$. Given the weighted samples, the posterior distribution can be approximated as:

$$p(\Theta_k|\mathbf{z}_{1:k}) \approx \sum_{i=1}^{N} w_k^{(i)} \delta(\Theta - \Theta_k^{(i)}), \tag{4.9}$$

where $\delta(\cdot)$ is the Dirac delta function. The sample weights are updated in a recursive manner by sequential importance sampling. At each time step, a new sample $\Theta_k^{(i)}$ is drawn from the proposal distribution $q(\Theta_k^{(i)})$, which should resemble $p(\Theta_k|\mathbf{z}_{1:k})$. The

corresponding sample weights are then updated according to:

$$\bar{w}_k^{(i)} = w_{k-1}^{(i)} \cdot \frac{p(\Theta_k^{(i)}|\Theta_{k-1}^{(i)})p(z_k(\mathbf{p}_k)|\Theta_k^{(i)})}{q(\Theta_k^{(i)}|\Theta_{k-1}^{(i)}, z_k)}. \tag{4.10}$$

By assuming a time-invariant source term (i.e. the source position is fixed and the emission rate is constant), we can assume the proposal distribution is equal to the posterior at time $k-1$, i.e. $q(\Theta_k^{(i)}) = p(\Theta_{k-1}|\mathbf{z}_{1:k-1})$. This leads to a simple algorithm where $\Theta_k^{(i)} = \Theta_{k-1}^{(i)}$ for $i = 1, ..., N$ [55]. Due to cancellation of terms in Eq. (4.10), the un-normalised particle weights are updated using the likelihood function and the previous weight as follows:

$$\bar{w}_k^{(i)} = w_{k-1}^{(i)} \cdot p(z_k(\mathbf{p}_k)|\Theta_k^{(i)}). \tag{4.11}$$

We then normalise the sample weights $w_k^{(i)} = \bar{w}_k^{(i)} / \sum_{i=1}^{N} \bar{w}_k^{(i)}$ to obtain the new approximation of the posterior.

Importance sampling is carried out sequentially at each time step. To avoid sample degeneracy, the random samples are re-sampled when the number of effective point estimates falls below a pre-specified threshold η. To improve sample diversity, re-sampled estimates are subject to a Markov chain Monte Carlo move step [196].

4.4.2 Decision making for mobile sensor control

To solve Eq. (4.8) when the future measurement $\hat{z}_{k+1}$ is unknown, the probability of the expected number of particle encounters $p(\hat{z}_{k+1}(\mathbf{a}_k)|\mathbf{z}_{1:k})$ at position $\mathbf{a}_k$ can be approximated using the current posterior distribution of source parameters. In other words, the future measurement is predicted using the knowledge that is currently available about the source:

$$p(\hat{z}_{k+1}(\mathbf{a}_k)|\mathbf{z}_{1:k}) \approx \int p(\hat{z}_{k+1}(\mathbf{a}_k)|\Theta_k)p(\Theta_k|\mathbf{z}_{1:k})\,\mathrm{d}\Theta_k. \tag{4.12}$$

This integral can be solved using the weighted sample approximation of the posterior $\{(\Theta_k^{(i)}, w_k^{(i)})\}_{1 \leq i \leq N}$. The first term on the right hand side can be obtained using Eq. (4.6), by replacing the measured data with potential data at the new position. The second term is the corresponding normalized particle weight $\{w_k^{(i)}\}$, resulting in:

$$p(\hat{z}_{k+1}(\mathbf{a}_k)|\mathbf{z}_{1:k}) \approx \sum_{i=1}^{N} \frac{\left(R(\mathbf{a}_k|\Theta_k^{(i)})t_0\right)^{\hat{z}_{k+1}(\mathbf{a}_k)}}{\hat{z}_{k+1}(\mathbf{a}_k)!} e^{-R\left(\mathbf{p}_k|\Theta_k^{(i)}\right)t_0} \cdot w_k^{(i)}. \tag{4.13}$$

Substituting this into Eq. (4.8), the entropy of the predictive measurement distribution for the manoeuvre $E\mathscr{I}(a_k)$ can be approximated by a summation over all possible future

measurements $\hat{z}_{k+1} = \{0, 1, 2, ..., \hat{d}^{max}\}$:

$$\mathbb{E}[\mathscr{I}(a_k)] \approx \sum_{\hat{z}_{k+1}=0}^{\hat{d}^{max}} p(\hat{z}_{k+1}(\mathbf{a}_k)|\mathbf{z}_{1:k}) \log p(\hat{z}_{k+1}(\mathbf{a}_k)|\mathbf{z}_{1:k}). \tag{4.14}$$

The predictive entropy $E\mathscr{I}(a_k)$ is calculated for each manoeuvre of the set ψ, and the maximum is selected in accordance to Eq. (4.7). The complete Entrotaxis algorithm is described in Algorithm 2. The stopping criteria (step 16) of the search can be set with regards to the spread of the posterior distribution or a maximum number of search steps.

Algorithm 2 Entrotaxis

0: $k = 0$
0: SEARCH = 'ON'
1: **while** SEARCH = 'ON' **do**
2: $k = k + 1$
3: $z_k \leftarrow$ read new sensor measurement
4: $\{(\Theta_{k-1}^{(i)}, w_{k-1}^{(i)})\}_{1 \le i \le N} \rightarrow \{(\Theta_k^{(i)}, w_k^{(i)})\}_{1 \le i \le N}$ update particle filter
5: **for** all $\mathbf{a}_k \in \psi$ **do**
6: consider potential position $\mathbf{a}_k = (\hat{x}_{k+1}^{\mathbf{a}_k}, \hat{y}_{k+1}^{\mathbf{a}_k})$
7: **for** i = 1:N **do**
8: determine $R\left(\mathbf{a}_k|\Theta_k^{(i)}\right)$
9: **for** $j = 1 : d_{max}$ **do**
10: determine $p(\hat{z}_{k+1}(\mathbf{a}_k)|\mathbf{z}_{1:k})$ using Eq. (4.13)
11: **end for**
12: **end for**
13: calculate $\mathbb{E}[\mathscr{I}(a_k)]$ using Eq. (4.14)
14: **end for**
15: $\mathbf{a}_k^* = \arg\max\{\mathbb{E}[\mathscr{I}(a_k)]\} \leftarrow$ new manoeuvre
16: $(x_{k+1}, y_{k+1}) = (x_k, y_k) + \mathbf{a}_k^* \leftarrow$ new position $\mathbf{p}_{k+1}$
17: **if** STOPPING-CRITERIA reached **then**
18: SEARCH = 'OFF'
19: **end if**
20: **end while**

4.5 Numerical simulations

In this section, an example run of the Entrotaxis algorithm is provided in order to illustrate the estimation and decision making process of the searcher using simulated data to generate measurements. Monte Carlo simulations are then performed under various conditions to validate the performance of the Entrotaxis search strategy in comparison to the state of the art Infotaxis approach [55].

4.5.1 Illustrative run

An example of a typical search carried out by the algorithm at various simulations steps is shown in Fig. 4.3. Simulation parameters used to generate the example are as follows:

$x_s = 6$, $y_s = 6.67$, $q_s = 1$, $u = 1$, $r = 1$, $\tau = 250$, $\sigma = 1$, $N = 10,000$. Uniform priors were provided within reasonably large bounds for the source location and release rates: $\pi(X_0) = \pi(Y_0) = \mathcal{U}[0, 10]$ and $\pi(Q_0) = \mathcal{U}[0, 4]$. The searcher, starting from $[x_1\ y_1] = [0.67\ 1.67]$, began by moving in a cross wind direction. Upon detection an emitted particle, represented by a black cross on the red path, it was typical for the searcher to circulate around the nearby area. This behaviour, demonstrated in Fig. 4.3(b), can be considered rational because in very sparse conditions, the most likely source position will initially be where a particle is detected. Furthermore, observations have shown a similar search pattern commonly performed by the male silkworm moth [43]. Once the searcher has circulated the particle, in response to subsequent null sensor readings, it proceeds to search elsewhere for the source. This behaviour is conducted autonomously during decision making under the single Entrotaxis framework. The random samples approximating the posterior distribution of the source location are represented by the green dots and the sequence of figures illustrate how the spread of the samples is decreased throughout the search. This is achieved by updating the sample weightings in response to new data, in the form of sporadic cues of particle encounters with the sensor, and subsequently re-sampling with a focus around highly weighted areas. The histogram in Fig. 4.3(d) displays the final estimate of the release rate q_s.

4.5.2 Monte Carlo simulations

Monte Carlo simulations are run to compare the performance of the Entrotaxis and Infotaxis algorithms. The mathematical formulation of the Infotaxis algorithm is first described and the computational benefit of the Entrotaxis algorithm is assessed. The paths traversed by the algorithms are then briefly assessed and the search performance of the techniques under various conditions are evaluated with Monte Carlo simulations.

4.5.2.1 Infotaxis

The Infotaxis II reward is described as it was proposed in [55]. This algorithm was shown to perform marginally better than the original Infotaxis reward by removing bias towards the source. Following the estimation of source parameters, which is carried out using the particle filter as described in Section 4.4, the Infotaxis II reward selects the manoeuvre that is expected to minimise the entropy of the posterior distribution:

$$\mathbb{E}[\mathscr{I}(a_k)] = -\int p(\hat{z}_{k+1}(\mathbf{a}_k)|\Theta_k)\mathscr{I}(\Theta_{k+1}|\hat{z}_{k+1}(\mathbf{a}_k), \mathbf{z}_{1:k})\,\mathrm{d}\hat{z}_{k+1}, \tag{4.15}$$

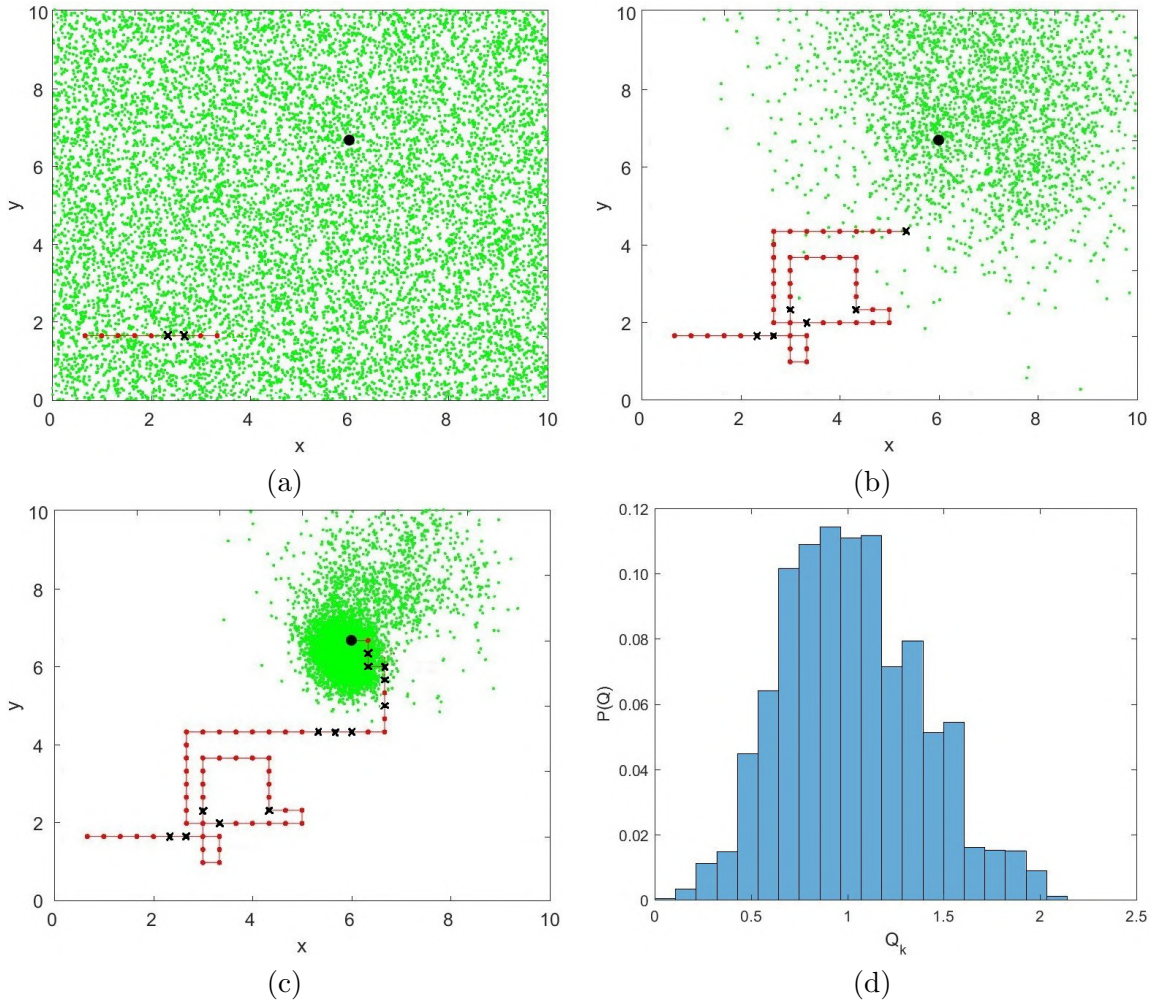

Figure 4.3: An illustrative run of the Entrotaxis algorithm at time steps: a) $k = 9$; b) $k = 41$; and c) $k = 71$. The histogram in d) displays the posterior estimate of the source release rate q_s at the end of the search. Simulation parameters are as follows: $[x_1\ y_1] = [0.67\ 1.67]$, $x_s = 6$, $y_s = 6.67$, $q_s = 1$, $u = 1$, $r = 1$, $\tau = 250$, $\sigma = 1$, $N = 10,000$. The true source location is indicated by a large black dot, green dots represent the random samples of the particle filter, the red line indicates the trajectory of the searcher, red dots indicate zero measurements and black crosses non-zero measurements.

where $\mathscr{I}(\Theta_{k+1}|\hat{z}_{k+1}, \mathbf{z}_{1:k})$ is the Shannon entropy of the expected posterior distribution given the hypothesised future measurement $\hat{z}_{k+1}$:

$$\begin{aligned}&\mathscr{I}(\Theta_{k+1}|\hat{z}_{k+1}(\mathbf{a}_k), \mathbf{z}_{1:k})\\ &= -\int p(\Theta_{k+1}|\hat{z}_{k+1}(\mathbf{a}_k), \mathbf{z}_{1:k}) \log p(\Theta_{k+1}|\hat{z}_{k+1}(\mathbf{a}_k), \mathbf{z}_{1:k})\, \mathrm{d}\Theta_k. \end{aligned} \tag{4.16}$$

The first term in Eq. (4.15) is the same as Eq. (4.12). The term $p(\Theta_{k+1}|\hat{z}_{k+1}, \mathbf{z}_{1:k})$ in Eq. (4.16) is solved by updating the current particle filter weightings $w_k^{(i)}$ to pseudo weights $\widehat{w}_{k+1}^{(i)}$, that would be produced in response to a hypothesised measurement $\hat{z}_{k+1}$. The overall expected reduction in posterior entropy is computed by a summation over all

possible future measurements $\hat{z}_{k+1} = \{0, 1, 2, ..., \hat{z}^{max}\}$:

$$\mathbb{E}[\mathscr{I}(a_k)] \approx \sum_{\hat{z}_{k+1}=0}^{\hat{z}^{max}} \sum_{i=1}^{N} p(\hat{z}_{k+1}(\mathbf{a}_k)|\Theta_k^{(i)}) \widehat{w}_{k+1}^{(i)} \log \widehat{w}_{k+1}^{(i)}. \tag{4.17}$$

In terms of computation, both algorithms see an increase in response to higher concentrations which, in turn, cause the value of $\hat{z}^{max}$ to increase. This is directly caused by the summation over potential measurements seen in both approaches Eqs. (4.14) and (4.17). For each potential measurement, Entrotaxis determines its corresponding probability, however Infotaxis must recompute the normalized posterior distribution, resulting in $2N|\psi|\hat{z}^{max}$ more operations, where $|\psi|$ is the cardinality of manoeuvres ψ. This is caused by extra operations in the innermost for loop of Algorithm 2. The result is 23% faster decision making made by the Entrotaxis algorithm whilst running on an Intel(R) Core(TM) i7-6700HQ 2.60GHz CPU.

4.5.2.2 Results

Typical search paths of the Entrotaxis and Infotaxis algorithms searching for a source of various release rates are shown in Fig. 4.4. The results after 100 Monte Carlo simulations for several values of release rate are provided in Table 4.1. The results indicate both approaches are adversely affected by weak sensing conditions, however, the Entrotaxis reward performs better in terms of the mean search time (MST). This is supported by the figures which display a more efficient path. The longer MST of the Infotaxis algorithm is due to its tendency to trace the domain boundary. Meanwhile, Entrotaxis would alter its search path sooner in response to the sensory cues. The increase in search time is caused by the larger ratio between the search area and the sensing area as reported in [55]. Essentially, the searcher spends much more time observing null sensor measurements, which are less informative than positive readings.

Table 4.1: Performance comparison for different values of release rate q_s for 100 Monte Carlo simulations. (SR = success rate [%]; MST = mean search time [number of measurements])

q_s	0.1	0.2	0.5	1	2	4
Entrotaxis						
SR	100	99	100	99	100	100
MST	196	140	96	79	62	49
Infotaxis II						
SR	100	99	100	100	100	99
MST	273	187	129	105	81	67

The algorithm's performance under various mean wind velocity u conditions were also analysed as subject to constant release rate $q_s = 2$. Typical search paths executed by Entrotaxis and Infotaxis are shown in Fig. 4.5, accompanied by Table 4.2 to summarise the

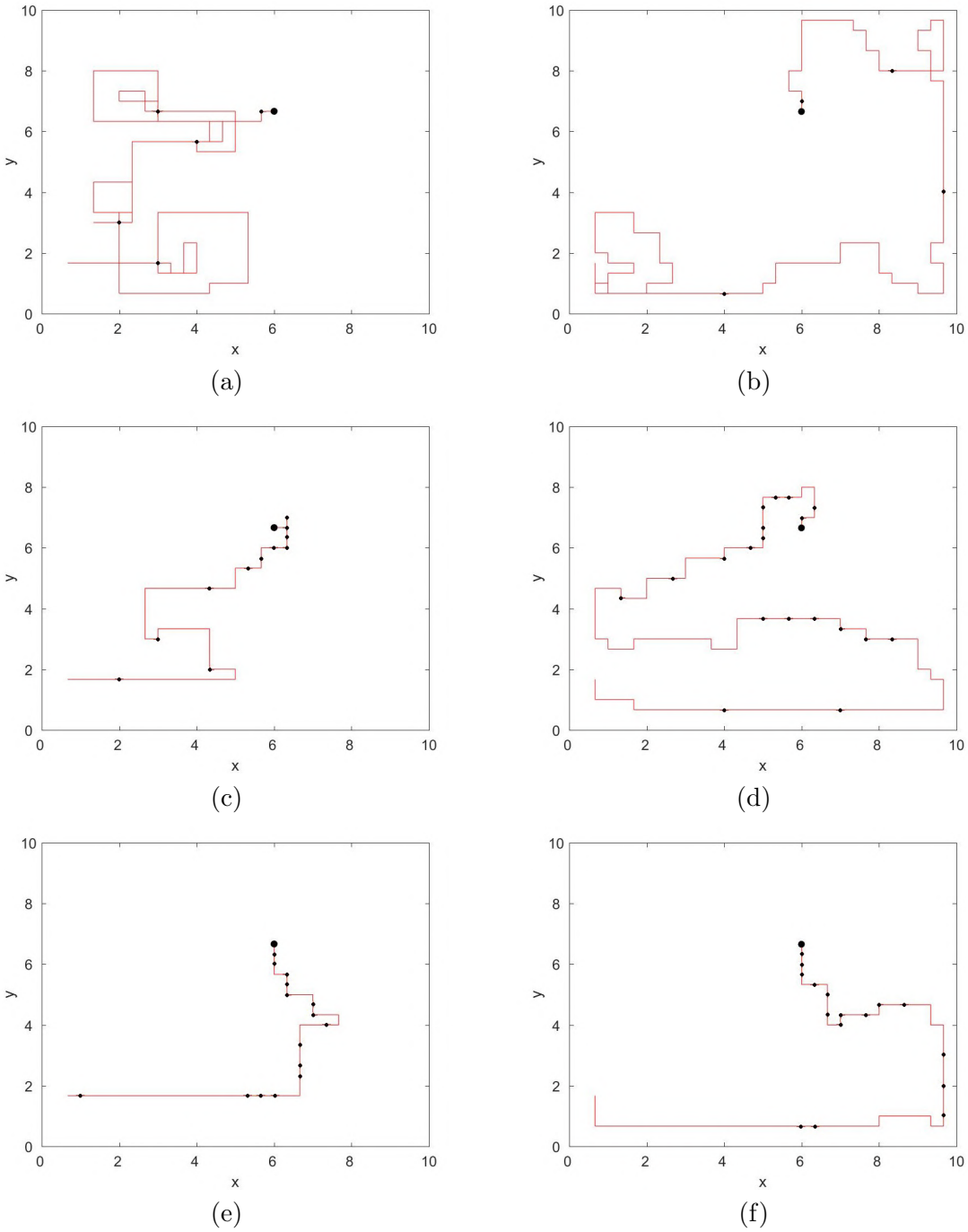

Figure 4.4: Search paths of Entrotaxis (left) and Infotaxis (right) strategies subject to various release rates: a,b) $q_s = 0.2$; c,d) $q_s = 1$; e,f) $q_s = 2$.

search performance. The table demonstrates the performance benefits of the Entrotaxis algorithm in low wind conditions, particularly as u goes to zero. The Infotaxis algorithm shows consistent performance improvements in response to increasing wind speeds, as was also observed by Ristic et al. [55].

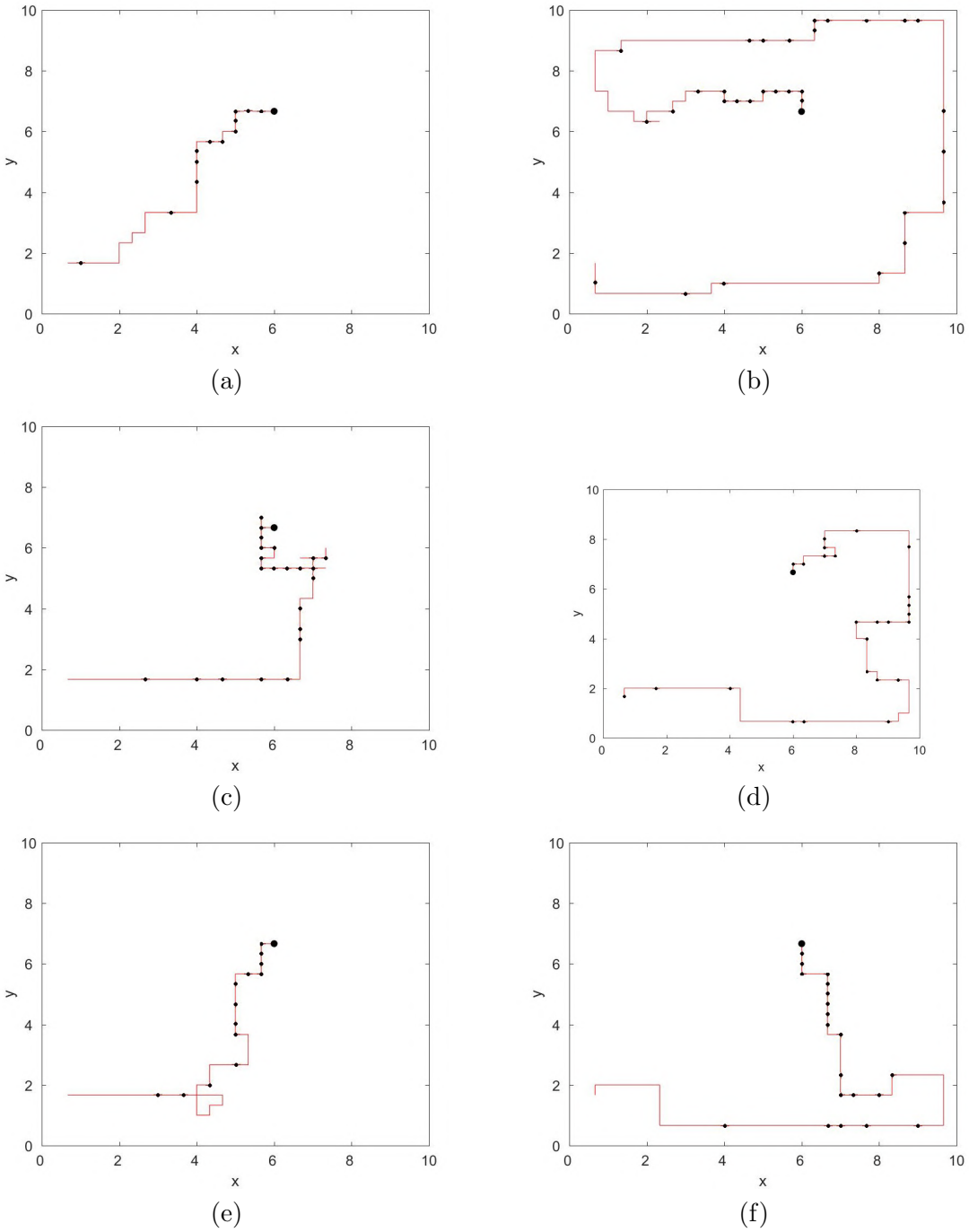

Figure 4.5: Search paths of Entrotaxis (left) and Infotaxis (right) strategies subject to various wind velocities: a,b) $u = 0$; c,d) $u = 0.5$; e,f) $u = 1.5$.

Thus far, the search strategies have considered favourable initial conditions, (with regards to searcher position in relation to the source and the bounds of the domain) where the searcher would start downwind of the source which is positioned near the upwind

Table 4.2: Search performance for different values of wind velocity u for 100 Monte Carlo simulations. (SR = success rate [%]; MST = mean search time [number of measurements])

v	0	0.25	0.5	1	1.5
Entrotaxis					
SR	100	100	99	100	99
MST	50	56	58	57	54
Infotaxis II					
SR	100	100	99	100	100
MST	103	99	87	79	75

centre of the domain. These assumptions are not valid for most scenarios seen by humans or in the natural world. In Table 4.3, we display Monte Carlo search results for various release rate q_s and wind velocity u combinations, where the source location and searcher starting locations are generated randomly within the domain, i.e. $[x_1\ y_1\ x_s\ y_s] = \mathcal{U}[0\ 10]$. The remaining parameters are set to the same values as Fig. 4.1.

The results in Table 4.3 follow a similar trend to Tables 4.1 and 4.2. Both algorithms performed worse in the low release rate conditions. The Infotaxis approach saw a significant improvement in performance in response to increased wind velocity and release rate, although Entrotaxis still had a more rapid MST. In most cases, the MST for both algorithms was lower than previous tables; however, this was expected, as most often the starting positions of the source and searcher would be closer together.

Table 4.3: Performance comparison with random starting and source positions. The results after 500 Monte Carlo simulations are shown for various release rate q_s and wind velocity u combinations.(SR = success rate [%]; MST = mean search time [number of measurements])

q_s	0.1	0.1	0.5	0.5	1	1	2	2
u	0	1	0	1	0	1	0	1
Entrotaxis								
SR	100	100	100	100	99.4	99.8	100	99.4
MST	197	180	92	73	68	59	58	50
Infotaxis II								
SR	100	100	99.6	99.6	99.2	99.8	100	99.8
MST	235	237	133	114	101	82	81	66

4.6 Experimental results

The Entrotaxis strategy is tested using an experimental dataset which was supplied by the DST Group [55]. The dataset was collected by the COANDA Research and Development Corporation using a large recirculating water channel. Fluoresceine dye was released at a constant rate from a narrow tube at the upwind end of the tunnel. Observations of the concentration of dye were obtained by using laser induced fluorescence. The dataset

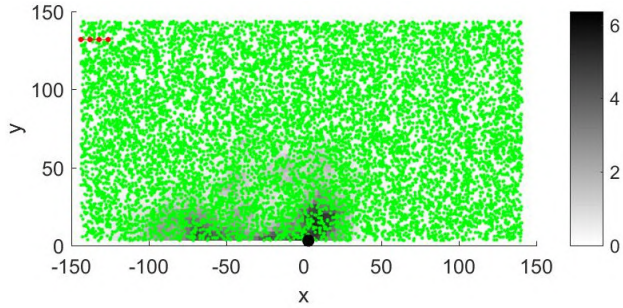

(a)

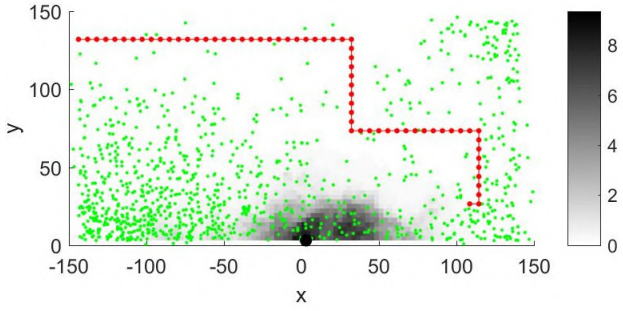

(b)

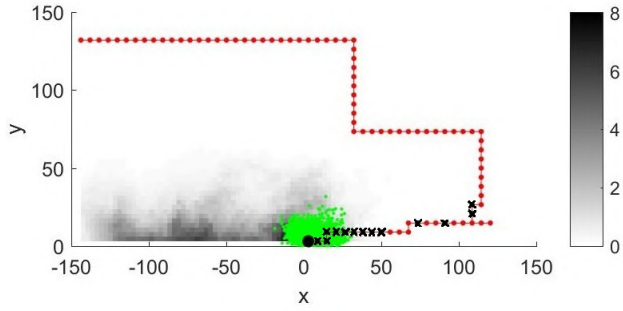

(c)

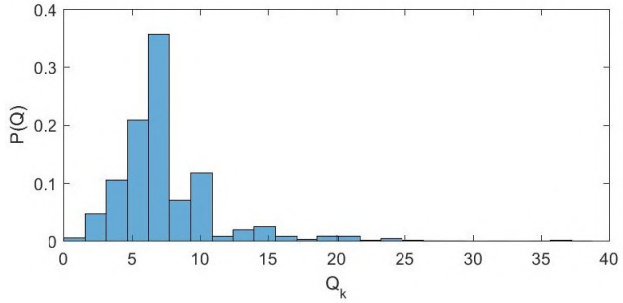

(d)

Figure 4.6: An illustrative run of the Entrotaxis algorithm at time steps: a) $k = 4$; b) $k = 64$; and c) $k = 90$ using the experimental dataset. The histogram in d) displays the posterior estimate of the source release rate Q_k at the end of the search. Simulation parameters are as follows: $[x_1\ y_1] = [0.67\ 1.67]$, $x_s = y_s = 2.935$, $u = 0$, $r = 2.935$, $\lambda = \sqrt{1000}$, $N = 10,000$. The true source location is indicated by a large black dot, green dots represent the random samples of the estimation algorithm, the red line indicates the trajectory of the searcher, red dots indicate zero measurements and black crosses non-zero measurements. The greyscale shading depicts the instantaneous concentration field at the current time step.

consists of a sequence of frames denoting the instantaneous concentration field in the vertical plane. Each frame consisted of 49×98 pixels, where each pixel corresponds to a $2.935 \times 2.935mm^2$ area. The nearest integer of a pixel was taken as the number of particle encounters with the sensor at the corresponding position and time. At each time step, the searcher would move to a neighbouring pixel to make an observation. We present a typical run of the Entrotaxis algorithm using the experimental dataset in Fig. 4.6. The source, located at $[x_s\ y_s] = [2.935\ 2.935]$, is represented by a large black dot. The greyscale shading depicts the instantaneous concentration field at the current time step k, and the histogram in Fig. 4.6(d) displays the posterior distribution of the source release rate q_k at the end of the search. The pdf for the release rate using the experimental dataset is of sometimes multimodel, however in the simulated scenarios (Fig. 4.3(d)) it is monomodal. This is caused by unforeseen mismatches between the modelling and the experimental dataset which can cause multiple modes.

The performance of Entrotaxis is assessed against the Infotaxis II algorithm on the experimental dataset using 200 Monte Carlo runs. Simulation parameters used in [55] are adopted (including a two dimensional version of the rate of encounters to replace Eq. (4.1)) as follows: $[x_1\ y_1] = [0.67\ 1.67]$, $x_s = y_s = 2.935$, $u = 0$, $r = 2.935$, $\lambda = \sqrt{1000}$, $N = 10,000$. During the Monte Carlo simulations a search is terminated if the spread of the posterior approximation falls below 5, the searcher lands on the source, or if the number of time steps k exceeds 1000. A search is considered successful if the distance between the estimated source position and the true source position is less than 10. Table. 4.4 compares the success rate (SR) and mean search time (MST) of the Entrotaxis and Infotaxis algorithms subject to various prior distributions for the release rate of the source $\pi(q_0)$. The prior distributions assessed include log-normal $\mathcal{L}(m, \sigma^2)$, uniform $\mathcal{U}(min, max)$ and normal $\mathcal{N}(m, \sigma^2)$ distributions. The table is ordered so that the more favourable priors are on the right hand side.

Whilst there is little difference in the SR of the approaches, the Entrotaxis approach has a faster MST for all the prior distributions. Under the more accurate normally distributed prior on the release rate, both strategies have a considerable reduction in the MST; this is caused by the overall larger prior on the release rate, leading both approaches to alter the search path further from the edge of the domain. The experimental results support the previous findings of Table 4.2, where Entrotaxis was the most successful strategy in low wind conditions. However, as the source was located very near to the edge of the domain, this was also favourable to the typical trajectories of Infotaxis shown in Figs. 4.5(b) and 4.5(d). The experimental results using the Infotaxis algorithm are noticeably different to those reported in [55]. This is expected to be caused by small differences in data processing, algorithm implementation and in the simulation parameters.

Table 4.4: Monte Carlo results using the experimental dataset after 200 runs with various prior distributions for the release rate. (SR = success rate [%]; MST = mean search time [number of measurements])

Method	$\mathcal{L}(1, 1.2)$	$\mathcal{U}(0, 20)$	$\mathcal{N}(7, 2)$
Entrotaxis			
SR	98	99	99.5
MST	93	93	76
Infotaxis			
SR	99	98.5	99
MST	101	96	80

4.7 Chapter summary

The Entrotaxis algorithm has been proposed to perform an autonomous search and reconstruction (i.e. STE) of a source emitting hazardous particles at an unknown, albeit minor, rate, in turbulent conditions. The ABMP method presented in the previous chapter was extended to perform STE using the recursive algorithm, sequential Monte Carlo, rather than the previous batch method. The Bayesian estimation algorithm was reformulated to consider discrete measurements from a particle count sensor, taking into account the large amount of non detections caused by the weak source and turbulent conditions. After demonstrating the benefit of an informative planning algorithm against conventional methods in the previous chapter, the method was compared with the current state of the art method, Infotaxis. The search characteristics of the Entrotaxis and Infotaxis algorithms were compared in simulations subject to various conditions. The observed search behaviour of the Entrotaxis algorithm supported its superior performance in Monte Carlo simulations. In addition, the methods were tested using experimental data collected from releasing dye into a water channel, the closest to real conditions that a STE algorithm incorporating a a mobile sensor had been assessed at the time. Overall, the results identified similar levels of performance between the Entrotaxis and Infotaxis algorithms in terms of the success rate of the algorithms, however, favourable conditions were observed for both approaches, with regards to achieving a faster mean search time. Entrotaxis performed better in most of our simulations, especially when subject to low winds or strong release rates. There was less difference in the mean search time of the strategies using the experimental data, where the source was located near to the domain edge, arguably a favourable position for the Infotaxis algorithm. Overall, the Entrotaxis approach typically located the source more rapidly than Infotaxis in our numerical simulations, using a less computationally demanding reward function and without degrading the rate of success. The Entrotaxis strategy is envisaged to be effective in several search scenarios where a model of the information source can be provided, such as tracking a ground target using a UAV, or other inverse problems involving data collection with a mobile sensor.

This chapter presented three main outcomes: an extension of the Information based search and STE algorithm to more sparse conditions whilst considering measurements from a particle count sensor; a comparison with the state of the art method in the literature; and tests in a more realistic scenario using an experimental dataset. The next step is to test the system using a real source and a sensor equipped autonomous unmanned vehicle. This task has not been achieved before, so several extensions will be required to facilitate successful experiments - such extensions and experiments are presented in the next chapter.

Chapter 5

Information based search for an atmospheric release using a mobile robot

In the previous chapter the information based search and STE algorithm was extended to perform the estimation of the source parameters in a more efficient manner by using a recursive algorithm. A more computationally efficient path planning algorithm was also developed. The developed STE method, named Entrotaxis, was compared with the current state of the art in the literature, the Infotaxis algorithm. After demonstrating the strong performance of the algorithm in simulations and on an experimental dataset, the next stage is to test the system using a real source and sensor. The real challenge of STE and search can be difficult to create in simulations and using datasets. Due to the difficulties in modelling the random nature of turbulence, the sensor response, and interactions the robot may have on the dispersion of HAZMAT.

This chapter presents developments on the previous work to enable successful experiments using a real mobile robot equipped with a low cost atmospheric concentration sensor, and a real dispersive source. In a similar manner to previous work in this thesis - a joint Bayesian estimation and search planning algorithm is used to guide the sensor equipped, mobile robot to collect informative measurements, allowing the parameters of a dispersive source to be estimated quickly and accurately. The work is extended in several areas to facilitate the successful experiments, for example, the Bayesian estimation is augmented to account for uncertainties in all of the parameters of the dispersion model, by inputting them as pdfs and a novel likelihood function is developed to address the intermittent, noisy readings from the low-cost gas sensor. Subsequently, this chapter presents the first experimental result of STE performed using a mobile robot in turbulent, diffusive conditions with a real sensor. The experiments used smoke from burning incense sticks to simulate a HAZMAT release, and electric fans to generate a turbulent wind field in the indoor test arena. A ground robot was equipped with a low-cost, metal oxide gas sensor

which responded to the smoke concentration. The experimental results demonstrated the effectiveness of the proposed estimation and search algorithm for STE using a mobile robot and a low-cost sensor.

The contents of this chapter can be summarised by several technical contributions that complement and facilitate one larger, more sincere, practical contribution. The latter is the fact that, to the best of the authors knowledge, this chapter reports the first online experimental STE results obtained using robot cognitive search in realistic conditions, which paves the way of deploying this algorithm in response to an accidental release or attack of HAZMAT into atmosphere. Technical contributions that facilitated this are as follows:

1. Inspired by the literature on source term estimation [2] (and after the literature review conducted in Chapter 2), an information based search algorithm is developed to accommodate the uncertainty in all dispersion parameters of the release, with key ones being the wind speed, direction and the diffusivity;

2. The sensor model used in the algorithm is extended from discrete particle encounter measurements (see e.g. [55]) to the continuous space of a low-cost sensor. More importantly, a novel likelihood function is designed to accommodate the intermittent reading of the low-cost sensor;

3. A modified dispersion model is also used to cater for an uncalibrated metal oxide sensor, to reflect an expected voltage reading instead of concentration. This is an important step, as calibration of metal oxide sensors is difficult and affected by numerous factors such as temperature, humidity and composition of the environment and the material of interest [197];

4. This is the first experimental study of a information based search that does not use a thermal source or assume the strength is of a known quantity, such that the release is turbulent and the meteorological conditions are inconsistent;

Finally, the overall experimental set-up is simple but effective, using inexpensive sensors and a safe, easily accessible source. It is hoped that this will benefit future source estimation researchers enabling quick development and testing of algorithms outside of simulations.

This chapter is based upon work that has been published by the author in [198]. The remainder of the chapter is organised as follows. First, more related work, specifically involving experimental validation of source localisation or STE algorithms, are reviewed in Section 5.1. A formal description of the problem addressed in this chapter is given in Section 5.2. In Section 5.3, the methodology is described, including the conceptual search solution, modelling required to implement the conceptual solution and the sequential Bayesian implementation. Section 5.4 outlines the experiment set-up and describes the robot searcher and the sensing environment. An illustrative run and numerical results

of the experiments are presented in Section 5.5. Finally, conclusions and future work are given in Section 5.6.

5.1 Related work

Autonomous search, with the goals of localising chemical leaks, sources of odour, or further understanding search patterns observed in nature, has been a popular subject of research for some time. Search is a quotidian task for animals during foraging, hunting or finding a mate. Due to the large amount of applications in nature and the extremely efficient and successful searches observed, many search algorithms have been biologically inspired. Most biologically inspired search strategies can be regarded as reactive, where observations trigger predefined movement sequences to localise a source [41, 53]. Alternatively, approaches have been developed based on a fusion of probabilistic and information theoretic principles, otherwise known as cognitive strategies [55]. Recent cognitive search strategies make decisions on-line, formulated as a POMDP [193]. The POMDP framework utilises state, action and reward. For the problem in this thesis, the state refers to the current knowledge about the source, the actions are potential future measurement locations and the reward is a quantity to describe the gain in information supplied by the corresponding action. Infotaxis is a cognitive search strategy proposed to be effective in the sparse sensing conditions where gradient based approaches would be unsuitable [10]. Assuming environmental parameters and the source strength were known, Bayes' rule was applied to update a probabilistic map of source location throughout the search, in response to sparse sensory cues in the form of particle encounters with a sensor [48]. Considering only one-step-ahead manoeuvres on a square lattice, the most informative actions were selected based on minimizing the expected entropy of the posterior distribution, with an adaptive term to bias the searcher's movements towards the source as levels of uncertainty were reduced. The strategy showed robustness to significantly sparse conditions and has thus inspired several studies proposing modifications and extensions [199, 194, 195].

A critical extension of the algorithm was its implementation in the sequential Monte Carlo framework, using a particle filter, alleviating its grid based implementation and allowing the source strength to be included in the parameter space [55]. This was essentially estimating the source term of the release. In the paper, the focus was on removing the assumption that the strength was known, so few details on the performance of the strength estimate were provided. Other strategies to perform source estimation with a mobile sensor include a genetic algorithm with an expert system for sensor planning [166], and MCMC sampling after a predefined sweeping path [167]. The information based probabilistic approaches are preferred in this thesis as they take into account the utility of the next measurement when making manoeuvre decisions. In simulations and on experimental datasets based studies, information based search planning strategies have been shown to outperform conventional approaches such as a uniform sweep [172]. However, experimental

results of STE performed on-line using a mobile sensor are yet to be found. Besides simulated data, previous work has used experimental datasets, whereby the artificial searcher could move to neighbouring locations to take a new measurement. This was done on a dataset collected in a turbulent water channel and for a radiological dataset [172, 55].

Note that there have been several source localisation experiments, rather than STE, that have been carried out in the past (see e.g.[36] and Section 2.2). These methods did not estimate important parameters of the release, such as its strength, and the robots were generally initiated downwind of the source within the dispersion. Furthermore, the experiments would typically use a constant and uniform wind flow, generated within a wind tunnel, creating a well defined plume; conditions which are rare in more realistic scenarios. There have been a few instances where localisation of the source has been demonstrated in more turbulent conditions, for example: particle filter based algorithms have been used in outdoor environments to locate a source of airborne material using metal oxide sensors [20, 32, 200]. To date, cognitive or information based search experiments are normally based on a thermal source with smooth dispersion, as opposed to turbulent airborne materials, and they have assumed known dispersion parameters and source strengths [201, 199, 53]. To this end, this chapter marks the first online implementation of an cognitive, or information based, search for STE using a mobile sensor, where both the location and parameters of the release are unknown.

5.2 Problem formulation

In this chapter, a ground robot is used without the ability to fly, therefore, the search for the HAZMAT source is considered in 2 dimensions.

Consider a flat rectangular search area $\Omega \subset \mathbb{R}^2$ that is expected to contain a hazardous release. A robot equipped with a metal oxide gas sensor is to navigate within the area to estimate the release parameters otherwise known as the source term. This shall provide the necessary inputs to an ATD model to produce a forecast of the hazard. For simplicity, it is assumed that at time index k the robot is aware of its own location $\mathbf{p}_k = \begin{bmatrix} x_k & y_k \end{bmatrix}^\mathsf{T} \in \Omega$ within the area. In practice, this can be achieved by using a GPS or a simultaneous localisation and mapping (SLAM) system.

The hazardous sensor outputs a continuous reading $z \in \mathbb{R}^+$ that can be related to the concentration of hazardous material in the air. This information can be used to predict the parameters of the source, i.e. the source term. The source term can include several parameters that depend on the type of release and the models used to forecast the dispersion. In this chapter, the source term is expanded to consider uncertainties in the source and the dispersion parameters. The source term is parametrised by:

- Cartesian coordinates of the source $\mathbf{p}_s = \begin{bmatrix} x_s & y_s \end{bmatrix}^\mathsf{T} \in \Omega$ in meters (m).
- Release rate/strength of the source $q_s \in \mathbb{R}^+$ in grams per second (g/s).

- The wind speed $u_s \in \mathbb{R}^+$ in meters per second (m/s) and direction $\phi_s \in \mathbb{R}$ in radians (rad).
- Diffusivity of the hazard in air $d_s \in \mathbb{R}^+$ in meters squared per second (m^2/s).
- Lifetime of the emitted material $\tau_s \in \mathbb{R}^+$ in seconds (s).

Hence, the parameter vector of the source term can be defined as:

$$\Theta_k = \begin{bmatrix} \mathbf{p}_s^\mathsf{T} & q_s & u_s & \phi_s & d_s & \tau_s \end{bmatrix}^\mathsf{T}. \tag{5.1}$$

The robot is to autonomously search the environment, collecting point observations $\mathbf{z}_{1:k} = \{z_1, \ldots, z_k\}$ from the hazardous sensor at discrete time steps $k = 1, \ldots, k$ and at known locations $\mathbf{p}_{1:k} = \{\mathbf{p}_1, \ldots, \mathbf{p}_k\}$. At each time step k, the robot updates its estimates of the source parameters Θ_k by drawing the inference on the probabilistic distribution $p(\Theta_k|\mathbf{z}_{1:k})$, and then chooses the next location $\mathbf{p}_{k+1}$ to make the next observation with the hazardous sensor by taking an action $\mathbf{a}_k$, such that $\mathbf{p}_{k+1} = \mathbf{p}_k + \mathbf{a}_k$. Note that the action $\mathbf{a}_k$ can be more generic than one step manoeuvres.

5.3 Methodology

To solve the formulated problem more efficiently, the goal is to navigate the robot to the most informative data collection locations so that the estimation of the source term can be performed more rapidly and accurately. The developed solution in this chapter is twofold. First, Bayes' theorem is used to update posterior density estimates of the source parameters and uncertain dispersion variables in response to the new sensor data. Secondly, an information based reward is derived to choose the next position to collect sensor data; that is expected to provide the most information given the current posterior results. In this section, the autonomous search and estimation algorithm is described; that is used to guide the robot to search for and estimate the parameters of a hazardous release. The proposed solution is outlined first, which explains further the framework of the approach, followed by descriptions of the models and assumptions required to implement the solution and then its algorithmic implementation.

5.3.1 Proposed solution

This subsection describes the autonomous search and estimation algorithm used to guide a robot to localise and reconstruct a source of hazardous material characterised by the unknown source term vector Θ_k. The key variables of the source to be identified are its location $\mathbf{p}_s$ and release rate q_s. The remaining parameters include the wind speed u_s, wind direction ϕ_s, diffusivity d_s and the average lifetime of the hazardous material τ_s. It is assumed that a good prior can be provided for those parameters but they are still included in the state vector to account for uncertainties. The robot, located at $\mathbf{p}_k$ at time step k

and equipped with the gas sensor, is to navigate the environment collecting measurements in the form of voltage readings relative to the hazard $z_k \in \mathbb{R}_{0 \leq z \leq 5}$. At each time step the robot will choose from the admissible set of actions $\Psi = \{\uparrow, \downarrow, \leftarrow, \rightarrow\}$, the move $\mathbf{a}_k^* \in \Psi$ that is expected to yield the most information. The most informative action is derived as an information based reward, inspired by the literature on optimal experiment design.

5.3.1.1 Estimation

A probabilistic framework is used to estimate the source parameters in response to large uncertainties in the observed data, in the form of a voltage reading from an uncalibrated sensor. The current state of knowledge regarding the source parameters is represented by a posterior probability distribution $p(\Theta_k|\mathbf{z}_{1:k})$, where $\mathbf{z}_{1:k}$ implies that the measurement data are collected at locations $\mathbf{p}_{1:k}$, respectively. The posterior distribution is subsequently updated according to Bayes' rule in response to new sensor data z_{k+1}, such that

$$p(\Theta_{k+1}|\mathbf{z}_{1:k+1}) = \frac{p(z_{k+1}|\Theta_{k+1})p(\Theta_{k+1}|\mathbf{z}_{1:k})}{p(z_{k+1}|\mathbf{z}_{1:k})} \tag{5.2}$$

where

$$p(z_{k+1}|\mathbf{z}_{1:k}) = \int p(z_{k+1}|\Theta_{k+1})p(\Theta_{k+1}|\mathbf{z}_{1:k})\,\mathrm{d}\Theta_{k+1}. \tag{5.3}$$

The initial prior distributions $\pi(\Theta_0) \equiv p(\Theta_0)$ of the source parameters are assumed to be given, these can be provided autonomously through sensory data or by user input. If information concerning the source term is available prior to the search, it can be exploited through an appropriate distribution to represent the prior knowledge known about the release. However, in the absence of information, the prior can be set to an uninformative distribution. For example, the prior distribution for the location of the source is a uniform distribution that is bounded by the domain Ω. In this Bayesian inference framework, it is also assumed that the source term is constant, i.e. $\Theta_{k+1} = \Theta_k$, which implies $p(\Theta_{k+1}|\mathbf{z}_{1:k}) = p(\Theta_k|\mathbf{z}_{1:k})$. In subsequent iterations, the prior distributions are replaced by the posteriors to reflect the information gained from the previous sequence.

5.3.1.2 Sensor planning

The goal of the robot path planning is to choose the manoeuvre $\mathbf{a}_k^*$ from an admissible set of actions $\Psi_k = \{\uparrow, \downarrow, \leftarrow, \rightarrow\}$, that is expected to be the most informative. The reward function for sensor planning is inspired by the literature on optimal experiment design [202], where it is referred to as the utility function $\Upsilon(z_{k+1}(\mathbf{a}_k))$. This is used to capture the information gain on the estimate of Θ_k given the next sensor data z_{k+1} after taking the action $\mathbf{a}_k$. Different utility functions can be adopted. Since the future measurement z_{k+1} is generally unknown, it is suggested that the optimal design of an experiment should be the one that maximises the expected utility of the subsequent measurement $\mathbb{E}[\Upsilon(\hat{z}_{k+1}(\mathbf{a}_k))]$, where the expectation is calculated with respect to the hypothetical future measurement

$\hat{z}_{k+1}$. The experimental design problem is adapted to direct a mobile sensor, where the choice of the next experiment is synonymous with the movement of the sensor. The maximization problem can be written as:

$$\mathbf{a}_k^* = \arg\max_{\mathbf{a}_k \in \Psi} \mathbb{E}\left[\Upsilon(\hat{z}_{k+1}(\mathbf{a}_k))\right]. \tag{5.4}$$

The expected utility of manoeuvre $\mathbf{a}_k$ can be further expressed as an integral based on the probability of a future measurement $\hat{z}_{k+1}(\mathbf{a}_k)$ and its corresponding utility $\Upsilon(\hat{z}_{k+1}(\mathbf{a}_k))$:

$$\mathbb{E}[\Upsilon(\hat{z}_{k+1}(\mathbf{a}_k))] = \int_{\hat{z}_{k+1}\in\mathcal{Z}} p(\hat{z}_{k+1}(\mathbf{a}_k)|\mathbf{z}_{1:k})\Upsilon(\hat{z}_{k+1}(\mathbf{a}_k))\, \mathrm{d}\hat{z}_{k+1}, \tag{5.5}$$

where $\mathcal{Z}$ is the range of the possible future measurement at the future sampling position. In this chapter, the utility of the manoeuvre $\mathbf{a}_k$ is defined as the Kullback-Leibler divergence between the predicted source term distributions before and after the measurement $\hat{z}_{k+1}(\mathbf{a}_k)$ being taken into account, i.e. between the distributions $p(\Theta_{k+1}|\mathbf{z}_{1:k})$ and $p(\Theta_{k+1}|\mathbf{z}_{1:k}, \hat{z}_{k+1}(\mathbf{a}_k))$. Thus, the utility function is defined as

$$\begin{aligned}\Upsilon(\mathbf{a}_k, \hat{z}_{k+1}) =& D_{KL}\left(p(\Theta_{k+1}|\mathbf{z}_{1:k}, \hat{z}_{k+1}(\mathbf{a}_k))||p(\Theta_{k+1}|\mathbf{z}_{1:k})\right) \\ =& \int_{\Theta_{k+1}} p(\Theta_{k+1}|\mathbf{z}_{1:k}, \hat{z}_{k+1}(\mathbf{a}_k)) \times \ln \frac{p(\Theta_{k+1}|\mathbf{z}_{1:k}, \hat{z}_{k+1}(\mathbf{a}_k))}{p(\Theta_{k+1}|\mathbf{z}_{1:k})}\, \mathrm{d}\Theta_{k+1}.\end{aligned} \tag{5.6}$$

Combining eq. (5.5) and eq. (5.6) leads to the following expression for the reward function

$$\begin{aligned}\mathbb{E}[\Upsilon(\mathbf{a}_k, \hat{z}_{k+1})] = \int_{\hat{z}_{k+1}} p(\hat{z}_{k+1}(\mathbf{a}_k)|\mathbf{z}_{1:k}) \int_{\Theta_{k+1}} & p(\Theta_{k+1}|\mathbf{z}_{1:k}, \hat{z}_{k+1}(\mathbf{a}_k)) \\ & \times \ln \frac{p(\Theta_{k+1}|\mathbf{z}_{1:k}, \hat{z}_{k+1}(\mathbf{a}_k))}{p(\Theta_{k+1}|\mathbf{z}_{1:k})}\, \mathrm{d}\Theta_{k+1}\, \mathrm{d}\hat{z}_{k+1}.\end{aligned} \tag{5.7}$$

The method applied to approximate Eq. (5.7) is described in the sequential Bayesian implementation section.

The sensor control strategy provides the full search algorithm under a single framework, which provides balanced exploration and exploitation by adapting to the state of the posterior density estimates of the source parameters. This is characterised by more explorative behaviour when the posterior distributions have a wide spread and are uninformative, and exploitative behaviour, directed towards the source, as the posterior distributions become more informative. The approach naturally moves towards the source location, as the posterior estimate becomes more certain.

5.3.2 Modelling

One of the great benefits and influencing factors of using Bayes' theorem is the ability to approach the problem from a probabilistic perspective, where variables and models can be given distributions to represent their level of certainty. In this subsection, the models

used for the gas sensor measurement and estimated observations from a dispersion model are derived and then combined to form the likelihood function used in Eq (5.2).

5.3.2.1 Dispersion model

To construct the likelihood function $p(z_{k+1}|\Theta_{k+1})$ used in Eq.((5.2)), there must be a method of linking sensor measurements z_k with the expected observations. To do this, a model of dispersion is required, which will provide the expected concentration at position $\mathbf{p}_k$ produced from a hypothesised source with parameters Θ_k. Any relevant model can be used; there exist highly complex particle tracking models, computational fluid dynamics techniques or equations derived from analytical solutions to the advection-diffusion equations such as the Gaussian plume dispersion model. The model is interchangeable without any other changes to the algorithm, and should be chosen to reflect the current scenario. For example, the NAME dispersion model is used by the UK Met Office to forecast long range ash dispersion from a volcanic eruption [68], whereas CFD based methods have been developed for complex geometries such as urban environments [134, 203]. In this chapter, a particular solution to the advection-diffusion equation is adopted from [10]. This is a simplified equation based on atmospheric statistics assuming homogeneous diffusion and a constant mean wind direction and speed. Although other approaches may be more accurate, this model is chosen as it is very fast running and expected to be useful in turbulent short-range conditions. The expected concentration to be read by a sensor at position $\mathbf{p}_k$ from a source at position $\mathbf{p}_s$, releasing gas at a rate of q_s with average lifetime τ_s in an environment with mean wind speed u_s, wind direction ϕ_s and diffusivity d_s is given by:

$$C\left(\mathbf{p}_k|\Theta_k\right) = \frac{q_s}{4\pi d_s||\mathbf{p}_k - \mathbf{p}_s||} \exp\left[\frac{-||\mathbf{p}_k - \mathbf{p}_s||}{\lambda}\right] \times \exp\left[\frac{-(x_k - x_s)u_s\cos\phi_s}{2d_s}\right] \exp\left[\frac{-(y_k - y_s)u_s\sin\phi_s}{2d_s}\right], \quad (5.8)$$

where

$$\lambda = \sqrt{\frac{d_s\tau_s}{1 + (u_s^2\tau_s)/(4d_s)}}. \quad (5.9)$$

An example of the modelled plume is given in Fig 5.1 where the sensor model to be described in the following section has been applied. From Eq (5.8), the state vector of the unknown source term and meteorological parameters is $\Theta_k = \begin{bmatrix} x_s & y_s & q_s & u_s & \phi_s & d_s & \tau_s \end{bmatrix}^\mathsf{T}$ where key parameters are the source location and strength. The remaining variables are included as uncertain parameters to increase robustness as these variables are rarely known with absolute certainty.

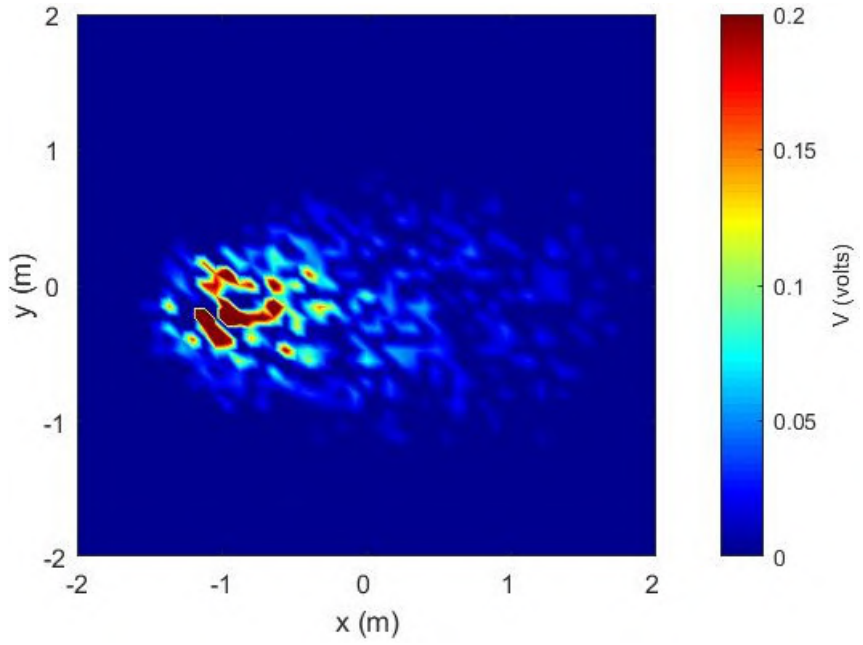

Figure 5.1: Example plot of the expected observation z_k of the robot in a square area, produced from a source Θ_k with parameters: $x_s = -1.2, y_s = -0.2, q_s = 0.1$, $u_s = 1, \phi_s = 90°, d_s = 0.1$ and $\tau_s = 2$.

5.3.2.2 Sensor model

The focus of this chapter is on validating a STE framework and demonstrating how a low cost set-up can be used for rapid prototyping and source estimation experiments. Therefore, a low-cost metal oxide (MOX) gas sensor is adopted. Its output is a voltage reading, which will vary due to a change in resistance of the sensor, caused by contact with atmospheric contaminants [197].

Typically, MOX sensors can be calibrated to a known gas so that meaningful concentration measurements, in physical units such as parts per million (ppm) can be found. This is done by using a lookup table or an equation to describe the relationship between output voltage and the sensed concentration. However, the calibrations are sensitive to uncontrollable atmospheric conditions such as temperature, humidity and pressure [197]. In many scenarios the atmospheric conditions can change, the equipment to measure them are not available, or the source of interest may be unknown or has not yet been calibrated to the sensor. To address this problem and make the proposed STE framework more applicable, the sensor used in this chapter is not calibrated. For simplicity, it is assumed that the expected voltage reading V from the contamination is directly proportional to the concentration of the substance. Based on the dispersion model defined in Eq. (5.8), the proportional relationship from the expected concentration to the expected voltage follows:

$$V\left(\mathbf{p}_k, \Theta_k\right) \propto C\left(\mathbf{p}_k|\Theta_k\right) \;\rightarrow\; V\left(\mathbf{p}_k, \Theta_k\right) = \frac{C\left(\mathbf{p}_k|\Theta_k\right)}{\alpha}, \tag{5.10}$$

where α is a calibration factor. This is a reasonable assumption based on figures in [197].

While the substance is unknown or the sensor is not calibrated to the specific material, a scaled release mass $A_0 = q_s/\alpha$ is estimated, resulting in the new model for the expected voltage reading:

$$V(\mathbf{p}_k, \Theta_k) = \frac{A_0}{4\pi d_s ||\mathbf{p}_k - \mathbf{p}_s||} \exp\left[\frac{-||\mathbf{p}_k - \mathbf{p}_s||}{\lambda}\right] \times \exp\left[\frac{-(x_k - x_s)u_s \cos\phi_s}{2d_s}\right] \exp\left[\frac{-(y_k - y_s)u_s \sin\phi_s}{2d_s}\right]. \quad (5.11)$$

With a slight abuse of notation, Θ_k is now used to represent the new source term where q_s is replaced by A_0. Moreover, to account for the unmodelled chemical concentration, an additive measurement noise $\bar{v}$ is assumed to associate with the expected voltage reading $V(\mathbf{p}_k, \Theta_k)$ due to the sensor noise.

Another challenge in using this low-cost sensor is that the sensor is not specific to a particular material. There exists a positive reading by the sensor in clean air, which in this chapter, is modelled as the background noise $\underline{v}$. This also implies that the chemical concentration from the source of interest may not be picked up by the sensor, when the concentration is relatively low.

5.3.2.3 Measurement likelihood

The likelihood function $p(z_k|\Theta_k)$ needs to be constructed to provide the probability of the sensor reading given a source term realisation. As described above, the observational data z_k is determined by a number of factors, including the expected voltage reading $V(\mathbf{p}_k, \theta)$ and different noises. In this chapter, it is assumed that both the additive measurement noise $\bar{v}_k$ and the background noise $\underline{v}_k$ follow Gaussian distributions, such that $\bar{v}_k \sim \mathcal{N}(\bar{v}_k; 0, \bar{\sigma}_k)$ and $\underline{v}_k \sim \mathcal{N}(\underline{v}_k; 0, \underline{\sigma}_k)$. The standard deviation of the background noise $\underline{\sigma}_k$ can be obtained experimentally which is set as a constant. In the contrast, $\bar{\sigma}_k$ is more difficult to quantify. Therefore, a common practice in STE is followed, where the errors are set as a percentage of the modelled concentration reading such that $\bar{\sigma}_k(V(\mathbf{p}_k, \Theta_k)) = 0.03 + (0.1 \times V(\mathbf{p}_k, \Theta_k))$.

While the noise distributions can be modelled, there still exists a phenomena to be accounted for in the sensing process due to the complicated nature of chemical dispersion and the low-cost sensor, which is the miss-detection of the sensor. In many previous studies, more comprehensive particle counter sensors were used, where a Poisson process is normally used to capture the uncertainty caused by the sporadic behaviour of the gas. To solve this problem, an event $\mathcal{D}$ is defined to describe the case where the gas has been picked up by the sensor ($\mathcal{D} = 1$) and the case where sensor did not respond to the gas ($\mathcal{D} = 0$). The probability of detection is defined as $P_d = \Pr\{\mathcal{D} = 1\}$, which is a tuning parameter to be set in the experiments. Therefore, the sensor model used in this chapter

can be expressed as

$$z_k = \begin{cases} V(\mathbf{p}_k, \Theta_k) + \bar{v}_k & \text{if } \mathcal{D} = 1 \\ \underline{v}_k & \text{if } \mathcal{D} = 0 \end{cases} \tag{5.12}$$

The corresponding likelihood function can be written as

$$p(z_k|\Theta_k) = (1 - P_d) \cdot \mathcal{N}(z_k; 0, \underline{\sigma}_k) + P_d \cdot \mathcal{N}(z_k - V(\mathbf{p}_k, \Theta_k); 0, \bar{\sigma}_k) \tag{5.13}$$

5.3.3 Sequential Bayesian implementation

The Bayesian estimation of source parameters is implemented in the sequential Monte Carlo framework using a particle filter. The output is an approximation of the posterior distribution $p(\Theta_k|\mathbf{z}_{1:k})$, which represents the current state of knowledge about the source parameters. Given the posterior distribution in the form of a weighted random sample, the integral in Eq. (5.7) is approximated so that the expected most informative manoeuvre can be chosen.

5.3.3.1 Sequential Monte Carlo estimation

The conceptual solution derived to estimate the source parameters is implemented using a particle filter. The posterior distribution from Eq. (5.2) is approximated by a set of weighted random samples $\{\Theta_k^{(i)}, w_k^{(i)}\}_{i=1}^N$, where

$$\Theta_k^{(i)} = \begin{bmatrix} x_{s,k}^{(i)} & y_{s,k}^{(i)} & A_{0,k}^{(i)} & u_{s,k}^{(i)} & \phi_{s,k}^{(i)} & d_{s,k}^{(i)} & \tau_{s,k}^{(i)} \end{bmatrix}^\mathsf{T} \tag{5.14}$$

is a sample representing a potential source term and $w_k^{(i)}$ is the corresponding normalised weighting such that $\sum_{i=1}^N w_k^{(i)} = 1$. Given the weighted samples, the posterior distribution is approximated as:

$$p(\Theta_k|\mathbf{z}_{1:k}) \approx \sum_{i=1}^{N} w_k^{(i)} \delta(\Theta_k - \Theta_k^{(i)}), \tag{5.15}$$

where $\delta(\cdot)$ is the Dirac delta function. The sample weights are updated in a recursive manner by sequential importance sampling [204]. At each time step, a set of new samples $\{\Theta_{k+1}^{(i)}\}_{i=1}^N$ can be drawn from a proposal distribution $q(\Theta_{k+1}^{(i)})$, which should resemble the distribution $p(\Theta_{k+1}|\mathbf{z}_{1:k+1})$. The corresponding un-normalised weights are then updated according to:

$$\bar{w}_{k+1}^{(i)} \propto w_k^{(i)} \cdot \frac{p(z_{k+1}|\Theta_{k+1}^{(i)}) p(\Theta_{k+1}^{(i)}|\Theta_k^{(i)})}{q(\Theta_{k+1}^{(i)}|\Theta_k^{(i)}, \mathbf{z}_{1:k+1})}. \tag{5.16}$$

The proposal distribution is typically used to update the samples to the next time step for estimating dynamic states. By assuming a time-invariant source term (i.e. the source position is fixed and the release rate is constant), the proposal distribution can be assumed to be identical to the posterior at time k. This leads to a simple algorithm where $\Theta_{k+1}^{(i)} = \Theta_k^{(i)}$ for $i = 1, ..., N$ [55]. Due to cancellation of terms in Eq. (5.16), the

un-normalised particle weights are updated using the likelihood function and the previous weight as follows:

$$\bar{w}_{k+1}^{(i)} = w_k^{(i)} \cdot p(z_{k+1}|\Theta_{k+1}^{(i)}). \tag{5.17}$$

The sample weights are then normalised as $w_{k+1}^{(i)} = \bar{w}_{k+1}^{(i)} / \sum_{i=1}^{N} \bar{w}_{k+1}^{(i)}$ to obtain the new approximation of the posterior.

Importance sampling is carried out sequentially at each time step. This can eventually lead to only a few particles with non-negligible weights, known as the degeneracy problem. To avoid sample degeneracy, the number of effective samples are estimated by:

$$N_{eff} = \frac{1}{\sum_{i=1}^{N} (w_k^{(i)})^2}. \tag{5.18}$$

When the number of effective point estimates N_{eff} falls below a pre-specified threshold η the sample points are re-sampled. This can lead to another problem where highly weighted particles will be multiplied many times, leading to a lack of diversity. This problem is referred to as sample impoverishment. To improve the diversity of the random samples, the re-sampled estimates are regularised by drawing new samples from a Gaussian kernel. The new samples undergo an MCMC move step [204], where they will be accepted with a probability proportional to their likelihood.

5.3.3.2 Sensor planning

The reward in Eq. (5.7) must be integrated over values of the future measurement z_{k+1}. This value is unknown until the manoeuvre has been made. Therefore, the distribution of the hypothetical measurement $\hat{z}_{k+1}$ needs to be generated based on the dispersion model and the current estimate of the source term through the likelihood function. Based on the current sample set $\{\Theta_k^{(i)}, \omega_k^{(i)}\}_{i=1}^{N}$ and using the law of total probability, the likelihood function can be approximated as:

$$\begin{aligned} p(\hat{z}_{k+1}(\mathbf{a}_k)|\mathbf{z}_{1:k}) &= \int_{\Theta_{k+1}} p(\hat{z}_{k+1}(\mathbf{a}_k), \Theta_{k+1}|\mathbf{z}_{1:k}) \, \mathrm{d}\Theta_{k+1} \\ &= \int_{\Theta_{k+1}} p(\hat{z}_{k+1}(\mathbf{a}_k)|\Theta_{k+1}) p(\Theta_{k+1}|\mathbf{z}_{1:k}) \, \mathrm{d}\Theta_{k+1} \\ &\approx \sum_{i=1}^{N} w_k^{(i)} \cdot p(\hat{z}_{k+1}(\mathbf{a}_k)|\Theta_{k+1}^{(i)}) \end{aligned} \tag{5.19}$$

where $\Theta_{k+1}^{(i)} = \Theta_k^{(i)}$. To generate a set of samples from this distribution, M particles $\{\hat{z}_{k+1}^{(j,i)}\}_{j=1}^{M}$ can be drawn from each $p(\hat{z}_{k+1}(\mathbf{a}_k)|\Theta_{k+1}^{(i)})$ based on Eq.(5.12), which yields a total of MN samples.

To reduce the computational load, a small number of samples $\{\Theta_k^{(l)}, \frac{1}{N_z}\}_{l=1}^{N_z}$ can be resampled from $\{\Theta_k^{(i)}, \omega_k^{(i)}\}_{i=1}^{N}$, where $N_z << N$. Moreover, $M = 1$ is set in this chapter, hence only one sample of $\hat{z}_{k+1}^{(l)}$ will be produced given a particular $\Theta_k^{(l)}$, for $l = 1, \ldots, N_z$.

Therefore, the distribution $p(\hat{z}_{k+1}(\mathbf{a}_k)|\mathbf{z}_{1:k})$ can be approximated by

$$p(\hat{z}_{k+1}(\mathbf{a}_k)|\mathbf{z}_{1:k}) \approx \frac{1}{N_z}\sum_{l=1}^{N_z}\delta(\hat{z}_{k+1}-\hat{z}_{k+1}^{(l)}) \tag{5.20}$$

The detailed process of generating $\{\hat{z}_{k+1}^{(l)}\}_{l=1}^{N_z}$ is provided in Algorithm 3.

Algorithm 3 Drawing samples for hypothetical measurement $\hat{z}_{k+1}$

Require: weighted samples: $\{\Theta_k^{(i)},\omega_k^{(i)}\}_{i=1}^{N}$; future location $\mathbf{p}_{k+1}$;
for $l=1,2,\ldots,N_z$ **do**
  draw sample $\Theta_k^{(l)} \sim \sum_{i=1}^{N}\omega_k^{(i)}\delta(\Theta_k-\Theta_k^{(i)})$
  $\Theta_{k+1}^{(l)}=\Theta_k^{(l)}$
  draw sample $\kappa \sim \mathcal{U}([0,1])$
  if $\kappa \le P_d$ **then**
    draw sample $\bar{v}_{k+1}\sim\mathcal{N}(\bar{v}_{k+1};0,\bar{\sigma}_{k+1})$
    set $\hat{z}_{k+1}^{(l)}=V(\mathbf{p}_{k+1},\Theta_{k+1}^{(l)})+\bar{v}_{k+1}$
  else
    draw sample $\underline{v}_{k+1}\sim\mathcal{N}(\underline{v}_{k+1};0,\underline{\sigma}_{k+1})$
    set $\hat{z}_{k+1}^{(l)}=\underline{v}_{k+1}$
  end if
end for
Ensure: weighted samples: $\{\hat{z}_{k+1}^{(l)},\frac{1}{N_z}\}_{l=1}^{N_z}$

Given the hypothetical future measurement $\hat{z}_{k+1}^{(l)}$, the utility function $\Upsilon(\cdot)$ defined in (5.6) can be evaluated. First, based on the set of samples $\{\Theta_k^{(i)},\omega_k^{(i)}\}_{i=1}^{N}$ resembling $p(\Theta_k|\mathbf{z}_{1:k})$ and the fact $\Theta_{k+1}^{(i)}=\Theta_k^{(i)}$, the same set of samples can be used to approximate the predicted distribution $p(\Theta_{k+1}|\mathbf{z}_{1:k})$. Then, the posterior distribution $p(\Theta_{k+1}|\mathbf{z}_{1:k},\hat{z}_{k+1}^{(l)})$ can be approximated by the sample set $\{\Theta_{k+1}^{(i,l)},\hat{w}_{k+1}^{(i,l)}\}_{i=1}^{N}$, where $\Theta_{k+1}^{(i,l)}=\Theta_k^{(i)}$ and the corresponding weight is updated based on the same Bayesian law (5.16)-(5.17), such that $\hat{w}_{k+1}^{(i,l)}\propto p(\hat{z}_{k+1}^{(l)}|\Theta_{k+1}^{(i)})\cdot w_k^{(i)}$ and $\sum_{i=1}^{N}\hat{w}_{k+1}^{(i,l)}=1$. Thus, the utility function can be approximated as

$$\Upsilon(\hat{z}_{k+1}^{(l)}(\mathbf{a}_k)) \approx \sum_{i=1}^{N}\hat{w}_{k+1}^{(i,l)}\ln\frac{\hat{w}_{k+1}^{(i,l)}}{w_k^{(i)}}. \tag{5.21}$$

At last, the expected utility function with respect to the hypothetical future measurement $\hat{z}_{k+1}$ can be expressed as

$$\mathbb{E}[\Upsilon(\hat{z}_{k+1}(\mathbf{a}_k))] \approx \frac{1}{N_z}\sum_{l=1}^{N_z}\sum_{i=1}^{N}\hat{w}_{k+1}^{(i,l)}\ln\frac{\hat{w}_{k+1}^{(i,l)}}{w_k^{(i)}}. \tag{5.22}$$

The expected utility is calculated for all the manoeuvres in the set Ψ, then the robot selects the move $\mathbf{a}_k^*$ that has the greatest expected utility. Following the manoeuvre, the robot takes a new observation z_{k+1} and the estimation and sensor control cycle is iterated until some stopping criteria are reached. The action selection algorithm is summarised in Algorithm 4.

Algorithm 4 Select optimal control action $\mathbf{a}_k^*$

Require: weighted samples: $\{\Theta_k^{(i)}, \omega_k^{(i)}\}_{i=1}^N$;
for all $\mathbf{a}_k \in \Psi$ **do**
  $\mathbf{p}_{k+1} = \mathbf{p}_k + \mathbf{a}_k$
  draw samples $\{\hat{z}_{k+1}^{(l)}\}_{l=1}^{N_z}$ using Algorithm 3
  for $l = 1, 2, \ldots, N_z$ **do**
    for $i = 1, 2, \ldots, N$ **do**
      $\hat{\Theta}_{k+1}^{(i,l)} = \Theta_{k+1}^{(i)}$
      $\tilde{\omega}_{k+1}^{(i,l)} = p(\hat{z}_{k+1}^{(l)} | \hat{\Theta}_{k+1}^{(i,l)}) \cdot \omega_k^{(i)}$
    end for
    set $\hat{\omega}_{k+1}^{(i,l)} = \tilde{\omega}_{k+1}^{(i,l)} / \sum_{i=1}^N \tilde{\omega}_{k+1}^{(i,l)}$, for $i = 1, 2, \ldots, N$
    calculate utility $\Upsilon^{(l)} = \sum_{i=1}^N \hat{w}_{k+1}^{(i,l)} \ln \frac{\hat{w}_{k+1}^{(i,l)}}{w_k^{(i)}}$
  end for
  $\mathbb{E}[\Upsilon(\hat{z}_{k+1}(\mathbf{a}_k))] = \frac{1}{N_z} \sum_{l=1}^{N_z} \Upsilon^{(l)}$
end for
$\mathbf{a}_k^* = \arg\max_{\mathbf{a}_k \in \Psi} \mathbb{E}[\Upsilon(\hat{z}_{k+1}(\mathbf{a}_k))]$
Ensure: $\mathbf{a}_k^*$

This concludes the methodology section of the current chapter. The estimation and sensor planning implementations describe the entire algorithm required for decision making of the robot to search for and estimate the source term of a hazardous source. All that remains is a system to take the output of the algorithm, a new position coordinate, and manoeuvre the robot to the desired location to take the following measurement. The robotic system and the experimental set-up are described in the next section and then the experimental results are presented.

5.4 Experiment setup

In this section the experiment set-up that is described is used to validate the proposed STE algorithm using a mobile robot. To the authors' knowledge, the experiment is the first of its kind, whereby a robot equipped with a gas sensor moves around autonomously to estimate the location and strength of a source releasing hazardous material into the atmosphere. The smoke produced from burning incense sticks is used to simulate a hazardous release and electric fans are used to create a wind field. The robot navigates the environment to the most informative measurement locations to make sensor observations, which are point measurements of the smoke concentration. The measurements are used to estimate the source term recursively, using the probabilistic algorithm described in Section 5.3.3.1. At each time step, the robot moves to the position dictated by the information based reward described in Section 5.3.3.2 to take a new measurement.

5.4.1 Environment

The smoke produced from burning incense sticks, as shown in Fig 5.2a, is used as the simulated, hazardous material during the experiments. Incense sticks, otherwise known as Joss sticks, are a popular item used by the public for aesthetic reasons, therapy, deodorizer or for meditation. Such an accessible source enabled simple, safe and easily repeated experiments that could be conducted in an indoor environment. An example of the highly turbulent smoke plume generated by the burning incense during the experiments is shown in Fig 5.2b, which is a snapshot from an experiment video. Multiple experiments are conducted with a varying number of burning sticks to analyse the response of the algorithm in different sensing conditions and to assess the accuracy of the scaled release rate estimates A_0.

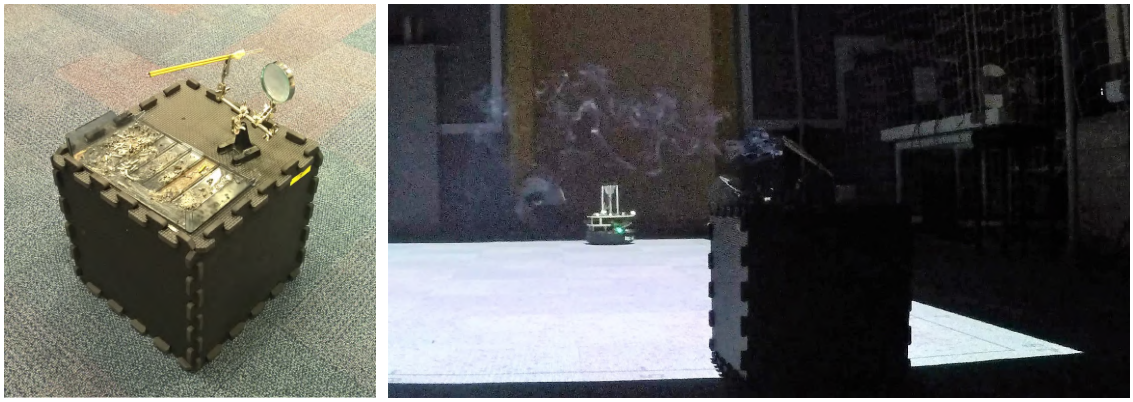

(a) (b)

Figure 5.2: (a) Incense stick used as a smoke source during experiments. (b) A snapshot of the burning incense during an experiment to illustrate the turbulence.

An illustration of the search environment is depicted in Fig 5.3a, the axis limits indicate the domain area Ω that is used to define the limits of the uniform prior on the source position. The red shaded area represents the area within which the robot can move, bounded by the field of view of the indoor positioning system. The location of the incense sticks $(-2.4, -0.8)$ during the experiments and the starting position of the robot $(1.8, 1.2)$ are indicated in the figure. A wind field is generated, roughly along the positive x-direction, using fans to the left and to the right of the search area. A photo of the experiment set-up during an experimental run is shown in Fig 5.3b, displaying the position of the robot during a search, and the source location at the bottom left. The localisation of the robot is provided by an indoor positioning system (Vicon). The image on the floor is produced by a downwards-facing projector that is used for visualisation during the experiments. The set-up was inside a large ventilated building, large enough for there to be little effect caused by trapped smoke or wall reflectance.

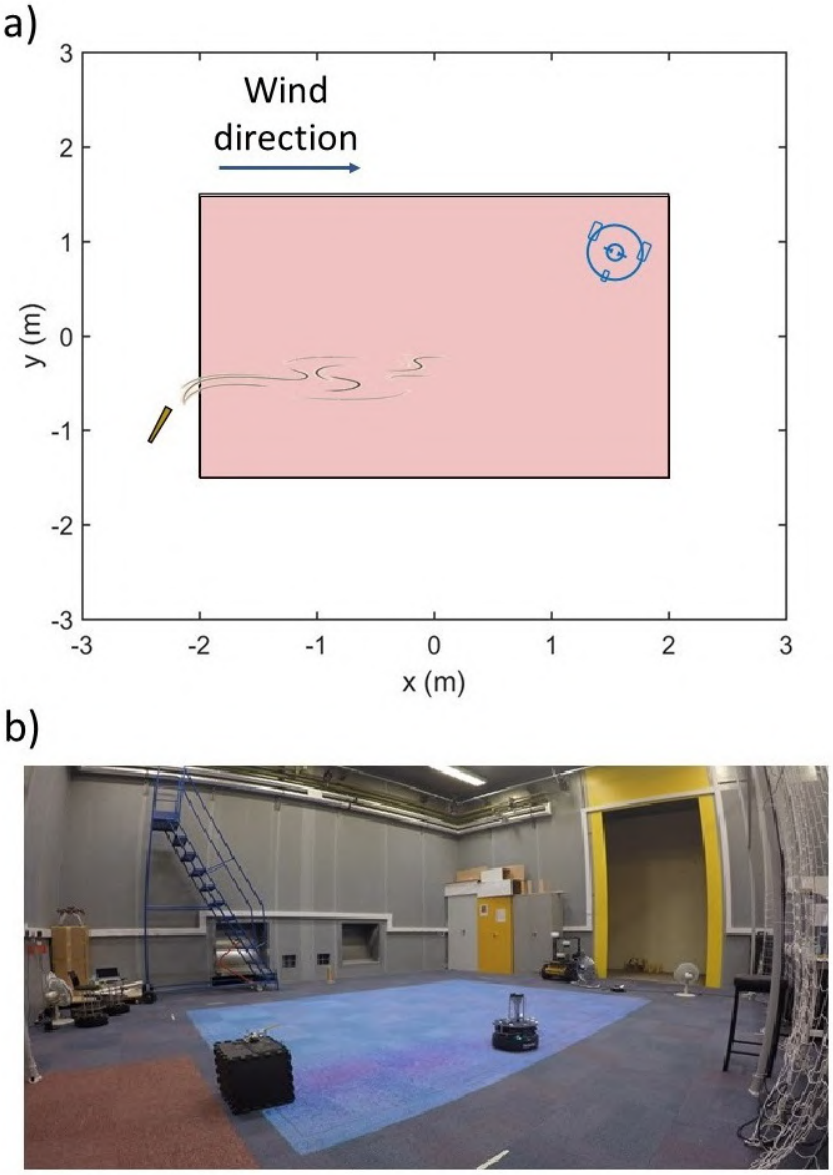

Figure 5.3: Experiment set-up used for the illustrative runs and experimental results. (a) A diagram of the environment displaying the starting position of the robot, the wind direction and the location of the incense sticks. The red shaded area indicated the bounds where the robot can move. (b) Photo of the experiment set-up with a down facing projector for data visualisation.

5.4.2 Search robot

A 'Turtlebot' is adapted for gas sensing experiments shown in Fig 5.4a. A MOX gas sensor is used to sense the smoke. There are a range of sensors available, each with different sensitivities towards materials. The MQ135 gas sensor shown in Fig 5.4b was chosen for the experiments due to its reported sensitivity to smoke. In order to improve the response of the sensor during the experiments, a cone and a CPU cooling fan were added to suck air into the sensor as is illustrated in Fig 5.4c. The sensor information is

sent via a serial connection to a laptop on-board the Turtlebot which sends it to a ground station. The robot operating system (ROS) is used for communications [205]. A custom ROS message is created to send the location stamped sensor data to the ground station. The ground station (Intel core i7 desktop PC) runs the sequential estimation of the source term parameters and outputs the new position command based on the online optimization.

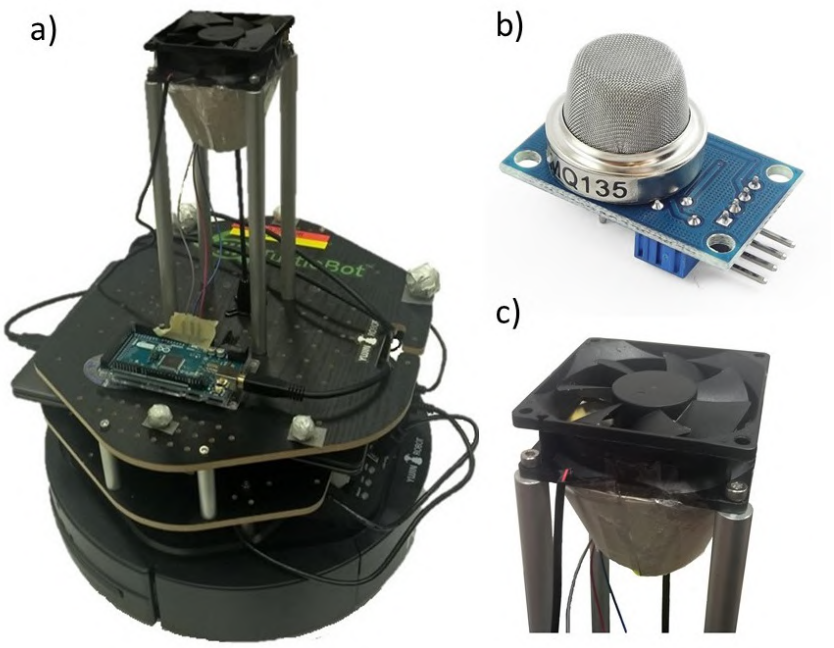

Figure 5.4: The gas sensing system: a) a Turtlebot robotic platform; b) MQ135 metal oxide gas sensor; and c) a fan and inlet cone used to draw air into the sensor.

5.5 Experimental results

Multiple experiments are conducted to validate the algorithm and assess its behaviour in response to varying source strengths. Illustrative runs are presented to show the characteristics of the cognitive search and source reconstruction with a strong and a weak source. Examples of the output are shown in the form of marginal posterior density curves for all the estimated parameters in the source term vector Θ_k. A table is provided which summarises the results of 3 trials each for experiments with 2, 4 and 6 burning incense sticks. The table indicates the accuracy of the location estimate of the algorithm and the time taken to complete the search. Finally, averaged marginal posterior densities of the release strength are included to demonstrate the performance of the release rate estimate.

5.5.1 Illustrative runs

The illustrative runs and experiments are conducted using the environment and robot that have been described. The starting position of the robot during the runs is $\mathbf{p}_0 = (1.8, 1.2)$. The number of random samples used in the particle filter is $N = 10,000$ and the number

of samples used to approximate the expected utility from Eq (5.22) is $N_z = 100$. The probability of detection during the runs was set to $P_d = 0.7$ and the standard deviation of the background noise was fixed at $\underline{\sigma}_k = 0.005$.

To initiate the experiments, prior distributions for the source parameters must be input to the algorithm. As discussed briefly in Section 5.3.1, the prior distributions should reflect information known about the release. To assess the algorithm in realistic conditions, it is assumed that there is little information known about the release beforehand. The prior distributions used to initiate the illustrative runs and the experimental results were set to the values shown in Table 5.1, where the true values are indicated if they were known. This is followed by a short discussion on the choice of the prior distributions.

Table 5.1: Illustrative run parameters and priors.

Parameter (Truth)	Prior
x_s (-2.4)	$\mathcal{U}(-3, 3)$
y_s (-0.84)	$\mathcal{U}(-2, 2)$
A_0	$\mathcal{G}(075, 0.5)$
u_s	$\mathcal{U}(0.01, 2.1)$
ϕ_s	$\mathcal{U}(80, 100)$
d_s	$\mathcal{U}(0.03, 13)$
τ_s	$\mathcal{U}(0.4, 1.4)$

- The prior distributions for the location of the source $(p_0(x_s), p_0(y_s))$ were set to uniform within the domain. This would be equivalent to a someone drawing a large rectangle to indicate "we think the source is within here" (the area could be very large).
- The scaled release strength prior $p_0(A_0)$ was given a Gamma distribution. This was used to indicate to the algorithm that the release is likely to be weak, causing the robot to display more explorative behaviour than it would it if was told the source was strong. This prior was fixed for every test, regardless of the real strength or the number of burning incense sticks.
- The meteorological variables $(p_0(\phi_s), p_0(u_s))$ and diffusivity $p_0(d_s)$ were assigned uniform distributions. Operationally these should be set using meteorological sensors and information about the hazardous material.
- The average lifetime prior $p_0(\tau_s)$, which in this case refers to the average time taken for the smoke particles to cool and fall to the ground (in other cases it may be a result of chemical reactions), was set to a uniform distribution as this parameter was unknown. In some circumstances, it could be given a more informative distribution based on information known about the hazard.

An illustrative run using 2 burning incense sticks is shown in Fig 5.5. Figures 5.5a-5.5d show the path of the robot and the measurement positions, at various time steps,

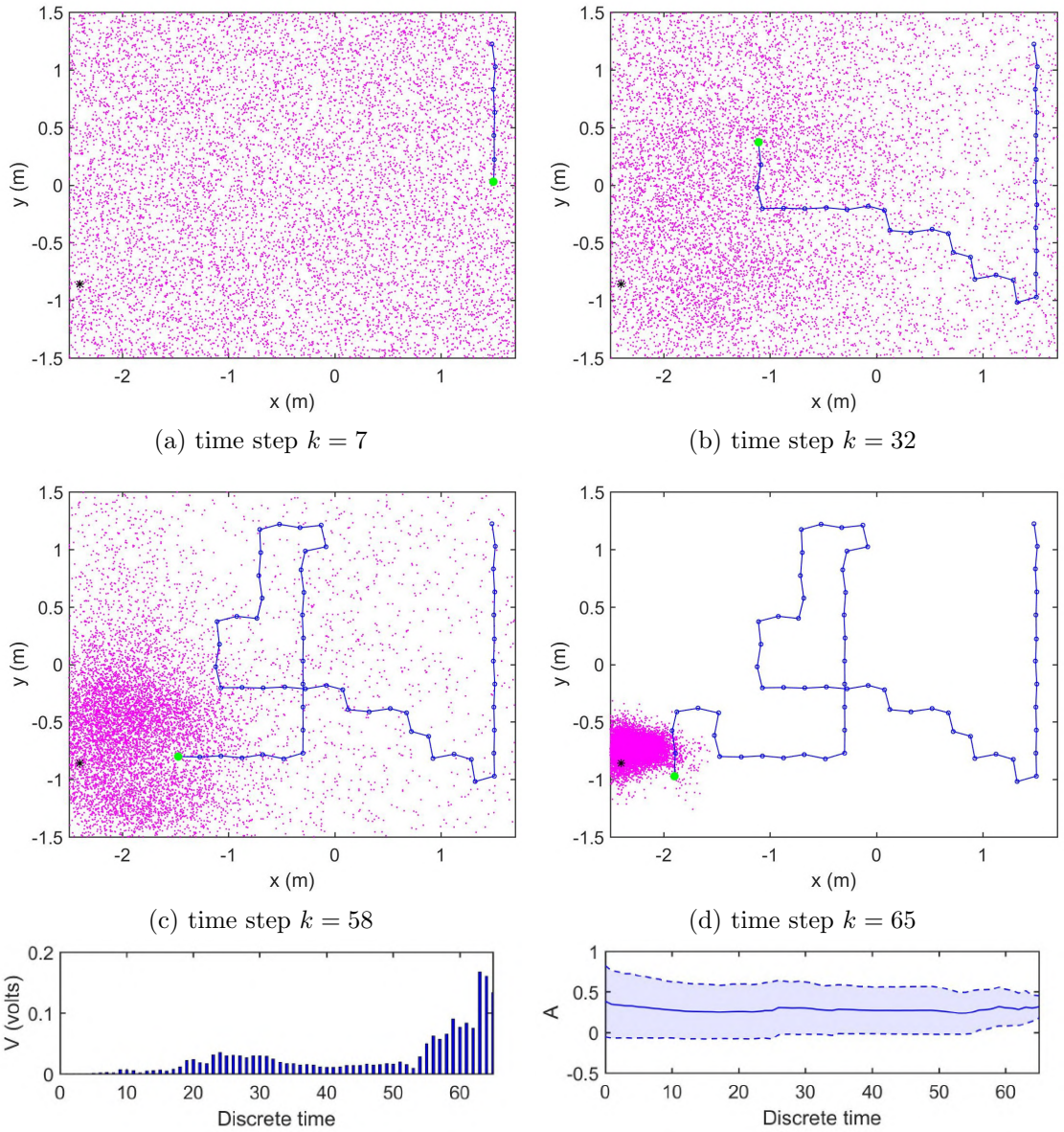

(a) time step $k = 7$

(b) time step $k = 32$

(c) time step $k = 58$

(d) time step $k = 65$

(e) Measurements

(f) q_s estimate

Figure 5.5: An illustrative run using 2 burning incense sticks at time steps: (a) $k = 7$; (b) $k = 32$; (c) $k = 58$; and (d) $k = 65$. The green dot represents the current position of the robot that has followed the blue line trajectory and taken observations at positions indicated by the blue dots. The location of the source is indicated by a black dot and the small pink dots represent the random samples of the estimation algorithm. (e) The voltage reading of the sensor throughout the experiment. (f) The mean and standard deviation of the release rate estimate over time.

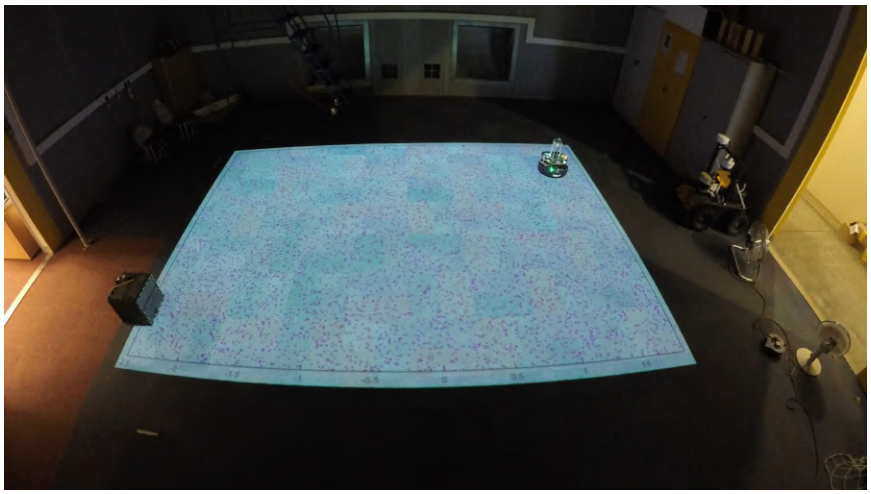

(a)

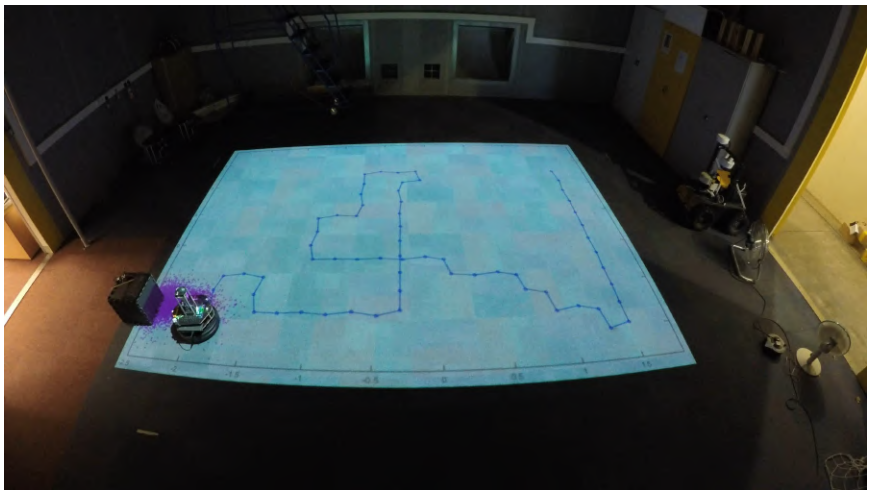

(b)

Figure 5.6: Photos at the a) start and b) end of the illustrative run with 2 sticks.

represented by the blue line and the blue dots. At each time step, the robot stops at the blue dot for one second to sample, updates the estimates of the source term and then decides where to move next. The current position of the robot is indicated by a larger, green circle and the true position of the source is at the black circle. The large amount of small pink dots represents the N random samples that are used to approximate the posterior estimates of the source parameters, as described in Section 5.3.3.1. The figure demonstrates how the robot begins the search by moving in a crosswind direction. In response to very little or no readings of smoke the robot moves slightly upwind while proceeding to travel crosswind in the other direction. By time step 32, shown in Fig 5.5b, the pink dots have moved away from the visited locations of the robot where no smoke was seen, however due to the large amount of uncertainty expected during the search, some dots still remain in this area in case the low or zero reading could have been caused by either sensor noise or atmospheric turbulence. By time-step $k = 58$, shown in Fig 5.5c, the robot has narrowed down the source position and the pink dots begin to converge into the

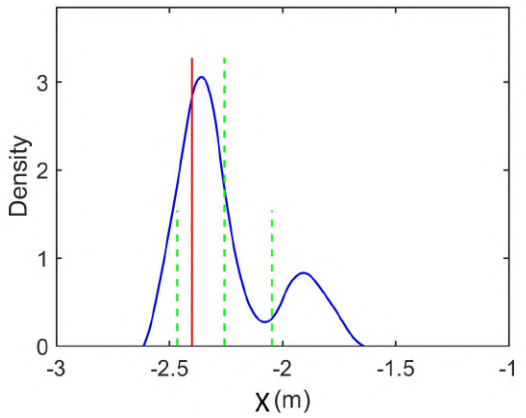

(a)

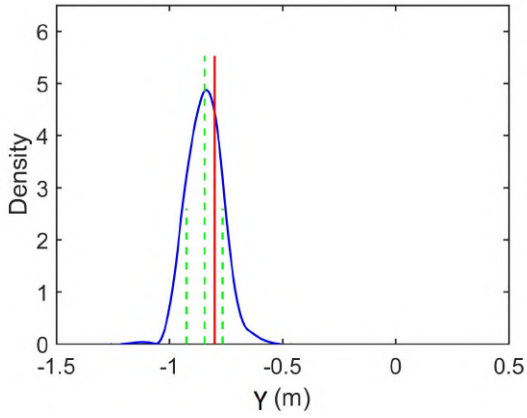

(b)

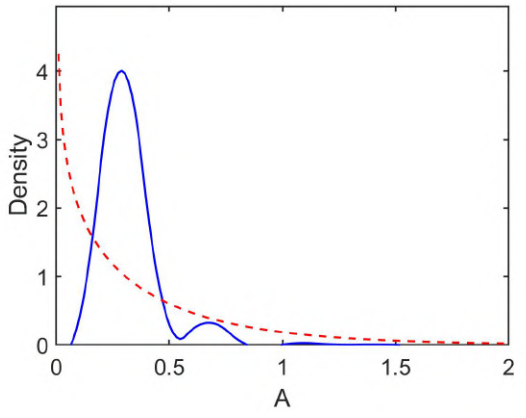

(c)

Figure 5.7: Outputs of the STE algorithm after an illustrative run with two sticks. Posterior density estimates of the location in the (a) x and (b) y coordinates. The blue curve indicates the posterior estimate and the vertical red line is the truth. The dashed green lines represent the mean and standard deviation of the estimate. (c) The posterior density of the scaled release rate A_0. The blue curve indicates the posterior estimate and the dashed red curve represents the prior distribution.

true source location. At the end of the search, shown in Fig 5.5d the robot has narrowed down the source estimate to within $10cm$ of the true source location.

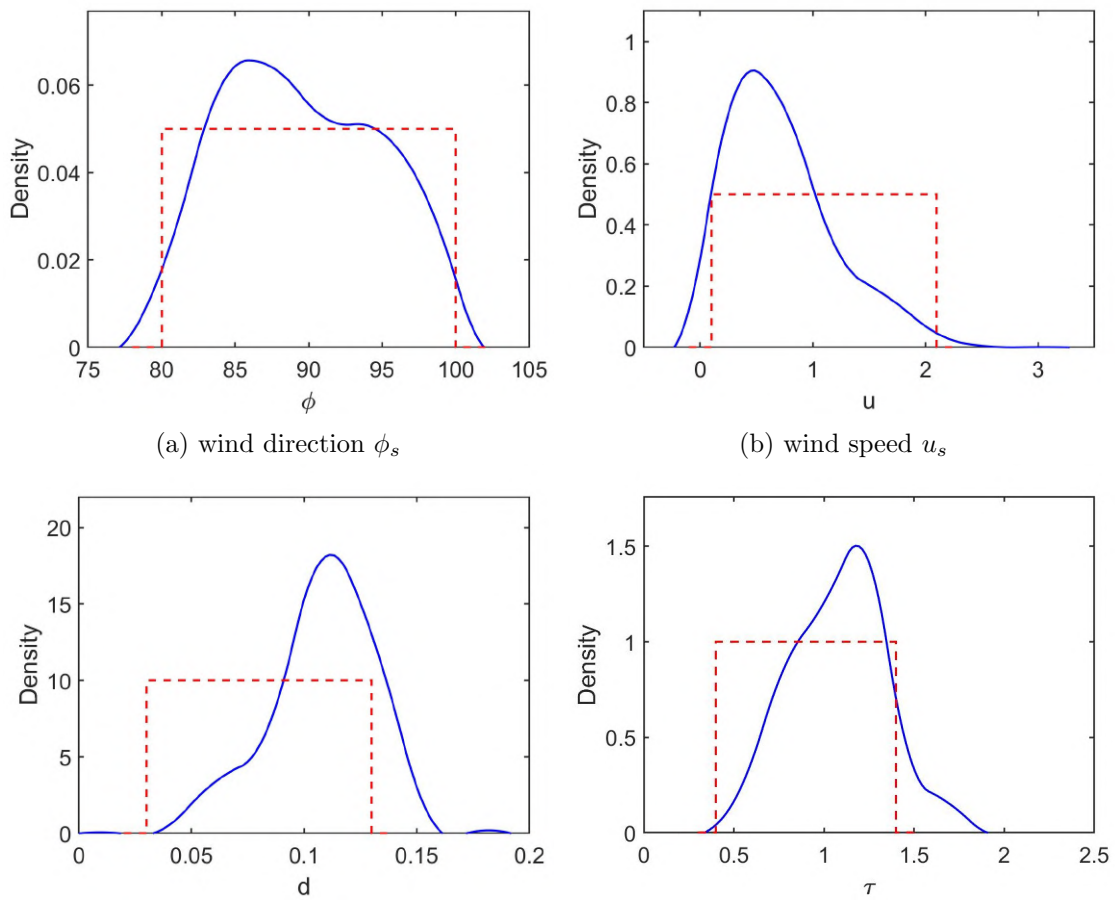

(a) wind direction ϕ_s

(b) wind speed u_s

(c) diffusivity d_s

(d) lifetime τ_s

Figure 5.8: The remaining source parameter estimates at the end of the illustrative run with 2 burning incense sticks. The dashed red line indicates the prior and the blue curve is the estimate.

The sensor output (in units of Volts) over time is shown in Fig 5.5e and the estimate of the source strength over time is given in Fig 5.5f, with shaded regions indicating confidence intervals of a single standard deviation. Photos taken at the beginning and the end of the experimental run are shown in Fig 5.6. The downward-facing projector shows the path of the robot and the particle representation of the source estimate similarly to Fig 5.5a-5.5d.

Posterior density estimates of the location of the source are shown in Figs 5.7a-b. The blue curve represents the estimate, the vertical red line is the true location, the tall green dashed vertical line is the mean and the shorter lines are standard deviations. It is clear how the red line, representing the mean, is close to the peak of the density curve for the estimates in the x and y coordinates. The posterior estimate of the source release rate is shown in Fig 5.7c, where the dashed red curve indicates the inverse Gamma prior and the blue line is the estimate. The performance of the release rate estimate is analysed in the results section where the output is compared for different amounts of sticks. Posterior densities of the remaining parameters are shown in Fig 5.8, these parameters are mainly included to add robustness to the algorithm in the presence of uncertain meteorological

conditions.

In Fig 5.9, an illustrative run is shown where four burning incense sticks were used as the smoke source. In this run, smoke was detected by the detector much earlier in the search, causing the robot to proceed towards the source earlier on as more information was available. Posterior densities at the end of the run for the location and strength estimates are given in Fig 5.10. The sensor readings throughout the search are given in Fig 5.9. The difference in the sensing conditions caused by changing the number of burning incense sticks can be seen by comparing figures 5.5e and 5.9.

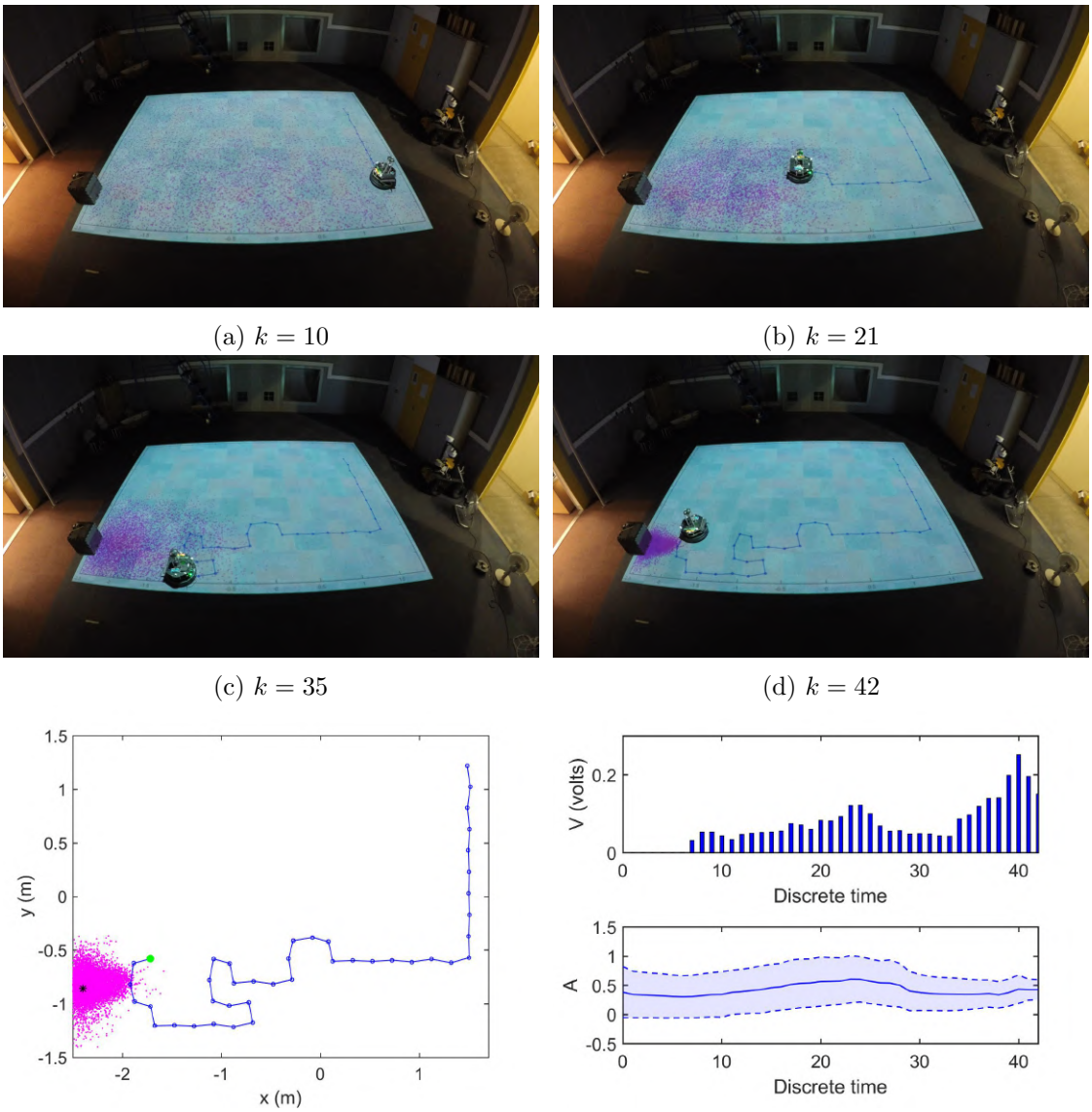

(a) $k = 10$ (b) $k = 21$

(c) $k = 35$ (d) $k = 42$

Figure 5.9: An illustrative run using four burning incense sticks. (a-d) Snapshots of the experiment at different time steps k. (e) Plot of the path at the end of the search. The path followed by the robot is indicated by the blue line. The location of the source is indicated by a black dot and the small pink dots represent the random samples of the estimation algorithm. (f) The voltage reading of the sensor throughout the experiment. (g) The mean and standard deviation of the release rate estimate over time.

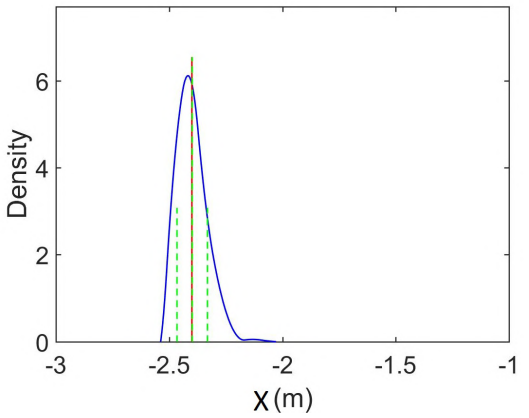

(a)

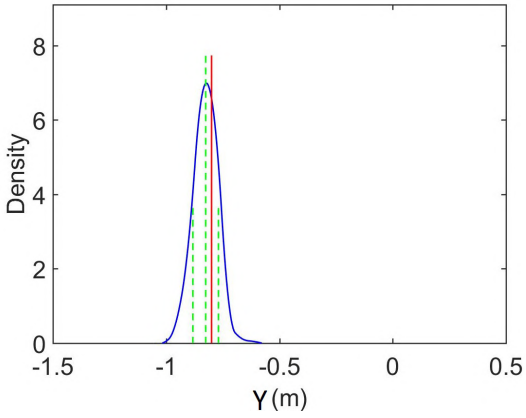

(b)

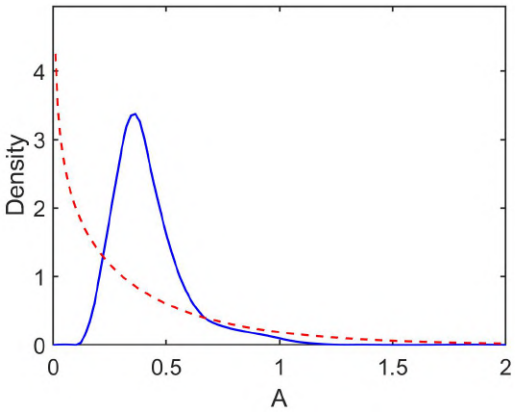

(c)

Figure 5.10: Outputs of the STE algorithm after an illustrative run with four sticks. Posterior density estimates of the location in the (a) X and (b) Y coordinates. The blue curve indicates the posterior estimate and the vertical red line is the truth. The dashed green lines represent the mean and standard deviation of the estimate. (c) The posterior density of the scaled release rate A_0. The blue curve indicates the posterior estimate and the dashed red curve represents the prior distribution.

5.5.2 Numerical results

The illustrative runs were repeated three times each for 2, 4 and 6 burning incense sticks. An autonomous stopping criteria was created based on the spread of the estimate. At each time step during the experiments, the spread of the posterior distribution was estimated as $S_k = \sqrt{\zeta_k(1,1) + \zeta_k(2,2)}$ where ζ_k is the covariance of the source position particles. The results are summarised in Table 5.2, where the mean estimates of the source location and strength are given, with details about the search time.

For all runs, the location estimate was very accurate, typically within 10cm of the true source position. In STE literature using static networks it is common for there to be greater error along the downwind x direction then crosswind y. However, in several of the experimental runs a more significant error was seen in the crosswind direction. This was caused by the slow recovery time of the MOX gas sensor. When the robot moved from an area of very high concentration, to very low, it was not reflected by the sensor, as it would still be recovering from its high reading. This is a negative property of metal oxide sensors reported previously in source localisation experiments [36] and is a current topic of research focused on reducing and modelling the response time [206]. There are other sensors available, slightly more expensive than the cheap MQ135 sensor used during the experiments, that are expected to perform better.

Table 5.2: Results for 3 trials using 2, 4 and 6 incense sticks.

	Truth	Trial 1	Trial 2	Trial 3
2 sticks				
x_s (m)	-2.4	-2.33	-2.39	-2.37
y_s (m)	-0.8	-0.70	-0.78	-0.82
A_0		0.237	0.293	0.227
Search time (s)		201	210	312
Euclidean position error (m)		0.12	0.02	0.04
Number of measurements		46	49	72
4 sticks				
x_s (m)	-2.4	-2.35	-2.40	-2.30
y_s (m)	-0.8	-0.81	-0.83	-0.86
A_0		0.333	0.362	0.433
Search time (s)		194	192	224
Euclidean position error (m)		0.05	0.03	0.12
Number of measurements		44	43	52
6 sticks				
x_s (m)	-2.4	-2.39	-2.38	-2.27
y_s (m)	-0.8	-0.77	-0.83	-0.85
A_0		0.588	0.589	0.535
Search time (s)		210	199	195
Euclidean position error (m)		0.03	0.04	0.14
Number of measurements		49	47	44

In response to more sticks, the robot could estimate the source term more quickly. This is due to higher, more informative concentration readings earlier on in the search. The difference in search time between 4 and 6 sticks is quite small; this is from the robot still moving crosswind, even though the posterior estimate clearly showed the source is upwind of the robots position. This behaviour can be expected, as the goal of the decision making is not to move directly towards the source, but to follow an informative path that collects information about the source location, strength and the meteorological parameters. Furthermore, by moving crosswind, the robot could gain an accurate crosswind position estimate of the source earlier on in the search from a stand-off position. Source localisation strategies have been assessed in the past, and it was found that a strategy that focused on moving directly towards the estimated source position was more prone to errors and failure. This is a result of making decisions based on getting close to the source, not on what might be learnt from the new measurement.

To assess the strength estimate of the algorithm one would usually compare the strength estimate directly with the true value. In these experiments, the true release strength of the incense sticks was unknown and the sensor did not output a concentration reading. Smoke itself can be a mixture of several materials, so the composition of the material that the sensor was reading was unknown. The sensor was uncalibrated to the smoke, and the output was a voltage not a reading of concentration, meaning that only a scaled release strength A_0 could be estimated as described in Section 5.3.2. Upon calibration of the sensor, this can easily be adjusted to a true physical value. To assess the strength estimate of the algorithm the outputs relative to one another using the varying amounts of sticks were compared.

The averaged marginal posterior densities of the release strength are shown in Fig 5.11, using all the runs from Table 5.2. The curves show the averaged posteriors for 2 sticks in blue, 4 in dotted cyan and 6 in dashed green. The red curve indicates the prior distribution. It is clear from the figure that the scaled strength estimate is proportional to the number of incense sticks, increasing by approximately 0.09 per stick. The individual output estimates from all the trials are shown in Fig 5.12

There are a number of reasons for the increased spread of the posterior for the larger release rate estimates: i) modelled variance was increased with sensed value and the sensed value was larger with higher release rates; ii) a larger release rate lead to the possibility of a stronger source further away causing increased spread of several posterior parameters; and iii) the final result was further from the prior distribution resulting in more spread. The strength estimate can be dependant on several of the unknown parameters due to coupling. It is beneficial for these parameters to be entered into the algorithm accurately, however, it has been shown that the algorithm is robust to quite uninformative prior information.

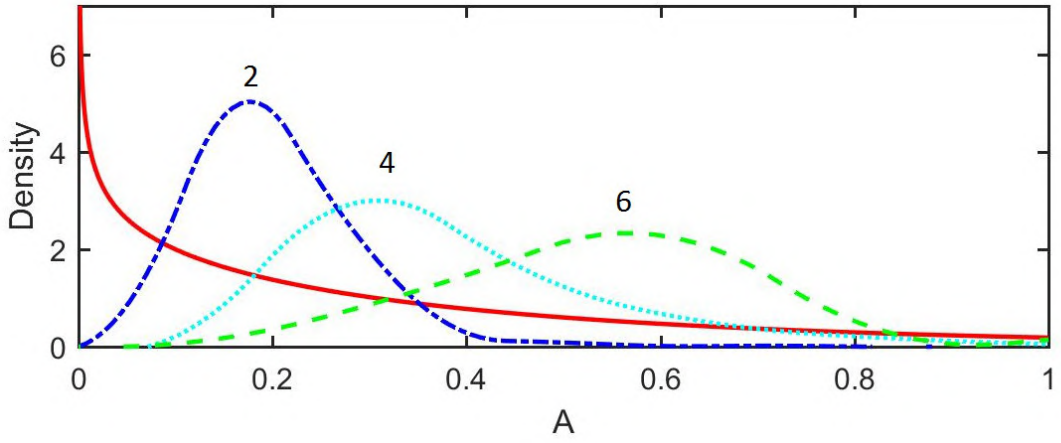

Figure 5.11: Averaged marginal estimates of the release rate A_0 of the source at the end of the experiments. The red solid line indicates the prior distribution. The blue curve is the average release rate estimate after 3 runs with 2 burning incense sticks. The dotted cyan curve is the average for 4 sticks and the dashed green line for 6.

5.6 Chapter summary

This chapter described a system and algorithms to navigate a robot to the expected most informative locations to estimate the source term of an atmospheric release. Subsequently, the approach was validated in experiments using a real sensor and dispersive source, a result which had not been achieved previously in the literature. The system was able to estimate important details about a release or leak of airborne HAZMAT into the atmosphere (i.e. the source term), such as its location or the rate of emission. This information permits a model to forecast the spread and deposition of the material into the surrounding area. An example of the forecast produced from the source estimates from the ilustrative run using four burning incense sticks is shown in Fig 5.13. All of the dispersion parameters used in the ATD model were assumed to be uncertain to improve the robustness of the algorithm. This includes the wind direction and the wind speed, as well as the key parameters of the source term; the origin of the release and the rate of emission. A new likelihood function was designed to accommodate the intermittent readings from the low cost MOX sensor that was mounted on the robot. Where the sporadicity was a consequence of a weak source, insufficient mixing of the airborne material, and the small size and low sensitivity of the sensor. An experiment set-up was devised, that is easily repeatable, cheap, fast and effective for early testing of STE techniques. Illustrative runs demonstrated the search behaviour of the algorithm and its accuracy in the location estimate. Numerical results showed the consistency of the algorithm and the effect of a stronger or weaker source. Finally, it was shown how the algorithm is able to predict the scaled release strength of the source relative to the other experimental runs. The results mark a first for a STE algorithm running on-line to guide a mobile sensor.

Following the successful validation of the information based search and STE algorithm

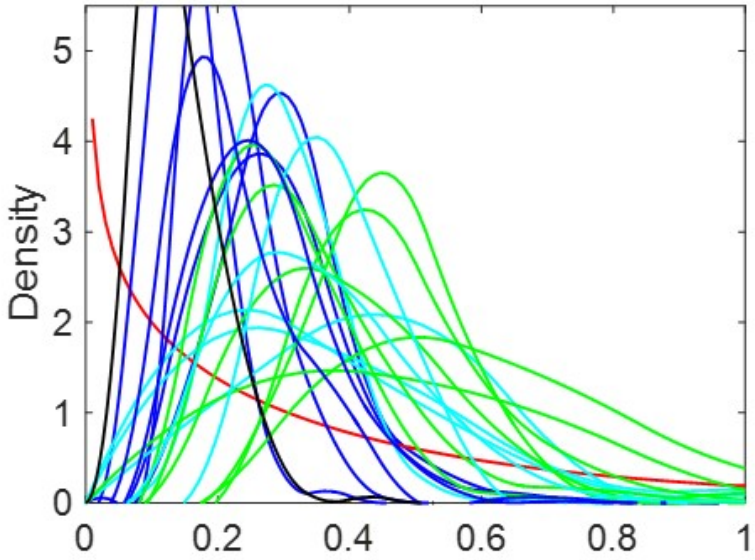

Figure 5.12: Marginal estimates of the release rate A_0 of the source at the end of all the experiments.

in the indoor arena, where fans were used to simulate a wind field, the next step is to test the system in natural outdoor conditions using a UAV. STE using an aerial vehicle is a new area of research, therefore, before extending the information based planning algorithm to work using the UAV outdoors the next step will be to focus on the estimation algorithm. The Bayesian estimation algorithm must be extended to work in the short range outdoor conditions that the UAV will operate in and it must be able to handle the sensor data that is provided by an aerial vehicle. The sensor data is expected to be effected by the UAVs rotors and the short averaging times of the sensor measurements to cope with the short flight time of a UAV and the requirement of a rapid response.

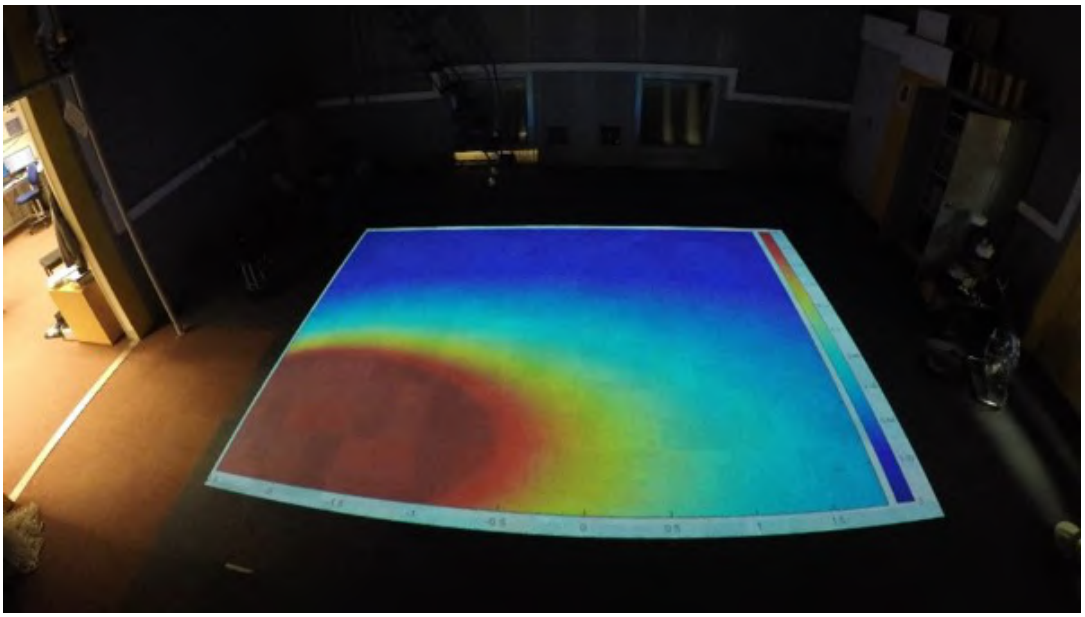

Figure 5.13: Example output plume estimate of the STE algorithm using the source estimate after an experiment with four burning incense sticks.

Chapter 6

Source term estimation of a hazardous airborne release using an unmanned aerial vehicle

In this chapter, the Bayesian based STE algorithm is extended to estimate the source term of a dispersive release using measurements from a UAV. The chapter focuses on validation of the estimation algorithm so a pre planned uniform sweep flight pattern is used rather than the information based planning method. The source term parameters that are estimated are extended to include the three dimensional location of the release rather than 2D. The parameters of the source are estimated by fusing concentration observations from a gas detector on-board the aircraft, with meteorological data and an appropriate model of dispersion. Two simple, fast running models are compared in this chapter, both derived from analytical solutions to the advection diffusion equation. The system is verified with novel, outdoor, fully automated experiments, where observations from the UAV are used to estimate the parameters of a real diffusive source. The estimation performance of the algorithm is assessed subject to various flight path configurations and wind speeds. Observations and lessons learned during these unique experiments are discussed and areas for future research are identified.

This chapter is based upon work by the author in [207]. The remainder of this chapter is outlined as follows. Firstly, the contributions of the chapter are outlined in the subsection below. In Section 6.1, the setup of the system is described in greater detail. A formal description of the problem is given in Section 6.2. In Section 6.3, the Bayesian estimation of the source parameters is described, including formulations of the models used and the computational implementation of the algorithm. Experimental trials are presented in Section 6.4, including the setup, implementation remarks, an illustrative run and the results. Discussions and lessons learned are provided in Section 6.5, and finally, conclusions and ideas for future research are given in Section 6.6.

6.0.1 Contributions of the chapter

Gas source localisation has been an active area of academic research for some time. In spite of this, existing experimental results have rarely been obtained in realistic environments or even outdoors. To the best of the authors knowledge, gas source localisation using a UAV has only been achieved with a single system [32]. This was a significant step forward, simultaneously extending previous work to an outdoor environment and utilising a UAV that could estimate the wind vector using its inertial measurement unit [200]. The experimental results were impressive, however, there were still some limitations at this stage: the search area was quite narrow and two dimensional, a fan at the source was used to create a nice flow to help spread the gas, the UAVs altitude was held manually, it was initiated from within the gas plume, and finally, the emission rate of the source was not estimated. All the former points are addressed in this chapter.

Source term estimation is popular area of research, with significant experimental results obtained using high quality datasets from experimental trials of tracer gas dispersion such as the Joint Urban 2003 study in Oklahoma [208]. Contributions in this area typically focused on using a network of static gas detectors [4, 2]. In the present study, a UAV is guided fully autonomously to collect the spatial temporal data required to estimate the parameters of a dispersive release. When using a static network, gas concentration samples are typically averaged over a period of a minute or more. Given the short flight time of a UAV this is greatly decreased, resulting in significantly different outputs from the sensor; characterised by greater intermittency, or non detections, and increased noise. A new likelihood function is used to handle the intermittent detections and greater uncertainty incurred by the shorter sampling periods. Another contribution is a comparison of two dispersion models, proposed in the literature for source term estimation, using the unique experimental data collected by the UAV. Modelling is a critical component of STE algorithms. For applications that do not require a rapid response, it would be reasonable to use more complex and potentially more accurate methods such as CFD to model the expected observations from the detectors. When a rapid response is required, the simple models may be more appropriate. In this work, two simple, fast running models, formulated from the advection diffusion equations with various assumptions, are compared using the unique data collected during the experimental trials: The Gaussian plume equation [209] and an Isotropic plume equation [10]. The predominant difference between the models lies in the specification of the diffusivity parameters. Furthermore, two simple, fast running dispersion models . To the best of the authors knowledge, the experimental trials described in this thesis mark the first occasion where a UAV is used, in realistic conditions, to search for and estimate the source term parameters of a gaseous release. This is a significant step towards an operational system.

The theoretical foundations of this chapter were predominantly a result of earlier work that has been verified in simple simulation studies, datasets collected in a turbulent water

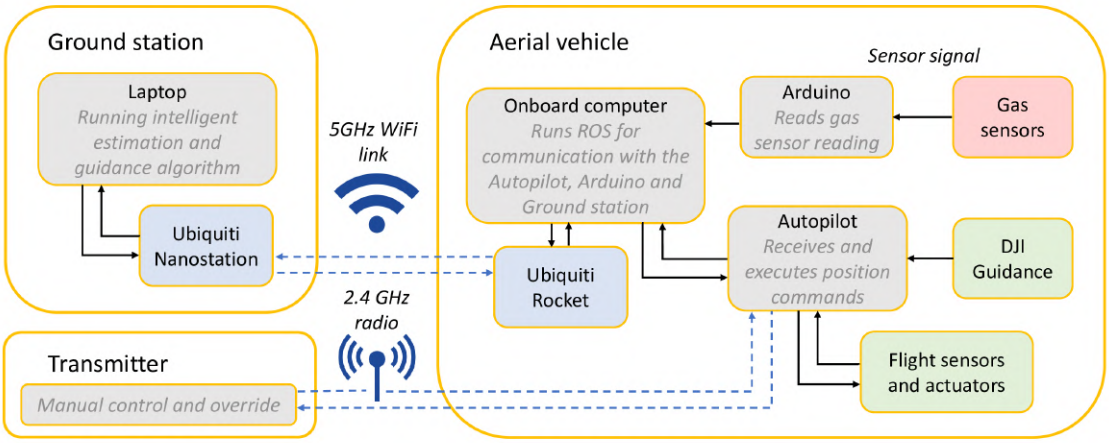

Figure 6.1: System overview: The measurements from the PID gas detector are read by an Arduino Uno. The ground station and the on-board computer communicate over 5GHz WiFi. The Arduino and autopilot communicate with the on-board computer via serial and UART connections. The transmitter is used to switch between manual and autonomous flight. The DJI Guidance system is connected to the autopilot to provide more accurate localisation in flight.

channel, or by using a ground robot indoors [198]. In addition to the moderate adjustments to enable the algorithms practical implementation with a UAV, such as a novel likelihood function, the main contributions of this work are of a practical and experimental nature, as follows:

- A complete UAV based gas source estimation system has been developed consisting of gas sensors, a UAV, a ground control station, and a source estimation algorithm.
- The trials mark the first experimental result of source term estimation performed using gas measurements from an autonomous UAV.
- The source estimation performance is assessed with regards to the UAVs altitude, the distance between gas measurements and the wind speed or atmospheric stability.
- The experiments in general are rare, where a gas source is localised in an outdoor environment rather than in more controlled indoor arenas where fans are used to generate wind.
- Two well known models are compared using the unique experimental data.

Given such an immature area to obtain experimental results there were several observations and lessons learned during the outdoor trials. This has lead to new insights and subsequently, new areas identified for future research.

Figure 6.2: System components: DJI Matrice 100 UAV, ground station laptop, WiFi equipment and radio transmitter.

6.1 System overview

The main components of the system are a quadrotor UAV platform, an on-board computer, a ground station laptop and the gas sensing payload. An overview of the system is outlined in Fig 6.1 and a photo of the equipment prior to an experimental trial is shown in Fig 6.2. The remainder of this section shall further describe the system components and its set-up.

The system primarily consists of a quadrotor UAV and a laptop as a base station. The quadrotor is equipped with a photoionisation detector (PID) which is used to measure the concentrations of the hazardous gas. Currently, the measured concentrations are sent to the ground station using a 5Ghz WiFi network. The system executes a systematic sweep search pattern to collect the data. The ground station will run the Bayesian estimation of the source parameters and send the next position demand to the UAV. This set-up is chosen to facilitate the development of a more efficient on-line planning algorithm in the future. Due to the very fast computational time of the algorithm the computation could potentially be performed by the on-board computer of the UAV, however, during the experimental trials the laptop was used for simplicity and to enable more seamless algorithm development [210]. Furthermore, the data sent consisted only of a concentration measurement and 3D location coordinates. The Robot Operating System (ROS) framework was used for all communications between the autopilot and the on board computer, and likewise between the on-board computer and the ground-station.

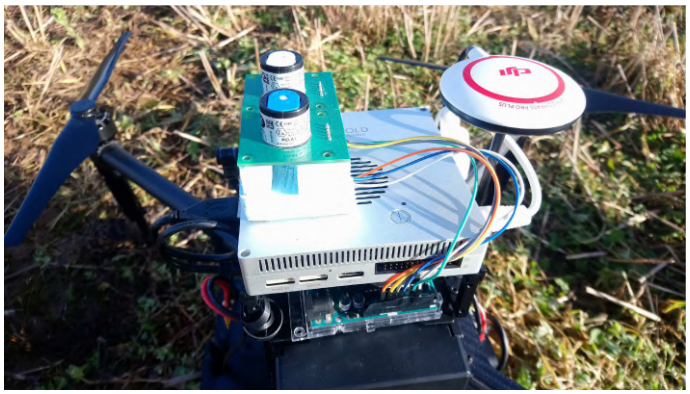

Figure 6.3: PID gas sensors connected to an Arduino Uno on-board the UAV.

6.1.1 Aerial platform

The aerial platform is a DJI Matrice 100 as shown in Fig 6.2. Among other components, it is equipped with: DJI's guidance system, to support accurate localisation; an autopilot; a GPS; and DJI's on-board computer called the manifold. The manifold is a reasonably powerful computer based off an Nvidia Tegra. Although, in the present study, the algorithms are run on the ground station laptop, in the future they could be deployed to run on-board the UAV. This would have great benefits in large or cluttered scenarios, such as urban areas, where wireless communication could become unstable. The on-board computer communicates with the autopilot via UART and with the ground station via 5GHz WiFi. The WiFi communication is achieved via a bridge between a Ubiquiti Rocket on-board the Matrice 100 and a Ubiquiti M5 Nanostation which is connected to the laptop on the ground. A 5GHz link is selected over the longer range 2.4GHz to avoid interference with the remote controller. The ROS[1] software framework is used for communication among the system components. The dji_sdk[2] package facilitates communication between the on-board computer and the autopilot. Additionally, the data from the gas sensor is read by an Arduino Uno and input to the ROS network using the rosserial_arduino[3] package. The ROS network allows the autopilot data, sensor data, and commands from the ground station to be shared among the connected components in the system.

The set-up of the system was motivated by the ability to quickly test algorithms developed in Matlab without the requirement to compile the code on the UAV. This enabled rapid development and adjustments to the algorithm whilst out in the field. During the experiments, the 3D position of the UAV and a sensor reading are sent from the on-board computer to the ground station. The ground station updates its estimates of the source term parameters using a sequential Bayesian algorithm, and sends a new position demand to the aerial vehicles on-board computer. The dji_sdk package performs the lower level control to manoeuvre the UAV to the new position.

[1] http://www.ros.org
[2] http://wiki.ros.org/dji_sdk
[3] http://wiki.ros.org/rosserial_arduino

6.1.2 Gas sensing payload

The UAV is equipped with a PID gas detector to take measurements of the hazardous gas, as shown in Fig 6.3. The PID sensors were chosen as they are a reasonable price and highly sensitive to a large number of chemicals. The output of the PID detector is a reading related to the concentration of a standard volatile organic compound (VOC), isobutelene. A data sheet is provided with the sensors to approximate this to a parts per billion (ppb) measurement of the target gas, which is subsequently converted to a concentration measurement in g/m^3. As shown in Fig 6.3, the sensor is wired to an Arduino Uno[4], which communicates with and draws power from the on-board computer via a serial connection.

One of the dominant factors to consider when measuring a gas using a UAV is the effect of the rotors on the dispersion of the gas and the output from the sensor. This effect has been taken into consideration in the past and research has been conducted to determine the optimal position of the gas detector and the effect on the sensor measurement [6, 25, 22]. Some of the potential sensor positions proposed include: under the rotors of the UAV, in the centre of the platform raised above or below it, in the space between the UAV rotors, and extended on an arm away from the platform and its effect on the gas. Through computational fluid dynamics (CFD) studies, smoke visualisation experiments, and pressure and airflow measurements around the UAV, some conclusions can be drawn, despite conflicting results. The general consensus is that the effect of the rotors is to decrease the measurement from the gas detector and increase its uncertainty [26]. The most accurate measurements would come from a sensor outside of the disturbed region of airflow, however, this would be more likely to cause stability issues whilst in flight. A pumped system could be implemented on the vehicle, where the inlet would be away from the platform, still, this would add undesirable weight to the system. For these reasons, the most common placement seen in the literature is in a raised position, in the centre of the platform [6, 28]. The focus of the present work is on validating a source term estimation algorithm using a UAV, consequently, the effect of the rotors has not been prioritised. Nevertheless, the effect on the source estimates is discussed in the results. Given the huge increase in applications and experiments involving gas sensing on UAVs, it is envisaged that bespoke new sensors, designed for UAVs will have a great benefit and will be an important area for future research.

In this chapter, we place the sensor in the most common area suggested in the literature: in an elevated position in the centre of the UAV, as shown in Fig 6.3. Although this is likely to effect the reading from the sensor, it is structurally more favourable than extending it on an arm, more lightweight than using a pumped system, and it will protect the sensor in the event of a hard landing. Sensor placement, and possibly correction factors to account for the UAVs rotor effect are left as an area for future research. However,

[4]https://www.arduino.cc/

the effect on the source estimation results are examined and discussed in Sections 6.4 and 6.5.

6.2 Problem description

After an event such as an earthquake or explosion, a large area of concern exists where there is the potential for a hazardous release from damaged pipes or chemical facilities. In response to a suspicious smell, it could be challenging to find the source or determine if it is hazardous. After an act of terrorism involving gas, it would be of paramount importance to locate the source without endangering the lives of responders. During an important event it may be desirable to monitor the surrounding area for signs of a dangerous release. Given such an area of interest, the goal of this work is to provide an algorithm to autonomously search for and estimate the parameters of a release, with a high degree of accuracy and in a short amount of time.

The zone of interest, parameterised by the three dimensional volume $\Omega \subset \mathbb{R}^3$, will be used to initialise the search area of the algorithm. This could be the region where a suspicious odour is reported, a region of interest to survey, an area along a pipeline or the area around a chemical facility. The UAV, equipped with the relevant gas detector payload, is to navigate within the area to estimate the release parameters otherwise known as the source term. This shall provide responders with information about the location of the release, as well as the necessary inputs to an ATD model to produce a forecast of the hazard.

The UAV is aware of its location $\mathbf{p}_k = \begin{bmatrix} x_k & y_k & z_k \end{bmatrix}^\mathsf{T} \in \Omega$ within the domain. In this present study, this is achieved via fusion of GPS, IMU, ultrasonic and stereo image data. The gas detector on-board the UAV observes point-wise measurements of the gas concentration $z_k \in \mathbb{R}^+$. The meteorological parameters are provided by a local weather station. The location stamped measurements and meteorological observations are used to estimate the parameters of the source Θ_k, which in this work, is given by:

- Cartesian coordinates of the source $\mathbf{p}_s = \begin{bmatrix} x_s & y_s & z_s \end{bmatrix}^\mathsf{T} \in \Omega$ in meters (m).
- Emission rate/strength of the source $q_s \in \mathbb{R}^+$ in grams per second (g/s).
- The wind speed $u_s \in \mathbb{R}^+$ in meters per second (m/s) and direction $\phi_s \in \mathbb{R}$ in radians (rad).
- Model dependant diffusion parameters $\zeta_s = \begin{bmatrix} \zeta_{s1} & \zeta_{s2} \end{bmatrix}^\mathsf{T} \in \mathbb{R}^+$ which relate to the spread of the gas concentration from the source.

Hence, the parameter vector of the source term can be defined as:

$$\Theta_k = \begin{bmatrix} \mathbf{p}_s^\mathsf{T} & q_s & u_s & \phi_s & \zeta_s \end{bmatrix}^\mathsf{T}. \tag{6.1}$$

The key parameters of the source term are its location and emission rate. The remaining parameters are incorporated to add robustness to the system and account for uncertainties.

The UAV is to autonomously search the environment, collecting point observations $\mathbf{z}_{1:k} = \{z_1, \ldots, z_k\}$ from the gas detector at discrete time steps $k = 1, \ldots, k$ and at known locations $\mathbf{p}_{1:k} = \{\mathbf{p}_1, \ldots, \mathbf{p}_k\}$. At each time step k, the estimates of the source parameters Θ_k are updated by drawing the inference on the probabilistic distribution $p(\Theta_k|\mathbf{z}_{1:k})$. The next location to make an observation with the gas detector $\mathbf{p}_{k+1}$ is then selected, and navigated towards, to begin the next iteration of the algorithm.

6.3 Source term estimation

In such a scenario where input variables, measurements and underlying models are fraught with uncertainty, a probabilistic approach is preferable so that the errors can be accounted for by designing a likelihood function to reflect such uncertain conditions. Under this approach, the uncertainty in the source term estimates can be captured within a probability density function (pdf). Bayes' theorem is used to update the estimates of the source parameter vector Θ_k in a recursive manner given the measurements from the gas detector $\mathbf{z}_{1:k}$ and prior information.

Using the Bayesian framework, the current state of knowledge regarding the source parameters is represented by a posterior probability distribution $p(\Theta_k|\mathbf{z}_{1:k})$, where $\mathbf{z}_{1:k}$ implies that the measurement data are collected at locations $\mathbf{p}_{1:k}$, respectively. In response to new measurement data from the gas detector z_{k+1}, the posterior distribution is updated according to Bayes' rule, such that

$$p(\Theta_{k+1}|\mathbf{z}_{1:k+1}) = \frac{p(z_{k+1}|\Theta_{k+1})p(\Theta_{k+1}|\mathbf{z}_{1:k})}{p(z_{k+1}|\mathbf{z}_{1:k})} \tag{6.2}$$

where

$$p(z_{k+1}|\mathbf{z}_{1:k}) = \int p(z_{k+1}|\Theta_{k+1})p(\Theta_{k+1}|\mathbf{z}_{1:k})\,\mathrm{d}\Theta_{k+1}. \tag{6.3}$$

The initial prior distributions $\pi(\Theta_0) \equiv p(\Theta_0)$ of the source parameters are assumed to be provided to the algorithm, these can be obtained autonomously through sensory data or by user input. For example, the prior distribution for the location of the source is a uniform distribution that is bounded by the domain Ω. In subsequent iterations, the prior distributions are replaced by the posteriors to reflect the information gained from the previous sequence.

6.3.1 The likelihood function

To construct the likelihood function $p(z_{k+1}|\Theta_{k+1})$ used in Eq. (6.2), there must be a method of linking sensor measurements z_k with the expected observations. To do this, a

model of the dispersion from a source and a model of the sensor response are required.

6.3.1.1 Dispersion models

The dispersion model will provide the expected concentration at position $\mathbf{p}_k$ produced from a hypothesised source with parameters Θ_k, given as $\mathcal{M}(\mathbf{p}_k, \Theta_k)$. Any relevant model can be used; there exist highly complex particle tracking models, CFD techniques, or equations derived from analytical solutions to the advection-diffusion equations such as the Gaussian plume dispersion model. The model is interchangeable without any other changes to the algorithm, and should be chosen to reflect the current scenario. For example, the NAME dispersion model is used by the UK Met Office to forecast long range ash dispersion from a volcanic eruption [68], whereas CFD based methods have been developed for complex geometries such as urban environments [134, 203]. In this work, two models are compared, both derived from analytical solutions to the advection diffusion equation with various assumptions: The standard gaussian plume (GP) model [209], and a more simplified model assuming isotropic diffusion [10] which shall be referred to as the isotropic plume (IP) model. Both models are fast running and based on the assumption of a steady state plume with a consistent mean wind velocity, source strength, and turbulent conditions. The principle difference among the methods is in the specification of the diffusion parameters $\zeta_{\mathbf{s}} = [\zeta_{s1}, \zeta_{s2}]$ and the assumptions therein.

6.3.1.1.1 Gaussian plume model The GP model approximates the spread of the gas from the source in the crosswind, horizontal and vertical directions using measurements or approximations of atmospheric stability. To account for uncertainties, the diffusion parameters are adopted from [142], resulting in $[\zeta_{s1}, \zeta_{s2}]$ representing stochastic diffusion terms in the horizontal and vertical directions. Subsequently, the expected concentration to be read by a detector at position $\mathbf{p}_k$ from a source with parameters Θ_k using the Gaussian plume model is given as

$$\mathcal{M}(\mathbf{p}_k, \Theta_k) = \frac{q_s}{u_s \sigma_{y,k} \sigma_{z,k} 2\pi} \exp\left(\frac{-c_k^2}{2\sigma_{y,k}^2}\right) \times \left[\exp\left(\frac{-(z_k - z_s)^2}{2\sigma_{z,k}^2}\right) + \exp\left(\frac{-(z_k + z_s)^2}{2\sigma_{z,k}^2}\right)\right], \tag{6.4}$$

where c_k is the crosswind distance from the source, and, given that the downwind distance from the source is d_k, the standard deviations of concentration in the crosswind and vertical directions are:

$$\sigma_{y,k} = \frac{\zeta_{s1} d_k}{\sqrt{(1 + 0.0001 d_k)}} \quad and \quad \sigma_{z,k} = \frac{\zeta_{s2} d_k}{\sqrt{(1 + 0.0001 d_k)}}. \tag{6.5}$$

6.3.1.1.2 Isotropic plume model The Isotropic model assumes isotropic diffusion from the source. Following [10], the diffusion terms $[\zeta_{s1}, \zeta_{s2}]$ represent the diffusivity of

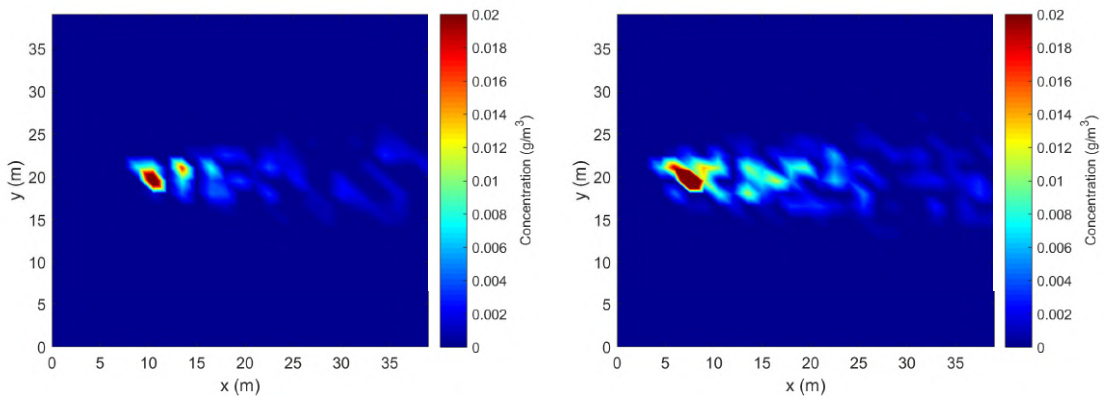

(a) Gaussian plume model

(b) Isometric plume model

Figure 6.4: Example plots of the expected observations z_k of the UAV flying at a 2.5m altitude using: (a) the GP model; and (b) the IP model. The source had parameters: $x_s = 4, y_s = 20, z_s = 1.5, q_s = 1$, $u_s = 5$, and $\phi_s = 90°$.

the gas in the environment, and the average lifetime of the gas. Given the model, the expected concentration to be read by a detector at position $\mathbf{p}_k$ from a source at position $\mathbf{p}_s$, releasing gas at a rate of q_s with average lifetime ζ_{s2} in an environment with mean wind speed u_s, wind direction ϕ_s and diffusivity ζ_{s1} is given by:

$$\mathcal{M}(\mathbf{p}_k, \Theta_k) = \frac{q_s}{4\pi\zeta_{s1}||\mathbf{p}_k - \mathbf{p}_s||} \exp\left[\frac{-||\mathbf{p}_k - \mathbf{p}_s||}{\lambda}\right] \times \exp\left[\frac{-(x_k - x_s)u_s \cos\phi_s}{2\zeta_{s1}}\right] \exp\left[\frac{-(y_k - y_s)u_s \sin\phi_s}{2\zeta_{s1}}\right], \quad (6.6)$$

where

$$\lambda = \sqrt{\frac{\zeta_{s1}\zeta_{s2}}{1 + (u_s^2\zeta_{s2})/(4\zeta_{s1})}}. \quad (6.7)$$

An example plot from each of the models is shown in Fig 6.4, where the sensor model to be described in the next section has been applied. The main difference in the outputs of the models is seen in the vicinity of the source, particularly upwind. Upwind of the source, the GP model (Fig 6.4a) assumes zero mean concentration from the source whereas the IP model (Fig 6.4b) does not. The GP model is more popular in the literature, it is extensively studied, and even accepted commercially. However, the model is typically used on a larger scale than the experiments conducted in this chapter and as depicted in the example figures.

6.3.1.2 Gas sensing model

To form the likelihood function used in Eq. (6.2), the measurements from the gas detector must be related to the expected observations deduced from the dispersion models. The measurement data $\mathbf{z}_{1:k}$ features detection events, where measurements from the gas de-

tector picked up some concentrations from the source, and non detection events, where the measurement did not surpass a pre-specified threshold z_{thr}. The threshold is set high enough to minimise false detections, whilst maintaining sufficient sensitivity. The observational data, and subsequently the likelihood function, can be split among these detections $\overline{z}_k$ and non detections $\underline{z}_k$ [211] as:

$$p(z_k|\Theta_k) = \begin{cases} p(\overline{z}_k|\Theta_k) & \text{if } z_k > z_{thr}, \\ p(\underline{z}_k|\Theta_k) & otherwise. \end{cases} \tag{6.8}$$

The observational model linking detection data $\overline{z}_k$ with the source term parameters Θ_k is given as

$$\overline{z}_k = \mathcal{M}(\mathbf{p}_k, \Theta_k) + \overline{v}_k, \tag{6.9}$$

where $\overline{v}_k$ encapsulates the various errors between the measured and modelled concentration at a particular position $\mathbf{p}_k$. The discrepancy can arise from measurement error, input error, model error and stochastic uncertainty [182]. Given the limited knowledge of the errors between predicted and measured concentrations, application of the maximum entropy principle suggests the Gaussian distribution as the most conservative choice for the likelihood function [212, 211]. Thus the likelihood function for a detection event is as follows:

$$p(\overline{z}_k|\Theta_k) = \frac{1}{\sigma_k\sqrt{2\pi}} \exp\left[-\frac{(\overline{z}_k - \mathcal{M}(\mathbf{p}_k, \Theta_k))^2}{2\sigma_k^2}\right], \tag{6.10}$$

where the variance σ_k is a function of the modelled concentration such that $\sigma_k \propto \mathcal{M}(\mathbf{p}_k, \Theta_k)$.

A non detection event on the other hand, can be caused by three hypothesised scenarios: The concentration measurement is only a result of background and instrument noise $\mathcal{E}_b$; the non detection is a result of intermittency caused by turbulence or a missed detection $\mathcal{E}_m$, typically exacerbated by the short sampling intervals of the UAV; or, the concentration includes contributions from both the source and background, although it did not amount to a value above the concentration threshold $\mathcal{E}_s$. Combining the three hypotheses results in the following likelihood of a non detection:

$$p(\underline{z}_k|\Theta_k) = p(\mathcal{E}_b) \cdot p(\underline{z}_k|\mathcal{E}_b, \Theta_k) + p(\mathcal{E}_m) \cdot p(\underline{z}_k|\mathcal{E}_m, \Theta_k) + p(\mathcal{E}_s) \cdot p(\underline{z}_k|\mathcal{E}_s, \Theta_k), \tag{6.11}$$

where the probability of each event is given as $p(\mathcal{E}_b) = P_b$, $p(\mathcal{E}_m) = P_m$ and $p(\mathcal{E}_s) = P_s$ and $P_b + P_m + P_s = 1$. Assuming the background noise and contributions from the source can be modelled as normal distributions the likelihood function for a non detection can

be written as

$$p(\underline{z}_k|\Theta_k) = \left(P_b \times \frac{1}{2}\left[1 + \text{erf}\left(\frac{z_{thr} - \mu_b}{\sigma_b\sqrt{2}}\right)\right]\right) + P_m \\ + \left(P_s \times \frac{1}{2}\left[1 + \text{erf}\left(\frac{z_{thr} - (\mu_b + \mathcal{M}(\mathbf{p}_k, \Theta_k))}{\sigma_k\sqrt{2}}\right)\right]\right), \tag{6.12}$$

where μ_b and σ_b are the mean and variance of the background noise and erf() denotes the error function. The values of P_b, P_m and P_s were set during the experiments.

Given the appropriate models and Bayesian formulations, the next section will describe a method to implement the probabilistic estimation of the source parameters.

6.3.2 Sequential Bayesian implementation

The Bayesian estimation of the source parameters is implemented in the sequential Monte Carlo framework using a particle filter. The output is an approximation of the posterior distribution $p(\Theta_k|\mathbf{z}_{1:k})$, which represents the current state of knowledge about the source parameters. The posterior distribution from Eq. (6.2) is approximated by a set of weighted random samples $\{\Theta_k^{(i)}, w_k^{(i)}\}_{i=1}^N$, where

$$\Theta_k^{(i)} = \begin{bmatrix} x_{s,k}^{(i)} & y_{s,k}^{(i)} & z_{s,k}^{(i)} & q_{s,k}^{(i)} & u_{s,k}^{(i)} & \phi_{s,k}^{(i)} & \zeta_{s1,k}^{(i)} & \zeta_{s2,k}^{(i)} \end{bmatrix}^\mathsf{T} \tag{6.13}$$

is a sample representing a potential source term and $w_k^{(i)}$ is the corresponding normalised weighting such that $\sum_{i=1}^N w_k^{(i)} = 1$. Given the weighted samples, the posterior distribution is approximated as:

$$p(\Theta_k|\mathbf{z}_{1:k}) \approx \sum_{i=1}^{N} w_k^{(i)} \delta(\Theta_k - \Theta_k^{(i)}), \tag{6.14}$$

where $\delta(\cdot)$ is the Dirac delta function. The sample weights are updated in a recursive manner by sequential importance sampling [204]. At each time step, a set of new samples $\{\Theta_{k+1}^{(i)}\}_{i=1}^N$ can be drawn from a proposal distribution $q(\Theta_{k+1}^{(i)})$, which should resemble the distribution $p(\Theta_{k+1}|\mathbf{z}_{1:k+1})$. The corresponding un-normalised weights are then updated according to:

$$\bar{w}_{k+1}^{(i)} \propto w_k^{(i)} \cdot \frac{p(z_{k+1}|\Theta_{k+1}^{(i)}) p(\Theta_{k+1}^{(i)}|\Theta_k^{(i)})}{q(\Theta_{k+1}^{(i)}|\Theta_k^{(i)}, \mathbf{z}_{1:k+1})}. \tag{6.15}$$

The proposal distribution is typically used to update the samples to the next time step for estimating dynamic states. By assuming a time-invariant source term (i.e. the source position is fixed and the release rate is constant), the proposal distribution can be assumed to be identical to the posterior at time k. This leads to a simple algorithm where $\Theta_{k+1}^{(i)} = \Theta_k^{(i)}$ for $i = 1, ..., N$ [55]. Due to cancellation of terms in Eq. (6.15), the un-normalised particle weights are updated using the likelihood function and the previous

weight as follows:

$$\bar{w}_{k+1}^{(i)} = w_k^{(i)} \cdot p(z_{k+1}|\Theta_{k+1}^{(i)}). \tag{6.16}$$

The sample weights are then normalised as $w_{k+1}^{(i)} = \bar{w}_{k+1}^{(i)} / \sum_{i=1}^{N} \bar{w}_{k+1}^{(i)}$ to obtain the new approximation of the posterior.

Importance sampling is carried out sequentially at each time step. This can eventually lead to only a few particles with non-negligible weights, known as the degeneracy problem. To avoid sample degeneracy, the number of effective samples are estimated by:

$$N_{eff} = \frac{1}{\sum_{i=1}^{N} (w_k^{(i)})^2}. \tag{6.17}$$

When the number of effective point estimates N_{eff} falls below a pre-specified threshold η the sample points are re-sampled. This can lead to another problem where highly weighted particles will be multiplied many times, leading to a lack of diversity. This problem is referred to as sample impoverishment. To improve the diversity of the random samples, the re-sampled estimates are regularised by drawing new samples from a Gaussian kernel. The new samples undergo an MCMC move step [204], where they will be accepted with a probability proportional to their likelihood.

6.4 Experimental trials

In this section the experiments used to verify the system are described and the results are presented and discussed. Firstly, the experiment setup is outlined including information about the environment, the equipment used, the inputs to the algorithm and remarks on its implementation. Given the setup, an illustrative run of one of the trials is provided to further illustrate the experimental procedure and the capabilities of the algorithm. The results of all the conducted experimental trials are then summarised. Finally, the output estimates of the algorithm are assessed with regards to the measurement altitude of the UAV, the step increment in the sweep pattern, and the wind speed or atmospheric stability.

6.4.1 Experiment setup

The experiments were conducted outdoors in an open field, in order to verify the algorithm for the first time in real world atmospheric conditions, outside of simulation. Acetone was released into the atmosphere using a source comprising of ultrasonic diffusers and an air pump, as depicted in Fig 6.5. The release rate of the source was obtained by measuring directly, the change in weight at the beginning and the end of the experiments and assuming that it was emitted at a constant rate. The release rate was typically 1.5g/s, however, this would vary depending on atmospheric conditions such as temperature and pressure.

The field used during the experiments was located nearby Loughborough University,

Leicestershire, UK. A large square within the field, containing the release, would represent the domain Ω which forms a part of the input to the algorithm. A photo of the environment is shown in Fig 6.6, featuring examples of the starting location of the UAV, the wind direction and the position of the source.

(a) (b)

Figure 6.5: (a) Source set-up for the experiments comprising of acetone, diffusers and an air pump. (b) A snapshot of the source and UAV during an experimental trial.

Figure 6.6: An example photo of the environment set-up for the experimental trials. The UAV begins the search at the white square and perform a sweep search pattern within the red area, which represents the prior distribution for the location of the diffusive source. The true position of the source is indicated by the black circle and the wind direction is implied by the red arrow.

6.4.2 Implementation remarks

In this section, the details on the implementation of the source estimation algorithm from Section 6.3 are outlined. This includes the specification of the prior distributions used to initialise the algorithm and the control of the UAV to collect the observational data.

6.4.2.1 Prior distributions

Initial distributions must be set for all of the parameters in the source vector Θ_k. Where possible the distributions are set based off sensory data, for example, the wind speed and direction distributions can be assigned from meteorological measurements. The prior distributions should reflect information known about the release, or lack thereof. For example, intelligence may exist as to the possible whereabouts of the source location, or there may exist some known bounds on the rate of emission. To assess the algorithm in realistic conditions, it is assumed, in the trials, that there is little information known about the release beforehand. The prior distributions are summarised as follows:

- The prior distributions for the location of the source $[p_0(x_s), p_0(y_s), p_0(z_s)]$ were set to uniform within the domain Ω. The size of the domain is the key input of a user, essentially, it is the area in which to search for the source. Multiple domain sizes were used during the experiments, ranging from 42x42m to 15x15m.
- A gamma distribution was used as the prior for the emission rate $p_0(q_s) = \mathcal{G}(1, 5)$. This is a long tailed distribution to account for a large amount of uncertainty in the emission rate of the source. This prior was fixed during all of the experimental trials.
- The meteorological variables $[p_0(\phi_s), p_0(u_s)]$ were assigned Normal distributions $\mathcal{N}(\mu, \sigma)$ upon initialisation of the algorithm. In the future, the meteorological variables should be measured in-situ, on-board the UAV, in order to alleviate dependence on other data sources.
- The dispersion parameters $[\zeta_{s1}, \zeta_{s2}]$ were given uniform distributions with an appropriate range.

6.4.2.2 UAV control

The UAV executes a systematic sweep search pattern to collect spatial temporal measurements of the gas concentration. The search pattern can be generated using coverage path planning algorithms. As the flight path is fixed, the flight could have been pre-planned and uploaded to the autopilot using some mission planning software. However, in order to facilitate on-line, more informative planning in the future, the position demands were sent directly from the laptop during flight. The control of the UAV was made fully autonomous by utilising the dji_sdk ROS package. This included take-off, landing and the uniform sweep flight pattern. Upon take-off, the minimum altitude of the UAV was set to 1.2m above ground, measured by ultrasonic sensors, to minimise the chance of a collision. Manual override was also possible throughout the experiments.

At each time step, the UAV would hover to take an averaged measurement of the concentration. The sample duration was set to 5 seconds. This was a short amount of time compared to source term estimation methods incorporating static sensors, where it is

more common to sample for a few minutes. This sampling time was chosen as a trade-off between the measurement accuracy and search time.

After the sample is collected and the source parameter estimates are updated, the UAV would proceed to the next measurement location defined by the uniform sweep pattern. The control of the UAV, to the next position, was handled autonomously by the dji_sdk ROS package. The incremental step size between each measurement location was set to 3, 4, 5 or 6m.

6.4.3 Illustrative run

An illustrative run of an experiment, Trial 25, is given in Fig 6.7. Overlaid on a map of the experimental field, the figure shows: the flight path of the UAV executing the sweep search pattern at various snapshots in time; the measurements at each sampling location; the true position of the source; and an indication of the wind direction. In this example the GP model was used as the underlying dispersion model in the estimation algorithm. To begin the search, the system is initialised at discrete time step $k = 0$ as shown in Fig 6.7a. The starting position of the UAV is indicated by the white square, the source is given by the black circle, and the red arrow points in the direction of the wind. The large number of red dots represent the random sample approximation used in the sequential Monte Carlo algorithm at the current time step, which in this figure, approximates the prior distribution. Each dot represents a weighted source term realisation $\{\Theta_k^{(i)}, w_k^{(i)}\}$, where only the marginalised position estimates are visualised in the figure. Figures 6.7b, 6.7c and 6.7d show the trajectory of the UAV, given by the white line, and the update of the Monte Carlo samples at time steps, $k = 6, 16$ and 36. The white circles indicate the positions where the UAV hovered to collect an averaged measurement from the gas detector; their size is representative of the measured value.

The illustrative run (Trial 25) was conducted in relatively high wind (8m/s) and neutrally stable atmospheric conditions, characterised by Pasquill's stability class D [213]. The search area was a 25x25m square in which measurements were taken at 5m intervals at 1.2m altitude. The sub figures in Fig 6.7, show how the estimate of the source location is narrowed down significantly in response to the gas measurements. Positive detections had a larger effect on the posterior distribution as they were associated with less uncertainties than zero sensor readings as had been reflected in the respective likelihood function in Eq. (6.10). The location of the source was narrowed down more quickly in the crosswind direction than upwind, as seen in Fig 6.7c. This is an expected attribute due to the concentration distributions and characteristics of both of the underlying dispersion models, where uncertainties and correlations in the wind speed and source strength incur a lot of uncertainty in the upwind location of the source.

The result of the illustrative run is summarised in Fig 6.8, in a manner that is used for comparisons in the results section. Figure 6.8a shows the resulting flight path (white

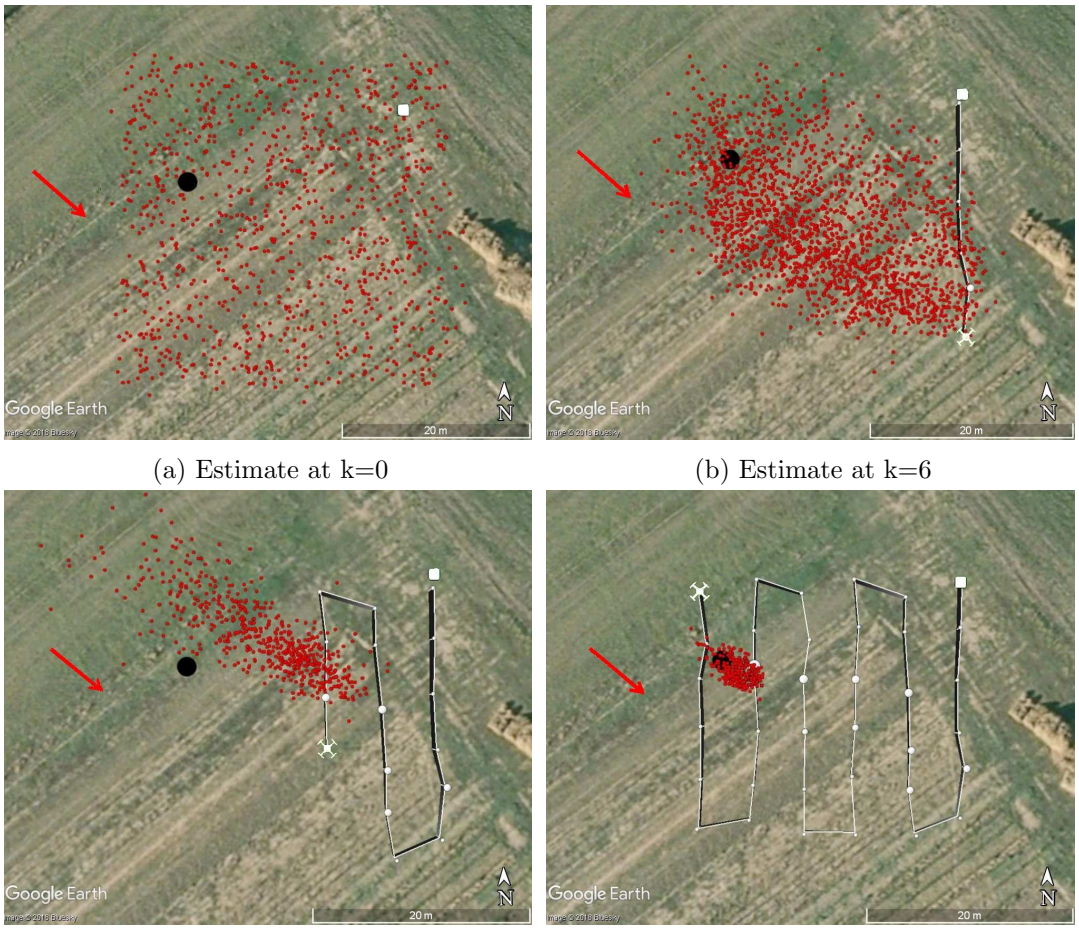

(a) Estimate at k=0

(b) Estimate at k=6

(c) Estimate at k=16

(d) Estimate at k=36

Figure 6.7: Example run of the algorithm at discrete time steps: (a) k=0, (b) k=6, (c) k=16 and (d) k=36. The white line indicates the path of the UAV and the black circle represents the true position of the source. The white square and quadrotor symbol indicate the starting and current location of the UAV. The red dots represent the random sample approximation of the source parameter estimates at the current time step and the red arrow indicates the wind direction.

line), wind direction (red arrow) and marginalised posterior estimate of the source location (heat map). The Monte Carlo samples used in Fig 6.7d are replaced by a heat map to display the posterior estimate more clearly. The starting and ending positions of the UAV are given by the white square and diamond. The true position of the source is indicated by the black circle filled with a white cross and the algorithms mean estimate is given by the hollow black circle. Figure 6.8b shows the probability density estimate of the emission rate of the source, $p(q_s|\mathbf{z}_{1:k})$, and the measurement data during the flight, $\mathbf{z}_{1:k}$. The blue curve represents the PDF of the emission estimate with mean and standard deviation indicated by the vertical dashed green lines. The black dashed curve shows the prior distribution provided to the algorithm, and the true value is given by solid red line. Bars in the lower figure of 6.8b indicate the measurement at the discrete time step. In this example the position estimate of the source was very accurate, with only a 2.43m Euclidean error. The emission estimate was also accurate, but underestimated by 0.58grams/s.

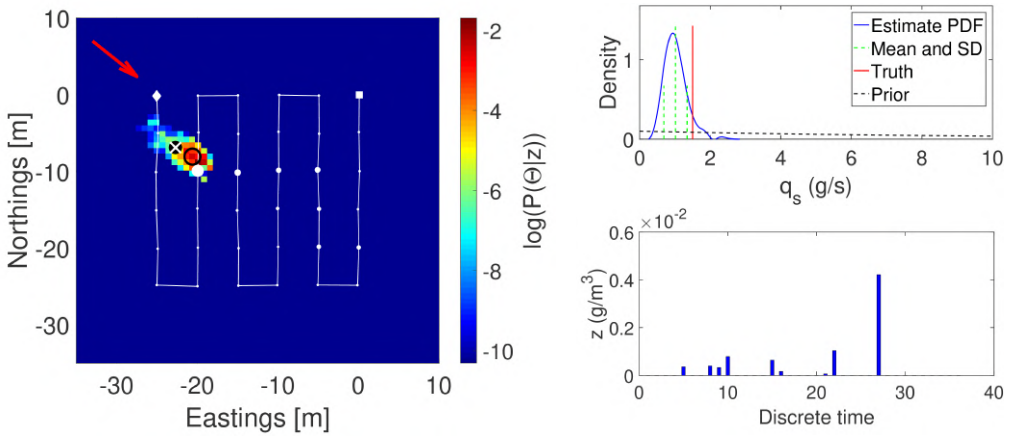

(a) (b)

Figure 6.8: Summary of the illustrative run (Trial 25). (a) The resulting UAV path (white line), gas sensor measurements (white dots), wind direction (red arrow), true source position (white cross), mean source estimate (black circle) and probability density (heat map). (b) Upper: Emission rate PDF (blue curve), truth (red line), prior (dashed black curve), mean and standard deviation (dashed green lines). (b) Lower: Sensor measurements at discrete time steps.

6.4.4 Results

In total, 27 experimental trials were conducted to test the system in the fairly realistic setting described. The experiments were conducted at various flight altitudes, wind speeds and scales. The results, using both the IP and GP dispersion models, are summarised in Table 6.1. The table includes details on the scale of the experiments, the step size or incremental distance between sensor measurements, the UAVs flight altitude, the duration of an experiment and the wind speed. The output Euclidean position error and the absolute emission errors are shown, where the true values are compared with the means of the estimation algorithm.

Overall, the Euclidean error was small considering the scale of the experiments, the severe amount of uncertainty in the dispersion process, and some uncertainty in the localisation of the UAV itself. In the majority of the experiments the error was noticeably within the step size used in the flight pattern. This was not always the case, due to changing meteorology and the large amount of intermittency in the gas detections in the vicinity of the source. The emission estimates from the algorithm using both models were encouraging, with errors typically under $1 g/s$. Given the brief review on gas sensing using UAVs in Section 6.1, the release estimate was expected to be under predicted due to decreased readings from the sensor caused by the rotor effect. However, the outcomes of the trials were varied; featuring very accurate estimates in addition to under or over predictions. Despite the reduced measurements, which may be responsible for the under predications of the emission rates; the over predictions are expected to be a result of the shorter sampling times that were adopted for data collection by the UAV. This lead to significantly more

Table 6.1: Summary of results for the 27 experimental trials, using the GP and IP models, including the errors in the source location and emission rate estimates, and flight pattern data.

Flight data						**Position error [m]**		**Emission error** $[g/s]$	
ID	**Scale[m]**	**Step size[m]**	**Altitude[m]**	**Time[mm:ss]**	**Wind speed**$[m/s]$	**GP model**	**IP model**	**GP model**	**IP model**
1	36x36	6	1.75	09:23	1.5	4.57	3.54	1.05	1.55
2	36x36	6	1.75	07:46	1.5	4.63	4.90	1.38	0.84
3	36x36	6	1.75	08:06	3	4.48	1.84	0.54	0.81
4	36x36	6	1.75	08:09	3	6.51	3.29	0.14	0.25
5	36x36	6	1.75	07:52	2	5.00	3.00	0.68	0.58
6	36x36	6	1.75	07:56	3	2.75	2.29	1.04	0.06
7	36x36	6	1.2	08:02	4	2.96	3.63	0.04	0.61
8	36x36	6	1.2	08:05	1	7.24	2.71	0.53	0.40
9	36x36	6	1.2	08:06	1	7.24	11.79	1.45	1.66
10	36x36	6	1.2	08:02	4	0.76	2.94	1.28	1.22
11	36x36	6	1.2	07:50	4	3.52	1.28	0.06	0.06
12	36x36	6	1.2	08:07	4	4.58	2.08	0.85	0.21
13	36x36	6	1.2	07:59	4	1.87	1.03	0.55	0.79
14	36x36	6	1.2	07:58	4	4.68	0.72	0.24	0.09
15	36x36	6	4	07:60	3	17.33	19.98	0.47	0.35
16	25x25	5	1.2	05:39	4	1.67	0.77	0.51	0.72
17	25x25	5	1.2	05:42	5	5.54	2.85	0.79	1.04
18	15x15	3	1.2	05:11	4	2.56	1.66	0.95	0.91
19	15x15	3	1.2	05:40	3	2.10	2.09	0.44	0.41
20	15x15	3	1.2	05:57	4	6.40	1.97	0.69	0.27
21	15x15	3	1.2	05:36	4	3.96	1.60	0.86	0.78
22	15x15	3	1.2	05:32	4	2.72	1.28	0.56	0.95
23	36x36	6	1.5	08:06	2	9.91	2.91	2.21	0.93
24	42x42	6	1.5	09:30	7	3.20	2.02	0.61	0.32
25	25x25	5	1.2	05:39	8	2.43	2.25	0.58	0.91
26	20x20	4	1.2	05:39	7	5.64	1.72	1.03	0.63
27	25x25	5	1.5	05:28	7	3.88	4.88	0.57	0.27

volatile measurements where there is the potential to average over a period of intermittency or during a large spike in concentration; which, given a larger sampling time, would typically be accompanied by smaller readings to smooth the average. This averaging over a spike is expected to be the cause of the over prediction of the emission rate that occurred in some of the trials. Other factors that had the most effect on the estimation accuracy were the flight altitude of the UAV, the step size between taking measurements and the wind speed.

Flying at different altitudes affected the estimation performance of the system as it changed the concentration observations made by the sensor onboard the UAV. Acetone is a dense material, so at high altitudes the UAV would be outside of the plume, where it would detect nothing with the gas sensor. Example results of flights conducted at 1.2m, 1.75m and 4m altitudes are shown in Fig 6.9, where the IP model was used in the estimation. For reference, the height of the source during the experiments was 1.4m. It was found, due to the density of the acetone, that at lower flight altitudes the sensor on-board the UAV picked up more positive detections, with less intermittency, which resulted in more accurate estimates of the source term with less spread, as observed in Fig 6.9. Note: in figure 6.9f, the scale of the sensor data axis is smaller for the flight conducted at 4m altitude. At altitudes greater than 4m there would generally be zero detections made by the gas sensor. All flights were of the same scale and step size and conducted in similar wind conditions.

The effect of the step size between measurements made by the gas sensor was as expected. The closer, more dense measurements resulted in more accurate estimates with less spread. This is illustrated in Fig 6.10 which shows example results of flights with samples taken at 3m, 5m, and 6m increments along the sweep path. All flights were conducted at 1.2m altitude in similar wind conditions and the IP model was used in the estimation.

The affects the wind speed has on the estimates made by the system are twofold: 1) In stronger winds more acetone remained airborne, rather than falling to the ground, resulting in more positive detections from the gas sensor and better matching between the observations and the dispersion models which did not account for the buoyancy of the material; 2) Stronger winds are linked with greater atmospheric stability [213] which leads to more consistent meteorological conditions. Examples of experiments conducted in 1, 4 and 7m/s winds at similar scales and altitudes are shown in Fig 6.11, where the IP model was used in the estimation. Studying the figures, it is clear how the sensing characteristics of the system are much better in higher winds. Figures 6.11a and 6.11b show the results in 1m/s mean wind speed on a hot sunny day which is associated with the most unstable atmospheric stability class (Pasquill's stability Class A). During this trial, the wind speed was negligible at times and the direction completely reversed. The poor sensing conditions, where acetone was detected only near the beginning of the flight, resulted in the inaccurate estimate of the source location. In higher wind, as shown in

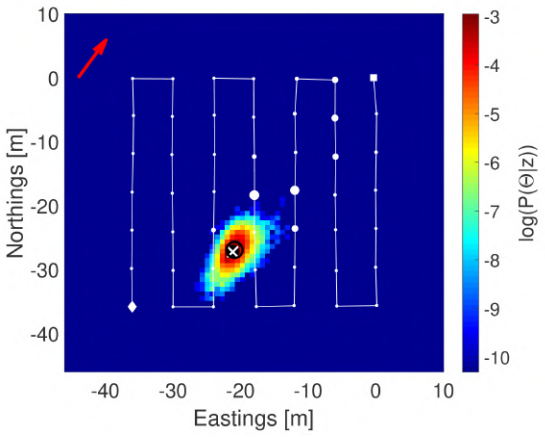

(a) Trial 14, position estimate.

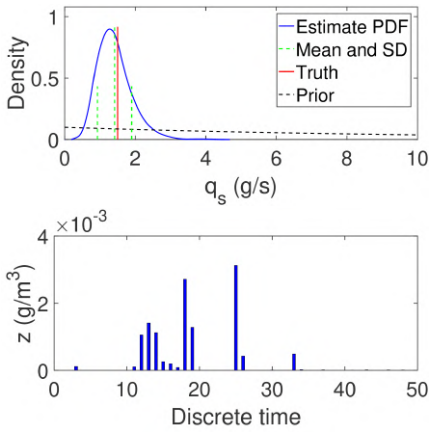

(b) Trial 14, q_s estimate and sensor data.

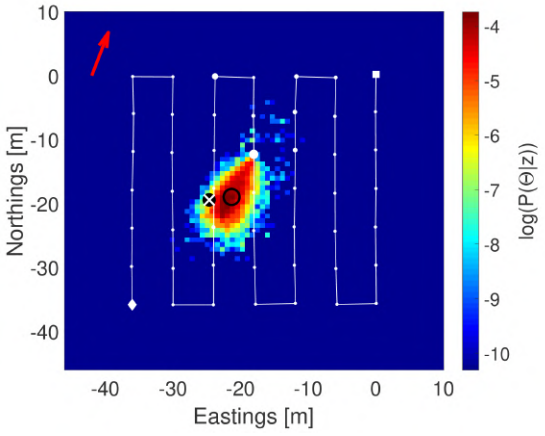

(c) Trial 4, position estimate.

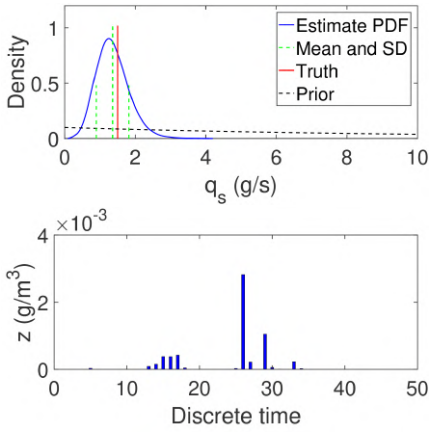

(d) Trial 4, q_s estimate and sensor data.

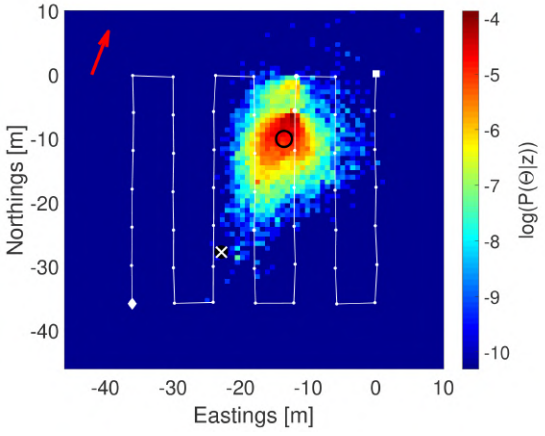

(e) Trial 15, position estimate.

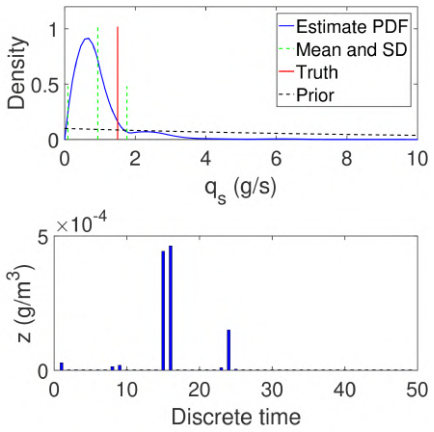

(f) Trial 15, q_s estimate and sensor data.

Figure 6.9: Results at altitudes (a-b) 1.2m: Trial 14, (c-d) 1.75m: Trial 4 and (e-f) 4m: Trial 15, using the IP model. The search area was 36x36m, the step size was 6m and wind speed 3-4m/s.

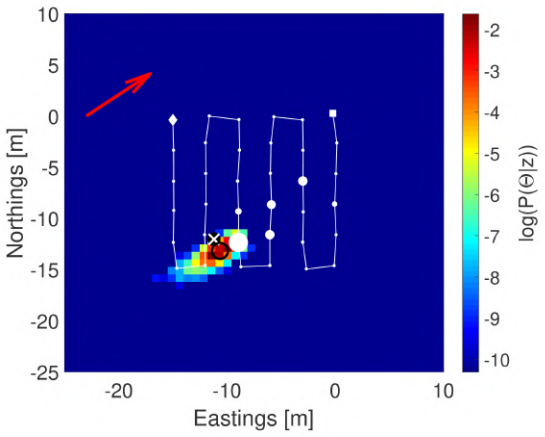

(a) Trial 22, position estimate.

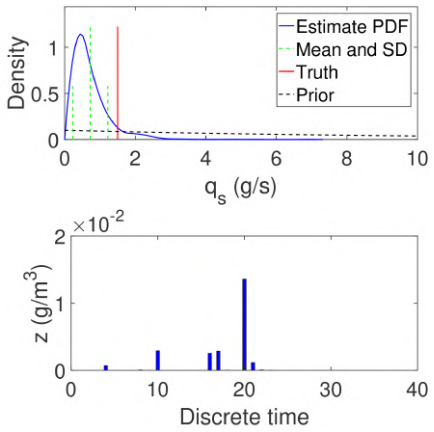

(b) Trial 22, q_s estimate and sensor data.

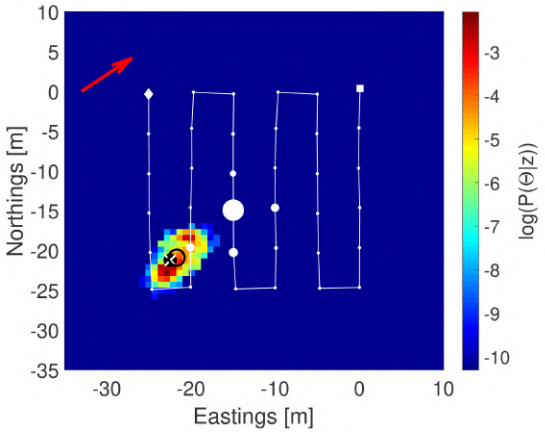

(c) Trial 16, position estimate.

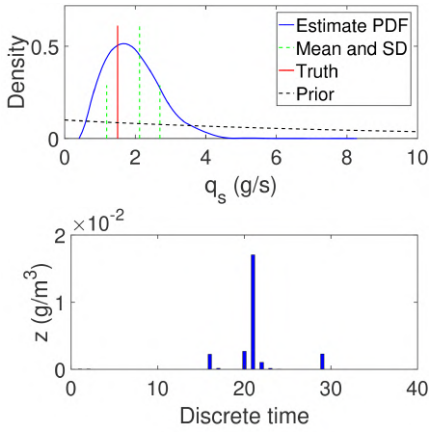

(d) Trial 16, q_s estimate and sensor data.

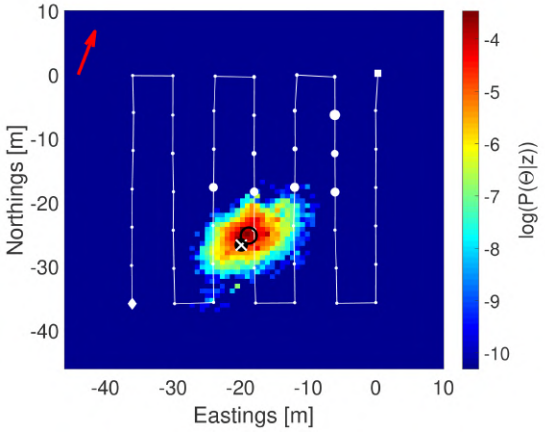

(e) Trial 12, position estimate.

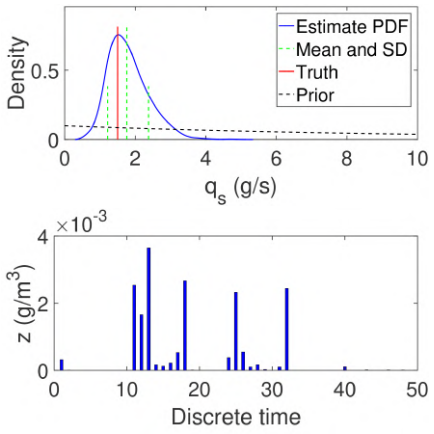

(f) Trial 12, q_s estimate and sensor data.

Figure 6.10: Results at step sizes (a-b) 3m: Trial 22, (c-d) 5m: Trial 16 and (e-f) 6m: Trial 12, using the IP model. The UAV altitude was 1.2m, the step size was 6m and wind speed 4m/s.

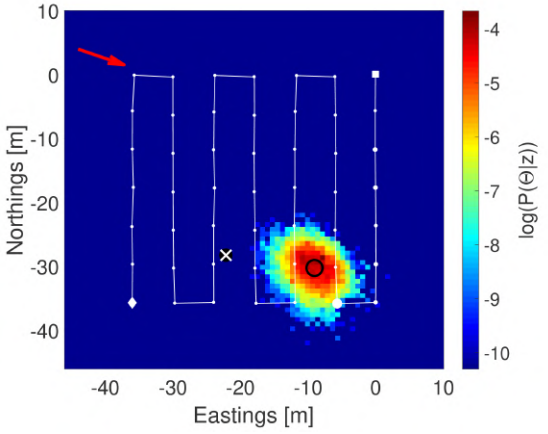

(a) Trial 9, position estimate.

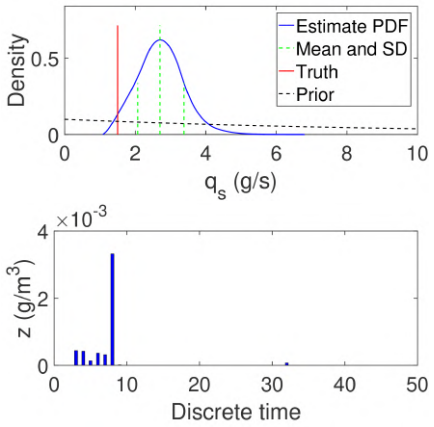

(b) Trial 9, q_s estimate and sensor data.

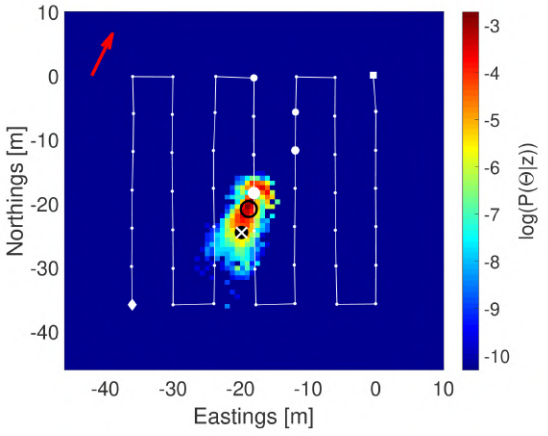

(c) Trial 7, position estimate.

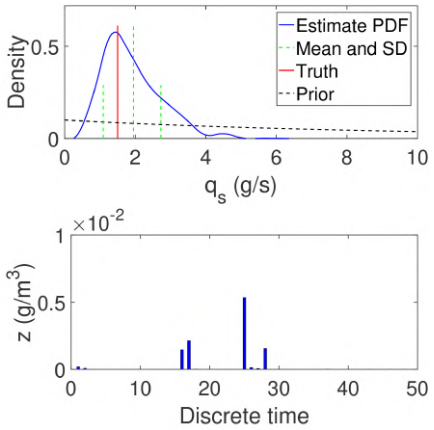

(d) Trial 7, q_s estimate and sensor data.

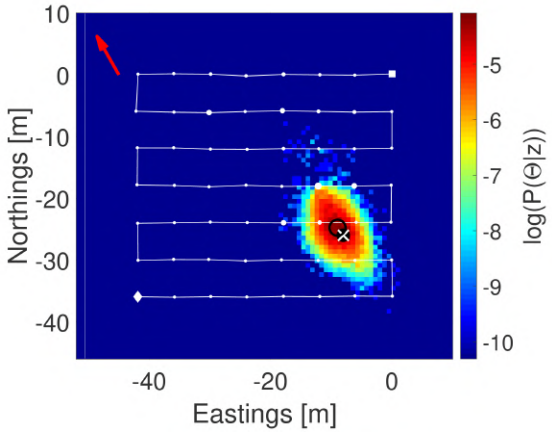

(e) Trial 24, position estimate.

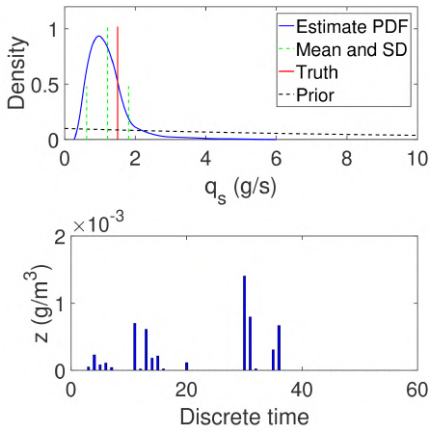

(f) Trial 24, q_s estimate and sensor data.

Figure 6.11: Results at wind speeds (a-b) 1m/s: Trial 9, (c-d) 4m/s: Trial 7 and (e-f) 7m/s: Trial 24, using the IP model. The UAV altitude was 1.2-1.5m and the step size was 6m.

figures 6.11e and 6.11f, the wind direction and speed was more consistent producing a better defined plume. The corresponding source position and emission estimates were very accurate with errors of 2.02m and 0.32grams/s.

The root mean squared errors (RMSE) and standard deviation (SD) of the position and emission estimates for the GP and IP models are shown in Table 6.2. The RMSEs and SDs are split among all the trials and subsets of the trials corresponding to different flight altitudes, step sizes and wind speeds. The IP model outperformed the GP model in all conditions with regards to the position estimates and in the majority of conditions for the emission estimates. The difference in performance is expected to be caused by the characteristics of the models near the source, for which the IP model more closely matched the data collected by the UAV in the particular experiments conducted in this thesis. The limiting characteristic of the GP model was its approximation of the width of the plume near the source, which was often wider than anticipated by the model. The wind speed appeared to have the greatest effect on the RMSE and SD of the estimates. In higher wind speeds the system produced consistently accurate estimates, resulting in low values of RMSE and SD. Small wind speeds ($\leq 3m/s$), which correspond to significantly more unstable atmospheric conditions, resulted in the most inaccurate and variable estimates. Considering Table 6.2, the best results are obtained with a smaller step size. However, a larger step size did not impede the results to the extent of weak wind speeds or flying at higher altitudes that are on the edge of the plume.

A common method to assess the performance of source localisation systems is the rate of successful localisations [214]. This metric introduces some ambiguity with regards to the definition of a successful localisation, which is usually given as a certain distance between the estimated and true source positions. Therefore, to provide a more explicit idea of the performance of the system, the success rate is plotted for various values of success criteria in Fig 6.12, where the success criteria is given as a range of Euclidean errors in the source position estimate. The success rate is shown for estimations made using the IP and GP models. Note: The result of Trial 15 (conducted at 4m altitude) was neglected as this was used to demonstrate the adverse effect of high altitudes. The figure shows the results of the remaining 26 trials and the subset where the wind speed was greater than 3m/s.

To conclude the results, the parameters of a gaseous release into the atmosphere have been estimated using point measurements of concentration from an autonomous UAV equipped with a gas detector. The results in Table 6.1 show accurate estimates for the source location and its emission rate obtained using the Bayesian inference method described in Section 6.3. Both dispersion models performed well but the IP model was more accurate in the experimental conditions described in this chapter. The overall accuracy of the source estimates was dependant on the measurements taken from the UAV, and how they matched the chosen ATD model featured in the likelihood function. The measurement data was affected by the meteorology, the altitude of the UAV, and the size of the increments between sampling the gas concentration.

Table 6.2: RMSE and SD in the position and emission rate estimates using the GP and IP dispersion models.

Data subset	Position RMSE (SD) [m]		Emission RMSE (SD) [g/s]	
	GP model	IP model	GP model	IP model
All data	4.75 (3.24)	3.35 (3.93)	0.75 (0.47)	0.65 (0.43)
Step size = 6m	5.37 (3.79)	4.08 (4.78)	0.77 (0.58)	0.63 (0.50)
Step size = 5m	3.38 (1.71)	2.69 (1.70)	0.61 (0.12)	0.73 (0.34)
Step size = 3m	3.55 (1.74)	1.72 (0.32)	0.70 (0.21)	0.66 (0.31)
Height $\geqslant$1.5m	5.22 (2.17)	3.33 (1.10)	0.95 (0.64)	0.66 (0.48)
Height <1.5m	3.88 (2.00)	2.45 (2.51)	0.67 (0.39)	0.69 (0.42)
Wind speed $\leqslant$3m/s	6.45 (4.43)	4.65 (5.45)	0.85 (0.60)	0.62 (0.43)
Wind speed >3m/s	3.86 (1.76)	2.63 (2.58)	0.69 (0.38)	0.66 (0.43)

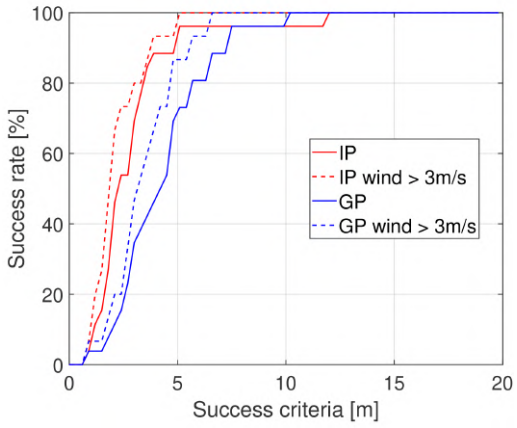

Figure 6.12: Success rates of the system.

6.5 Discussions and lessons learned

The results of the experimental trials presented are, to the best of the authors knowledge, the first time an autonomous UAV has been used to collect gas concentration measurements to estimate the source term (location and strength) of a release. Given such an immature area of work, there are valuable observations and lessons learned during the experiments that will be described in this section. These are related to the position of the UAV, gas sensing with an aerial vehicle, and the local meteorology.

6.5.1 UAV altitude

Given the chosen method to estimate the parameters of the release, it is important to know the location of the gas concentration measurements accurately, so that they can be related to the predictions from a model. In the horizontal directions, this was achieved through fusion of GPS data, IMU data and the guidance system on-board the aircraft. The

Figure 6.13: Visualisation of the UAVs effect on the gas dispersion using coloured smoke. A gap in the plume can be seen directly downwind of the platform, highlighted by the red lines.

altitude of the UAV was more challenging. When relying on barometric data, the UAV altitude could drift by a couple of meters. Although this is not very large, on the small scale of the experiments it would have an adverse effect on the results, especially given the low altitude of the UAV and the small size of the acetone plume. Down facing ultrasonic sensors of the guidance system provided an accurate estimate of the height above ground, however, this source of information was only suitable for level terrain. Consequently, this assumption was made during the experiments.

6.5.2 Gas sensing with a UAV

The rotors of the UAV did reduce the concentration readings of the gas detector. This was visible when the UAV was stationary on the ground and the rotors would turn off and on. Despite this, the results of the experiments were extremely positive, with the source emission rate only slightly underestimated. As discussed in Section 6.1, the sensor inlet could be moved outside the region of influence of the rotors or, in future research, a new model for the sensor response could be formulated. In addition, during visualisation experiments performed using coloured smoke, it was found that the UAV seemed to split the plume; as captured in Fig 6.13. This is a feature that may become important in path planning research in the future or when cooperating multiple vehicles.

6.5.3 Gas Buoyancy

The diffused acetone is dense, reducing how the gas would rise from the source. This results in low altitudes required by the UAV in order to make contact with the plume, and it causes the gas dispersion to be less buoyant than modelled by the simple transport

equations considered in this thesis. Adding the effect of buoyancy to the model could improve the accuracy of the estimation. This could be included as a parameter with uncertainty, and inferred as part of an extension of the source vector Θ_k.

6.5.4 Changing meteorology

In this work, and commonly in the literature, source term estimation algorithms for atmospheric releases assumed steady state conditions in the underlying dispersion model. This assumption holds in simulations and in wind tunnel datasets. Outside of simulation the condition is often not fulfilled, particularly on highly unstable, low wind speed conditions, where the direction of the wind is much more random. This incurs a large error on the estimation of the source location. This may be overcome by employing a different model, such as a Gaussian Puff, which does not make a steady state assumption. However, some assumptions on the wind field would still be required, and the model would be more computationally expensive.

6.5.5 Sampling time and step size

The sampling time, or how long the UAV hovers to take an averaged measurement of concentration, had been set to a fixed value based on a trade-off between search time and performance. The step size, or movement distance between each sample, was selected in a similar manner. Given a larger area to search, it may be necessary to reduce the sampling time or increase the movement distance so that the UAV can search the area in less time. In future work, these parameters of the planning algorithm should be selected adaptively based on the current information available, or even removed altogether by considering observations from a continuously moving platform.

6.6 Chapter summary

This chapter described a system to enable estimation of the parameters of a dispersive atmospheric release using a UAV. It extended the estimation algorithm to perform in 3D and to handle the noisy measurements from a sensor on-board the UAV. The Bayesian framework from the previous work in the thesis has been extended to accommodate a new sensor model which accounts for noisy background readings and intermittency in the measured concentration. The set-up and development of a UAV has been described to enable the experimental validation of the algorithm in an outdoor open field. To the best of the authors knowledge, this has been the first experimental testing of a source term estimation algorithm using an autonomous UAV, where a static network of gas detectors has been used in the past. Extensive experiments were conducted in various meteorological conditions and with different sweeping flight path configurations. Using the data generated from a total of 27 experiments, the effect of the UAVs attitude, the

incremental step size between taking measurements, and the wind speed was assessed. It was found, in the experiments conducted, which used a relatively dense material as a source, that the system performed better, in terms of estimation accuracy, flying at lower altitudes and in higher wind speeds (stronger atmospheric stability [213]). The wind speed, and hence the atmospheric stability, was found to have a significant effect on the accuracy of the algorithm and the SD of the estimation errors. As expected, the smaller incremental step sizes between gas measurements, resulted in more accurate source estimates with less spread. However, this would incur significant penalties on the size of the area covered over time. Additionally, two simple, fast running dispersion models were compared using the data from the unique experiments conducted in the chapter. Overall, the Isotropic plume model noticeably outperformed the standard Gaussian model. This is expected to be due to the characteristics of the models in the vicinity of the source, suggesting the IP model is more appropriate for estimation on a smaller scale. Overall, the experimental results demonstrated strong performance of the system making it closer to use in real scenarios.

Given the validation of a STE algorithm using the UAV, the next step in this thesis is to test the information based search algorithm in the challenging outdoor conditions using the UAV. The information based algorithm will be able to capitalise on the information gained during flight, improving the the search time and potentially the accuracy of the source term estimate. Furthermore, after the discovery of the adverse effect of low or changing wind conditions on the STE performance, a mapping method is also explored as a potential response in these situations. The mapping response is described in Chapter 9.

Chapter 7

Information based search for a hazardous airborne release using an unmanned aerial vehicle

This chapter presents results of experiments to test the information based search algorithm in outdoor conditions using the UAV. The chapter is essentially an experimental evaluation of an integration of the work from the previous two chapters. The information based planning algorithm that was verified in controlled indoor experiments in Chapter 5 is extended to three dimensions and integrated with the improved estimation algorithm from Chapter 6. After the comparison of dispersion models conducted in Chapter 6 the Isotropic plume model is used as the underlying model for the information based experiments. The Chapter begins with an outline of the combined algorithms, followed by the descriptions of the experiment set-up and the user interface that was developed to ease initialisation of the algorithm for each of the experimental trials. The results using the information based planning algorithm are compared with the uniform sweep results from the previous Chapter and some characteristics of the information based search in real outdoor experiment conditions are discussed.

The chapter is organised as follows. In Section 7.1 the source term estimation and path planning algorithms are described. In Section 7.2 the experiment set-up is described including a user interface for the system used to initiate the algorithm in the outdoor trials. In Section 7.3, an illustrative run of the intelligent search algorithm in 3D outdoor conditions is shown, followed by the results of multiple experiments and a comparison with the sweep search pattern approach from the previous chapter. The chapter is then summarised in Section 7.4.

7.1 Algorithms

7.1.1 Formal problem formulation

A zone of interest, parameterised by the three dimensional volume $\Omega \subset \mathbb{R}^3$, will be used to initialise the search area of the algorithm. This could be the region where a suspicious odour is reported, a region of interest to survey, an area along a pipeline or the area around a chemical facility. The UAV, equipped with the relevant payload, is to navigate within the area to estimate the release parameters otherwise known as the source term.

The UAV is aware of its location $\mathbf{p}_k = \begin{bmatrix} x_k & y_k & z_k \end{bmatrix}^\mathsf{T} \in \Omega$ within the domain. The detector on-board the UAV observes point-wise measurements of the HAZMAT concentration $z_k \in \mathbb{R}^+$. The meteorological parameters are provided by a local weather station. The location stamped measurements and meteorological observations are used to estimate the parameters of the source Θ_k, which in this work, is given by:

- Cartesian coordinates of the source $\mathbf{p}_s = \begin{bmatrix} x_s & y_s & z_s \end{bmatrix}^\mathsf{T} \in \Omega$ in meters (m).
- Emission rate/strength of the source $q_s \in \mathbb{R}^+$ in grams per second (g/s).
- The wind speed $u_s \in \mathbb{R}^+$ in meters per second (m/s) and direction $\phi_s \in \mathbb{R}$ in radians (rad).
- Model dependant diffusion parameters $\zeta_s = \begin{bmatrix} \zeta_{s1} & \zeta_{s2} \end{bmatrix}^\mathsf{T} \in \mathbb{R}^+$ which relate to the spread of the atmospheric concentration from the source.

Hence, the parameter vector of the source term can be defined as:

$$\Theta_k = \begin{bmatrix} \mathbf{p}_s^\mathsf{T} & q_s & u_s & \phi_s & \zeta_s \end{bmatrix}^\mathsf{T}. \tag{7.1}$$

The UAV is to autonomously search the environment, collecting point observations $\mathbf{z}_{1:k} = \{z_1, \ldots, z_k\}$ from the chemical detector at discrete time steps $k = 1, \ldots, k$ and at known locations $\mathbf{p}_{1:k} = \{\mathbf{p}_1, \ldots, \mathbf{p}_k\}$. At each time step k, the estimates of the source parameters Θ_k are updated by drawing the inference on the probabilistic distribution $p(\Theta_k|\mathbf{z}_{1:k})$. The next location to make an observation with the HAZMAT detector $\mathbf{p}_{k+1}$ is then selected by approximating an information based reward function, and choosing the action $\mathbf{a}_k$ such that $\mathbf{p}_{k+1} = \mathbf{p}_k + \mathbf{a}_k$.

7.1.2 Source estimation algorithm

The focus of this Chapter is on the extension of the information based search algorithm to 3D and experiments using a UAV. The estimation aspect of the system used in this Chapter is described in Chapter 6 Section 6.3. Note that only the Isotropic plume model, which performed best in the previous Chapter, is extended for information based experiments with the UAV.

7.1.3 Planning algorithm

The information theoretic path planner chooses the manoeuvre $\mathbf{a}_k^*$ from an admissible set of actions $\Psi_k = \{\uparrow, \downarrow, \leftarrow, \rightarrow, \odot, \times\}$, that is expected to be the most informative. Here, the arrows refer to moves in the crosswind, upwind and downwind directions, and $(\odot, \times)$ refer to an increase or reduction in UAV altitude. Besides an extension of the admissible set of actions to 3D and the replacement of the estimation algorithm with that described above, the remainder of this Section follows from Chapter 5, Sections 5.3.1.2 and 5.3.3.2.

The output of the planning algorithm is a new goal position for the UAV which is expected to provide the most information from the subsequent measurement. Following a manoeuvre to the goal position the UAV takes a new observation z_{k+1} and the estimation and sensor control cycle is iterated until some stopping criteria are reached, such as a threshold on the spread of the location estimate of the source term.

7.2 Experiment setup

The experiments conducted used the same environment set-up as the previous chapter, where acetone was used to simulate a hazardous release in an outdoor open field. The UAV set-up also remained the same, a DJI Matrice 100 UAV equipped with a PID sensor. The ROS framework was used for communications between the UAV and the ground station laptop. At each time step, the UAV would send its location stamped sensor measurement to the ground station. The laptop would run the estimation and planning algorithm and send a new position demand to the on-board computer of the UAV. In a similar manner to Chapter 5 where the indoor experiments were discussed, the mission was terminated if the robot tried to move onto the source or if the covariance of the position estimate was reduced below a threshold.

7.2.1 User interface

The search algorithm was set-up and initialised from the ground station laptop, however, in the future, it is envisioned that this would be done via an app on a phone/tablet that would also be used to control the UAV. An example of the user interface developed for the experiments is shown in Fig 7.1, where the top right video feed would be replaced by the on-board camera of the UAV. Note, for the purposes of this chapter, the top right part of the figures shows a video taken by a filming drone during the experiments in order to better visualise the result than what would be provided by the on-board camera of the searching platform.

The figure in 7.1 show the user interface at various time steps. The left portion of the figures shows the search area, the path of the UAV and the true position of the source during the experiments. The right portion shows a video of the UAV executing the mission in real time. The bottom of the figures indicate the real time data from the on-board PID

sensor.

The initialisation of the information based autonomous search and source term estimation algorithm is as follows

1. The user draws an area on a map where the source may be, as indicated by the red box in the following figure. (Note: the algorithm is quite robust to finding source outside of the search area.)

2. Another area is drawn to define the flight area, which will limit where the UAV can move.

3. The final input is a position to initialise the search, alternatively, this can simply be the take-off position of the platform.

4. Press GO!

After pressing GO, the UAV will fully autonomously: take-off, search for the source, return, and land. Throughout this fully autonomous mission, the path, current position and real time gas measurements from the UAV are transmitted to the ground station as shown in the following figures. At the end of the mission, the source position and a plume estimate are displayed to the user, as shown in the Fig 7.1c.

7.3 Results

An illustrative run of an experiment using the information based planning algorithm is given in Fig 7.2. Overlaid on a map of the experimental field, the figure shows: the flight path of the UAV executing the information based search at various snapshots in time; the measurements at each sampling location; and the true position of the source. To begin the search, the system is initialised at discrete time step $k = 0$. The starting position of the UAV is indicated by the green square and the true location of the source is given by the blue circle. The large number of orange dots represent the random sample approximation used in the sequential Monte Carlo algorithm at the current time step (i.e. the current posterior distribution). Each dot represents a weighted source term realisation $\{\Theta_k^{(i)}, w_k^{(i)}\}$, where only the marginalised position estimates are visualised in the figure.

Figures 7.2a-7.2d show the path of the robot and the measurement positions, at various time steps. The figure demonstrates how the robot begins the search by moving in a crosswind direction. In response to positive detections from the PID detector the algorithm is able to narrow down the location of the source in the crosswind direction as shown in Fig 7.2b. At this point it begins to travel upwind towards the source. By time-step $k = 29$, shown in Fig 7.2d, the UAV had narrowed down the source position and the orange dots converged into the true source location. At the end of the illustrative run using the information based search algorithm the position estimate of the source was very accurate, with only a 1.42m Euclidean error. However, the emission rate was reasonably

(a)

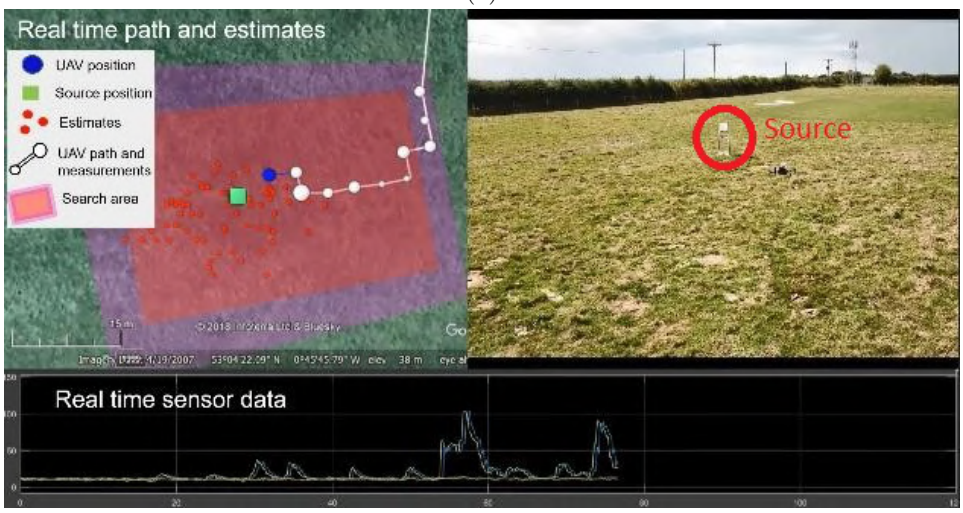

(b)

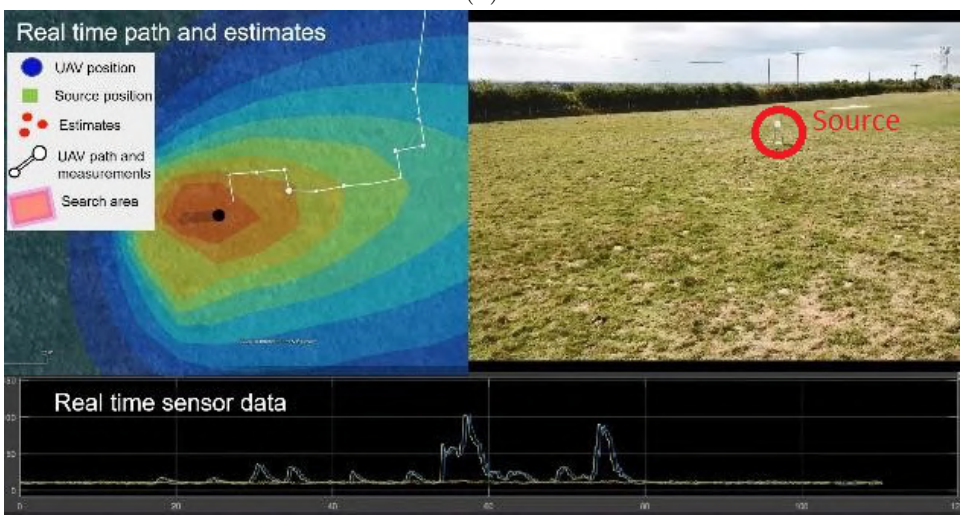

(c)

Figure 7.1: Snapshots of the user interface during an experimental trial at various time steps. (a) snapshot at the beginning of a mission, the UAV is on its way to the starting position. (b) snapshot towards the end of a mission, the source estimate is converging on the true position. (c) output plume estimate using the posterior distribution of the source parameters.

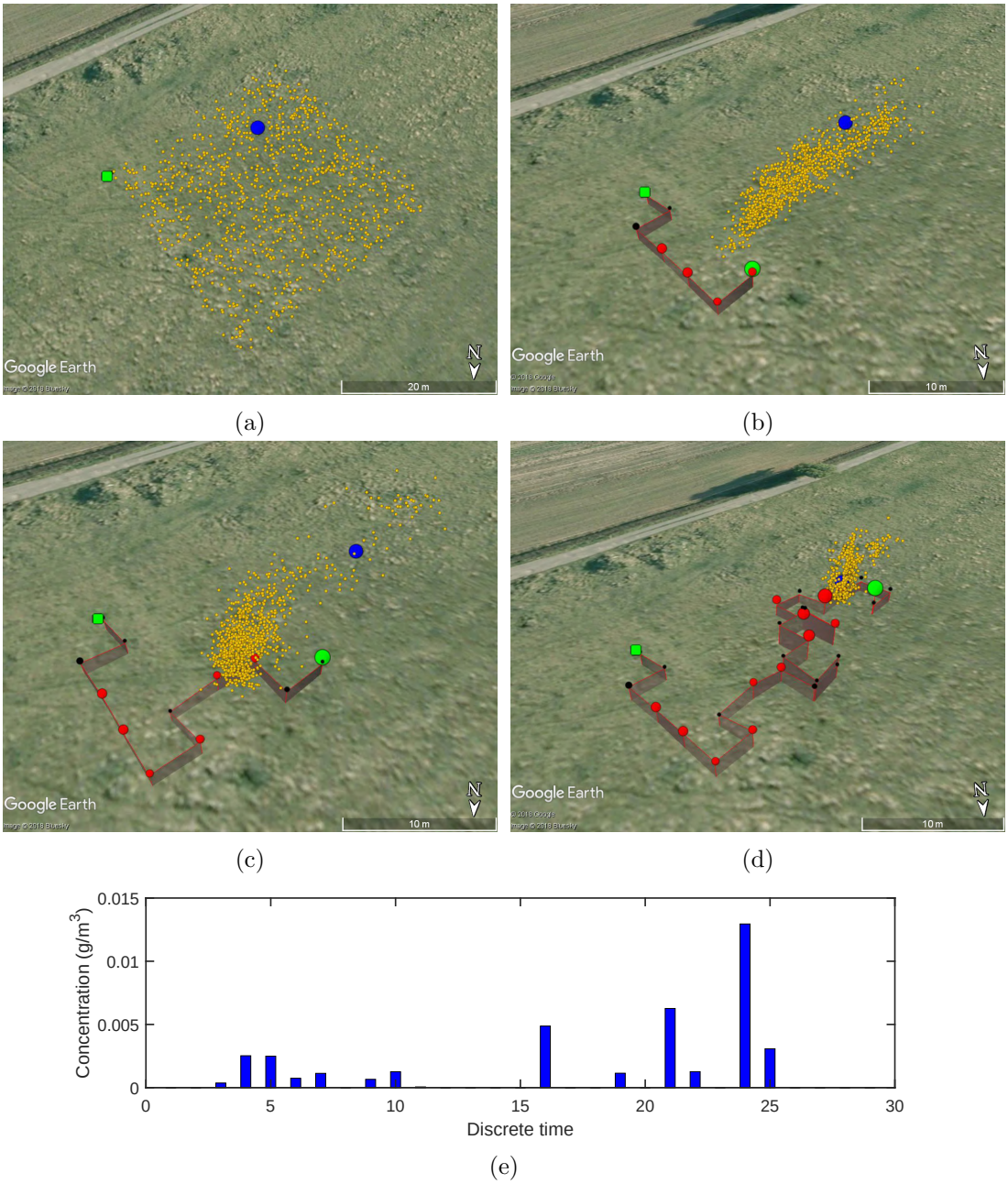

Figure 7.2: Example run of the intelligent search algorithm at discrete time steps: (a) k=0 and (b) k=7 (c) k=12 and (d) k=29. The red line indicates the path of the UAV and the blue circle represents the true position of the source. The green square and circle indicate the starting and current location of the UAV. Finally, the orange dots represent the random sample approximation of the source parameter estimates at the current time step. (e) The observations from the detector at discrete time steps.

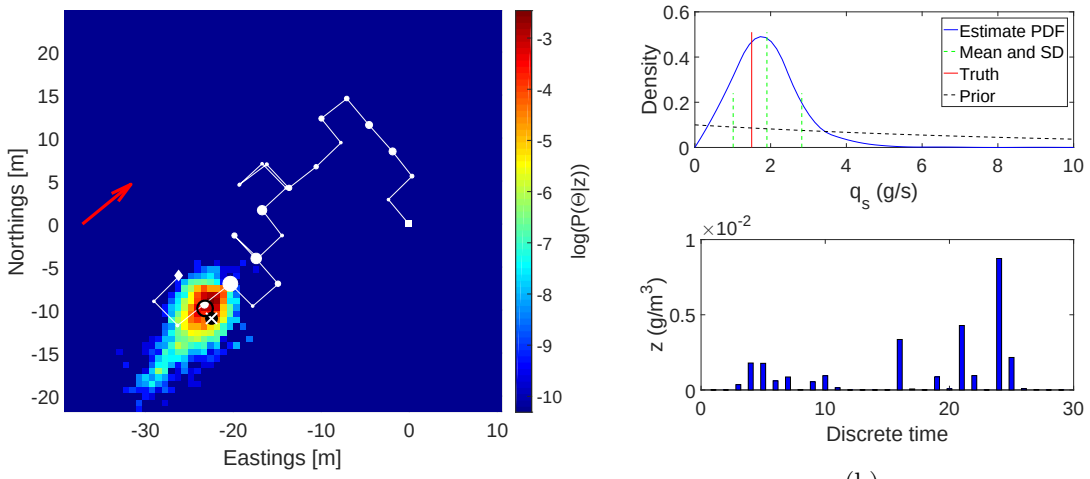

(a) (b)

Figure 7.3: Summary of the example run of the information based search algorithm using the UAV. (a) The resulting UAV path (white line), gas sensor measurements (white dots), wind direction (red arrow), true source position (white cross), mean source estimate (black circle) and probability density (heat map). (b) Upper: Emission rate PDF (blue curve), truth (red line), prior (dashed black curve), mean and standard deviation (dashed green lines). (b) Lower: Sensor measurements at discrete time steps.

accurate, but over predicted by 1.26grams/s. The measurements from the PID sensor during the search are shown in Fig 7.2e.

A summary of the Trial in a condensed form is given in Fig 7.3. Figure 7.3a shows the resulting flight path (white line), wind direction (red arrow) and marginalised posterior estimate of the source location (heat map). The starting and ending positions of the UAV are given by the white square and diamond. The true position of the source is indicated by the black circle filled with a white cross and the algorithms mean estimate is given by the hollow black circle. Figure 7.3b shows the probability density estimate of the emission rate of the source, $p(q_s|\mathbf{z}_{1:k})$, and the measurement data during the flight, $\mathbf{z}_{1:k}$. The blue curve represents the PDF of the emission estimate with mean and standard deviation indicated by the vertical dashed green lines. The black dashed curve shows the prior distribution provided to the algorithm, and the true value is given by solid red line. Bars in Fig 7.3b indicate the measurements at discrete time steps. In this example the position and emission rate estimates of the source were very accurate. The results of 3 other trials using the information based search algorithm are summarised in Fig 7.4.

The results of 10 trials using the information based algorithm are summarised in Table 7.1, including information about the source location estimates, emission estimates and some flight data. Overall, the Euclidean error is small given the scale of the experiments, moreover, given the severe amount of uncertainty in the dispersion process and even some uncertainty in the localisation of the UAV itself. Similarly to the experiments using a uniform sweep flight pattern, the emission estimates from the algorithm were encouraging, with errors typically within $1g/s$.

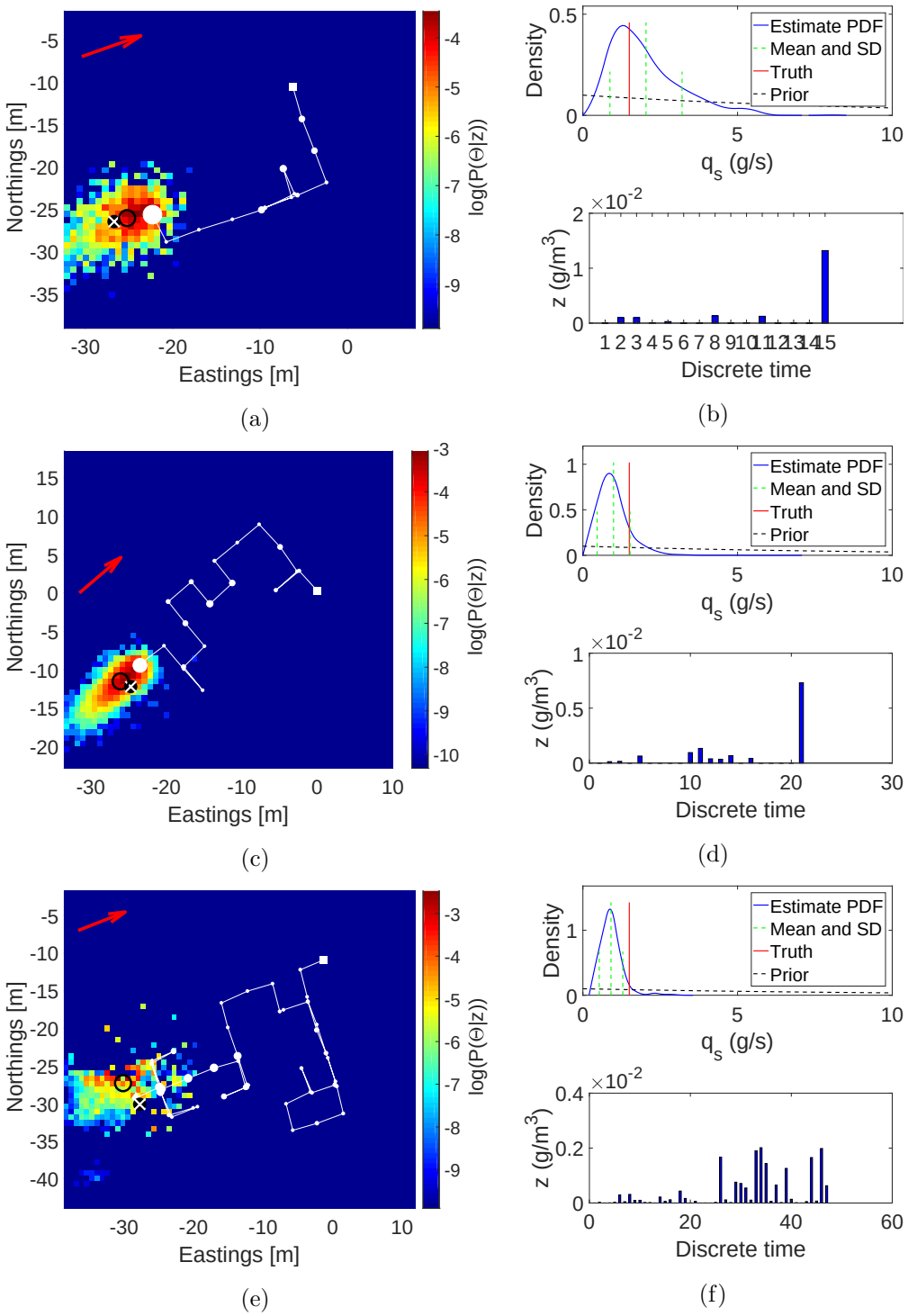

Figure 7.4: Summary of information based experiments using the UAV. (a-b) Trial 7, (c-d) Trial 4 and (e-f) Trial 10

Table 7.1: Summary of results for the information based experimental trials, using the IP model, including the accuracy of the source location and emission rate estimates, and some flight data.

Flight data					**Result**	
ID	**Scale [m]**	**Step size [m]**	**Time [mm:ss]**	**Wind speed** $[m/s]$	**Position error [m]**	**Emission error** $[g/s]$
1	36x36	4	05:31	5	1.44	1.26
2	36x36	4	04:05	6	1.22	0.09
3	36x36	4	04:48	4	2.39	1.27
4	36x36	4	05:12	3	7.04	0.16
5	36x36	4	03:05	4	1.31	0.55
6	36x36	4	06:02	3	1.76	1.09
7	36x36	4	08:28	4	2.76	0.23
8	36x36	4	06:51	5	2.08	0.63
9	36x36	4	02:37	5	1.52	0.50
10	36x36	4	07:01	4	3.81	0.73

7.3.1 Comparison with sweep flight pattern

The results of the information based experiments are compared with the uniform sweep results from Chapter 6. The uniform sweep results are restricted to where the Isotropic plume model was used and where the scale of the experiments was similar to the that used in the information based trials. The average search time, the source position estimate RMSE, and the source emission rate RMSE using both methods is shown in Table 7.2. Overall, in agreement with the simulations conducted in Chapter 3, the informative search algorithm attained more accurate source position estimates and a significantly lower average search time. The emission rate RMSE was less effected; this is expected to be due to the large amount of noise in the sensor measurements for both strategies, and the lower number of measurements taken during the informative search before the source was found. It is expected that a longer sampling time, whilst taking atmospheric concentration measurements, would improve the emission rate estimate for both approaches, whilst penalising the search time.

Table 7.2: Accuracy of methods

Method	**Average search time [mm:ss]**	**Position RMSE [m]**	**Emission RMSE** $[g/s]$
Sweep search pattern	08:05	4.21	0.65
Informative search	05:22	2.83	0.65

7.4 Chapter summary

This chapter presented experiments to test the information based search and Bayesian source term estimation algorithms developed throughout this thesis. The hardware used to test the system was the same as the previous chapter to make a fair comparison of the methods. A user interface was developed in order to enable more seamless experimentation and to look at how an end user may interact with the system. The interface was simple to use, involving only 4 steps to initiate the algorithm and begin the fully autonomous search. The information based algorithm from Chapter 5 was simply extended to 3D and combined with the Bayesian estimation algorithm from the previous chapter. The system performed well in multiple experiments. The results show the benefits of the information based approach over the uniform sweep path with regards to search time and the accuracy of the location estimate. However, the accuracy of the emission rate was relatively unchanged. To the best of the authors knowledge, this has been the first experimental testing of an information based search and source term estimation algorithm using a UAV, building upon the novel result of indoor experiments presented in Chapter 5.

After the successful experimental assessment of the methods developed throughout this thesis the next steps will be to extend the system to work in different scenarios, such as a non-continuous release (which is described in the next chapter), and to improve the reliability of the system with regards to handling changing meteorological conditions.

Chapter 8

Information based search for a non-continuous atmospheric release using a UAV

In previous chapters, simulations and experiments have verified the application of a UAV to estimate the source term of a continuously emitting release using a Bayesian and information based approach. Given the success of the method, in this chapter it is extended to estimate the source term of an instantaneous release, namely, its origin and emission mass. In an instantaneous release, it is assumed that all the hazardous material is emitted at one time rather then at a constant rate. In this more challenging scenario, there will not be any concentrations to detect at the source origin after some time after the release has occurred as it will all have blown downwind. The hazardous area from an instantaneous release is commonly referred to as a puff, rather then a plume. In a similar manner to the previous chapters the estimation is formulated as an inverse problem. In this chapter the concentration observations from a mobile sensor are fused with meteorological information and a Gaussian puff dispersion model to characterise the source. Note, that the puff model is used now not plume. Bayes' theorem is still applied to estimate the parameters of the release so that the uncertainty that exists in the dispersion parameters and meteorological variables can be taken into consideration. The information based reward is still used to guide an unmanned aerial vehicle equipped with a chemical sensor to the expected most informative measurement locations. The method is assessed in simulations and the performance is compared between using a single mobile sensor and various amounts of static sensors. The characteristics of the estimation performance are discussed subject to different relase parameters and meteorological conditions.

This chapter is based upon the research previously published by the author in [215]. The remainder of this chapter is organised as follows. Background on the specific problem is given in Section 8.1. In Section 8.2, the problem is presented including information about the domain and modelling used within the algorithm and for the simulations. In

Section 8.3, the conceptual solution is described. An illustrative run and Monte Carlo simulations with other strategies are presented in Section 8.4, and finally, the chapter is concluded in Section 8.5.

8.1 Background

As has been discussed throughout this thesis, searching for the source of an atmospheric release of dispersing material is an important task for mankind and also in the natural world. The reason for finding the source may vary, for humans it is often in an emergency response to some hazardous release, searching for useful resources or inspecting an area for mines [216]. In nature the intentions are more virtuous, such as searching for a food source or even a mate [10]. In almost all cases, especially within the literature on source localisation, it is assumed that the source is continuously emitting. This assumption simplifies the problem, allowing techniques to attempt to track the concentration of the material to its source [36].

In this chapter, a more challenging problem is considered, estimating the source location of an instantaneous release using point-wise concentration observations from a mobile sensor. In this scenario, reactive or control based algorithms will be unable to track towards the source, still, they may be able to track the instantaneous puff of material downwind of the release which could also provide a useful response. The goal in this thesis however, is to estimate the source term of the release. As has been mentioned throughout this thesis, the source term encapsulates all of the information required to produce a forecast of the spread of the material using an atmospheric transport and dispersion (ATD) model, regardless of whether the release is continuous, instantaneous or discrete. It is also of importance in understanding the cause of the release in an emergency event. As a minimum, the details required are the release mass and the location/origin of the release source. Other important variables that can be included will depend on the scenario and the chosen ATD model including: stack height, uncertain meteorological variables, release time and the duration of the release. The release time is particularly important in the response to an instantaneous release, as the release time and the wind speed have a significant effect on the current location of the hazardous concentrations.

Since the source can not be tracked towards directly, the model based STE techniques must be applied to estimate the source location of the instantaneous or puff release. Several limitations and opportunities arise when applying a mobile sensor on a UAV to the problem. The main limitation will be with respect to the start time of the release, the wind speed and the time that the UAV is deployed, where the UAV may simply have to "chase" the puff downwind, until some positive readings of concentration are found. Spatial-temporal measurements of the hazard can be improved but are also limited if there is only one mobile sensor. The advantages arise from the movement of the sensor, so that measurements can be taken from more desirable locations.

The only record of application of mobile sensors to estimate the parameters of an instantaneous release is found in [217], however it had been assumed that the source location was known a priori, so only the strength of the release was estimated.

8.2 Problem description and modelling

An instantaneous or puff release undergoing atmospheric transport and dispersion can be characterised by the Gaussian puff equation [121] using the source term vector $\Theta = [\mathbf{p}_s \ m_s \ u_s \ \phi_s \ \zeta_s^x \ \zeta_s^y]^\mathsf{T}$. Where m_s is the mass of the release with origin position $\mathbf{p}_s = [x_s, y_s, z_s]^\mathsf{T}$. u_s is the wind speed, ϕ_s is the wind direction, and (ζ_s^x, ζ_s^y) are stochastic dispersion parameters adopted from [142].

A sensor equipped UAV with position vector $\mathbf{p}_k = [x_k, y_k, z_k, t_k]^\mathsf{T}$ (where x_k, y_k, z_k are the Cartesian coordinates of the sensor at time t_k) is to make concentration observations to estimate the release parameters. The mean concentration observed by the sensor from an instantaneous source Θ can be modelled using the Gaussian Puff model as:

$$C(\mathbf{p}_k, \Theta) = \frac{m_s}{(2\pi)^{\frac{3}{2}}\sigma_x\sigma_y\sigma_z} \exp[-\frac{(x_k - x_c)^2}{2\sigma_x^2} - \frac{(y_k - y_c)^2}{2\sigma_y^2}] \times (\exp[-\frac{(z_k - z_s)^2}{2\sigma_z^2}] + \exp[-\frac{(z_k + z_s)^2}{2\sigma_z^2}]) \quad (8.1)$$

where x_c and y_c are the coordinates of the centroid of the puff that is translated by the wind over time, defined as:

$$x_c = x_s - u_s \sin(\phi_s)(t - t_s) \quad (8.2)$$

$$y_c = y_s - u_s \cos(\phi_s)(t - t_s) \quad (8.3)$$

and $(\sigma_x, \sigma_y, \sigma_z)$ are dispersion parameters defined as a function of downwind distance $\bar{x}$ using the Karlsruhe-Jülich system [218] as:

$$\sigma_x = \sigma_y = a\bar{x}^b \quad and \quad \sigma_z = c\bar{x}^d. \quad (8.4)$$

The variables (a, b, c, d) are a function of stability category [180]. For example at Pascal stability category C: $a = 0.66, b = 0.81, c = 0.17$ and $d = 1$. Inspired by the work in [142], where the constants in the dispersion parameter equations were replaced by stochastic parameters (ζ_1, ζ_2) the equations for the dispersion parameters are reformulated as:

$$\sigma_x = \sigma_y = \zeta_1\bar{x}^b \quad and \quad \sigma_z = \zeta_2\bar{x}^d, \quad (8.5)$$

where b and d are still selected based on the stability class.

An example run of the Gaussian puff model from Eq (8.1) is shown in Fig 8.1, where

the red dot denotes the source position and the colour map represents the concentration at positions in the x, y and z frames. The figure shows examples 50 seconds and 300 seconds after the release, with a 4m/s wind speed directed 20 degrees from the x axis.

At time step k the UAV will be at the position $\mathbf{p}_k$, the sensor observes a concentration z_k defined as:

$$z_k = z_k^{true} + e \tag{8.6}$$

where e refers to the error in the measurement. The observations of concentration from a sensor z_k and from predictions with a model $C(\mathbf{p}_k, \Theta)$ are infected with several sources of error that can arise from sensor noise and drift, modelling errors or errors in other dispersion variables such as the wind speed. An appropriate distance metric or likelihood function must determine the probability of the observed data given an expected reading from the model. Several distributions have been used in the past. Application of the maximum entropy principle [212] suggests that the most conservative choice of likelihood function is Gaussian. This leads to the following likelihood function between observed and modelled concentrations which encapsulates the errors from modelling and sensing:

$$p(z_k|\Theta) = \frac{1}{\sigma_k(z_k)\sqrt{2\pi}} \exp\left[-\frac{(z_k - C(\mathbf{p}_k, \Theta))^2}{2(\sigma_k(z_k))^2}\right], \tag{8.7}$$

where the variance is defined as: $\sigma_k(z_k) = 0.1z_k$. In the next section, Bayes' theorem is introduced which will use the likelihood function to update estimates of the source parameters.

8.3 Conceptual solution

A sensor equipped UAV is released to estimate the parameters of the Gaussian puff. At each time step the parameters of the source are estimated using Bayes' theorem [2] and then the sensor chooses the next position to take a measurement by maximising an information based reward. Bayes' theorem is chosen to estimate the source parameters as it can be robust to uncertainty as the errors expected in the observations can be modelled to reflect such uncertain conditions. We have chosen an information based reward as it takes into account the effect that the future measurement may have on the estimates of the source parameters. Furthermore, it has previously been shown to be effective for continuously releasing scenarios [179].

Using Bayes' theorem, the posterior distribution of the source parameters $p(\Theta|\mathbf{z}_{1:k})$ is updated recursively as new sensor observations become available as:

$$p(\Theta|\mathbf{z}_{1:k}) = \frac{p(z_k|\Theta)p(\Theta|\mathbf{z}_{1:k-1})}{p(z_k|\mathbf{z}_{1:k-1})}, \tag{8.8}$$

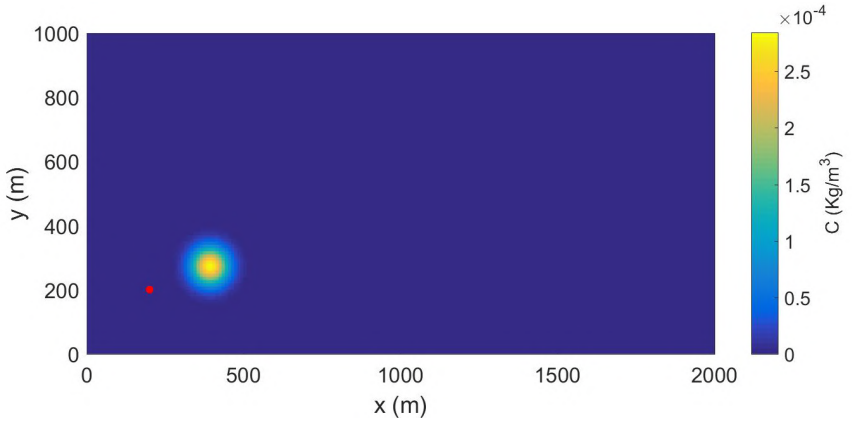

(a)

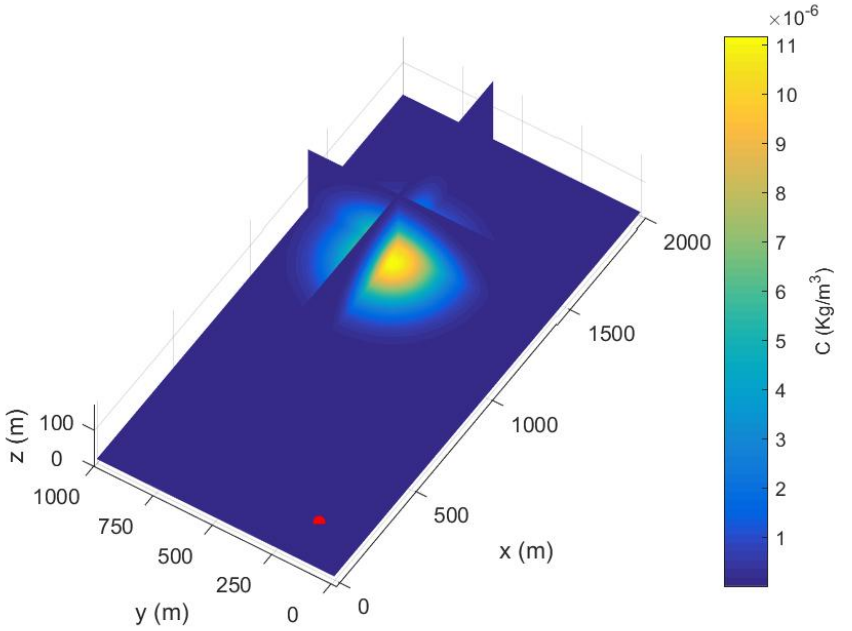

(b)

Figure 8.1: Example plot of the concentration from the puff model at a) 50 seconds and b) 300 seconds after the release. The red dot indicates the origin of the source and the colour map denotes the concentration at the correspondence position, generated from a puff with parameters: $\mathbf{p}_s = [200, 200, 1]^{\mathsf{T}}$, $m_s = 150$, $u_s = 4$, $\phi_s = 20$ and $[a, b, c, d] = [0.14, 0.95, 0.53, 0.73]$.

where

$$p(z_k|\mathbf{z}_{1:k-1}) = \int p(z_k|\Theta)p(\Theta|\mathbf{z}_{1:k-1})\,\mathrm{d}\Theta. \tag{8.9}$$

At each iteration, the previous result replaces the posterior distributions of the parameters. To initialise the algorithm, prior distributions for each of the parameters in the source vector must first be selected. Where possible, these can be given informative distributions. For example, assuming that meteorological sensors are available, a normal distribution is used for the prior on the wind speed u_s and direction ϕ_s. The remaining priors are set as uniform distributions within some reasonable bounds. Bayes' theorem is implemented using a particle filter as described in the implementation section.

Once the posterior distribution at the current time step is obtained, the UAV must choose where to take the next measurement by maximising the expected gain in information:

$$\mathbf{a}_k^* = \arg\ \max_{\mathbf{a}_k \in \Psi} \{\mathbb{E}[\Upsilon(a_k)]\}, \tag{8.10}$$

where $\mathbf{a}_k \in \Psi$ is the set of manoeuvres that the UAV can make. In this chapter, the manoeuvre set is limited to a single move in the x, y, or z directions with a fixed step size: $\Psi = \{+x, -x, +y, -y, +z, -z\}$.

Inspired by the work on optimal experiment design, the expected utility of manoeuvre $\mathbf{a}_k$ is given as the product of the likelihood of an observation/measurement and its corresponding utility $\Upsilon(\Theta, \hat{z}_{k+1}, \mathbf{a}_k)$ [202]:

$$\mathbb{E}[\Upsilon(\mathbf{a}_k)] = \int_{\hat{z}_{k+1}} p(\hat{z}_{k+1}|\Theta, \mathbf{a}_k)\Upsilon(\Theta, \hat{z}_{k+1}, \mathbf{a}_k)d\hat{z}_{k+1}, \tag{8.11}$$

where $\hat{z}_{k+1}$ is the range of possible future measurements at the potential sampling position. The utility of the manoeuvre is defined as the Kullback-Leibler divergence between the source parameter distributions before $p(\Theta)$ and after $p(\Theta|\hat{z}_{k+1}, \mathbf{a}_k)$ the new measurement.

$$\Upsilon(\Theta, \hat{z}_{k+1}, \mathbf{a}_k) = z_{KL}(p(\Theta|\hat{z}_{k+1}, \mathbf{a}_k)||p(\Theta)) = \int_\Theta p(\Theta|\hat{z}_{k+1}, \mathbf{a}_k) \ln \frac{p(\Theta|\hat{z}_{k+1}, \mathbf{a}_k)}{p(\Theta)} d\Theta \tag{8.12}$$

Combining (8.11) and (8.12) leads to the following expression for the reward function.

$$\mathbb{E}[\Upsilon(\mathbf{a}_k)] = \int_{\hat{z}_{k+1}} p(\hat{z}_{k+1}|\Theta, \mathbf{a}_k) \int_\Theta p(\Theta|\hat{z}_{k+1}, \mathbf{a}_k) \ln \frac{p(\Theta|\hat{z}_{k+1}, \mathbf{a}_k)}{p(\Theta)} d\Theta d\hat{z}_{k+1} \tag{8.13}$$

The complex double integral in Eq (8.13) can be approximated efficiently by importance sampling.

The estimation of the parameters of the instantaneous release via the particle filter and the computational implementation of the information based reward are as described in Chapter 5.

8.4 Simulations

Simulations are used to assess the performance and feasibility of performing source term estimation of an instantaneous release using a single mobile sensor. The results are compared with the more common approach: using an array of varying amounts of static sensors. The simulations are designed to provide a fair comparison between the two approaches, both of which can have limitations. For example, it would not be a fair comparison if the hazardous material did not pass any or even a couple of the static sensors. Likewise, it would not be fair if the wind speed was faster than the speed of the UAV platform or if it was initialised a long time after the release or from a very poor starting position. Therefore, in this preliminary study, the simulations are constrained to a scenario where the UAV can move 2 times faster than the wind and at least half of the puff passes over the static network.

An example run is provided to demonstrate the behaviour of the algorithm during a typical source term estimation task. The scenario described will be ran multiple times to produce a Monte Carlo comparison between the mobile sensor and a static network.

8.4.1 Illustrative runs

An illustrative run of the algorithm is given in Fig 8.2. Simulated data was generated from the model described by Eq (8.1) and infected with Gaussian noise. An instantaneous release of 150kg that occurred 50 seconds prior to the search start was simulated. The wind had a speed of $4m/s$, 20° from the x-axis. The UAV, started the search from $\mathbf{p}_k = [100, 300, 31]^\mathsf{T}$ and followed the path indicated by the red line, where red dots represent the positions where measurements were taken. The discrete time step used during the simulations was 3 seconds, during this interval, it was assumed the UAV could move 36m. The large number of green dots represents the random sample approximation of the location estimate of the source and the shaded contour shows the concentration of the puff at the current time. The posterior estimates of the source parameters at the end of the illustrative run are shown in the histograms in Fig 8.3, where the red line is the true value of the parameter. Similarly, an illustrative run is shown in Fig 8.4 in the same conditions, where a static network of sensors was used in place of a UAV. The static sensors were distributed on the circumference of a circle with centre $(1400, 400)$ and radius 300. The figures and histograms in Figs 8.3 and 8.5 demonstrate how the UAV can produce a more certain posterior estimate of the source.

8.4.2 Results

The results after 100 Monte Carlo simulations using the set-up illustrated in Figs 8.2 and 8.4 are summarised in Table 8.1. Other scenarios also shown include various wind speeds $u = 2, 4, 6$, release masses $M = 75, 150$ and a different amount of static sensors. The root

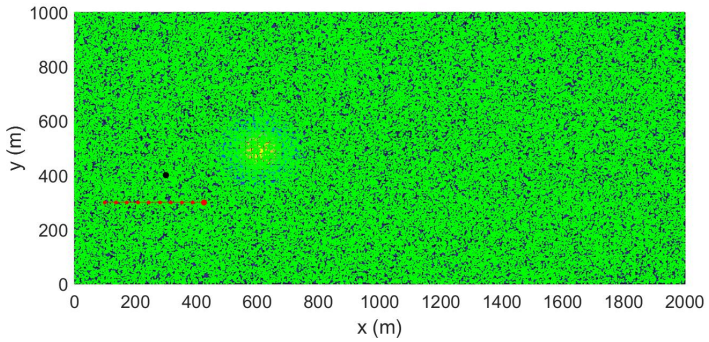

(a) k=10

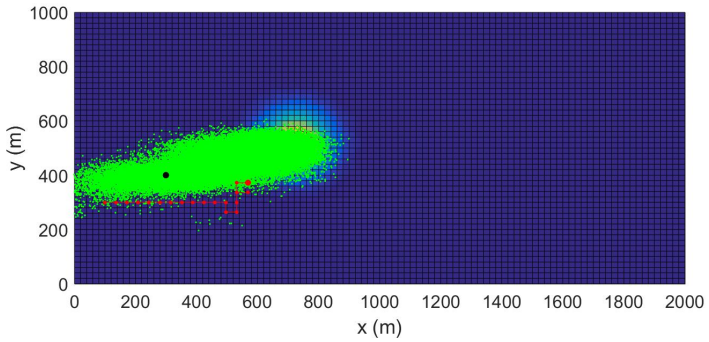

(b) k=20

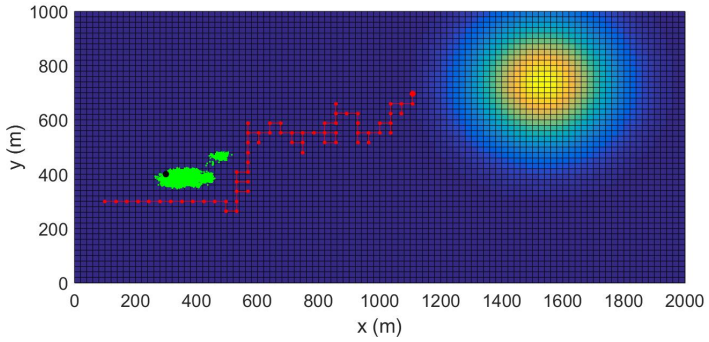

(c) k=90

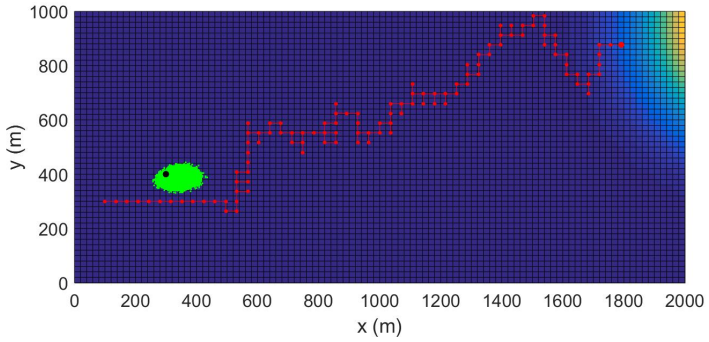

(d) k=160

Figure 8.2: Illustrative run using a single UAV at time steps a) k=10; b) k=20; c) k=90; and d) k=160. The UAV starts at (100,300) and follows the red lined path taking measurements at the red dots. The green dots represent the random sample approximation of the posterior distribution of the source with true position indicated by the black dot at $(300, 400)$.

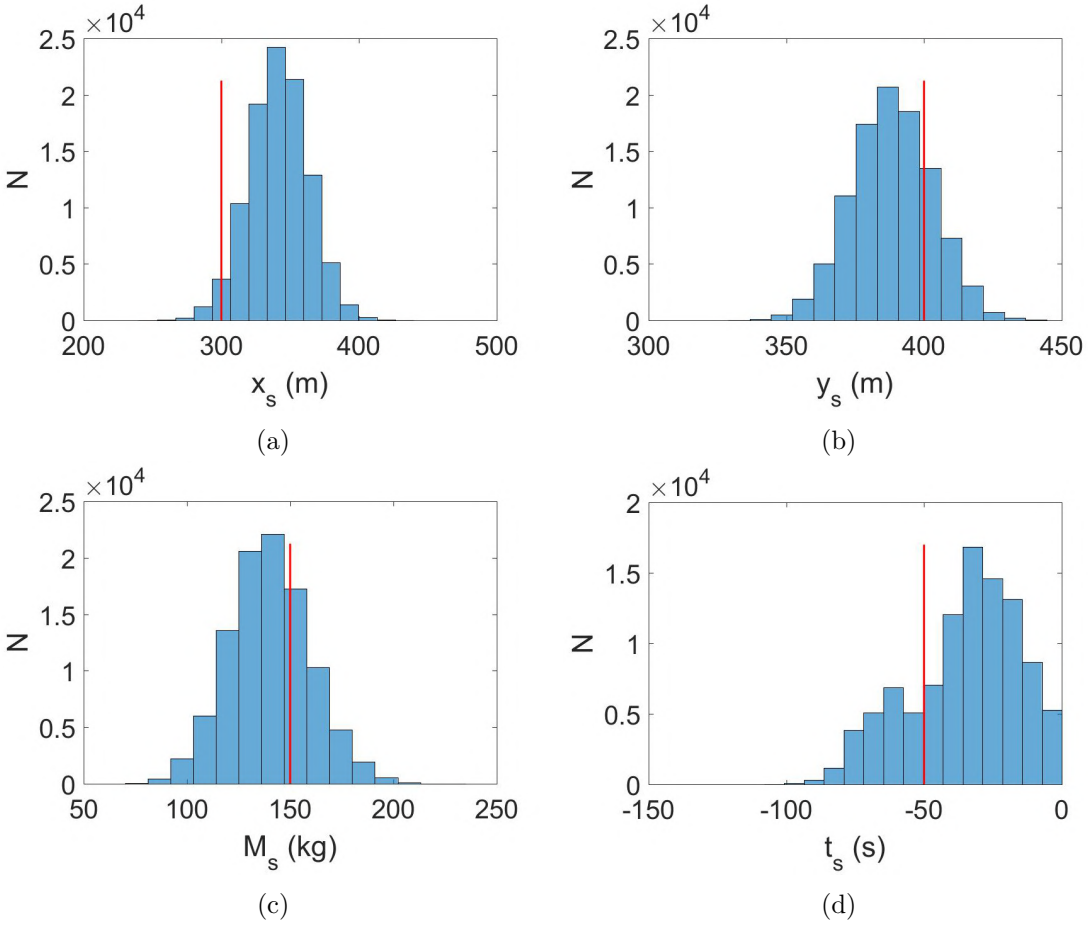

Figure 8.3: Posterior density estimates at the end of the illustrative run using a single UAV for the source parameters: a-b) x_s and y_s coordinates; c) release mass m_s; and d) the start time t_s.

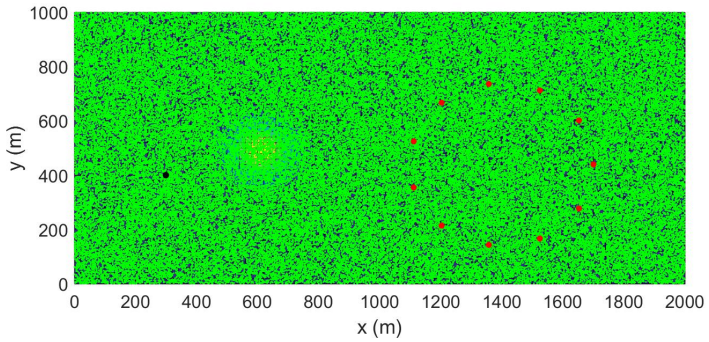

(a) k=10

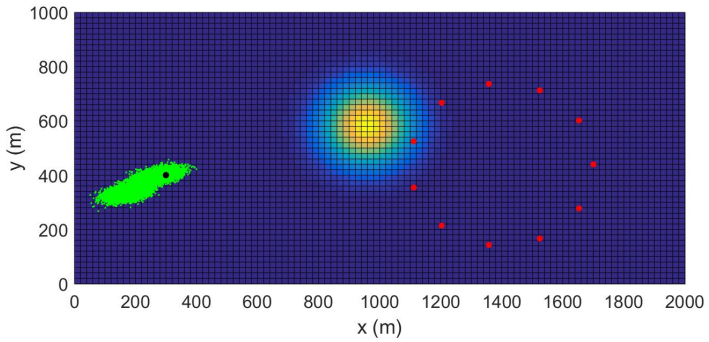

(b) k=40

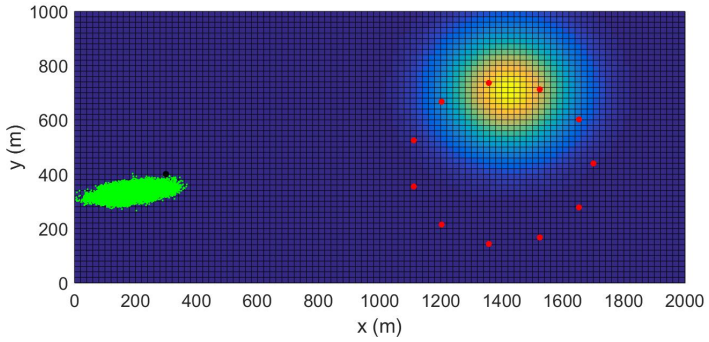

(c) k=80

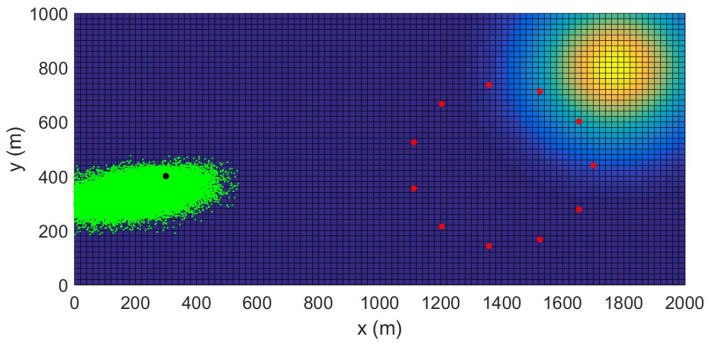

(d) k=110

Figure 8.4: Illustrative run using a circular array of 12 static sensors at time steps a) k=10; b) k=40; c) k=80; and d) k=110. Red dots denote the locations of the sensors. The green dots represent the random sample approximation of the posterior distribution of the source with true position indicated by the black dot at $(300, 400)$.

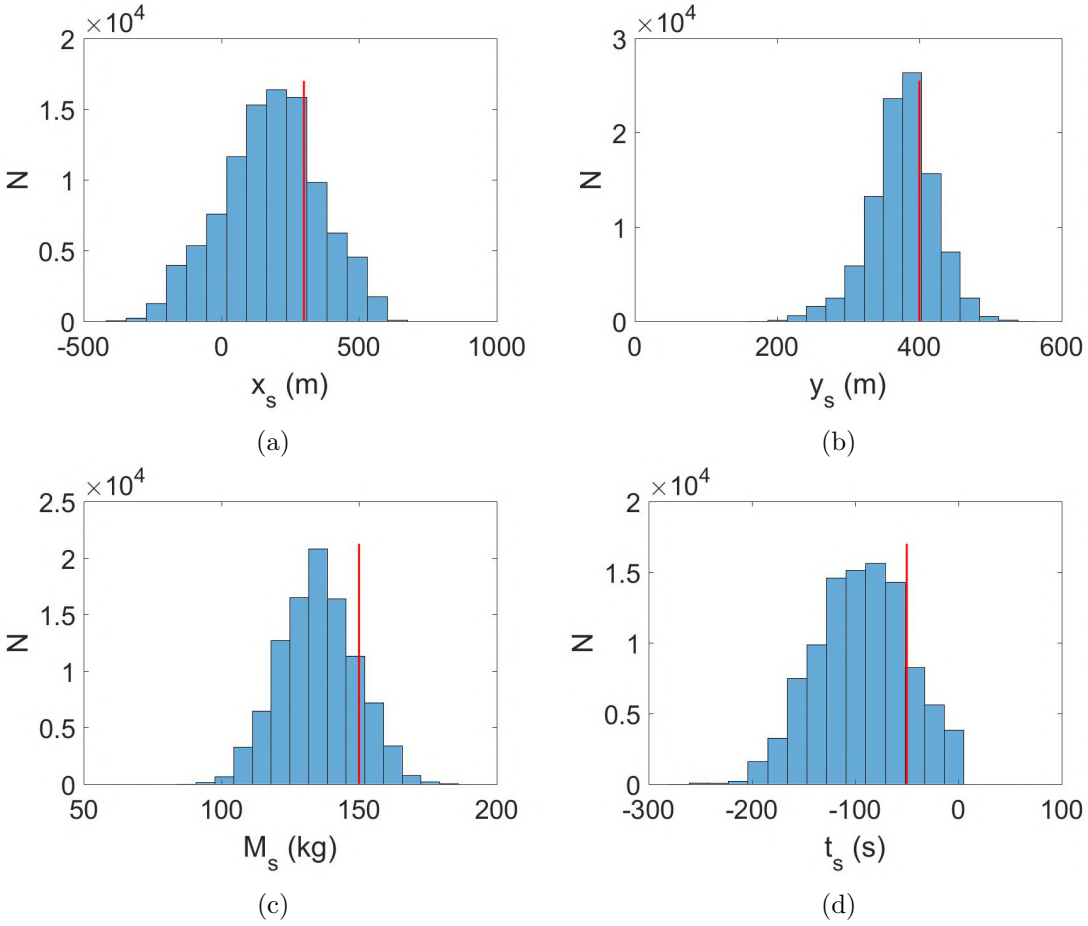

Figure 8.5: Posterior density estimates at the end of the illustrative run using 12 static sensors for the source parameters: a-b) x_s and y_s coordinates; c) release mass m_s; and d) the start time t_s.

Table 8.1: Performance comparison over a hundred Monte Carlo simulations

	True mass m_s	75	75	75	150	150	150
	Wind speed u_s	2	4	6	2	4	6
1 mobile sensor	RMSE in $x_s(m)$	55.78	108.10	159.65	63.77	137.89	169.86
	RMSE in $y_s(m)$	38.39	43.70	54.48	33.15	51.52	56.23
	RMSE in $z_s(m)$	1.65	1.58	1.60	1.58	1.72	1.69
	RMSE in $m_s(kg)$	28.14	27.85	24.58	76.18	49.18	27.10
	RMSE in $t_s(s)$	73.44	29.59	22.17	60.69	36.11	28.83
12 static sensors	RMSE in $x_s(m)$	109.52	165.66	186.35	102.66	145.59	179.38
	RMSE in $y_s(m)$	46.80	49.72	52.16	38.66	44.75	50.16
	RMSE in $z_s(m)$	2.80	2.22	1.73	2.54	1.92	1.85
	RMSE in $m_s(kg)$	10.07	9.73	5.97	15.18	8.86	8.29
	RMSE in $t_s(s)$	53.34	44.11	33.05	54.81	42.69	32.53
25 static sensors	RMSE in $x_s(m)$	134.62	152.21	158.51	144.44	145.15	153.31
	RMSE in $y_s(m)$	49.88	45.40	54.30	46.41	46.22	41.05
	RMSE in $z_s(m)$	2.54	2.07	2.67	2.25	2.22	1.68
	RMSE in $m_s(kg)$	20.89	18.38	16.15	22.76	18.45	19.83
	RMSE in $t_s(s)$	89.84	68.63	35.61	107.73	51.37	40.11

mean squared errors (RMSEs) are shown for the mean estimates of the location (x_s, y_s, z_s), release mass m_s and start time t_s of the release. The remaining variables in the source vector are not shown as they are mainly included in the vector as nuisance parameters. The benefits of using a UAV to estimate the source term in lower wind conditions are clear, however, at higher wind speeds the static network begins to outperform the UAV based system. Interestingly, the difference in the number of static sensors had less effect than expected. This may be caused by the considerable amount of data read by the sensors after the large amount of time steps. The static sensors could typically estimate the mass of the release much more accurately, this is caused by the greater amount of observations of the puff, reducing the effects of noise. Moreover, the static networks took observations simultaneously from several locations within the puff at a single instance, including observations near its centroid where the concentrations are greatest. On the other hand, the singular UAV would have less observations of the puff, which were more typically taken from its edge.

In general, more accurate estimates of the release parameters were obtained for both static and mobile sensors when the release was stronger, as shown in the Table, where the results for a release mass of 150kg were more accurate than 75kg. For both amounts of sensors, more accurate estimates were obtained in lower wind conditions, besides those for the start time of the release. This is caused by the large amount of correlation between variables estimated using the particle filter, which makes them more dependant on the prior distributions provided at the beginning of the simulations. There are several causes of correlation, for example downwind location, wind speed and release time are highly

correlated as is shown by Eq (8.2). The release time and mass of release are also correlated, where a release from long time ago produces smaller measurements, similarly to a smaller mass.

8.5 Chapter summary

After the successful experiments of STE performed in realistic outdoor conditions using a UAV, this chapter aimed to extend the method to a scenario where the HAZMAT source is not continuously emitting. This was achieved by augmenting the information based search and source estimation algorithm with a puff model and its associated model parameters. In simulations, the system was shown to successfully estimate the parameters of the release including its location, start time and the quantity of released material. The method was comparable in performance to that of a static network, whilst overcoming issues such as positioning of the sensors, and the costs of powering and maintenance of a large network of sensors. The UAV based system was able to estimate the parameters of the release more accurately in simulations with a wind speed less than half that of the UAV. The difficulty of estimating all the dispersion parameters of a puff due to coupling between variables was highlighted and is an area that should be addressed in future work, although it is outside of the scope of this thesis. It may also be useful to perform many more simulations to test the algorithm with alternative starting conditions. These may be built from further information regarding the operational circumstances the system is expected to be deployed into.

Chapter 9

Plume mapping using point measurements from autonomous unmanned vehicles

In the low or changing wind conditions that cause the source search and estimation algorithm to lose performance or fail, the hazardous area can be mapped instead. This functionality is described independently in this chapter, however, in the future, it is envisioned that a method could be developed to perform both simultaneously or to make a decision whether to perform STE or mapping autonomously.

Mapping the spatial distribution of the concentration of a gas has several important applications in environmental monitoring, air quality assessments, and in response to accidents or deliberate spills of hazardous chemicals [87]. A spatial approximation of the spread of the gas can provide valuable information for urban planning, about emissions, and to support emergency responders with valuable knowledge to help them act effectively. Mapping of a gas cloud typically involves linking several spatial temporal observations from point-wise concentration detectors which can be spread on the ground or placed upon unmanned vehicles.

Mapping the distribution of a gas has an advantage over other response methods, including STE, as it can provide a detailed map of the hazard using observations from sensors without relying on a model. The approach can still be affected by noisy observations, turbulence, and intermittent readings from the sensors, however, these phenomena can be handled by a robust algorithm. Moreover, to the best of the authors knowledge, proper experimental evaluation of gas distribution or plume mapping algorithms is not available in the literature. The previous work, discussed in the literature review in Chapter 2, had been assessed in simulations, empirically, or by using sensor data taken at different times in uncontrolled environments, which does not represent a proper ground truth (In an uncontrolled environment, such as natural conditions outdoors or indoors, the gas distribution changes over time predominantly due to small variations in the wind. Therefore,

point measurements of the plume taken at different times cannot be used to form learning data and ground truth data.). Furthermore, the effect of measurement sampling times has not yet been considered. Sampling times in the literature were high meaning a long time was taken to produce a map of the plume, typically at least one hour [219], which is unacceptable for emergency response.

The main contribution of this chapter is from thorough experiments that have been performed to assess the plume mapping performance of unmanned autonomous vehicles. Several mapping algorithms are compared including Gaussian Process regression, Neural networks and polynomial and piecewise linear interpolation. The methods are compared in Monte Carlo simulations using a well known plume model and in indoor experiments using a ground robot. Unlike previous work on mapping using unmanned vehicles, the indoor experiments were performed in a controlled manner so that a ground truth could be obtained in order to properly assess the various regression methods using data from a real dispersive source and sensor. The effect of sampling time during data collection was assessed with regards to the mapping accuracy, a parameter which had previously been neglected in the literature even though it has a significant effect on the noise of the measurement data. Overall, the Gaussian Process method was found to perform the best among the regression algorithms, showing more robustness to the noisy measurements obtained from short sampling periods, enabling an accurate map to be produced in significantly less time. After thorough assessments in simulations and repeatable experiments, the plume mapping results are presented in uncontrolled outdoor conditions, using an unmanned aerial vehicle, to demonstrate the system in a realistic uncontrolled environment.

This chapter is based upon work that has is currently under review [220]. Note: the nomenclature used in this final chapter of the thesis is described in a manner to match the convention of the Gaussian Process machine learning literature. The remainder of the chapter is outlined as follows. The problem is further described in Section 9.1. The Gaussian process regression algorithm used to generate an approximation of the gas distribution is outlined in Section 9.2. Simulation results are provided in Section 9.3 followed by indoor experimental results using a ground robot in Section 9.4. Outdoor experiments using a UAV are given in Section 9.5 and finally, conclusions and ideas for future research are given in Section 9.6.

9.1 Problem description

After a release of hazardous material, or during an environmental monitoring task, an unmanned vehicle equipped with a relevant gas concentration detector is sent into an area to collect measurements. This enables responders to assess the hazard without direct contact, or environmental researchers to gather a large amount of data in a short amount of time. The data from the vehicle consists of an $N \times 1$ vector of observations from the

gas detector given by $\mathbf{y} \in \mathbb{R}^{N\times 1}$, taken at positions given by the $N \times 2$ matrix $\mathbf{x} \in \mathbb{R}^{N\times 2}$. Here, N refers to the number of measurements made by the gas detector. The unmanned vehicle performs a full coverage search pattern, such as a parallel sweep, over a predefined area to collect the data. The goal is to provide an approximate map of the gas distribution given these observations that are likely to be corrupt with noise and intermittency [219]. In this chapter, the accuracy of the map generated using different regression algorithms is compared.

9.2 Gaussian process regression

9.2.1 Gaussian Process

Gaussian Process (GP) is employed to model the distribution of gas concentration using the noisy readings from the gas detector. GP is a machine learning technique which can be used to solve regression problems [221]. The key advantage of the Gaussian Process method is that it does not rely on pre-specified parameters to fit a function to the available data, making it suitable to variety of different gas releases and meteorological conditions without the need for pre-training or adjusting parameters.

Generally, Gaussian Process is denoted as:

$$f \sim \mathcal{GP}(\boldsymbol{m}(\mathbf{x}), \boldsymbol{k}(\mathbf{x}', \mathbf{x})), \tag{9.1}$$

where $\boldsymbol{m}(\mathbf{x})$ and $\boldsymbol{k}(\mathbf{x}', \mathbf{x})$ are $N \times 1$ vectors of mean and covariance functions, respectively. $\mathbf{x}'$ is an $M \times 2$ matrix of positions at which GP predicts the value and M is a number of data points at which predictions are made. The mean and covariance functions are discussed in more detail later, at this point, it is worth noting that both $\boldsymbol{m}(\mathbf{x})$ and $\boldsymbol{k}(\mathbf{x}', \mathbf{x})$ are characterised by a set of hyperparameters, which describe how the data are correlated internally within those functions. The number of hyperparameters and their impact is unique to the choice mean and covariance functions. The set of hyperparameters is given as $\boldsymbol{\theta}$.

To fit the function to the collected data points, the values of $\boldsymbol{\theta}$ are adjusted until the chosen mean and covariance function have the best fit. This is achieved by firstly defining a log marginal likelihood as:

$$L = \log(\mathbf{y}|\mathbf{x}, \boldsymbol{\theta}) = -\frac{1}{2}(\mathbf{y} - \boldsymbol{m}(\mathbf{x}))^T(\boldsymbol{C_n})^{-1}(\mathbf{y} - \boldsymbol{m}(\mathbf{x})) - \frac{1}{2}\log|\boldsymbol{C_n}| - \frac{n}{2}\log(2\pi), \tag{9.2}$$

where $\boldsymbol{C_n} = \Sigma + \sigma_N^2 I$ in which Σ denotes a set of covariance functions of $N \times N$ size with entries $k_{ij} = k(x_i, x_j)$ for $i, j = 1, ..., N$. σ_N^2 is a hyperparameter responsible for accounting for noisy data and $\mathbf{y}$ is the set of point-wise gas concentration measurements from the UAV. The conjugate gradient method [222] has been adopted in order to find $\boldsymbol{\theta}$:

$$\boldsymbol{\theta}^* = \arg\max_{\boldsymbol{\theta}}(L) \tag{9.3}$$

Once the hyperparameters are optimised, prediction can be made in form of mean and variance outputs at the positions $\mathbf{x}'$ as:

$$\mu_p(\mathbf{x}') = \boldsymbol{m}(\mathbf{x}') + \boldsymbol{\mu}(\mathbf{x}') + (\boldsymbol{C_n}^{-1}(\boldsymbol{y} - \boldsymbol{m}(\mathbf{x}')) \tag{9.4}$$

$$\sigma_p(\mathbf{x}') = \boldsymbol{k}(\mathbf{x}', \mathbf{x}') - \boldsymbol{k}(\mathbf{x}, \mathbf{x}')^T(\boldsymbol{C_n})^{-1}\boldsymbol{k}(\mathbf{x}, \mathbf{x}'). \tag{9.5}$$

The variance $\sigma_p(\mathbf{x}')$ is a valuable parameter that represents the magnitude of uncertainty in the prediction.

9.2.2 Mean and covariance function

To make a good prediction, the choice of mean and covariance functions need to be suitable for the data expected. In general there are two types of covariance functions: (i) stationary; and (ii) non-stationary. A stationary covariance function is used in this work as it is applicable when mathematical patterns are present. In the case of a gas release, information gained in one place has implications about the shape of the fitted functions in others. For example, using gradient information is helpful to determine the overall shape of the plume. In light of this, the Squared Exponential with an automatic relevance determination covariance function is used:

$$k(x', x) = \sigma_f^2 exp\bigg((x - x')^T\boldsymbol{\Lambda}^-2(x - x')\bigg), \tag{9.6}$$

where σ_f and $\boldsymbol{\Lambda} = (\Lambda_1, \Lambda_2)$ are the hyperparameters. This covariance function is complimented with a constant mean function:

$$m(x) = c, \tag{9.7}$$

where c is a hyperparameter to optimise, resulting in the hyperparameter set $\boldsymbol{\theta} = \{\sigma_f, \boldsymbol{\Lambda}, c\}$.

9.3 Simulations

The GP regression algorithm is compared with other methods in simulations using data generated from a plume model. The regression methods compared are a neural network based technique, and linear and locally weighted scatterplot smoothing interpolation methods from MATLAB's Deep learning and curve fitting toolboxes. To simulate the dispersion, 50 different Gaussian plumes are generated using the model described in [209]. The measurements from the sensor are modelled using a 30% chance of a miss detection, and then additionally infected with zero mean normally distributed noise with standard

deviation equal to the expected reading from the model. The mobile sensor undergoes a uniform sweep pattern collecting sensor measurements every 2 meters on its path. This data are then used to train the regression algorithms to predict shape of the dispersion at arbitrary locations.

The average root mean squared error (RMSE) is calculated between the predicted concentrations within the plume and the simulated plume prior to adding the noise model. The results are summarized in Table 9.1 including the relative percentage RMSE relative to the output of the Gaussian process (which performed best). It can be seen that Neural Network based approach comes closest to GP method with an average greater error of approximately 17%. The two interpolation methods have a significantly greater average RMSE.

Example surfaces generated by each method and their corresponding errors are shown in Fig 9.1. Comparing these surfaces can reveal the issues of the different techniques. Both interpolation predictions are very noisy, due to the nature of the reading from the sensor. The Neural Network based approach tended to over estimate the area of influence for each of the points. The resulting surface was robust to noise, however, it was over-fitted in many places. Finally, analysing the Gaussian Process output, it can be seen that it predicts the shape as good as interpolation without an over-fitting issue, thus, it results in the best prediction.

Table 9.1: Accuracy of methods

Method	Average RMSE error	RMSE error as a percentage of GP RMSE error
Gaussian Process (GP)	0.004	0%
Neural Network for regression	0.0048	20%
Locally weighted scatterplot smoothing interpolation	0.0056	40%
Piecewise linear interpolation	0.0052	30%

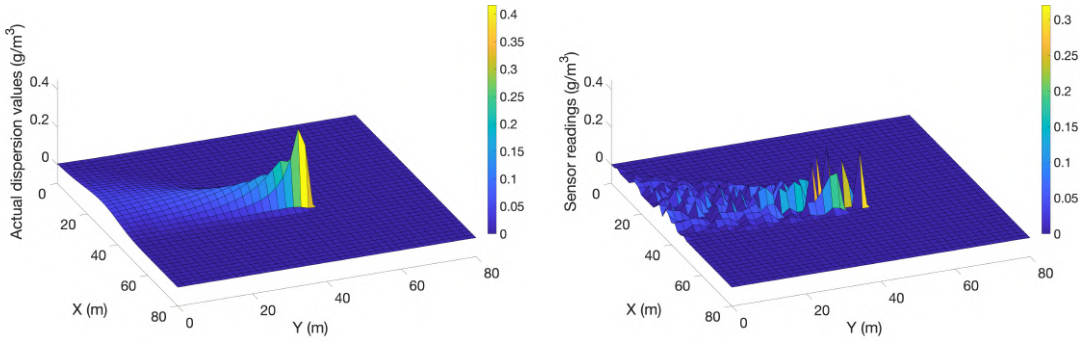

(a) True map of dispersion

(b) Sensor reading

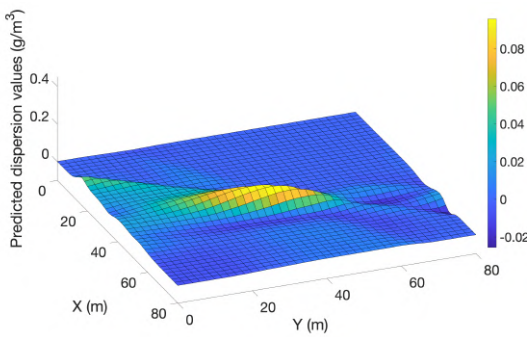

(c) Dispersion map predicted by NN

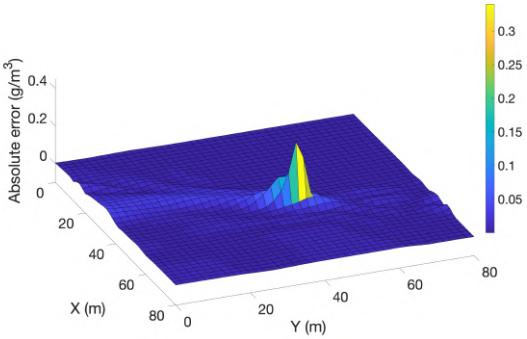

(d) RMSE error of NN

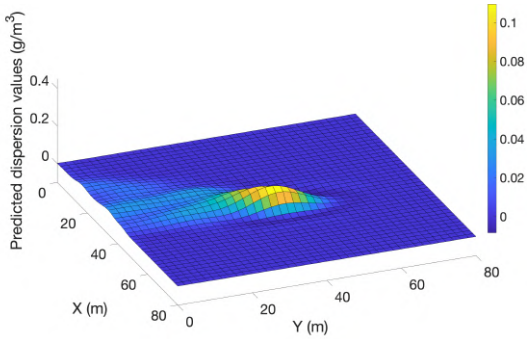

(e) Dispersion map predicted by GP

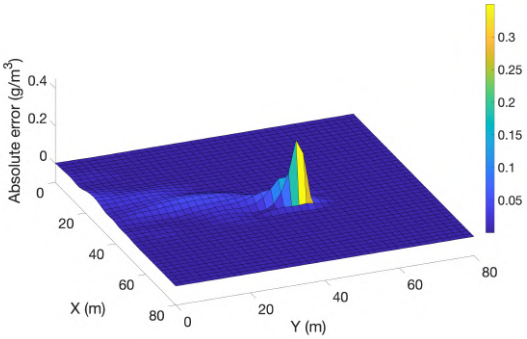

(f) RMSE error of GP

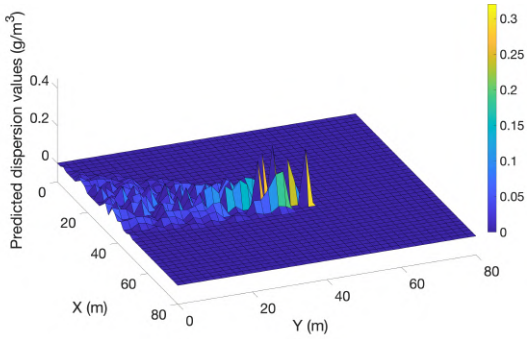

(g) Dispersion map predicted by interpolation

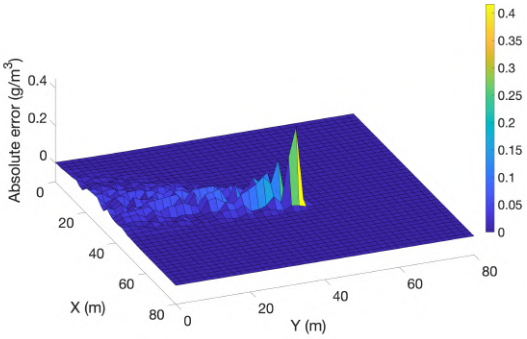

(h) RMSE error of interpolation

Figure 9.1: A sample scenario from the set of 50 Monte Carlo simulations. The sensor reading as shown in (b) is quite noisy, resulting in poor prediction from interpolation (g). NN results in (c) tend to over-fit the data resulting in larger errors where zeros should have been predicted. Gaussian Process (e) fixes the issue of overfitting while suffering less from noise.

9.4 Indoor validation experiments

9.4.1 Experiment setup

The indoor system consisted of a Turtlebot 3 ground robot equipped with a PID gas sensor and a vicon motion capture system for indoor positioning. The system is shown in Fig. 9.2. The Robot Operating System (ROS) was used for all communications among the system components.

A small open bottle of acetone and a heat gun was used to produce a constant emission rate of dispersive material. Fans at either side of the room were used to generate a constant wind field. The experiment environment is shown in Fig. 9.2 where the ground truth is displayed on the floor. The controlled environment meant that the plume would reach a steady state, where sufficient sampling times would result in repeatable measurements. It was found that 30 seconds was sufficient producing repeatable measurements at the same locations.

During the experiments, the Turtlebot performed a uniform sweep flight pattern, moving 0.2 meters in y-axis and 0.4 meters in x-axis between samples. Multiple runs with 30 second samples were shown to produce consistent measurements, and were used as a ground truth. 5s and 1s samples were used to collect noisy data to compare the algorithms.

9.4.2 Results

Twenty seven experiments were conducted in total to assess the mapping performance of the algorithms. 3 runs were conducted with a 30s sampling time to prove the experiments were repeatable and to establish a ground truth. 12 runs were conducted with 5s sampling times and 12 with 1s. The results of the experiments are summarised in Fig. 9.3 and in Table 9.2. Fig. 9.3 shows the error between predicted measurements and the ground truth. The more the distribution is skewed to the right, the better the result as it means a greater number of data points were predicted with less error. It can be seen that for both 5s and 1s sampling times, GP has the best prediction quality followed by interpolation and NN based regression. However, the performance advantage offered by GP is not as significant as shown in simulations and comes with an additional computational cost compared to linear interpolation. Thus, depending on the application, sampling time and computational time, there are advantages of both interpolation over GP regression for plume mapping.

9.5 Outdoor experiments

Following the validation of the algorithms in controlled indoor experiments, outdoor experiments were conducted to demonstrate the algorithm in an uncontrolled environment using a UAV for data collection. Such experiments are rare in the literature, where a UAV

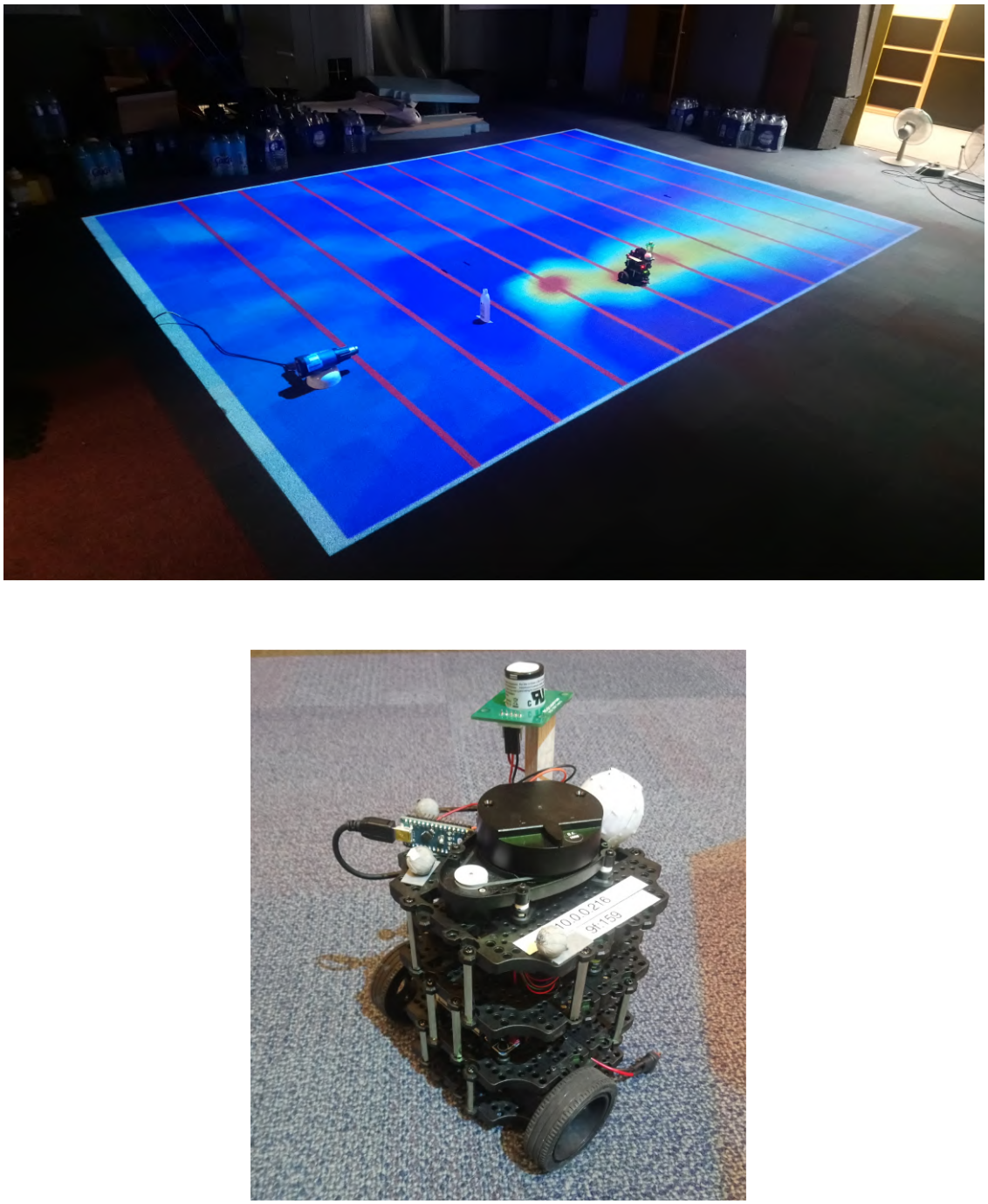

Figure 9.2: Experiment setup to validate the mapping algorithms. The bottle of acetone and a heater are shown on the floor near the centre of the left figure. The red line on the ground denote the robots path during the experiments and the colourmap is generated by running the GP algorithm on the ground truth data.

is employed to gather gas concentration data in the presence of a chemical release. This section describes the set-up of the UAV and the experiments, followed by the results.

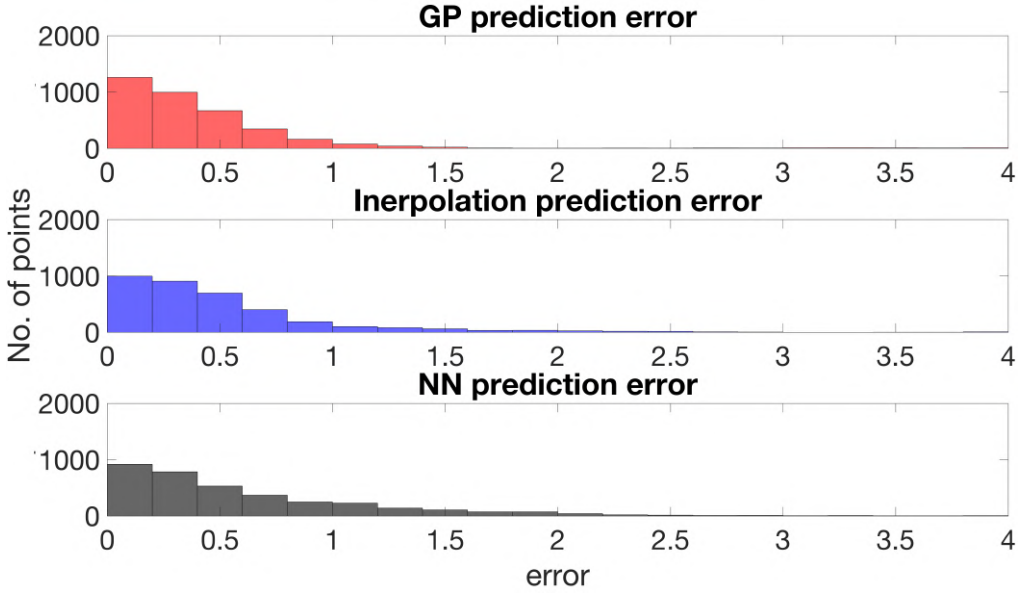

(a) Errors with 5 second sampling times.

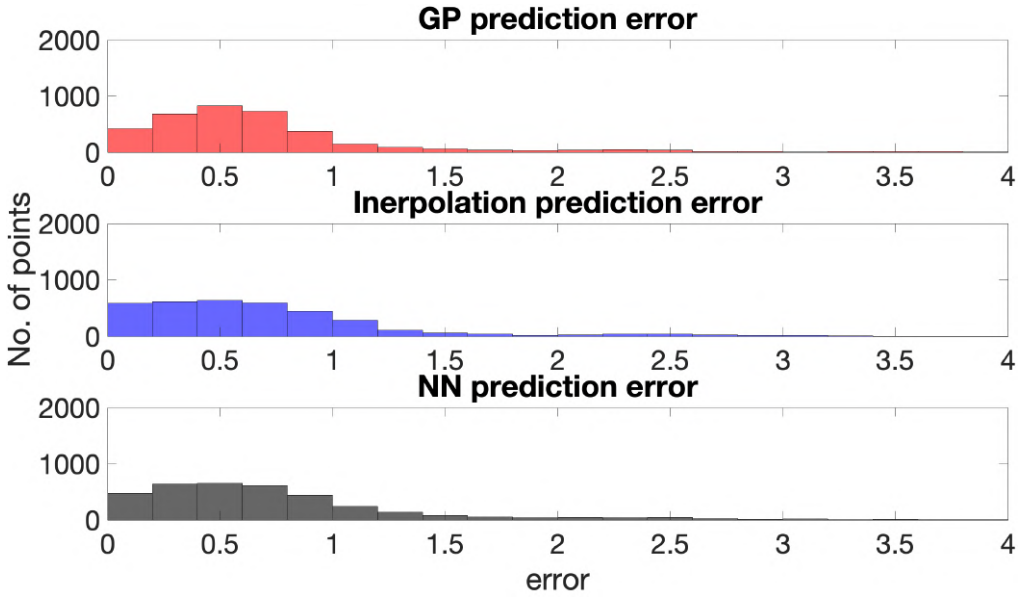

(b) Errors with 1 second sampling times.

Figure 9.3: Histograms of Errors for three regression methods. Results are shown for predictions made using measurement data collected using a) 5 seconds and b) 1 second sampling times. The predictions are compared against 30 seconds ground truth data collected at different runs, in different positions.

Table 9.2: Accuracy of methods

Method	Average RMSE error for 5 seconds	Average RMSE error for 1 second
Gaussian Process (GP)	0.4875	0.8407
Neural Network for regression	0.7661	0.9074
Piecewise linear interpolation	0.6623	0.8779

9.5.1 UAV setup

The system primarily consisted of a quadrotor UAV and a laptop as a base station. The quadrotor platform was a DJI Matrice 100 as shown in Fig 9.4. It was equipped with a PID gas sensor which was used to measure the concentration of the hazardous gas. The Robot Operating System (ROS) framework was used for all communications to enable location stamped data collection in the field. Such a system applied to UAVs is further described in [210].

9.5.2 Experiment setup

Acetone was released into the atmosphere using a source comprising of ultrasonic diffusers and an air pump. The source would release acetone at a rate of approximately 1.5g/s, however, this would vary slightly depending on atmospheric conditions such as temperature and pressure. The field used during the experiments was located nearby Loughborough University, Leicestershire, UK. A snapshot during an experiment is shown in Fig 9.4 where, for clarity, the UAV and source are highlighted blue and red. The UAV would execute a uniform sweep pattern, at a constant height of 2m, stopping every 5 meters for 5 seconds to take an averaged measurement of the concentration measured by the gas sensor. The sweep covered a 25m by 25m square area.

9.5.3 Results

The output approximations of the distribution of gas concentration for the corresponding trials produced by the Gaussian process regression algorithm are displayed in figures 9.5a and 9.5b. The heat map indicates the approximated concentration at the corresponding location in $grams/m^3$. The location of the acetone source producing the hazard is indi-

Figure 9.4: Aerial platform used during the experimental trials showing the gas sensor mounted on top of the platform and a photo during an experiment. The source and the UAV are highlighted red and blue.

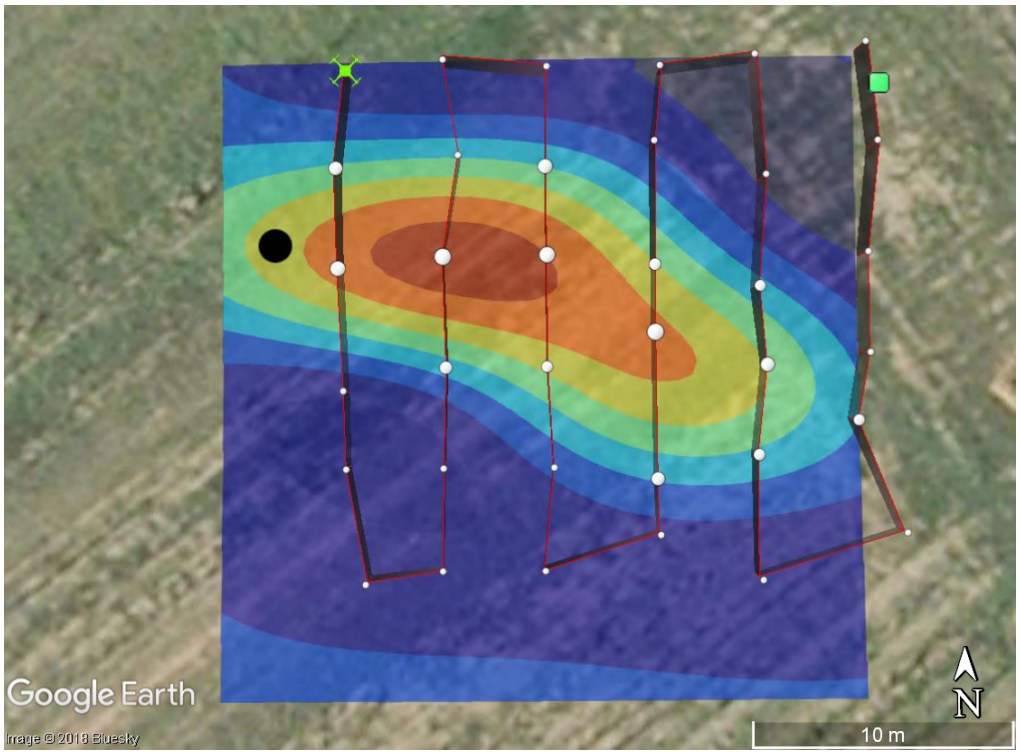

(a)

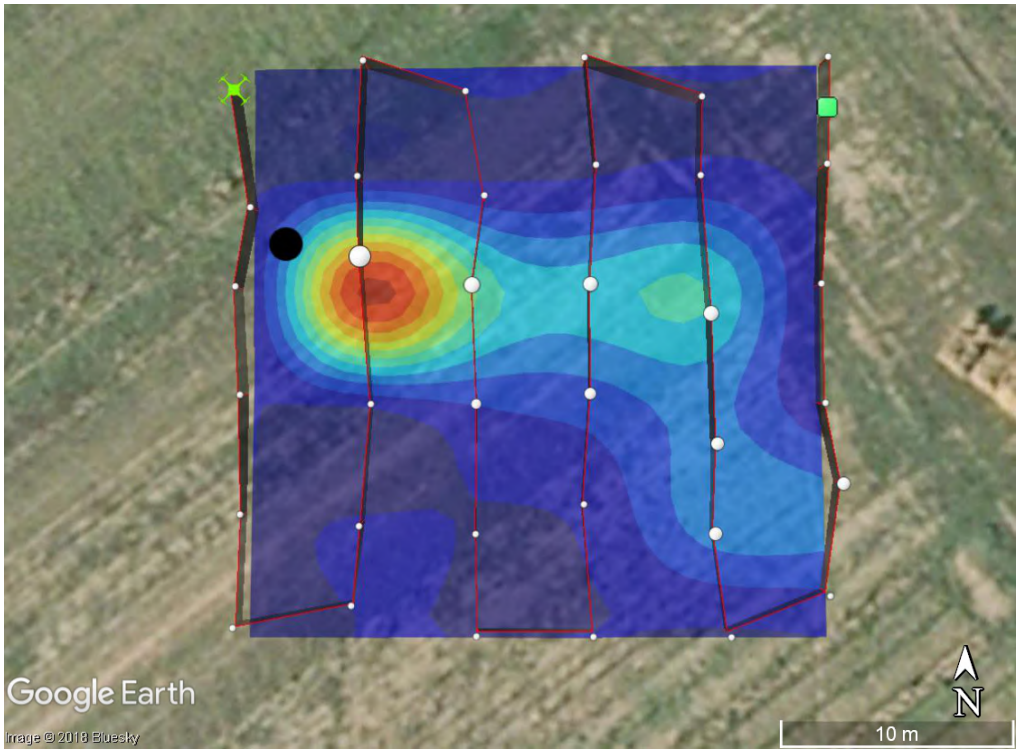

(b)

Figure 9.5: Output maps produced by the GP Regression algorithm after two experimental trials. The UAV followed the red line path, starting at the green square and ending at the UAV symbol. White dots on the path indicate measurements made by the onboard gas detector. The location of the source is given the black circle.

cated by the black circle. The raw data output from the gas sensor is indicated by the size of the white dots on the UAVs path which is indicated by the red line. The datasets were not large enough to use half the data for training and half for comparison and the uncontrolled environment meant that they were not repeatable. The results demonstrate the output of the algorithm during a realistic experiment after previously validating its performance in simulations and controlled indoor experiments.

9.6 Chapter summary

This chapter assessed several regression algorithms to map the distribution of a plume of dispersing material using point-wise measurements of the concentration. Firstly, simulations were used to assess the performance of the methods using a well known plume model. Then, controlled indoor experiments were performed to test the methods in repeatable conditions in order to validate the algorithms using a real source and sensor. Given the successful validation of the algorithms in the controlled experiments, the system was demonstrated in realistic uncontrolled experiments, outdoors, using a UAV for data collection. The mapping response that has been described in this chapter will be useful in conditions where the performance of the STE algorithm suffers or in scenarios where there is not a relevant ATD model to run a forward prediction.

There are two main areas for future work that are expected to improve the performance of the mapping system: Firstly, the algorithms should be extended to learn the map on-line, as data are gathered, rather than using a batch process method. Given this extension, it will also be useful to plan the path of the UAV on-line using the information available, rather than executing a uniform sweep flight pattern.

Chapter 10

Conclusions

10.1 Summary

This thesis described a method of response to releases of airborne material or gases into the atmosphere using a sensor equipped UAV. The main aim and contribution of the thesis was an extension of previous information based probabilistic source term estimation methods to work in real experiments, outdoors, using a UAV.

The thesis began with a general overview of the potential methods of response proposed in the literature which included source localisation, boundary tracking, mapping and source term estimation using static or mobile sensors. Subsequently, mapping and source term estimation methods using unmanned autonomous vehicles were identified as the most promising approaches to research during the remainder of the thesis.

To begin research in the area of source term estimation using information theoretic path planning principles the most common and tested Bayesian method used to estimate the source term of a release, previously using static detectors, was combined with an information based path planning algorithm which was adapted from the field of optimal experiment design. In numerical simulations the information based planning algorithm was shown to outperform conventional path planning methods such as a parallel sweep search pattern.

Following the support for an information based planning approach to STE, the Bayesian estimation algorithm was reformulated and implemented in a recursive manner, more appropriate for the problem where sensor data is collected sequentially. The information based path planning algorithm was also made more efficient by using the predictive measurement entropy as the planning reward, which lead to the new algorithm termed "Entrotaxis". The method was compared with the state of the art approaches in the literature using a simulated scenario and an experimental dataset, where it was shown to achieve a more efficient autonomous search.

Before attempting to perform STE using a UAV outdoors, the next stage was to test the algorithm outside of simulations but in a controlled environment. This involved designing

an appropriate experiment and setting up a robotic platform. Successful experiments were conducted in an indoor area with fans to simulate wind and a ground robot equipped with a low cost gas sensor. Several contributions were made in order to facilitate the successful experiments, particularly the development of a sensor model that could account for missed detections. The experiments conducted were the first of their kind in the literature, where the source term of a diffusive release was estimated using a ground robot.

With the successful indoor result, the system was assessed in outdoor conditions using an aerial vehicle. As STE had not previously been performed using a UAV, the estimation side of the algorithm was first verified using a parallel sweep flight pattern rather than the information based on-line planner. The experiments marked another first achievement of the thesis in the literature. The unique data collected during the experiments was used to compare the performance of two popular ATD models used in the literature. Furthermore, the effect on the results of the UAVs altitude, the step size in the sweep pattern, and the wind speed were assessed. The information based on-line planner was then tested in similar experimental conditions and the results were compared.

Following successful outdoor experiments using the UAV, the method was extended to handle a non-continuous release of hazardous material. The UAV based approach was compared to using static sensors in simulations.

During the outdoor experiments using the UAV it had been discovered that the system performed less well in low wind, highly unstable atmospheric conditions. In response to this a mapping algorithm was developed. Several regression based algorithms for mapping were compared in controlled indoor experiments using a ground robot and then demonstrated in uncontrolled outdoor tests using a UAV.

To conclude the thesis as a whole, the information based probabilistic methods of source term estimation have been extended from simulations to real world experiments using a UAV. The contributions herein facilitate the evolution of previous work in the area from theory to application.

10.2 Discussions on future work

In this thesis the ability to perform STE using a UAV with an information based path planning algorithm has been demonstrated in real world experiments for the first time. This motivates extension of the method to work in more environments and conditions in order to produce a system that could be used to potentially save lives in HAZMAT incidents or to support environmental monitoring missions. The future work described below should enable the method to work in more challenging environments, and to autonomously handle different release types. It should also make the estimation and path planning more reliable and efficient. Following the description of how the system can be improved, the use of the method in other applications areas is discussed.

Extend to more environments

In this thesis the method was validated in experiments conducted in an outdoors open field. To enable its application in more general environments it should be extended to work in urban, cluttered, or even indoor environments. This will require extensions to the estimation and path planning side of the algorithms. On the estimation side, the system should be extended to account for the disturbances caused by obstacles on the dispersion of atmospheric concentrations. On the path planning side a multiple step ahead planning algorithm should be integrated with a SLAM system to plan informative paths around obstacles. One such method that could be applied is rapidly exploring random trees (RRT) which has been popular in the area of informative path planning [223, 224].

Estimation improvements

During outdoor experiments the estimation performance was strongly dependant on the consistency of the wind direction. This was due to the assumptions on constant wind direction made in the underlying dispersion models. The estimation performance could be made more reliable by taking into account changing winds. This could be achieved my measuring the wind direction during the search, similarly to [200], and then accounting for changes in the estimation algorithm. Potentially through using a time dependant dispersion model, such as a Gaussian puff or directly solving the PDEs, or by adjustments to the algorithm itself.

Another area to extend the estimation algorithm was to remove the assumption that the source is continuously emitting, such as an instantaneous release or a discrete time release where the type of release is not known a priori. This has been achieved using static sensors in the literature by extending the parameter vector to include the start and stop times of the release, using a time dependant dispersion model such as SCIPUFF, and using an MCMC algorithm. It has not been done in a recursive manner or using a UAV.

An autonomous search for multiple sources is another area where the estimation algorithm could be extended. STE of multiple sources has been achieved in the literature

using static sensors and a reversible jump MCMC algorithm but not in a recursive manner or using a UAV. It is envisaged that a hybrid state or multiple model based particle filter could handle this scenario.

Path planning improvements

Besides the ability to cope with unknown release types or multiple releases the path planning should be extended to consider multiple steps ahead to improve efficiency and to handle cluttered environments.

Another area that could greatly improve the performance of the algorithm would be to remove the requirement to stop, or hover, to take an averaged sample of the hazard concentration. This may be achieved by taking a sensor average whilst moving, or by using the instantaneous observations of the sensor. This will introduce new problems due to the dynamics of the sensor, and designing an appropriate likelihood function to account for the new sampling technique. The source term estimation methods in the past, which used static sensors, had much longer sampling times which resulted in less intermittency and spread in the measurements making this a new problem to be solved.

Explore sensor types

The Bayesian and information based algorithms should be extended to handle different sensor types. In particular, an integral stand off concentration sensor such as a tunable diode laser absorption spectroscopy (TDLAS) sensor could yield many benefits and should be explored in the future.

Swarm based response

Using multiple cooperating vehicles, or a swarm, could produce a significantly more effective response with regards to accuracy and speed. For STE, multiple vehicles could work cooperatively by extending the information based planning algorithm to optimise the joint rewards from all the vehicles. For mapping, an informative path planing based algorithm or a multiple vehicle coverage algorithm should be developed to produce a map of the hazardous area more quickly and to monitor the dynamics of the plume. To facilitate this extension, the mapping algorithm should learn the map on-line, as data are gathered, rather than using a batch process method.

Other applications areas of the system

After the successful experiments and simulations throughout this thesis have demonstrated the performance improvements of using an information based path planning algorithm over conventional methods, it would be interesting to apply the work to other application areas. It is envisaged that the system could be applied to inverse problems in general that can benefit from measurements with a moving sensor. For example, tracking a car with a UAV and a monocular camera.

References

[1] LG Mastin, M Guffanti, R Servranckx, P Webley, S Barsotti, K Dean, A Durant, JW Ewert, A Neri, William I Rose, et al. A multidisciplinary effort to assign realistic source parameters to models of volcanic ash-cloud transport and dispersion during eruptions. *Journal of Volcanology and Geothermal Research*, 186(1):10–21, 2009.

[2] Michael Hutchinson, Hyondong Oh, and Wen-Hua Chen. A review of source term estimation methods for atmospheric dispersion events using static or mobile sensors. *Information Fusion*, 36:130–148, 2017.

[3] Nicholas S Holmes and Lidia Morawska. A review of dispersion modelling and its application to the dispersion of particles: an overview of different dispersion models available. *Atmospheric Environment*, 40(30):5902–5928, 2006.

[4] K Shankar Rao. Source estimation methods for atmospheric dispersion. *Atmospheric Environment*, 41(33):6964–6973, 2007.

[5] S. Susca, F. Bullo, and S. Martinez. Monitoring environmental boundaries with a robotic sensor network. *IEEE Transactions on Control Systems Technology*, 16(2):288–296, March 2008.

[6] Juan Jesús Roldán, Guillaume Joossen, David Sanz, Jaime del Cerro, and Antonio Barrientos. Mini-uav based sensory system for measuring environmental variables in greenhouses. *Sensors*, 15(2):3334–3350, 2015.

[7] Tommaso Francesco Villa, Felipe Gonzalez, Branka Miljievic, Zoran D Ristovski, and Lidia Morawska. An overview of small unmanned aerial vehicles for air quality measurements: Present applications and future prospectives. *Sensors*, 16(7):1072, 2016.

[8] Lars Yndal Sørensen, Lars Toft Jacobsen, and John Paulin Hansen. Low cost and flexible uav deployment of sensors. *Sensors*, 17(1):154, 2017.

[9] Boris I Shraiman and Eric D Siggla. Scalar turbulence. *Nature*, 405(6787):639, 2000.

[10] Massimo Vergassola, Emmanuel Villermaux, and Boris I Shraiman. 'infotaxis' as a strategy for searching without gradients. *Nature*, 445(7126):406–409, 2007.

[11] Julius Adler. Chemotaxis in bacteria. *Science*, 153(3737):708–716, 1966.

[12] Jiri Janata. *Principles of chemical sensors*. Springer Science & Business Media, 2010.

[13] Michael B Frish, Richard T Wainner, Matthew C Laderer, BDavid Green, and Mark G Allen. Standoff and miniature chemical vapor detectors based on tunable diode laser absorption spectroscopy. *IEEE Sensors Journal*, 10(3):639–646, 2010.

[14] Marco Trincavelli. Gas discrimination for mobile robots. *KI-Künstliche Intelligenz*, 25(4):351–354, 2011.

[15] Victor Hernandez Bennetts, Achim J Lilienthal, Ali Abdul Khaliq, Vıctor Pomareda Sesé, and Marco Trincavelli. Gasbot: A mobile robotic platform for methane leak detection and emission monitoring. In *Workshop on Robotics for Environmental Monitoring at the IEEE/RSJ International Conference on Intelligent Robots and Systems*, 2012.

[16] Victor Manuel Hernandez Bennetts, Achim J Lilienthal, Ali Abdul Khaliq, Victor Pomareda Sese, and Marco Trincavelli. Towards real-world gas distribution mapping and leak localization using a mobile robot with 3d and remote gas sensing capabilities. In *Robotics and Automation (ICRA), 2013 IEEE International Conference on*, pages 2335–2340. IEEE, 2013.

[17] Victor Hernandez Bennetts, Erik Schaffernicht, Todor Stoyanov, Achim J Lilienthal, and Marco Trincavelli. Robot assisted gas tomography—localizing methane leaks in outdoor environments. In *Robotics and Automation (ICRA), 2014 IEEE International Conference on*, pages 6362–6367. IEEE, 2014.

[18] Achim J Lilienthal, Matteo Reggente, Marco Trincavelli, Jose Luis Blanco, and Javier Gonzalez. A statistical approach to gas distribution modelling with mobile robots-the kernel dm+ v algorithm. In *Intelligent Robots and Systems, 2009. IROS 2009. IEEE/RSJ International Conference on*, pages 570–576. IEEE, 2009.

[19] W Jatmiko, F Jovan, RYS Dhiemas, Alvissalim M Sakti, Fanany M Ivan, T Fukuda, and K Sekiyama. Robots implementation for odor source localization using pso algorithm. *WSEAS Transactions on Circuits and Systems*, 10(4):115–125, 2011.

[20] Ji-Gong Li, Qing-Hao Meng, Yang Wang, and Ming Zeng. Odor source localization using a mobile robot in outdoor airflow environments with a particle filter algorithm. *Autonomous Robots*, 30(3):281–292, 2011.

[21] Qing-Hao Meng, Wei-Xing Yang, Yang Wang, and Ming Zeng. Collective odor source estimation and search in time-variant airflow environments using mobile robots. *Sensors*, 11(11):10415–10443, 2011.

[22] Brendan Smith, Garrett John, Brandon Stark, Lance E Christensen, and YangQuan Chen. Applicability of unmanned aerial systems for leak detection. In *Unmanned Aircraft Systems (ICUAS), 2016 International Conference on*, pages 1220–1227. IEEE, 2016.

[23] Brendan J Smith, Garrett John, Lance E Christensen, and YangQuan Chen. Fugitive methane leak detection using suas and miniature laser spectrometer payload: System, application and groundtruthing tests. In *Unmanned Aircraft Systems (ICUAS), 2017 International Conference on*, pages 369–374. IEEE, 2017.

[24] Bing Luo, Qing-Hao Meng, Jia-Ying Wang, and Ming Zeng. A flying odor compass to autonomously locate the gas source. *IEEE Transactions on Instrumentation and Measurement*, 67(1):137–149, 2018.

[25] Chih-Chung Chang, Jia-Lin Wang, Chih-Yuan Chang, Mao-Chang Liang, and Ming-Ren Lin. Development of a multicopter-carried whole air sampling apparatus and its applications in environmental studies. *Chemosphere*, 144:484–492, 2016.

[26] Tommaso Francesco Villa, Farhad Salimi, Kye Morton, Lidia Morawska, and Felipe Gonzalez. Development and validation of a uav based system for air pollution measurements. *Sensors*, 16(12):2202, 2016.

[27] J Aurell, W Mitchell, V Chirayath, J Jonsson, D Tabor, and B Gullett. Field determination of multipollutant, open area combustion source emission factors with a hexacopter unmanned aerial vehicle. *Atmospheric Environment*, 166:433–440, 2017.

[28] Miguel Alvarado, Felipe Gonzalez, Peter Erskine, David Cliff, and Darlene Heuff. A methodology to monitor airborne pm10 dust particles using a small unmanned aerial vehicle. *Sensors*, 17(2):343, 2017.

[29] Colin Greatwood, Thomas S Richardson, Jim Freer, Rick M Thomas, A Rob MacKenzie, Rebecca Brownlow, David Lowry, Rebecca E Fisher, and Euan G Nisbet. Atmospheric sampling on ascension island using multirotor uavs. *Sensors*, 17(6):1189, 2017.

[30] Patrick P Neumann, Harald Kohlhoff, Dino Hüllmann, Achim J Lilienthal, and Martin Kluge. Bringing mobile robot olfaction to the next dimension—uav-based remote sensing of gas clouds and source localization. In *Robotics and Automation (ICRA), 2017 IEEE International Conference on*, pages 3910–3916. IEEE, 2017.

[31] Miguel Alvarado, Felipe Gonzalez, Andrew Fletcher, and Ashray Doshi. Towards the development of a low cost airborne sensing system to monitor dust particles after blasting at open-pit mine sites. *Sensors*, 15(8):19667–19687, 2015.

[32] Patrick P Neumann, Victor Hernandez Bennetts, Achim J Lilienthal, Matthias Bartholmai, and Jochen H Schiller. Gas source localization with a micro-drone using bio-inspired and particle filter-based algorithms. *Advanced Robotics*, 27(9):725–738, 2013.

[33] Jay A Farrell, Shou Pang, Wei Li, and Richard Arrieta. Chemical plume tracing experimental results with a remus auv. In *OCEANS 2003. Proceedings*, volume 2, pages 962–968. IEEE, 2003.

[34] Muhammad Fahad, Yi Guo, Brian Bingham, Kristopher Krasnosky, Laura Fitzpatrick, and Fernando A Sanabria. Robotic experiments to evaluate ocean plume characteristics and structure. In *Intelligent Robots and Systems (IROS), 2017 IEEE/RSJ International Conference on*, pages 6098–6104. IEEE, 2017.

[35] Gideon Kowadlo and R Andrew Russell. Robot odor localization: a taxonomy and survey. *The International Journal of Robotics Research*, 27(8):869–894, 2008.

[36] Hiroshi Ishida, Yuta Wada, and Haruka Matsukura. Chemical sensing in robotic applications: A review. *IEEE Sensors Journal*, 12(11):3163–3173, 2012.

[37] Lino Marques and Anibal T De Almeida. Electronic nose-based odour source localization. In *Advanced Motion Control, 2000. Proceedings. 6th International Workshop on*, pages 36–40. IEEE, 2000.

[38] Lino Marques, Nuno Almeida, and AT De Almeida. Olfactory sensory system for odour-plume tracking and localization. In *Sensors, 2003. Proceedings of IEEE*, volume 1, pages 418–423. IEEE, 2003.

[39] Hiroshi Ishida, Kin-ichiro Suetsugu, Takamichi Nakamoto, and Toyosaka Moriizumi. Study of autonomous mobile sensing system for localization of odor source using gas sensors and anemometric sensors. *Sensors and Actuators A: Physical*, 45(2):153–157, 1994.

[40] R Andrew Russell. Laying and sensing odor markings as a strategy for assisting mobile robot navigation tasks. *IEEE Robotics & Automation Magazine*, 2(3):3–9, 1995.

[41] R Andrew Russell, Alireza Bab-Hadiashar, Rod L Shepherd, and Gordon G Wallace. A comparison of reactive robot chemotaxis algorithms. *Robotics and Autonomous Systems*, 45(2):83–97, 2003.

[42] John S Kennedy and D Marsh. Pheromone-regulated anemotaxis in flying moths. *Science*, 184(4140):999–1001, 1974.

[43] Ring T Cardé and Mark A Willis. Navigational strategies used by insects to find distant, wind-borne sources of odor. *Journal of chemical ecology*, 34(7):854–866, 2008.

[44] Dimitri Zarzhitsky and Diana F Spears. Swarm approach to chemical source localization. In *Systems, Man and Cybernetics, 2005 IEEE International Conference on*, volume 2, pages 1435–1440. IEEE, 2005.

[45] Dimitri Zarzhitsky, Diana Spears, David Thayer, and William Spears. Agent-based chemical plume tracing using fluid dynamics. In *Formal Approaches to Agent-Based Systems*, pages 146–160. Springer, 2004.

[46] Dimitri Zarzhitsky, Diana F Spears, William M Spears, and David R Thayer. A fluid dynamics approach to multi-robot chemical plume tracing. In *Proceedings of the Third International Joint Conference on Autonomous Agents and Multiagent Systems-Volume 3*, pages 1476–1477. IEEE Computer Society, 2004.

[47] Dimitri Zarzhitsky, Diana F Spears, and William M Spears. Swarms for chemical plume tracing. In *Swarm Intelligence Symposium, 2005. SIS 2005. Proceedings 2005 IEEE*, pages 249–256. IEEE, 2005.

[48] Shuo Pang and Jay A Farrell. Chemical plume source localization. *IEEE Transactions on Systems, Man, and Cybernetics, Part B (Cybernetics)*, 36(5):1068–1080, 2006.

[49] Adam T Hayes, Alcherio Martinoli, and Rodney M Goodman. Swarm robotic odor localization: Off-line optimization and validation with real robots. *Robotica*, 21(4):427–441, 2003.

[50] JB Masson, M Bailly Bechet, and Massimo Vergassola. Chasing information to search in random environments. *Journal of Physics A: Mathematical and Theoretical*, 42(43):434009, 2009.

[51] Eduardo Martin Moraud and Dominique Martinez. Effectiveness and robustness of robot infotaxis for searching in dilute conditions. *Frontiers in neurorobotics*, 4, 2010.

[52] Carlo Barbieri, Simona Cocco, and Rémi Monasson. On the trajectories and performance of infotaxis, an information-based greedy search algorithm. *EPL (Europhysics Letters)*, 94(2):20005, 2011.

[53] Nicole Voges, Antoine Chaffiol, Philippe Lucas, and Dominique Martinez. Reactive searching and infotaxis in odor source localization. *PLoS Comput Biol*, 10(10):e1003861, 2014.

[54] Hadi Hajieghrary, M Ani Hsieh, and Ira B Schwartz. Multi-agent search for source localization in a turbulent medium. *Physics Letters A*, 380(20):1698–1705, 2016.

[55] Branko Ristic, Alex Skvortsov, and Ajith Gunatilaka. A study of cognitive strategies for an autonomous search. *Information Fusion*, 28:1–9, 2016.

[56] Victor Hernandez Bennetts, Achim Josef Lilienthal, Patrick Neumann, and Marco Trincavelli. Mobile robots for localizing gas emission sources on landfill sites: is bio-inspiration the way to go? *Frontiers in neuroengineering*, 4:20, 2012.

[57] P Menon and Debasish Ghose. Boundary mapping of 3-dimensional regions. In *American Control Conference (ACC), 2013*, pages 2984–2989. IEEE, 2013.

[58] M Kemp, AL Bertozzi, and D Marthaler. Multi-uuv perimeter surveillance. In *2004 IEEE/OES Autonomous Underwater Vehicles (IEEE Cat. No. 04CH37578)*, pages 102–107. IEEE, 2004.

[59] Zhipu Jin and Andrea L Bertozzi. Environmental boundary tracking and estimation using multiple autonomous vehicles. In *Decision and Control, 2007 46th IEEE Conference on*, pages 4918–4923. IEEE, 2007.

[60] Abhijeet Joshi, Trevor Ashley, Yuan R Huang, and Andrea L Bertozzi. Experimental validation of cooperative environmental boundary tracking with on-board sensors. In *American Control Conference, 2009. ACC'09.*, pages 2630–2635. IEEE, 2009.

[61] Justin Clark and Rafael Fierro. Cooperative hybrid control of robotic sensors for perimeter detection and tracking. In *American Control Conference, 2005. Proceedings of the 2005*, pages 3500–3505. IEEE, 2005.

[62] Jerry Towler, Bryan Krawiec, and Kevin Kochersberger. Radiation mapping in post-disaster environments using an autonomous helicopter. *Remote Sensing*, 4(7):1995–2015, 2012.

[63] Juliane Brink. Boundary tracking and estimation of pollutant plumes with a mobile sensor in a low-density static sensor network. *Urban Climate*, 14:383–395, 2015.

[64] Alexey S Matveev, Hamid Teimoori, and Andrey V Savkin. Method for tracking of environmental level sets by a unicycle-like vehicle. *Automatica*, 48(9):2252–2261, 2012.

[65] Kirill Ovchinnikov, Anna Semakova, and Alexey Matveev. Decentralized multi-agent tracking of unknown environmental level sets by a team of nonholonomic robots. In *Ultra Modern Telecommunications and Control Systems and Workshops (ICUMT), 2014 6th International Congress on*, pages 352–359. IEEE, 2014.

[66] K.Ovchinnikov, A.Semakova, and A.Matveev. Cooperative surveillance of unknown environmental boundaries by multiple nonholonomic robots. *Robotics and Autonomous Systems*, 72:164–180, 2015.

[67] Prathyush P Menon, Christopher Edwards, Yuri B Shtessel, Debasish Ghose, and Jim Haywood. Boundary tracking using a suboptimal sliding mode algorithm. In *Decision and Control (CDC), 2014 IEEE 53rd Annual Conference on*, pages 5518–5523. IEEE, 2014.

[68] Andrew Jones, David Thomson, Matthew Hort, and Ben Devenish. The uk met office's next-generation atmospheric dispersion model, name iii. *Air Pollution Modeling and its Application XVII*, pages 580–589, 2007.

[69] Fumin Zhang and Naomi Ehrich Leonard. Generating contour plots using multiple sensor platforms. In *SIS*, pages 309–316, 2005.

[70] Fumin Zhang, Edward Fiorelli, and Naomi Ehrich Leonard. Exploring scalar fields using multiple sensor platforms: Tracking level curves. In *Decision and Control, 2007 46th IEEE Conference on*, pages 3579–3584. IEEE, 2007.

[71] Wencen Wu and Fumin Zhang. Cooperative exploration of level surfaces of three dimensional scalar fields. *Automatica*, 47(9):2044–2051, 2011.

[72] Brian A White, Antonios Tsourdos, Immanuel Ashokaraj, S Subchan, and Rafał Żbikowski. Contaminant cloud boundary monitoring using network of uav sensors. *Sensors Journal, IEEE*, 8(10):1681–1692, 2008.

[73] Subchan Subchan, Brian A White, Antonios Tsourdos, Madhavan Shanmugavel, and R Zbikowski. Dubins path planning of multiple uavs for tracking contaminant cloud. In *Proceedings of the 17th World Conference on the International Federation of Automatic Control, Seoul, Korea*, pages 6–11, 2008.

[74] Arpita Sinha, Antonios Tsourdos, and Brian White. Multi uav coordination for tracking the dispersion of a contaminant cloud in an urban region. *European Journal of Control*, 15(3):441–448, 2009.

[75] A.Sinha, A.Tsourdos, and B.White. Multi uav negotiation for coordinated tracking of contaminant cloud. In *Control Conference (ECC), 2009 European*, pages 109–114. IEEE, 2009.

[76] Cheng Zhang and Hailong Pei. Oil spills boundary tracking using universal kriging and model predictive control by uav. In *Intelligent Control and Automation (WCICA), 2014 11th World Congress on*, pages 633–638. IEEE, 2014.

[77] Juliane Euler, Alex Horn, Dominik Haumann, Jurgen Adamy, and Oskar Stryk. Cooperative n-boundary tracking in large scale environments. In *Mobile Adhoc and Sensor Systems (MASS), 2012 IEEE 9th International Conference on*, pages 1–6. IEEE, 2012.

[78] Woojin Kim, Dongjun Kwak, and H Jin Kim. Joint detection and tracking of boundaries using cooperative mobile sensor networks. In *Robotics and Automation (ICRA), 2013 IEEE International Conference on*, pages 889–894. IEEE, 2013.

[79] Sumana Srinivasan and Krithi Ramamritham. Contour estimation using collaborating mobile sensors. In *Proceedings of the 2006 workshop on Dependability issues in wireless ad hoc networks and sensor networks*, pages 73–82. ACM, 2006.

[80] Sumana Srinivasan, Krithi Ramamritham, and Purushottam Kulkarni. Ace in the hole: Adaptive contour estimation using collaborating mobile sensors. In *Information Processing in Sensor Networks, 2008. IPSN'08. International Conference on*, pages 147–158. IEEE, 2008.

[81] KN Krishnanand and Debasish Ghose. Detection of multiple source locations using a glowworm metaphor with applications to collective robotics. In *Swarm Intelligence Symposium, 2005. SIS 2005. Proceedings 2005 IEEE*, pages 84–91. IEEE, 2005.

[82] Prathyush P Menon and Debasish Ghose. Simultaneous source localization and boundary mapping for contaminants. In *American Control Conference (ACC), 2012*, pages 4174–4179. IEEE, 2012.

[83] T.Sun, H.Pei, Y.Pan, and C.Zhang. Robust adaptive neural network control for environmental boundary tracking by mobile robots. *International Journal of Robust and Nonlinear Control*, 23(2):123–136, 2013.

[84] Shuai Li, Yi Guo, and Brad Bingham. Multi-robot cooperative control for monitoring and tracking dynamic plumes. In *Robotics and Automation (ICRA), 2014 IEEE International Conference on*, pages 67–73. IEEE, 2014.

[85] Muhammad Fahad, Nathaniel Saul, Yi Guo, and Brian Bingham. Robotic simulation of dynamic plume tracking by unmanned surface vessels. In *Robotics and Automation (ICRA), 2015 IEEE International Conference on*, pages 2654–2659. IEEE, 2015.

[86] Muhammad Fahad, Yi Guo, Brian Bingham, Kristopher Krasnosky, Laura Fitzpatrick, and Fernando A Sanabria. Ocean plume tracking with unmanned surface vessels: Algorithms and experiments. *arXiv preprint arXiv:1804.08669*, 2018.

[87] Robin R Murphy, Joshua Peschel, Clint Arnett, and David Martin. Projected needs for robot-assisted chemical, biological, radiological, or nuclear (cbrn) incidents. In *Safety, Security, and Rescue Robotics (SSRR), 2012 IEEE International Symposium on*, pages 1–4. IEEE, 2012.

[88] Mirbek Turduev, Gonçalo Cabrita, Murat Kırtay, Veysel Gazi, and Lino Marques. Experimental studies on chemical concentration map building by a multi-robot system using bio-inspired algorithms. *Autonomous agents and multi-agent systems*, 28(1):72–100, 2014.

[89] Cyrill Stachniss, Christian Plagemann, and Achim J Lilienthal. Learning gas distribution models using sparse gaussian process mixtures. *Autonomous Robots*, 26(2-3):187–202, 2009.

[90] Patrick P Neumann, Sahar Asadi, Achim J Lilienthal, Matthias Bartholmai, and Jochen H Schiller. Autonomous gas-sensitive microdrone: Wind vector estimation and gas distribution mapping. *IEEE robotics & automation magazine*, 19(1):50–61, 2012.

[91] Kamarulzaman Kamarudin, Ali Yeon Md Shakaff, Victor Hernandez Bennetts, Syed Muhammad Mamduh, Ammar Zakaria, Retnam Visvanathan, Ahmad Shakaff Ali Yeon, and Latifah Munirah Kamarudin. Integrating slam and gas distribution mapping (slam-gdm) for real-time gas source localization. *Advanced Robotics*, 32(17):903–917, 2018.

[92] Matteo Reggente and Achim J Lilienthal. Using local wind information for gas distribution mapping in outdoor environments with a mobile robot. In *Sensors, 2009 IEEE*, pages 1715–1720. IEEE, 2009.

[93] Matteo Reggente and Achim J Lilienthal. Three-dimensional statistical gas distribution mapping in an uncontrolled indoor environment. In *AIP Conference Proceedings*, volume 1137, pages 109–112. AIP, 2009.

[94] Sahar Asadi, Han Fan, Victor Hernandez Bennetts, and Achim J Lilienthal. Time-dependent gas distribution modelling. *Robotics and Autonomous Systems*, 96:157–170, 2017.

[95] Javier G Monroy, Jose-Luis Blanco, and Javier Gonzalez-Jimenez. Time-variant gas distribution mapping with obstacle information. *Autonomous Robots*, 40(1):1–16, 2016.

[96] Sarvesh Kumar Singh, Maithili Sharan, and Jean-Pierre Issartel. Inverse modelling methods for identifying unknown releases in emergency scenarios: an overview. *International Journal of Environment and Pollution*, 57(1-2):68–91, 2015.

[97] Daniel Marthaler and Andrea L Bertozzi. Tracking environmental level sets with autonomous vehicles. In *Recent developments in cooperative control and optimization*, pages 317–332. Springer, 2004.

[98] Nathan Platt and Dennis DeRiggi. Comparative investigation of source term estimation algorithms using fusion field trial 2007 data: linear regression analysis. *International Journal of Environment and Pollution*, 48(1-4):13–21, 2012.

[99] M Redwood. Source term estimation and event reconstruction : a survey. Technical report, Atmospheric Dispersion Modelling Liaison Committee report : ADMLC-R6, 2011.

[100] Sarvesh Kumar Singh and Raj Rani. A least-squares inversion technique for identification of a point release: Application to fusion field trials 2007. *Atmospheric Environment*, 92:104–117, 2014.

[101] Maithili Sharan, Jean-Pierre Issartel, Sarvesh Kumar Singh, and Pramod Kumar. An inversion technique for the retrieval of single-point emissions from atmospheric concentration measurements. In *Proceedings of the Royal Society of London A: Mathematical, Physical and Engineering Sciences*, pages rspa–2008. The Royal Society, 2009.

[102] Xiaoping Zheng and Zengqiang Chen. Back-calculation of the strength and location of hazardous materials releases using the pattern search method. *Journal of hazardous materials*, 183(1):474–481, 2010.

[103] Laura C Thomson, Bill Hirst, Graham Gibson, Steve Gillespie, Philip Jonathan, Kenneth D Skeldon, and Miles J Padgett. An improved algorithm for locating a gas source using inverse methods. *Atmospheric Environment*, 41(6):1128–1134, 2007.

[104] Christopher T Allen, George S Young, and Sue Ellen Haupt. Improving pollutant source characterization by better estimating wind direction with a genetic algorithm. *Atmospheric Environment*, 41(11):2283–2289, 2007.

[105] Sue Ellen Haupt, George S Young, and Christopher T Allen. A genetic algorithm method to assimilate sensor data for a toxic contaminant release. *Journal of Computers*, 2(6):85–93, 2007.

[106] Christopher T Allen, Sue Ellen Haupt, and George S Young. Source characterization with a genetic algorithm-coupled dispersion-backward model incorporating scipuff. *Journal of applied meteorology and climatology*, 46(3):273–287, 2007.

[107] Maithili Sharan, Sarvesh Kumar Singh, and JP Issartel. Least square data assimilation for identification of the point source emissions. *Pure and applied geophysics*, 169(3):483–497, 2012.

[108] Jean-Pierre Issartel. Rebuilding sources of linear tracers after atmospheric concentration measurements. *Atmos. Chem. Phys*, 3:2111–2125, 2003.

[109] JP Issartel. Emergence of a tracer source from air concentration measurements, a new strategy for linear assimilation. *Atmospheric Chemistry and Physics*, 5(1):249–273, 2005.

[110] Grégory Turbelin, Sarvesh Kumar Singh, and Jean-Pierre Issartel. Reconstructing source terms from atmospheric concentration measurements: Optimality analysis of an inversion technique. *Journal of Advances in Modeling Earth Systems*, 6(4):1244–1255, 2014.

[111] Jean-Pierre Issartel, Maithili Sharan, and Manish Modani. An inversion technique to retrieve the source of a tracer with an application to synthetic satellite measurements. In *Proceedings of the Royal Society of London A: Mathematical, Physical and Engineering Sciences*, volume 463, pages 2863–2886. The Royal Society, 2007.

[112] Maithili Sharan, Anil Kumar Yadav, MP Singh, P Agarwal, and S Nigam. A mathematical model for the dispersion of air pollutants in low wind conditions. *Atmospheric Environment*, 30(8):1209–1220, 1996.

[113] Maithili Sharan, Jean-Pierre Issartel, and Sarvesh Kumar Singh. A point-source reconstruction from concentration measurements in low-wind stable conditions. *Quarterly Journal of the Royal Meteorological Society*, 138(668):1884–1894, 2012.

[114] Sarvesh Kumar Singh, Maithili Sharan, and Jean-Pierre Issartel. Inverse modelling for identification of multiple-point releases from atmospheric concentration measurements. *Boundary-layer meteorology*, 146(2):277–295, 2013.

[115] DP Storwold. Detailed test plan for the fusing sensor information from observing networks (fusion) field trial 2007 (fft 07. *US Army Dugway Proving Ground West Desert Test Center Doc. WDTC-TP-07-078*, 2007.

[116] Sarvesh Kumar Singh and Raj Rani. Assimilation of concentration measurements for retrieving multiple point releases in atmosphere: A least-squares approach to inverse modelling. *Atmospheric Environment*, 119:402–414, 2015.

[117] Pramod Kumar, Amir-Ali Feiz, Sarvesh Kumar Singh, Pierre Ngae, and Grégory Turbelin. Reconstruction of an atmospheric tracer source in an urban-like environment. *Journal of Geophysical Research: Atmospheres*, 120(24):12589–12604, 2015.

[118] Pramod Kumar, Sarvesh Kumar Singh, Amir-Ali Feiz, and Pierre Ngae. An urban scale inverse modelling for retrieving unknown elevated emissions with building-resolving simulations. *Atmospheric Environment*, 140:135–146, 2016.

[119] Pramod Kumar, Amir-Ali Feiz, Pierre Ngae, Sarvesh Kumar Singh, and Jean-Pierre Issartel. Cfd simulation of short-range plume dispersion from a point release in an urban like environment. *Atmospheric Environment*, 122:645–656, 2015.

[120] C. G. BROYDEN. The convergence of a class of double-rank minimization algorithms: 2. the new algorithm. *IMA Journal of Applied Mathematics*, 6(3):222–231, 1970.

[121] Paul E Bieringer, Luna M Rodriguez, Francois Vandenberghe, Jonathan G Hurst, George Bieberbach, Ian Sykes, John R Hannan, Jake Zaragoza, and Richard N Fry. Automated source term and wind parameter estimation for atmospheric transport and dispersion applications. *Atmospheric Environment*, 122:206–, 2015.

[122] William C Davidon. Variable metric method for minimization. *SIAM Journal on Optimization*, 1(1):1–17, 1991.

[123] Xiaoping Zheng and Zengqiang Chen. Inverse calculation approaches for source determination in hazardous chemical releases. *Journal of Loss Prevention in the Process Industries*, 24(4):293–301, 2011.

[124] Scott Kirkpatrick. Optimization by simulated annealing: Quantitative studies. *Journal of statistical physics*, 34(5-6):975–986, 1984.

[125] Robert B Goldberg, Susan J Barker, and Luis Perez-Grau. Regulation of gene expression during plant embryogenesis. *Cell*, 56(2):149–160, 1989.

[126] Sue Ellen Haupt. A demonstration of coupled receptor/dispersion modeling with a genetic algorithm. *Atmospheric Environment*, 39(37):7181–7189, 2005.

[127] Kerrie J Long, Sue Ellen Haupt, and George S Young. Assessing sensitivity of source term estimation. *Atmospheric environment*, 44(12):1558–1567, 2010.

[128] Andrew J Annunzio, George S Young, and Sue Ellen Haupt. Utilizing state estimation to determine the source location for a contaminant. *Atmospheric environment*, 46:580–589, 2012.

[129] Andrew J Annunzio, George S Young, and Sue Ellen Haupt. A multi-entity field approximation to determine the source location of multiple atmospheric contaminant releases. *Atmospheric environment*, 62:593–604, 2012.

[130] Denglong Ma, Jianqiang Deng, and Zaoxiao Zhang. Comparison and improvements of optimization methods for gas emission source identification. *Atmospheric Environment*, 81:188–198, 2013.

[131] Vladimir Naumovich Vapnik and Vlamimir Vapnik. *Statistical learning theory*, volume 1. Wiley New York, 1998.

[132] G Johannesson, B Hanley, and J Nitao. Dynamic bayesian models via monte carlo-an introduction with examples. *Lawrence Livermore National Laboratory, UCRL-TR-207173*, 2004.

[133] Mieczyslaw Borysiewicz, Anna Wawrzynczak, and Piotr Kopka. Bayesian-based methods for the estimation of the unknown model's parameters in the case of the localization of the atmospheric contamination source. *Foundations of Computing and Decision Sciences*, 37(4):253–270, 2012.

[134] Andrew Keats, Eugene Yee, and Fue-Sang Lien. Bayesian inference for source determination with applications to a complex urban environment. *Atmospheric environment*, 41(3):465–479, 2007.

[135] Ajith Gunatilaka, Branko Ristic, Alex Skvortsov, and Mark Morelande. Parameter estimation of a continuous chemical plume source. In *Information Fusion, 2008 11th International Conference on*, pages 1–8. IEEE, 2008.

[136] Anna Wawrzynczak, Piotr Kopka, and Mieczyslaw Borysiewicz. Sequential monte carlo in bayesian assessment of contaminant source localization based on the sensors concentration measurements. In *International Conference on Parallel Processing and Applied Mathematics*, pages 407–417. Springer, 2013.

[137] RO Lane, M Briers, and K Copsey. Approximate bayesian computation for source term estimation. *Mathematics in Defence 2009*, 2009.

[138] P Robins, VE Rapley, and N Green. Realtime sequential inference of static parameters with expensive likelihood calculations. *Journal of the Royal Statistical Society: Series C (Applied Statistics)*, 58(5):641–662, 2009.

[139] Reza Madankan, Parveen Singla, and Taranveer Singh. Application of conjugate unscented transform in source parameters estimation. In *American Control Conference (ACC), 2013*, pages 2448–2453. IEEE, 2013.

[140] Walter R Gilks. *Markov chain monte carlo*. Wiley Online Library, 2005.

[141] Nicholas Metropolis, Arianna W Rosenbluth, Marshall N Rosenbluth, Augusta H Teller, and Edward Teller. Equation of state calculations by fast computing machines. *The journal of chemical physics*, 21(6):1087–1092, 1953.

[142] Inanc Senocak, Nicolas W Hengartner, Margaret B Short, and W Brent Daniel. Stochastic event reconstruction of atmospheric contaminant dispersion using bayesian inference. *Atmospheric Environment*, 42(33):7718–7727, 2008.

[143] Eugene Yee. Bayesian probabilistic approach for inverse source determination from limited and noisy chemical or biological sensor concentration measurements. In *Defense and Security Symposium*, pages 65540W–65540W. International Society for Optics and Photonics, 2007.

[144] Enzo Marinari and Giorgio Parisi. Simulated tempering: a new monte carlo scheme. *EPL (Europhysics Letters)*, 19(6):451, 1992.

[145] Eugene Yee. Bayesian inversion of concentration data for an unknown number of contaminant sources. Technical report, DTIC Document, 2007.

[146] Peter J Green. Reversible jump markov chain monte carlo computation and bayesian model determination. *Biometrika*, 82(4):711–732, 1995.

[147] Eugene Yee. Validation of a bayesian inferential framework for multiple source reconstruction using fft-07 data. HARMO13-1-4 June 2010, Paris, France-13 th Conference on Harmonisation within Atmospheric Dispersion Modeling for Regulatory Purposes, 2010.

[148] E.Yee. Inverse dispersion for an unknown number of sources: model selection and uncertainty analysis. *ISRN Applied Mathematics*, 2012.

[149] Derek Wade and Inanc Senocak. Stochastic reconstruction of multiple source atmospheric contaminant dispersion events. *Atmospheric Environment*, 74:45–51, 2013.

[150] Eugene Yee, Ian Hoffman, and Kurt Ungar. Bayesian inference for source reconstruction: A real-world application. *International Scholarly Research Notices*, 2014.

[151] Arnaud Doucet, Nando De Freitas, and Neil Gordon. An introduction to sequential monte carlo methods. In *Sequential Monte Carlo methods in practice*, pages 3–14. Springer, 2001.

[152] Branko Ristic, Ajith Gunatilaka, Ralph Gailis, and Alex Skvortsov. Bayesian likelihood-free localisation of a biochemical source using multiple dispersion models. *Signal Processing*, 108:13–24, 2015.

[153] Branko Ristic, Ajith Gunatilaka, and Ralph Gailis. Localisation of a source of hazardous substance dispersion using binary measurements. *Atmospheric Environment*, 142:114–119, 2016.

[154] B.Ristic, A.Gunatilaka, and R.Gailis. Achievable accuracy in gaussian plume parameter estimation using a network of binary sensors. *Information Fusion*, 25:42–48, 2015.

[155] Cajo JF Ter Braak. A markov chain monte carlo version of the genetic algorithm differential evolution: easy bayesian computing for real parameter spaces. *Statistics and Computing*, 16(3):239–249, 2006.

[156] Peter Robins, Veronica E Rapley, and Paul A Thomas. Biological source term estimation using particle counters and immunoassay sensors. In *2006 9th International Conference on Information Fusion*, pages 1–8. IEEE, 2006.

[157] Peter Robins and Paul Thomas. Non-linear bayesian cbrn source term estimation. In *Information Fusion, 2005 8th International Conference on*, volume 2, pages 8–pp. IEEE, 2005.

[158] Peter Robins, Veronica Rapley, and Paul Thomas. A probabilistic chemical sensor model for data fusion. In *2005 7th International Conference on Information Fusion*, volume 2, pages 7–pp. IEEE, 2005.

[159] Norbert Wiener. The homogeneous chaos. *American Journal of Mathematics*, 60(4):897–936, 1938.

[160] K Dalbey, AK Patra, EB Pitman, MI Bursik, and MF Sheridan. Input uncertainty propagation methods and hazard mapping of geophysical mass flows. *Journal of Geophysical Research: Solid Earth*, 113(B5), 2008.

[161] Nagavenkat Adurthi, Parveen Singla, and Taranveer Singh. The conjugate unscented transform—an approach to evaluate multi-dimensional expectation integrals. In *American Control Conference (ACC), 2012*, pages 5556–5561. IEEE, 2012.

[162] Chunfeng Huang, Tailen Hsing, Noel Cressie, Auroop R Ganguly, Vladimir A Protopopescu, and Nageswara S Rao. Bayesian source detection and parameter estimation of a plume model based on sensor network measurements. *Applied Stochastic Models in Business and Industry*, 26(4):331–348, 2010.

[163] Branko Ristic, Ajith Gunatilaka, and Ralph Gailis. Achievable accuracy in parameter estimation of a gaussian plume dispersion model. In *Statistical Signal Processing (SSP), 2014 IEEE Workshop on*, pages 209–212. IEEE, 2014.

[164] Yan Wang, Hong Huang, and Wei Zhu. Stochastic source term estimation of hazmat releases: algorithms and uncertainty.

[165] Denglong Ma, Simin Wang, and Zaoxiao Zhang. Hybrid algorithm of minimum relative entropy-particle swarm optimization with adjustment parameters for gas source term identification in atmosphere. *Atmospheric Environment*, 94:637–646, 2014.

[166] Yuki Kuroki, George S Young, and Sue Ellen Haupt. Uav navigation by an expert system for contaminant mapping with a genetic algorithm. *Expert Systems with Applications*, 37(6):4687–4697, 2010.

[167] Bill Hirst, Philip Jonathan, Fernando González del Cueto, David Randell, and Oliver Kosut. Locating and quantifying gas emission sources using remotely obtained concentration data. *Atmospheric environment*, 74:141–158, 2013.

[168] Leslie Pack Kaelbling, Michael L. Littman, and Anthony R. Cassandra. Planning and acting in partially observable stochastic domains. *Artificial Intelligence*, 101(1–2):99 – 134, 1998.

[169] Solomon Kullback and Richard A Leibler. On information and sufficiency. *The annals of mathematical statistics*, 22(1):79–86, 1951.

[170] ALFRPED RRNYI. On measures of entropy and information. 1961.

[171] Branko Ristic and Ajith Gunatilaka. Information driven localisation of a radiological point source. *Information Fusion*, 9(2):317–326, 2008.

[172] Branko Ristic, Mark Morelande, and Ajith Gunatilaka. Information driven search for point sources of gamma radiation. *Signal Processing*, 90(4):1225–1239, 2010.

[173] Branko Ristic, Alex Skvortsov, and Andrew Walker. Autonomous search for a diffusive source in an unknown structured environment. *Entropy*, 16(2):789–813, 2014.

[174] Branko Ristic, Alex Skvortsov, and Ajith Gunatilaka. A study of cognitive strategies for an autonomous search. *Information Fusion*, 28:1 – 9, 2016.

[175] Reza Madankan, Puneet Singla, and Tarunraj Singh. Optimal information collection for source parameter estimation of atmospheric release phenomenon. In *2014 American Control Conference*, pages 604–609. IEEE, 2014.

[176] Thomas Wiedemann, Christoph Manss, Dmitriy Shutin, Achim J Lilienthal, Valentina Karolj, and Alberto Viseras. Probabilistic modeling of gas diffusion with partial differential equations for multi-robot exploration and gas source localization. In *Mobile Robots (ECMR), 2017 European Conference on*, pages 1–7. IEEE, 2017.

[177] Thomas J Loredo. Bayesian adaptive exploration. *arXiv preprint astro-ph/0409386*, 2004.

[178] A Keats, Eugene Yee, and F-S Lien. Information-driven receptor placement for contaminant source determination. *Environmental Modelling & Software*, 25(9):1000–1013, 2010.

[179] Michael Hutchinson, Hyondong Oh, and Wen-Hua Chen. Adaptive bayesian sensor motion planning for hazardous source term reconstruction. *IFAC-PapersOnLine*, 50(1):2812–2817, 2017.

[180] Hans A Panofsky and JA Dutton. *Atmospheric Turbulence: Models and Methods for Engineering Applications, 397 pp.* John Wiley, New York, 1984.

[181] Paola Sebastiani and Henry P Wynn. Maximum entropy sampling and optimal bayesian experimental design. *Journal of the Royal Statistical Society: Series B (Statistical Methodology)*, 62(1):145–157, 2000.

[182] K Shankar Rao. Uncertainty analysis in atmospheric dispersion modeling. *Pure and applied geophysics*, 162(10):1893–1917, 2005.

[183] G Johannesson, KM Dyer, WG Hanley, B Kosovic, SC Larsen, GA Loosmore, and A MIRIN. Sequential monte-carlo based framework for dynamic data-driven event reconstruction for atmospheric release. In *Proc. Joint Statistical Meeting, Minneapolis, MN, American Statistical Association and Cosponsors*, pages 73–80, 2005.

[184] W Keith Hastings. Monte carlo sampling methods using markov chains and their applications. *Biometrika*, 57(1):97–109, 1970.

[185] Michael Hutchinson, Hyondong Oh, and Wen-Hua Chen. Entrotaxis as a strategy for autonomous search and source reconstruction in turbulent conditions. *Information Fusion*, 42:179–189, 2018.

[186] Lance Champagne, R Greg Carl, and Raymond Hill. Agent models ii: search theory, agent-based simulation, and u-boats in the bay of biscay. In *Proceedings of the 35th conference on Winter simulation: driving innovation*, pages 991–998. Winter Simulation Conference, 2003.

[187] Martin Müller and Rüdiger Wehner. The hidden spiral: systematic search and path integration in desert ants, cataglyphis fortis. *Journal of Comparative Physiology A*, 175(5):525–530, 1994.

[188] Gandhimohan M Viswanathan, V Afanasyev, SV Buldyrev, EJ Murphy, PA Prince, H Eugene Stanley, et al. Lévy flight search patterns of wandering albatrosses. *Nature*, 381(6581):413–415, 1996.

[189] Nicolas E Humphries, Nuno Queiroz, Jennifer RM Dyer, Nicolas G Pade, Michael K Musyl, Kurt M Schaefer, Daniel W Fuller, Juerg M Brunnschweiler, Thomas K Doyle, Jonathan DR Houghton, et al. Environmental context explains lévy and brownian movement patterns of marine predators. *Nature*, 465(7301):1066–1069, 2010.

[190] Graham H Pyke. Understanding movements of organisms: it's time to abandon the lévy foraging hypothesis. *Methods in Ecology and Evolution*, 6(1):1–16, 2015.

[191] Andrew M Reynolds, Jennifer L Swain, Alan D Smith, Andrew P Martin, and Juliet L Osborne. Honeybees use a lévy flight search strategy and odour-mediated anemotaxis to relocate food sources. *Behavioral Ecology and Sociobiology*, 64(1):115–123, 2009.

[192] John M Danskin. A theory of reconnaissance: I. *Operations Research*, 10(3):285–299, 1962.

[193] Edwin KP Chong, Christopher M Kreucher, and Alfred O Hero III. POMDP approximation using simulation and heuristics. In *Foundations and Applications of Sensor Management*, pages 95–119. Springer, 2008.

[194] He Yuyao, Song Cheng, Yang Panpan, and Lei Xiaokang. Bio-inspired guiding strategy for robot seeking intermittent information source. In *2016 13th International Bhurban Conference on Applied Sciences and Technology (IBCAST)*, pages 161–166. IEEE, 2016.

[195] AW Eggels, RPJ Kunnen, B Koren, and AS Tijsseling. Infotaxis in a turbulent 3d channel flow. *Journal of Computational and Applied Mathematics*, 2016.

[196] Neil Gordon, B Ristic, and S Arulampalam. *Beyond the kalman filter: Particle filters for tracking applications*. Artech House, London, 2004.

[197] Chengxiang Wang, Longwei Yin, Luyuan Zhang, Dong Xiang, and Rui Gao. Metal oxide gas sensors: sensitivity and influencing factors. *Sensors*, 10(3):2088–2106, 2010.

[198] Michael Hutchinson, Cunjia Liu, and Wen-Hua Chen. Information-based search for an atmospheric release using a mobile robot: Algorithm and experiments. *IEEE Transactions on Control Systems Technology*, (99):1–15, 2018.

[199] Jean-Baptiste Masson. Olfactory searches with limited space perception. *Proceedings of the National Academy of Sciences*, 110(28):11261–11266, 2013.

[200] Patrick P Neumann and Matthias Bartholmai. Real-time wind estimation on a micro unmanned aerial vehicle using its inertial measurement unit. *Sensors and Actuators A: Physical*, 235:300–310, 2015.

[201] Eduardo Martin Moraud and Dominique Martinez. Effectiveness and robustness of robot infotaxis for searching in dilute conditions. *Frontiers in neurorobotics*, 4:1, 2010.

[202] Dennis V Lindley. On a measure of the information provided by an experiment. *The Annals of Mathematical Statistics*, pages 986–1005, 1956.

[203] George C. Efthimiou, Ivan V. Kovalets, Alexandros Venetsanos, Spyros Andronopoulos, Christos D. Argyropoulos, and Konstantinos Kakosimos. An optimized inverse modelling method for determining the location and strength of a point source releasing airborne material in urban environment. *Atmospheric Environment*, 2017.

[204] Branko Ristic, Sanjeev Arulampalam, and Neil James Gordon. *Beyond the Kalman filter: Particle filters for tracking applications*. Artech house, 2004.

[205] Morgan Quigley, Ken Conley, Brian P. Gerkey, Josh Faust, Tully Foote, Jeremy Leibs, Rob Wheeler, and Andrew Y. Ng. Ros: an open-source robot operating system. In *ICRA Workshop on Open Source Software*, 2009.

[206] Yu-Feng Sun, Shao-Bo Liu, Fan-Li Meng, Jin-Yun Liu, Zhen Jin, Ling-Tao Kong, and Jin-Huai Liu. Metal oxide nanostructures and their gas sensing properties: a review. *Sensors*, 12(3):2610–2631, 2012.

[207] Michael Hutchinson, Cunjia Liu, and Wen-Hua Chen. Source term estimation of a hazardous airborne release using an unmanned aerial vehicle. *Journal of Field Robotics*, 2018.

[208] KJ Allwine, MJ Leach, LW Stockham, JS Shinn, RP Hosker, JF Bowers, and JC Pace. J7. 1 overview of joint urban 2003–an atmospheric dispersion study in oklahoma city. 2004.

[209] Yan Wang, Hong Huang, Lida Huang, and Branko Ristic. Evaluation of bayesian source estimation methods with prairie grass observations and gaussian plume model: A comparison of likelihood functions and distance measures. *Atmospheric Environment*, 152:519 – 530, 2017.

[210] Pawel Ladosz, Matthew Coombes, Jean Smith, and Michael Hutchinson. A generic ros based system for rapid development and testing of algorithms for autonomous ground and aerial vehicles. In *Robot Operating System (ROS)*, pages 113–153. Springer, 2019.

[211] Eugene Yee. Automated computational inference engine for bayesian source reconstruction: Application to some detections/non-detections made in the ctbt international monitoring system. *Applied Mathematical Sciences*, 11(32):1581–1618, 2017.

[212] Edwin T Jaynes. *Probability theory: The logic of science*. Cambridge university press, 2003.

[213] Frank Pasquill. The estimation of the dispersion of windborne material. *Meteorol. Mag*, 90(1063):33–49, 1961.

[214] Lino Marques. Good experimental methodologies for mobile robot olfaction. In *Proceedings of the Robotics: Science and Systems Conference (RSS2009), Workshop on Good Experimental Methodology in Robotics, Seattle, WA, USA*, volume 28, pages 291–294, 2011.

[215] Michael Hutchinson, Cunjia Liu, and Wen-Hua Chen. Information based mobile sensor planning for source term estimation of a non-continuous atmospheric release. In *2018 IEEE International Conference on Robotics and Automation (ICRA)*, May 2018. accepted.

[216] Behzad Bayat, Naveena Crasta, Alessandro Crespi, António M Pascoal, and Auke Ijspeert. Environmental monitoring using autonomous vehicles: a survey of recent searching techniques. *Current opinion in biotechnology*, 45:76–84, 2017.

[217] Reza Madankan, Puneet Singla, and Tarunraj Singh. Parameter estimation of atmospheric release incidents using maximal information collection. In *Dynamic Data-Driven Environmental Systems Science*, pages 310–321. Springer, 2015.

[218] S Thykier-Nielsen, S Deme, and T Mikkelsen. Description of the atmospheric dispersion module rimpuff. *Riso National Laboratory, PO Box*, 49, 1999.

[219] Matteo Reggente and Achim J Lilienthal. Statistical evaluation of the kernel dm+ v/w algorithm for building gas distribution maps in uncontrolled environments. In *Eurosensors 23rd Conference; Lausanne; Switzerland; 6 September 2009 through 9 September 2009*, volume 1, pages 481–484. Elsevier, 2009.

[220] Michael Hutchinson, Pawel Ladosz, Cunjia Liu, and Wen-Hua Chen. Plume mapping using point measurements from autonomous unmanned vehicles. In *2019 IEEE International Conference on Robotics and Automation (ICRA)*, May 2019. under review.

[221] Carl Edward Rasmussen. Gaussian processes in machine learning. In *Advanced lectures on machine learning*, pages 63–71. Springer, 2004.

[222] Anthony J Carfang, Neeti Wagle, and Eric W Frew. Improving data ferrying by iteratively learning the radio frequency environment. In *Intelligent Robots and Systems (IROS 2014), 2014 IEEE/RSJ International Conference on*, pages 1182–1188. IEEE, 2014.

[223] Daniel Levine, Brandon Luders, and Jonathan How. Information-rich path planning with general constraints using rapidly-exploring random trees. In *AIAA Infotech@ Aerospace 2010*, page 3360. 2010.

[224] Geoffrey A Hollinger and Gaurav S Sukhatme. Sampling-based robotic information gathering algorithms. *The International Journal of Robotics Research*, 33(9):1271–1287, 2014.